



**Development of a plant-based
strategy for water status monitoring
and stress detection in grapevine**

ir. Annelies Baert



Promoter Prof. dr. ir. Kathy STEPPE
Laboratory of Plant Ecology
Department of Applied Ecology and Environmental Biology
Faculty of Bioscience Engineering
Ghent University

Members of the examination board

dr. Brendan CHOAT
Prof. dr. ir. Ingmar NOPENS
Prof. dr. ir. Marie-Christine VAN LABEKE (Secretary)
Prof. dr. ir. Marc VAN MEIRVENNE (Chairman)

Dean Prof. dr. ir. Guido VAN HUYLENBROECK

Rector Prof. dr. Anne DE PAEPE

ir. Annelies Baert

DEVELOPMENT OF A PLANT-BASED STRATEGY
FOR WATER STATUS MONITORING AND STRESS
DETECTION IN GRAPEVINE

Thesis submitted in fulfilment of the requirements
for the degree of Doctor (PhD) in Applied Biological Sciences

Dutch translation of the title:

Ontwikkeling van een plantgebaseerde strategie voor het opvolgen van de waterstatus en stressdetectie bij druif

Illustrations on the cover:

Front: Grapevine (*Vitis vinifera* L. cv. Muller Thurgau) at St. Peter's Abbey, Ghent, Belgium (© Annelies Baert)

Back: Detail of grape clusters in Elqui valley, Coquimbo, Chile (© Annelies Baert)

Citation of this thesis:

Baert A. 2013. Development of a plant-based strategy for water status monitoring and stress detection in grapevine. PhD thesis, Ghent University, Belgium.

ISBN-number: 978-90-5989-669-7

The author and the promoter give the authorisation to consult and to copy parts of this work for personal use only. Every other use is subject to the copyright laws. Permission to reproduce any material contained in this work should be obtained from the author.

Dankwoord

Deze eerste pagina's zou ik graag gebruiken om iedereen te bedanken die rechtstreeks of onrechtstreeks bijgedragen heeft tot het behalen van mijn doctoraat. Ik zou het zonder jullie niet hebben gehaald.

Ten eerste wil ik mijn promotor Prof. Kathy Steppe bedanken. Toen ik negen jaar geleden aan de opleiding Bio-Ingenieur begon had ik nooit gedacht dat ik ooit een doctoraat zou afleggen. Het was Kathy haar aanstekelijke enthousiasme tijdens de lessen terrestrische ecologie en later tijdens het begeleiden van mijn masterproef die me niet meer deden twifelen over de richting die ik wou inslaan. Kathy, bedankt voor de boeiende onderwerpen die je hebt aangebracht en helpen uitwerken. Bedankt voor je belangrijke bijdragen voor het behalen van mijn doctoraatsbeurs, het schrijven van publicaties en het uitdenken van proefopzetten. Ik kon na elke vergadering weer aan de slag met tal van nieuwe ideeën. Ik heb de kans gekregen een opleiding te volgen bij Kris Villez en mocht mijn onderzoek voorstellen op congressen met nogal exotische bestemmingen, zoals Canada en Chili. Ik ben heel blij dat je mij daar telkens in gesteund hebt.

I would like to thank the members of the examination board, dr. Brendan Choat, prof. dr. ir. Ingmar Nopens, prof. dr. ir. Marie-Christine Van Labeke and prof. dr. ir. Marc Van Meirvenne, for the opportunity to present my work and for your thoughtful review of this PhD thesis.

Het Agentschap voor Innovatie door Wetenschap en Technologie (IWT) wil ik bedanken voor het financieren van mijn doctoraatsonderzoek.

Daarnaast wil ik de collega's van Labo Plantecologie graag bedanken. Jullie hebben me hier een uiterst aangename tijd bezorgd. Geert en Philip, voor het helpen bij de technische aspecten van mijn experimenten, het meerijden in de veel te grote Jumper om de allereerste druivelaars op te halen, en het wintervervoer van de talrijke kleine druivelaars naar de faculteit, en terug naar Latem, en terug naar de faculteit, en dan opnieuw terug... Jullie deden het steeds met de glimlach,

waarvoor dank! Ann, bedankt voor je luisterend oor en het samen met Pui Yi en Margot steeds in orde brengen van mijn administratie en de leuke praatjes tijdens de koffiepauzes. Ik weet nu alles over Chinese draken die sla eten en fasciatherapie. Deze pauzes en labo-activiteiten werden ook steeds opgevrolijkt door Thomas, Erik, Hannes, Jackie, Ingvar, Michiel en Niels. Jullie wisten altijd interessante en vooral grappige onderwerpen aan te snijden. Hans, Wouter en ex-collega's Tom, Maja en Bruno, bij jullie kon ik elk moment langs voor raad en info. Elizabeth, ik ben enorm onder de indruk van je durf om naar Congo te reizen en Lidewei voor het trotseren van beren in de Oeral. Maurits, heerlijk dat je altijd de rustheid zelf uitstraalt. Ik verwacht nog veel baanbrekend werk van jou, of het nu gaat over de mangroves in Australië, de regenwouden van Brazilië of een problematiek in Vlaanderen. Bart, was jij er niet geweest om mijn drie thesisstudenten dit jaar te helpen begeleiden, dan had ik me nooit kunnen focussen op het schrijven van dit doctoraat. Ik wist dat ik op je kon rekenen. Ik apprecieer het enorm. Hopelijk neem je mijn passie voor de druivelaar over en kan je hierop verder werken. Het is een aanrader: een leuke wereld en geen congres gaat voorbij zonder wijnproeverij. Graag wil ik ook mijn enthousiaste thesisstudent Lies bedanken, het samen ontdekken van het XYL'ém toestel was... interessant. Ik ben blij dat ik het niet alleen moest ontrafelen. Ten slotte, mijn bureaugenoten Jochen, Jasper, Marjolein en Veerle (je kan die muur moeilijk een echte scheiding noemen eh!). Jullie waren er bij de leuke en minder leuke momenten telkens bij van op de eerste rij en hebben me altijd gesteund. We hadden vele wetenschappelijke en vooral ook niet-wetenschappelijke leuke babbels. Ik heb veel gelachen en me goed geamuseerd samen met jullie. Jullie zijn top collega's, ik had me geen betere bureaugenoten kunnen wensen.

Prof. Kris Villez, je introduceerde me niet alleen in de wereld van de principale componenten en functionele data analyse, maar liet me ook de VS en hun soms eigenaardige manier van redeneren ontdekken. Ik heb veel bijgeleerd tijdens mijn verblijf daar en kon er mijn eerste twee publicaties uit schrijven. Ik apprecieer dit enorm. Bedankt ook voor de uitstekende ontvangst in West-Lafayette en toffe koffiebreaaks.

De wijnbouwers en wijnmakers die ik in de afgelopen vier jaar heb ontmoet toonden stuk voor stuk veel passie voor hun vak en introduceerden me maar al te

graag in de wondere wereld van druiven en wijn. Vooral bedankt aan de lesgevers op Syntra, voor de goede introductie tot jullie bijzonder mooie stiel.

Daarnaast zijn er ook een aantal personen die ik wil bedanken omdat ze minstens even belangrijk zijn geweest voor mijn doctoraat door er altijd voor mij te zijn en te zorgen voor uitstekende ontspanning na het werk. Annelien, Lieve, Sara, Eline en the girls uit Latem: Nele, Elke, Charlotte, Julie. Bedankt voor ons groot avontuur naar China (maar ook de zee en de Ardennen waren ons niet te min), de heerlijke chocolade fondues, girls nights en avondjes op terras of café. Bart, jammer genoeg zal je het zelf nooit weten, maar je hebt me sterker gemaakt en tegenslagen in een ander perspectief leren plaatsen. Je loopt voor mij voor altijd voorop. Mijn mede milieu Bio-Ingieurs waaronder Cilia, Kim, Elena, de Ellens, Astrid en Willem, voor jullie vriendschap en deugddoende gesprekken. Ik ben blij dat we elkaar ook na onze studies nog vaak zien. Eef, Elena en Ellen wil ik nog speciaal bedanken omdat ik enorm heb genoten van onze wekelijkse lunches en de looptochtjes na het werk. Jullie begrijpen als geen ander wat doctoreren inhoudt.

Mijn twee schatten van ouders, bedankt voor het helpen opkweken van mijn druivelaars, de gelukkige en zorgeloze jeugd en de vele kansen die jullie mij gegeven hebben. En jullie onvoorwaardelijke steun, zelfs nu ik het huis uit ben (althans zo'n 6 dagen op 7). Mijn allerliefste broer Frederik en zus Elien, dat geldt ook voor jullie, het doet me veel deugd dat we zo goed overeenkomen. Ik wil ook mijn oma's en opa, meter, peter en anderen uit mijn familie, alsook de ouders van Cédric bedanken, omdat jullie altijd oprecht geïnteresseerd waren in mijn onderzoek en ook mijn doen en laten in het algemeen. Ten slotte, Cédric (lieve schat, snoek, (AB)Cé), je bent er al zoveel jaren voor mij geweest en ik ben er zeker van dat je dat altijd zal zijn. Je weet me altijd te doen lachen en op te vrolijken als ik een minder moment hebt en je bent mee uitbundig als ik gelukkig ben. Dank je wel hiervoor, je bent een schat!

November 2013

Annelies Baert

Contents

Dankwoord	i
Contents	v
Abbreviations and symbols	xi
Samenvatting	xv
Summary	xix
Chapter 1 Introduction	1
1.1 Global climate change	2
1.2 Belgium and the Netherlands: upcoming wine regions?	4
1.3 Thesis motivation and structure	5
Chapter 2 Water transport and its crucial role for grape and wine quality	9
2.1 Water transport in the soil-plant-atmosphere continuum	9
2.1.1 Basic principles of water transport	9
2.1.2 Hydraulic resistance	11
2.1.3 Cavitation	13
2.2 Influence of plant water status on grapevine development and productivity	16
2.3 Influence of plant water status on grape and wine composition	19
2.3.1 What defines grape and wine quality?	19
2.3.2 Growth phases of the grape	19
2.3.3 Grape and wine composition	23
2.4 Using plant measurements as indicators for plant water status	26
2.4.1 Stem diameter variations	27
2.4.2 Sap flow rate	27

2.4.3 Stem water potential	29
2.4.4 Combination of plant measurements	29
2.4.5 Vulnerability curve	30
2.5 Conclusions	33
Chapter 3 Introduction of two statistical techniques for automatic stress detection based on stem diameter variations	37
3.1 Introduction	38
3.2 Material and methods	42
3.2.1 Plant material and experimental set-up	42
3.2.2 Plant and microclimatic measurements	43
3.2.3 Unfold Principal Component Analysis	43
3.2.4 Functional Unfold Principal Component Analysis	48
3.3 Results	52
3.3.1 The UPCA model	52
3.3.2 Stress detection with UPCA	54
3.3.3 Functional data analysis	54
3.3.4 Stress detection with FUPCA	56
3.4 Discussion	58
3.4.1 UPCA and FUPCA to automatically detect plant stress	58
3.4.2 Comparison of UPCA and FUPCA	60
3.5 Conclusions	60
Chapter 4 Automatic drought stress detection in grapevines without using conventional threshold values	63
4.1 Introduction	64
4.2 Materials and methods	67
4.2.1 Plant material and experimental set-up	67

4.2.2 Microclimatic and plant physiological measurements	69
4.2.3 Unfold Principal Component Analysis	70
4.2.4 Functional Unfold Principal Component Analysis	72
4.3 Results	74
4.3.1 UPCA and FUPCA for drought stress detection	74
4.3.2 Selection of the calibration period	80
4.4 Discussion	81
4.4.1 Loadings of the principal components	81
4.4.2 UPCA and FUPCA for drought stress detection	81
4.4.3 Selection of the calibration period	85
4.5 Conclusions	86
Chapter 5 Development of a mechanistic water transport and storage model for grapevine	87
5.1 Introduction	88
5.2 Materials and methods	90
5.2.1 Experimental set-up	90
5.2.2 Microclimatic and soil measurements	90
5.2.3 Plant physiological measurements	91
5.2.4 Model description	91
5.3 Results	95
5.3.1 R^X exponentially increases with decreasing Ψ_{soil}	95
5.3.2 Drought stress simulated with constant or variable R^X	97
5.3.3 Vulnerability curve	98
5.3.4 Dynamics in the hydraulic resistances R^X and R^S during soil drying	99
5.4 Discussion	100
5.4.1 Plant drought response modelling requires variable hydraulic resistances	100

5.4.2 Advantage of an integrated soil-to-stem hydraulic resistance	101
5.4.3 Modelled soil-stem integrated vulnerability curve	102
5.4.4 Dynamics in axial and radial hydraulic resistances	103
5.5 Conclusions	104
Chapter 6 Real-time water status monitoring	107
6.1 Introduction	108
6.2 Material and methods	110
6.2.1 Plant material and set-up	110
6.2.2 Microclimatic, soil and plant measurements	111
6.2.3 Model description	112
6.2.4 Model calibration and simulation	112
6.2.5 Size of the moving window	114
6.3 Results and discussion	117
6.3.1 Daily model recalibration	117
6.3.2 Real-time simulation of the plant behaviour and water status	118
6.3.3 Size of the moving window	122
6.3.4 Step toward accurate irrigation scheduling	123
6.4 Conclusions	124
Chapter 7 Dynamic thresholds for stem water potential	125
7.1 Introduction	126
7.2 Material and methods	127
7.2.1 Plant material and experimental set-up	127
7.2.2 Water status monitoring	128
7.3 Results and discussion	132
7.3.1 Calculation of stem water potential thresholds and uncertainty bands	132
7.3.2 Dynamic thresholds for water status monitoring	132

7.3.3 Performance of generic thresholds for drought stress detection	136
7.3.4 Accuracy of automatic water status monitoring	137
7.3.5 Comparison between VPD and λE_p -based thresholds	139
7.4 Conclusions	140
Chapter 8 General conclusions and future perspectives	141
8.1 General conclusions	141
8.1.1 Data-driven modelling	142
8.1.2 Mechanistic modelling	146
8.1.3 Model calibration	148
8.1.4 Threshold for drought stress detection	149
8.1.5 Distinguishing between different levels of drought stress	150
8.1.6 Data interpretation and practical application	151
8.2 Future research	153
8.2.1 From greenhouse experiments to practice	153
8.2.2 Virtual fruit model	155
Appendix	157
References	167
Curriculum vitae	189

Abbreviations and symbols

Abbreviations

C1, C2	Control treatment 1, 2
D	Stem diameter variations
DOY	Day of the year
FPE	Final prediction error
FUPCA	Functional Unfold Principal Component Analysis
IID	Independent and identically distributed
LVDT	Linear Variable Displacement Transducer
MDS	Maximum daily shrinkage
MDS _i	Actual maximum daily shrinkage
MDS _{ref}	Maximum daily shrinkage of a reference (full-irrigated) group of plants
PAR	Photosynthetic active radiation
PCA	Principal Component Analysis
PC(s)	Principal component(s)
PLC	Percentage loss of hydraulic conductivity
R1 to R5	Repetition 1 to 5
RCV	Relative cumulative variance
RH	Relative humidity
RV	Relative variance
SF	Sap flow rate
SF _i	Actual sap flow rate
SF _{ref}	Sap flow rate of a reference (full-irrigated) group of plants
SSE	Sum of squared errors
UPCA	Unfold Principal Component Analysis
V ₁ , V ₂	Xylem vessel 1, 2
VD	Verzadigingsdeficit
VPD	Vapour pressure deficit

Latin symbols

a	Allometric parameter
b	Allometric parameter
c	Number of principal components
C	Number of coefficients
CO ₂	Carbon dioxide
C _{stem}	Capacitance of the water storage tissues in the stem compartment
D	Stem diameter variations (outer stem diameter)
D _i	Inner stem diameter
d ^s	Thickness of the storage compartment
E	Residuals
e ₁ , e ₂	Parameters for calculation of a dynamic stem water potential threshold based on potential evapotranspiration
F	Mass flow rate
f _{stem}	Water flow between xylem and storage compartment
F _{stem}	Water flow between the roots and the stem
H ₂ O	Water
i	Hour
I _{cal}	Days for calibration
k	Number of knots
K	Hydraulic conductance/conductivity
K _{max}	Maximum hydraulic conductance/conductivity
K ^X	Integrated hydraulic conductance in the soil-to-stem segment
l	Length of the stem segment
M _R	Matrix of residuals
n, n-1	Order, degree of a function
N	Number of data points or measurements
O ₂	Oxygen
p	Number of estimated parameters
P	Hydrostatic pressure
P ₅₀	Stem water potential at which 50% of hydraulic conductance is lost

P (JK x c)	Loading matrix P with dimensions $IJ \times c$, in which I stands for the day, J the time within the day and c the loading vector
R	Hydraulic resistance
r_1, r_2	Proportionality parameters for calculation of the integrated soil-to-stem hydraulic resistance
R^2	Coefficient of determination
r_a	Aerodynamic resistance
R_N	Net radiation
R_{leaves}	Hydraulic resistance of the leaves
R_{roots}	Hydraulic resistance of the roots
R^S	Radial hydraulic resistance between the xylem and elastic living tissues
R_{soil}	Hydraulic resistance of the soil
R_{stem}	Hydraulic resistance of the stem
R^X	Integrated hydraulic resistance in the soil-to-stem segment
s	Slope of the curve relating saturation vapour pressure with temperature
S	Soil heat flux
S_1, S_2	Proportionality parameters for calculation of the radial hydraulic resistance between xylem and elastic living tissues
T_{air}	Air temperature
T (I x c)	Score matrix T with I observations and c principal components
v	Wind speed
v_1, v_2	Parameters for calculation of a dynamic stem water potential threshold based on vapour pressure deficit
V^S	Volume of the storage compartment
W_{stem}^{max}	Maximum water content of the storage compartment
W_{stem}	Water content of the storage compartment
X (I x J x K)	Three-dimensional measurement matrix X with dimensions $I \times J \times K$, in which I stands for the day, J the time within the day and K the variable

Greek symbols

γ	Psychrometric constant
ΔP	Pressure gradient
$\Delta \Psi$	Water potential difference
ε_0	Proportionality constant for calculation of the bulk elastic modulus
λ	Latent heat of evaporation
λ_c	c^{th} largest eigenvalue
λE_p	Potential evapotranspiration
ρ_w	Density of water
ρ_v, ρ_v^0	Actual vapour concentration, saturated vapour concentration
Γ	Critical threshold at which cell wall-yielding (growth) occurs
ϕ	Cell wall extensibility
Ψ	Water potential
Ψ_{50}	Stem water potential at which 50% of hydraulic conductance is lost
Ψ_{air}	Air water potential
Ψ_g	Gravitational water potential
Ψ_{leaves}	Leaves water potential
Ψ_m	Matric water potential
Ψ_p	Pressure water potential
Ψ_p^s	Turgor pressure potential of the storage compartment
Ψ_{root}	Root water potential
Ψ_{soil}	Soil water potential
Ψ_{stem}	Stem water potential
$\Psi_{\text{stem},50}$	Stem water potential at which 50% of hydraulic conductance is lost
$\Psi_{\text{stem},90}$	Stem water potential at which 90% of hydraulic conductance is lost
Ψ_{stem}^s	Water potential of storage compartment
Ψ_{π}^s	Osmotic potential of the storage compartment
Ψ_{π}	Osmotic water potential
Ω	Decoupling coefficient

Samenvatting

Door de toenemende problematiek van waterbeschikbaarheid en globale klimaatsverandering stijgt de vraag naar efficiënte en precieze irrigatiecontrole, zelfs op plaatsen waar tot voorheen nooit werd geïrrigeerd. De aangewezen hoeveelheid water tijdens irrigatie wordt bij druivelaars (*Vitis vinifera* L.) niet zozeer bepaald door hun absolute vraag naar water, maar is eerder een kwestie van optimale timing en hoeveelheid, alsook een goede opvolging van het behoud van de waterstatus van de druivelaar. Bepaalde gradaties van lichte droogte op specifieke momenten in het groeiseizoen spelen zelfs een sleutelrol voor de productie van kwaliteitsdruiven en resulterende wijnen. Zowel te sterke als geen droogtestress zijn echter niet gewenst, aangezien ze het potentieel van druiven en wijnen negatief beïnvloeden. Om dit cruciaal evenwicht te bereiken zijn nieuwe, innovatieve technologieën nodig die de plant waterstatus kunnen monitoren en die de meest geschikte irrigatiehoeveelheid kunnen opleggen. Internationaal is men ervan overtuigd dat zulke technologieën op plantmetingen moeten gebaseerd zijn, en niet alleen op bodem- of microklimaatmetingen, omdat enkel dan informatie bekomen wordt over de werkelijke waterstatus van de plant.

Het doel van deze thesis was het ontwikkelen en evalueren van een plantgebaseerde strategie voor het opvolgen van de waterstatus en stressdetectie bij druif, gebruikmakend van automatische plantmetingen en modellen. Zowel experimenten als modelgebaseerde studies werden uitgevoerd op druivelaars in pot die onderworpen werden aan condities gaande van volledig geïrrigeerd tot sterke droogte.

Twee plantgebaseerde benaderingen voor opvolging van de plant waterstatus werden getest en vergeleken. In een eerste benadering werd een accurate opvolging van de druivelaar waterstatus en snelle droogtedetectie (i.e. verscheidene dagen vóór duidelijke visuele symptomen verschenen) bereikt met twee datagedreven modellen: Unfold Principle Component Analysis (UPCA) en Functional Unfold Principle Component Analysis (FUPCA). Deze modellen werden

oorspronkelijk ontwikkeld voor statistische procesopvolging van multivariabele datasets waar accurate kennis over het proces ontbreekt of moeilijk te achterhalen is. In deze studie bestonden de multivariabele datasets uit metingen van het microklimaat en een plantmeting die optrad als indicator van plant waterstatus, ofwel sapstroom ofwel stamdiametervariaties. De modellen gebruikten een grote hoeveelheid data uit goed bewaterde condities om de onderliggende informatie en patronen van deze gemeten variabelen te extraheren. Hieruit werd een profiel op van normaal datagedrag voor druivelaars onder goed bewaterde condities opgesteld. De nieuwe data werden aan dit patroon van normale condities getoetst. De modellen detecteerden abnormaal gedrag wanneer nieuwe data afweek van het normaal patroon, wat in deze studie kon gerelateerd worden aan het afwijken van de waterstatus of droogtestress.

In tegenstelling tot de datagedreven benadering waar voorafgaande kennis over onderliggende plantmechanismen minder cruciaal was, werd in de tweede benadering gefocust op de ontwikkeling van een mechanistisch watertransport en opslag model voor druivelaar. Dit mechanistische model beschrijft het axiale en radiale watertransport en de dynamiek van de stamdiameter van druivelaars wiskundig. De basisprincipes kwamen voort uit een bestaand watertransport en opslag model voor bomen dat accurate simulaties van onder andere stamwaterpotentialiaal (Ψ_{stem}), één van de beste indicatoren voor plant waterstatus, toeliet onder goed bewaterde condities. In deze doctoraatsstudie werden de constante hydraulische plantweerstand in het model vervangen door vergelijkingen om betere droogterespons simulaties te verkrijgen. Zowel de geïntegreerde hydraulische weerstand die water ervaart tijdens opwaarts watertransport doorheen het bodem-tot-stam segment (R^X), als de hydraulische weerstand tijdens radiaal watertransport tussen xyleemvaten en elastische levende weefsels (R^S) bleken afhankelijk van de bodemwaterpotentialiaal. Om deze ingebouwde mechanismen te verifiëren werden gemodelleerde waarden vergeleken met gemeten data.

Het mechanistisch model bewees zijn toepasbaarheid voor twee aspecten. Doordat het model nieuwe inzichten onthulde droeg het ten eerste bij tot het doorgronden van het functioneren van druivelaars tijdens droogte. In de meeste andere plantmodellen worden R^X and R^S als constant beschouwd, nochtans

demonstreerde het verbeterde model dat zowel R^X als R^S dagelijkse fluctuaties vertoonden en, bovenop deze fluctuaties, exponentieel stegen onder toenemende droogte. Bovendien werd aangetoond dat de gemiddelde turgordruk in de elastische opslagweefsels snel afnam tijdens droogte. Ten slotte kon een *in situ* bodem-tot-stam vatbaarheidcurve voor droogte (zogenaamde vulnerability curve) gegenereerd worden die de hydraulische geleidbaarheid in bodem en plant integreert ($K^X = 1/R^X$). Een dergelijke vatbaarheidcurve voor droogte geeft het verlies aan K^X weer in functie van afnemende Ψ_{stem} en wordt in de literatuur vaak toegepast om te bepalen hoe kwetsbaar soorten zijn voor droogte. Ten tweede werd het mechanistisch model uitgewerkt als een tool om de real time druivelaar waterstatus op te volgen. Met uitzondering van de meest extreme condities die niet geschikt zijn voor druif- en wijnkwaliteit en dus te vermijden zijn in de praktijk, kon het model Ψ_{stem} goed simuleren en behield het een strenge supervisie over druivelaar waterstatus. Ψ_{stem} kon immers continu worden getoetst aan te verwachten gedrag gedefinieerd voor goed bewaterde condities. Ψ_{stem} simulaties beschreven de werkelijke waterstatus van de druivelaar en werden vergeleken met een dynamische grenswaarde. Eens een druivelaar deze grenswaarde overschreed werd droogtestress verondersteld. De range waarin Ψ_{stem} verwacht werd onder goed bewaterde condities werd in deze studie gedefinieerd op basis van onzekerheidsbanden op een geschatte dynamische grenswaarde. Twee verschillende dynamische Ψ_{stem} grenswaarden werden getest. Een eerste benadering gebruikte verzadigingsdeficit (VD) als input. Een tweede, meer uitgebreide aanpak, gebruikte potentiële evapotranspiratie (λE_p). Hierbij werd zowel VD als straling beschouwd, beide gekend als drijvende krachten voor transpiratie bij planten. Zowel het gebruik van een VD- of een λE_p -gebaseerde dynamische grenswaarde en onzekerheidsband resulteerde in een snelle droogtedetectie en strenge supervisie over de plant waterstatus tijdens droogte experimenten op druivelaars.

Uit dit onderzoek kan ten slotte gesteld worden dat zowel de datagedreven als de mechanistische modelbenadering veelbelovende plantgebaseerde strategieën zijn voor opvolging van de waterstatus van druivelaars. Er blijven echter nog enkele uitdagingen over vooraleer deze strategieën in de praktijk kunnen worden toegepast om druif- en wijnkwaliteit te optimaliseren. Aangezien alle experimenten

in deze studie werden uitgevoerd op druivelaars in pot, zouden toekomstige experimenten de prestatie en toepasbaarheid van de modellen moeten testen in veldomstandigheden. Om in de toekomst druif- en wijnkwaliteit te kunnen sturen zou bovendien de exacte impact van verschillende niveaus van droogtestress op specifieke momenten tijdens het droogteseizoen op de druiven moeten worden nagegaan.

Summary

Water shortage has become a major problem, leading to a growing interest for efficient and precise irrigation scheduling even in areas that were completely rain-fed so far. Appropriate irrigation for grapevines (*Vitis vinifera* L.) is not exclusively a story of fulfilling water demand, but rather of defining the optimum level and timing and having a good knowledge of the grapevine water status. Specific levels of soil water deficit at specific times in the growing season are known to play a key role in the production of high quality grapes and resulting wines, but both severe and no drought stress are not desired as they negatively influence the grape's and wine's potential. Innovative techniques for monitoring the plant water status and for applying an adequate irrigation scheduling are required to achieve this crucial water balance for a grapevine. It is internationally recognised that such tools should rely on plant measurements, as they provide information on the actual plant water status, rather than be based on soil or microclimatic measurements.

The aim of this thesis was to develop and evaluate a strategy for water status monitoring and stress detection in grapevine based on automated plant measurements. To this end, both experimental and modelling work was carried out on potted grapevines that were subjected to conditions ranging from fully irrigated to severe drought.

Two different plant-based monitoring approaches were tested and compared. In a first approach, an accurate monitoring of the grapevine water status and a fast detection of drought stress (i.e. several days before the first clear visible symptoms appeared) were accomplished using two data-driven models: Unfold Principle Component Analysis (UPCA) and Functional Unfold Principle Component Analysis (FUPCA). These models were originally developed for statistical process monitoring of multivariate data sets where accurate mechanistic knowledge is lacking or difficult to achieve. In this study, the multivariate data set consisted of measured microclimatic variables and a plant measurement that served as indicator for plant water status, either sap flow rate or stem diameter variations. Using a large amount of data from well-watered conditions, the models extracted

the information and patterns underlying these measured variables and made a profile of normal, expected data behaviour under sufficient water availability. Monitoring new data then implied checking these data against this pattern. When a discrepancy between new data and this normal pattern was observed, the models indicated abnormality, which was in this study related to a deviating water status or drought stress.

Unlike the data-driven approach in which a priori information on underlying plant mechanisms was not crucial, the second approach focused on developing a comprehensive mechanistic water transport and storage model for grapevine. This mechanistic model mathematically describes the axial and radial water transport and stem diameter dynamics of grapevine. The basic principles originated from an existing tree water transport and storage model, which enabled among others accurate simulations of the stem water potential (Ψ_{stem}) under well-watered conditions, which is one of the best indicators for plant water status. To obtain better drought response simulations with the model, the constant hydraulic plant resistances were replaced by equations in this PhD study. Both the integrated hydraulic resistance experienced during upward water transport through the soil-to-stem segment (R^X) and the hydraulic resistance encountered during radial water transport between xylem and elastic living tissues (R^S) were dependent on soil water potential. Modelled and measured data were compared to verify the implemented mechanisms.

The mechanistic model was applied twofold. First, the model contributed to our understanding of grapevine functioning during drought conditions, as it revealed new insights. Despite the generally assumed constant R^X and R^S behaviour in several other plant models, the improved model demonstrated that both R^X and R^S showed daily fluctuations and, superimposed on these fluctuations, exponentially increased when drought progressed. Furthermore, it was shown that mean turgor in the elastic storage tissues rapidly decreased with drought. Finally, an *in situ* soil-to-stem vulnerability curve that integrated the hydraulic conductance in soil and plant ($K^X = 1/R^X$) was generated using the model. Such a curve depicts the loss in K^X as a function of declining Ψ_{stem} and is often applied in the literature to assess vulnerability of species to drought. Second, the mechanistic model was elaborated as a tool to monitor grapevine water status in real-time. Except under most severe

drought stress conditions, which are not favourable for grape and wine quality and should be avoided in practice, the model simulated Ψ_{stem} well and kept a tight supervision over the grapevine water status, as Ψ_{stem} could be continuously compared against expected plant behaviour defined under well-watered conditions. Simulated Ψ_{stem} , representing the actual water status of the grapevine, were then compared with a dynamic threshold beyond which the grapevine is considered to experience drought stress. In this study, the uncertainty band on the dynamic threshold estimation was used to represent the range within which Ψ_{stem} was expected to occur under well-watered conditions. Two different dynamic Ψ_{stem} thresholds were tested: an approach using vapour pressure deficit (VPD) as input, and a more elaborate approach using potential evapotranspiration (λE_p). The latter includes VPD and radiation, both known as key driving variables for plant transpiration. The use of both the VPD- or the λE_p -based dynamic threshold and uncertainty band allowed a fast detection of drought stress and tight supervision over the plant water status during a drought experiment on grapevines.

To conclude, both the data-driven and the mechanistic modelling approach were judged promising as plant-based strategy for monitoring the grapevine water status. To apply these strategies for optimising grape and wine quality in practice, some challenges remain. As all experiments in this study were conducted on potted grapevines, future experiments should test the performance of the models under field conditions. In addition, the exact impact on the grape berries of different drought levels at specific times during the growing season should be investigated, in order to be able to steer grape and wine quality in the future.

Chapter 1

Introduction

Since ancient times, grapevines have intrigued people. Grapevines can grow in the most unlikely places and grapes were among the first fruits to be domesticated (Fig. 1.1). They are adaptable plants that can be shaped in different forms, while their fruits can be transformed into a wide spectrum of products with diverse appearances, tastes and aromas. Currently, grapevines are cultivated between latitudes 4° and 51° in the northern hemisphere and 6° and 45° in the southern hemisphere, covering six out of seven continents and very diverse climates



Fig. 1.1 Wall paintings from 1500 B.C. in Thebes, the ancient capital of Egypt, indicate that grape cultivation and wine making originated in ancient times (after <http://www.thecultureconcept.com/circle/wine-women-and-song-a-tripartite-motto-for-all-time>).

(Schultz and Stoll, 2010). Grapevines are one of the major economically important crop industries in the world and cover around 7.1 million ha, yielding almost 70 million tonnes of grapes. They are the number one produced fruit crop around the world on a basis of planted area, and the number three on a basis of produced tonnes (2011 statistics by the Food and Agriculture Organisation of the United Nations). More than 70% of the harvested grapes are used for wine production, 27% as table grapes and the remaining is consumed as raisins or applied for juice or brandy production (Keller, 2010b).

1.1 Global climate change

Contrary to many other agricultural crops, grapevines are often cultivated under suboptimal conditions, mainly water deficits, whether or not deliberately imposed to enhance grape quality. Water deficit is the prevailing climatic constraint in current wine producing areas. Even in moderate climates, grapevines are often prone to some levels of drought stress during certain periods of the growing season (Gaudillère et al., 2002; Schultz and Stoll, 2010). Grapevines are thus often subjected to drought. This may become even more common, and grape growing more challenging, because of global climate change (Schultz, 2000; Jones et al., 2005; Chaves et al., 2010; Keller, 2010a; Schultz and Stoll, 2010).

Due to global climate change, the mean air temperature is predicted to rise and precipitation patterns are expected to change. Not only the amount of precipitation (annual total) will shift, but also the distribution among the different seasons, which can cause an increased shortage of water (IPCC, 2007; 2013). In Europe, more extreme temperatures (2.2 up to 5.3°C annual mean warming by 2080-2099 compared to 1980-1999), a higher frequency of summer drought periods and a reduction in soil moisture are expected to occur (Christensen et al., 2007). Significant warming has in fact already been observed in viticultural regions in the last decades (1.26°C increase in the average growing season temperature in the world's high-quality wine regions from 1950 to 1999 (Jones et al., 2005)), with a trend toward a prolongation of the growing season and accelerated vegetative and reproductive growth (Schultz, 2000; Jones et al., 2005; Keller, 2010a; Schultz and Stoll, 2010). The resulting earlier flowering, veraison and harvest are critical

aspects, because they strongly influence the ability to ripen grapes to optimum levels of sugar, acid and flavour, necessary to produce balanced and superior wines (Jones et al., 2005). In particular the timing of veraison is important, as an earlier veraison implies that the crucial ripening period shifts toward the warmest part of the season (Keller, 2010a).

Changes in temperature and precipitation cause a gradual shift of the margins where cultivation of grapevines is (economically) suitable. Since the northern limit tends to shift northward, grapevine cultivation currently occurs in areas that were considered unfeasible so far. In addition, the most suitable grapevine cultivars and wine types for a certain area change (Schultz, 2000; Jones et al., 2005; Creasy and Creasy, 2009; Chaves et al., 2010; Keller, 2010a; Hannah et al., 2013a). The switch to new varieties, however, encounters a resistance from both a practical and traditional point of view. Indeed, switching to new varieties requires a great investment and challenging decisions, especially taking into consideration that (microclimatic) conditions at the time of vineyard plantation may be profoundly different from those in the further lifetime of the vineyard (typically > 30 years) (Creasy and Creasy, 2009; Keller, 2010a). Furthermore, wine has developed a strong and broad historical, social and cultural identity derived from its typical grape growing, production, weather and climate. The finest and typical wines are associated with geographically distinct viticulture regions entailing specific climatic conditions, as the latter has a pronounced influence on the quality of grapes and resulting high-quality wines (Jones et al., 2005). According to Jones et al. (2005), many of the European wine regions are presently at or near their ideal climate for their respective grape cultivars and wine styles, underlining their sensitivity to changes. Warming may exceed the optimum temperature for the currently grown varieties, making a balanced ripening of its grapes and the production of the current wine styles challenging, if not infeasible. Hannah et al. (2013a) predict a remarkable decline (25% to 73%) of suitable areas for viticulture in major wine producing regions by 2050, however, the impact will most likely be less dramatic when growers take adaptation measures (Hannah et al., 2013b; van Leeuwen et al., 2013).

1.2 Belgium and the Netherlands: upcoming wine regions?

While global climate change makes viticulture more challenging in some regions, other regions become more viable (e.g. the northern regions of Europe) (Schultz, 2000; Jones et al., 2005). Belgium and the Netherlands appear among the latter. Earlier spring warming and budburst in combination with a later autumn cooling are expected for currently cooler climates, which would result in a prolongation of the growing season and could improve grapevine cold hardiness and winter reserves (Keller, 2010a). In addition to the putatively improving climate, the emergence of new grape varieties play a role in the growing interest for viticulture in Belgium and nearby areas. German, Austrian, Swiss, Czech and Hungarian institutes developed varieties that are better adapted to cool climates, while more resistant to diseases like downy mildew (*Plasmopara viticola*, fungus that likes humid, rainy weather and cool to moderate temperatures). These new varieties came on the market in the early nineties (<http://www.wijngaardeniersgilde.nl>).

The growing interest in viticulture in Belgium and the Netherlands is manifested by the steadily increasing amount of wine domains and the increasing quality of the wines (VILT website, 8 October 2007; 5 October 2009; <http://www.brabantsewijnbouwers.nl>; <http://www.dewijnhoek.nl>; <http://www.neerlandswijnmakerij.nl>). Obtained golden and silver medals at international competitions are proof of this (Belgian wines website, 16 June 2013; <http://www.wijngaardeniersgilde.nl>), as well as various educations on wine growing and making set up the last years, both for amateurs as professionals (e.g. <http://www.syntra.be>; <http://www.wijnacademie.nl>; <http://www.wijninstituut.nl>). Recently, the Flemish Prime Minister Kris Peeters took several supportive measures for the wine growing and making sector and underlined that it is an upcoming and promising sector for Belgium (VILT website, 16 September 2012; 22 October 2012). Belgium has around 100 vineyards with a total area of 150 ha, among which 50 professionals in Flanders and 25 in the Walloon provinces (VILT website, 16 September 2012; <http://www.dewijnhoek.nl>). They are predominantly located in Hageland between Diest and Leuven (<http://www.dewijnhoek.nl>). Besides Hageland, the main Belgian viticultural areas are Haspengouw, Sambre-

et-Meuse and Heuvelland (<http://www.45nwf.be>). Since the first appellation was founded in 1997, the area of vineyards is increased fourfold, with a doubling over the last five years (Belgian wines website, 16 June 2013). Under the impulse of Unizo, the Union for Independent Entrepreneurs, and the increasing awareness of its necessity, eight major Belgian wine growers founded the non-profit organisation *vzw Belgische Wijnbouwers* in 2009, which now has 66 members (<http://www.belgischewijnbouwersvzw.be>). The organisation provides training, commercial cooperation, a link with the several governments and acts in the Belgian wine grower's interest. In 2011, Belgian wine growers produced 539.550 L wine (78% white, 18% red and 4% rosé wine), which is a 14.7% increase compared to 2010 (VILT website, 22 October 2012). The Netherlands, with approximately 200 vineyards (170 commercial ones) on approximately 200 ha, produced around 1.353.400 bottles of wine in 2011 (<http://www.dewijnhoek.nl>). Although Belgian and Dutch wines do not contribute on a quantity level, it is clear that these wines become much appreciated because of their quality.

1.3 Thesis motivation and structure

On a global scale, climate change has an important impact on grape and wine production. Water shortage has become a major problem, leading to a growing interest for sustainable irrigation scheduling even in areas that were completely rain-fed so far. Together with the growing necessity, however, also the costs of and competition for (irrigation) water are increasing (Schultz, 2000; Schultz and Stoll, 2010; Hannah et al., 2013a). Efficient and accurate irrigation scheduling is thus an important and crucial issue for the future. Besides fulfilling water demand, the growing interest in efficient and accurate irrigation scheduling originates from the increasing evidence and awareness that both grape quality and quantity are greatly affected by the grapevine's water availability. Specific levels of water deficits at specific times play a key role in the production of high-quality grapes and resulting wines. However, both severe or no drought stress are not desired as they negatively affect the grape's and wine's potential (van Leeuwen et al., 2009). Too much water will induce excessive vegetative growth and decrease grape quality. A severe scarcity of water, on the other hand, limits important processes

such as growth and photosynthesis (Möller et al., 2007; Creasy and Creasy, 2009). Appropriate irrigation scheduling can thus assist in improving grape and resulting wine quality, but the balance between sufficient water availability for plant functioning and certain periods of drought stress is crucial. Defining and imposing this appropriate water status balance at a certain time during the growing season is difficult without additional tools for monitoring the plant water status and the ability to apply such an adequate irrigation scheduling. This thesis therefore aimed at developing a plant-based strategy for water status monitoring and stress detection in grapevine.

The thesis is divided in eight chapters (Fig. 1.2). **Chapter 2** summarises the basic principles of water transport and discusses the influence of plant water status on grapevine, its grapes and the resulting wine. Since information on the plant water status is crucial for improving grape and wine quality, **Chapter 2** explains how plant measurements can be used as indicators for this purpose and how they can be applied for automatic water status monitoring and drought stress detection.

Subsequently, two different monitoring strategies were developed and evaluated: one strategy based on data-driven modelling and another one based on mechanistic modelling. **Chapter 3** introduces Unfold Principle Component Analysis (UPCA) and Functional Unfold Principal Component Analysis (FUPCA), both data-driven strategies, to detect drought stress automatically in an early stage based on measurements of the stem diameter. **Chapter 4** elaborates on UPCA and FUPCA, explores drought stress detection based on measurements of sap flow rate and discusses the potential of UPCA and FUPCA to circumvent conventional threshold values.

Because data-driven models are less suitable to infer underlying mechanisms, crucial for understanding plant responses, **Chapter 5** presents the development of a mechanistic water transport and storage model. An existing tree water transport and storage model was adapted for monitoring the plant water status in grapevines and required changes to perform well under dry conditions. This adapted model was applied to describe plant responses during drought. **Chapter 6** focuses on the applicability of the mechanistic water transport and storage model in practice and tests its contribution to obtaining information on plant responses in real-time. Finally, to apply plant measurements as automatic indicators for the

plant water status, thresholds beyond which the plant starts sensing a certain level of drought stress are required. Such a threshold should not be defined as a fixed constant value, as it is not only influenced by soil water availability but also by microclimatic conditions. Although several approaches have been proposed to determine dynamic thresholds, the step toward a more practical, high time-resolution dynamic threshold, especially for grapevine stem water potential, is still lacking. **Chapter 7** therefore gives a detailed description of calculating and applying dynamic thresholds for the water status.

The last chapter, **Chapter 8**, compares the data-driven strategy with the mechanistic one, and links the results of **Chapters 3 to 7**. General conclusions are drawn concerning the applicability of mathematic models as automatic systems for water status monitoring and drought stress detection. Finally, perspectives for ongoing and future research are formulated.

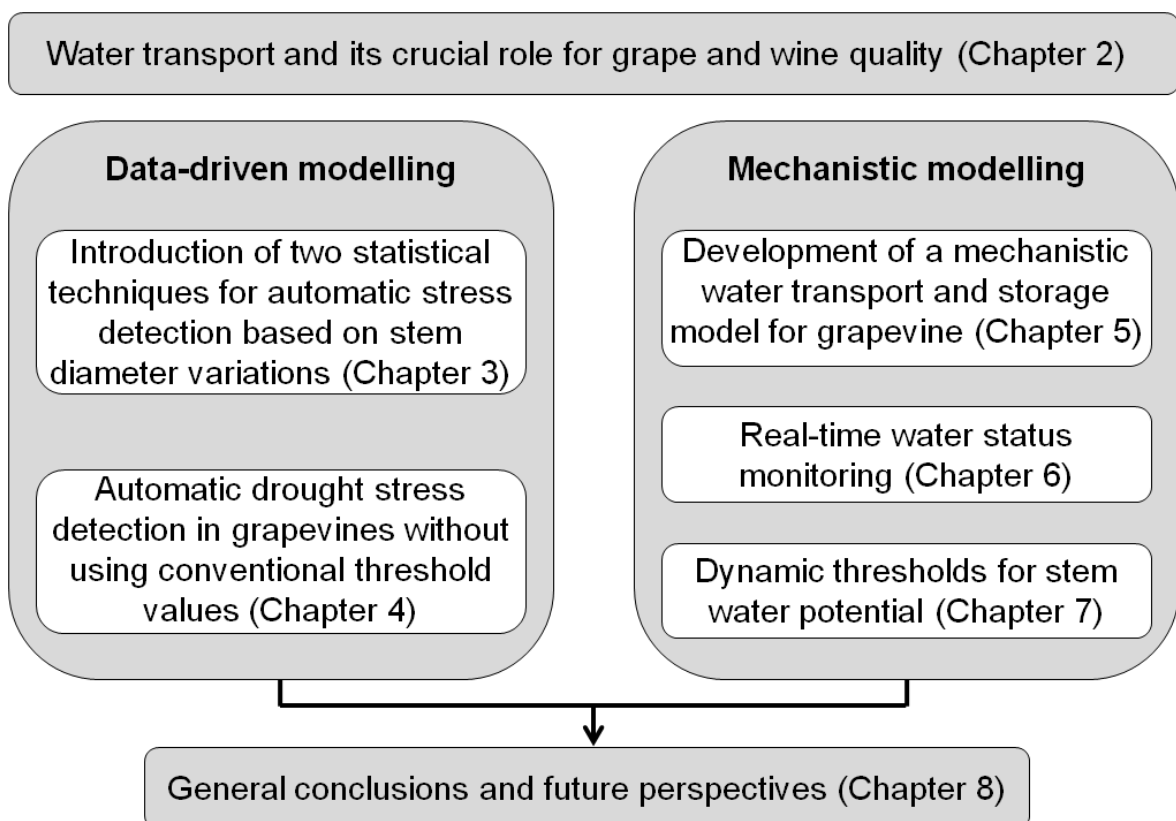


Fig. 1.2 Thesis structure

Chapter 2

Water transport and its crucial role for grape and wine quality

2.1 Water transport in the soil-plant-atmosphere continuum

2.1.1 Basic principles of water transport

As all plants, grapevines can exert energy from the sun to fix atmospheric carbon dioxide (CO₂). This photosynthesis process mainly occurs in the leaves (called sources). The captured energy is stored in the plant as photosynthetic assimilates, which are transported through the phloem (Fig. 2.1) toward energy demanding organs (called sinks). There it is used for maintenance and synthetic process (Jones, 1992). While the stomata (micro-pores imbedded in the lower epidermis of

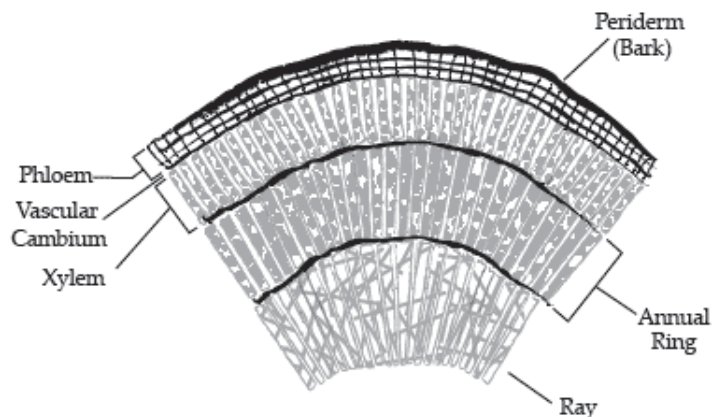


Fig. 2.1 Cross section of a three-year-old grapevine. Phloem for sugar transport from the leaves (called sources) to energy demanding organs (called sinks) and xylem for upward water transport from the roots are shown (after <http://rieslingrules.com>).

the leaves) are open during the day to capture CO_2 , water escapes to the atmosphere. This process, called transpiration, is the driving force for water transport in the plant (Fig. 2.2).

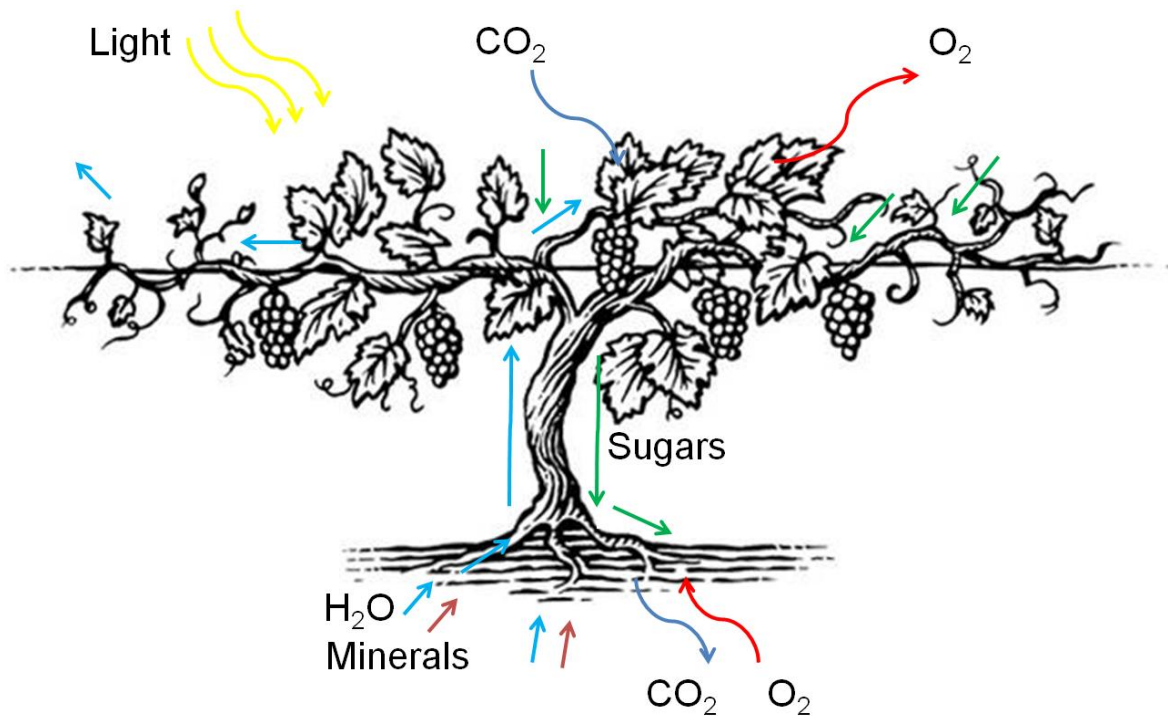


Fig. 2.2 Schematic overview of sugar and water transport in a grapevine. During photosynthesis, light and carbon dioxide (CO_2) are converted into oxygen (O_2) and sugars, which are transported from the leaves toward energy demanding organs through the phloem. While the stomata are open for photosynthesis, water vapour (H_2O) is lost to the atmosphere. This transpiration process induces an upward water flow, whereby water and minerals are absorbed by the roots and transported upward through the xylem (adapted from <http://www.stevennoble.com>).

Water transport in plants mainly occurs in the xylem (Fig. 2.1). Xylem in grapevines consists of dead conducting vessels and transports water, minerals and other substances (e.g. amino acids) from the roots to all plant organs. This upward water stream, also called sap flow, can be explained by the cohesion tension theory, which is introduced by Dixon and Joly (1895) and is still generally accepted as mechanism for describing water movement in plants. The cohesion tension theory states that water in the xylem vessels is under tension as a result of water loss in the leaves during transpiration. This tension overcomes the downward gravitational force and pulls water up by a combination of two forces: cohesion and adhesion. Water molecules are linked together by hydrogen bonds

that provide a strong intermolecular attraction. This cohesion force results in strongly connected water strings going from soil particles around the roots up to the cell walls where transpiration occurs. Water in plants thus forms one continuum, also referred to as the soil-plant-atmosphere continuum. Adhesion, on the other hand, exerts a force between the water continuum and the surrounding cell walls of the water conducting vessels and allows the water to rise upward (Cruiziat and Tyree, 1990).

Water transport and plant water status are often expressed in terms of Gibbs free energy by using the term water potential (Ψ), which can be seen as a measure of water demand. The reference state ($\Psi = 0$) is freely available water, while Ψ decreases to negative values when water demand is higher. Ψ is composed of four major components, resulting from osmotic (Ψ_{π} [MPa]), pressure (Ψ_p [MPa]), matric (Ψ_m [MPa]) and gravitational (Ψ_g [MPa]) forces:

$$\Psi = \Psi_{\pi} + \Psi_p + \Psi_m + \Psi_g = \Psi_{\pi} + P + \Psi_g \quad (2.1)$$

Since it is difficult to distinguish between pressure in the xylem vessels (Ψ_p) or in the cell walls (capillary forces or Ψ_m), Ψ_p and Ψ_m are generally considered together as the hydrostatic pressure (P). Turgor pressure is expressed as a positive P , while tension is expressed as a negative P . Differences in potential energy caused by a difference in height are represented by Ψ_g , but are often neglected when describing (small) plant systems. Finally, Ψ_{π} represents the attraction of water by dissolved solutes and is always negative. As xylem sap has only few osmotic components, Ψ_{π} can be omitted as well. It is thus acceptable to consider only hydrostatic pressure potentials to describe water transport in the xylem. Water moves passively (spontaneously) from higher Ψ to lower (more negative) Ψ , and is thus driven by water potential gradients (Fig. 2.3) (Jones, 1992; Williams, 2000; Jones, 2007; Keller, 2010b).

2.1.2 Hydraulic resistance

Water transport through the soil-plant-atmosphere continuum can be explained in analogy with electrical circuits, as introduced by van den Honert (1948). According to this theory, water flowing through the soil-plant-atmosphere continuum encounters a hydraulic resistance in each compartment: soil, roots, stem and leaves, such as electrical currents encounter electrical resistances. Similar to

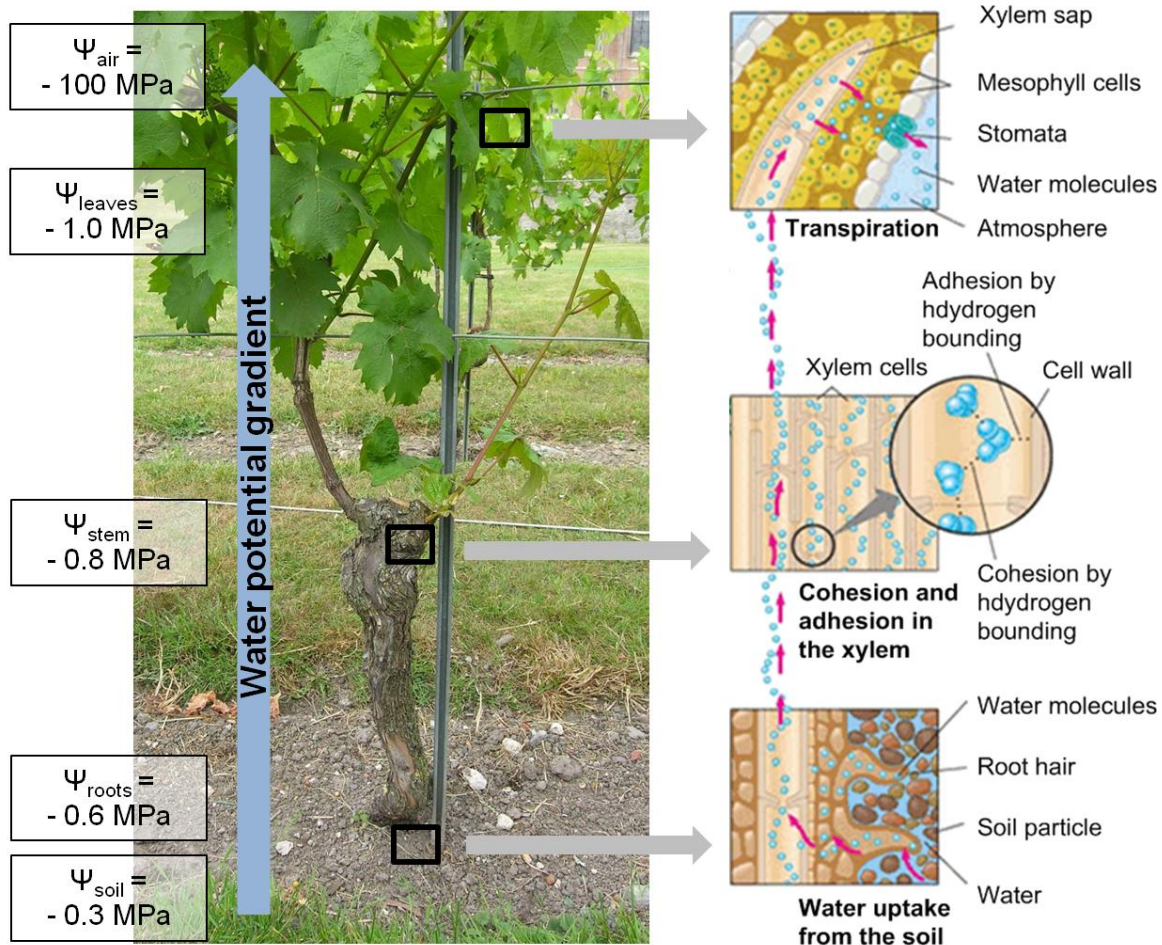


Fig. 2.3 Schematic overview of the water transport pathway through the soil-plant-atmosphere continuum and principle of the cohesion tension theory. Leaf transpiration creates a water potential gradient between the soil and the atmosphere. Typical values for air, leaves, stem, roots and soil water potential are shown (Ψ_{air} , Ψ_{leaves} , Ψ_{stem} , Ψ_{roots} and Ψ_{soil}). As water flows from a region with higher water potential to a region with lower water potential, water is pulled up through the xylem by a combination of adhesion and cohesion forces (adapted from Campbell and Reece (2008)).

electrical currents that are driven by potential differences, water transport is driven by water potential gradients (Fig. 2.4), as also stated by the cohesion tension theory. The water potential is higher near the roots and decreases (becomes more negative) in the direction of the leaves, creating a water potential gradient. This gradient results in water uptake near the roots and upward water transport toward the leaves (Fig. 2.3 and 2.4). Introducing the electrical analogy allows quantifying steady-state water flow (SF [$\text{g}\cdot\text{h}^{-1}$]) by applying Ohm's law:

$$\text{SF} = \frac{\Delta\Psi}{R} = \Delta\Psi K \quad (2.2)$$

with R the hydraulic resistance [$\text{MPa}\cdot\text{h}\cdot\text{g}^{-1}$], $\Delta\Psi$ the water potential difference [MPa] and K the often used reciprocal of R , i.e. hydraulic conductance [$\text{g}\cdot\text{MPa}^{-1}\cdot\text{h}^{-1}$]. Note that Eq. 2.2 only applies for steady-state flows and therefore a simplification of actual plant water flow, which is dynamic. Internal water storage or capacitive aspects are not considered, although they play an important role. Internal water storage pools contribute to the transpiration stream to compensate for the time lag of several minutes to hours that has been observed between transpiration (water loss through the leaves) and water uptake by the roots (Tyree, 1988; Meinzer et al., 2001; Steppe et al., 2006).

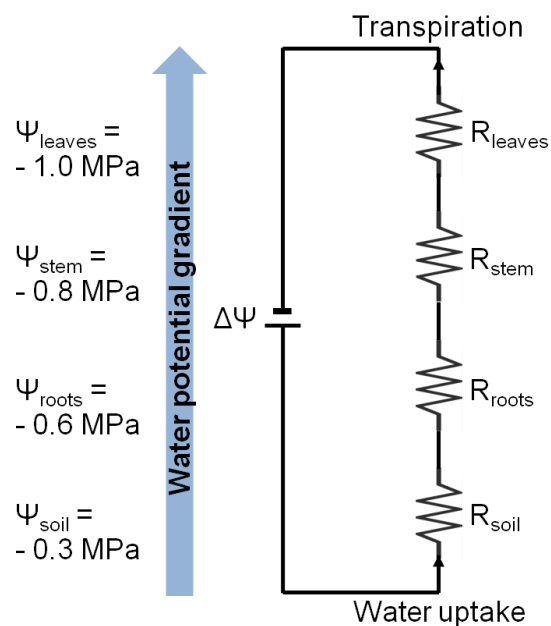


Fig. 2.4 Illustration of water transport through the soil-plant-atmosphere continuum as a result of decreasing water potentials (Ψ) (left) and its electrical analogy (right). Water transport is driven by water potential differences ($\Delta\Psi$) and encounters a specific hydraulic resistance (R) in each compartment (e.g. soil, roots, stem and leaves).

2.1.3 Cavitation

The xylem is built out of rigid vessels, necessary to avoid collapse under the continuous prevailing tension. Since water under such tensions is in a physically metastable condition, the presence of any air bubble may be sufficient to break the cohesion between the water molecules. The resulting breakage of the water continuum is called cavitation. During this process, the liquid water at negative pressure in the vessel is replaced by air (Fig. 2.5), this vessel loses its hydraulic function and the overall hydraulic resistance in the xylem increases. Cavitation

especially occurs when plants experience drought stress because the water potential strongly decreases during drought conditions and may surpass a critical threshold value. When this critical water potential threshold is surpassed, air bubbles are sucked into the xylem vessel and interrupt the water column (explained in Fig. 2.6) (Sperry and Tyree, 1988; Cruziat and Tyree, 1990; Tyree and Zimmermann, 2002; Hölttä et al., 2009; Lovisolo et al., 2010). Although more pronounced during drought, cavitation, as well as refilling of cavitated vessels, are common processes in many plant species (McCully et al., 1998; McCully, 1999; Bucci et al., 2003), including grapevines (Lovisolo et al., 2008; Brodersen et al., 2010; Zufferey et al., 2011; Schenk et al., 2013). Recent findings indicate that refilling can even occur when nearby vessels are still under considerable negative pressures (Meinzer et al., 2013; Schenk et al., 2013). As a consequence, hydraulic resistance (section 2.1.2) depends on the balance between cavitation formation and refilling and can vary throughout the day (Meinzer et al., 2013). Allowing some level of cavitation may actually benefit the plant, because the water pressure of the surrounding vessels increases when liquid water is released to the transpiration stream during cavitation, positively affecting the plant water status in the short-term. Cavitation thus entails a capacitive effect (Meinzer et al., 2001; Tyree and Zimmermann, 2002; Hölttä et al., 2009). Furthermore, this effect may delay closure of the stomata, allowing the plant to gain more carbon (Hölttä et al., 2009). Wheeler et al. (2013) however question the above findings and attribute observed diurnal variation in level of cavitation to artefacts of the methods used to quantify this cavitation, indicating that further research is still needed on this topic.

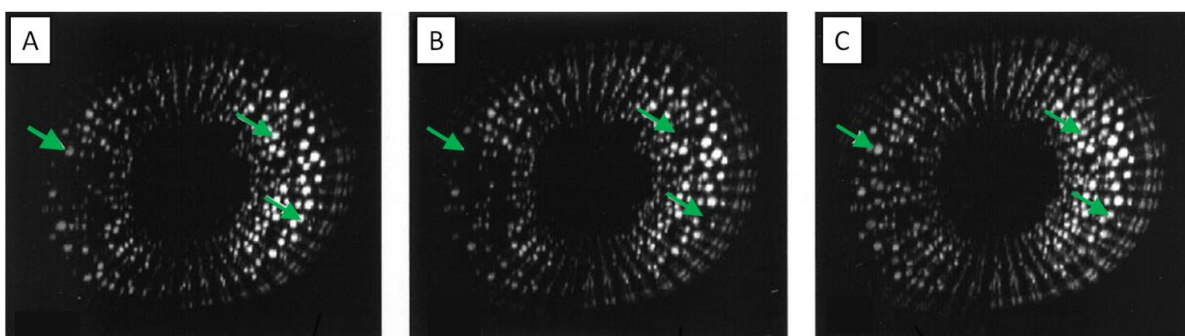


Fig. 2.5 Cross section of a grapevine stem obtained by magnetic resonance imaging: green arrows indicate vessels that were initially filled with water (A), then cavitated under declining water potential, thus filled with gas and not visible (B), and finally refilled after water supply was resumed (C) (after Holbrook et al. (2001)).

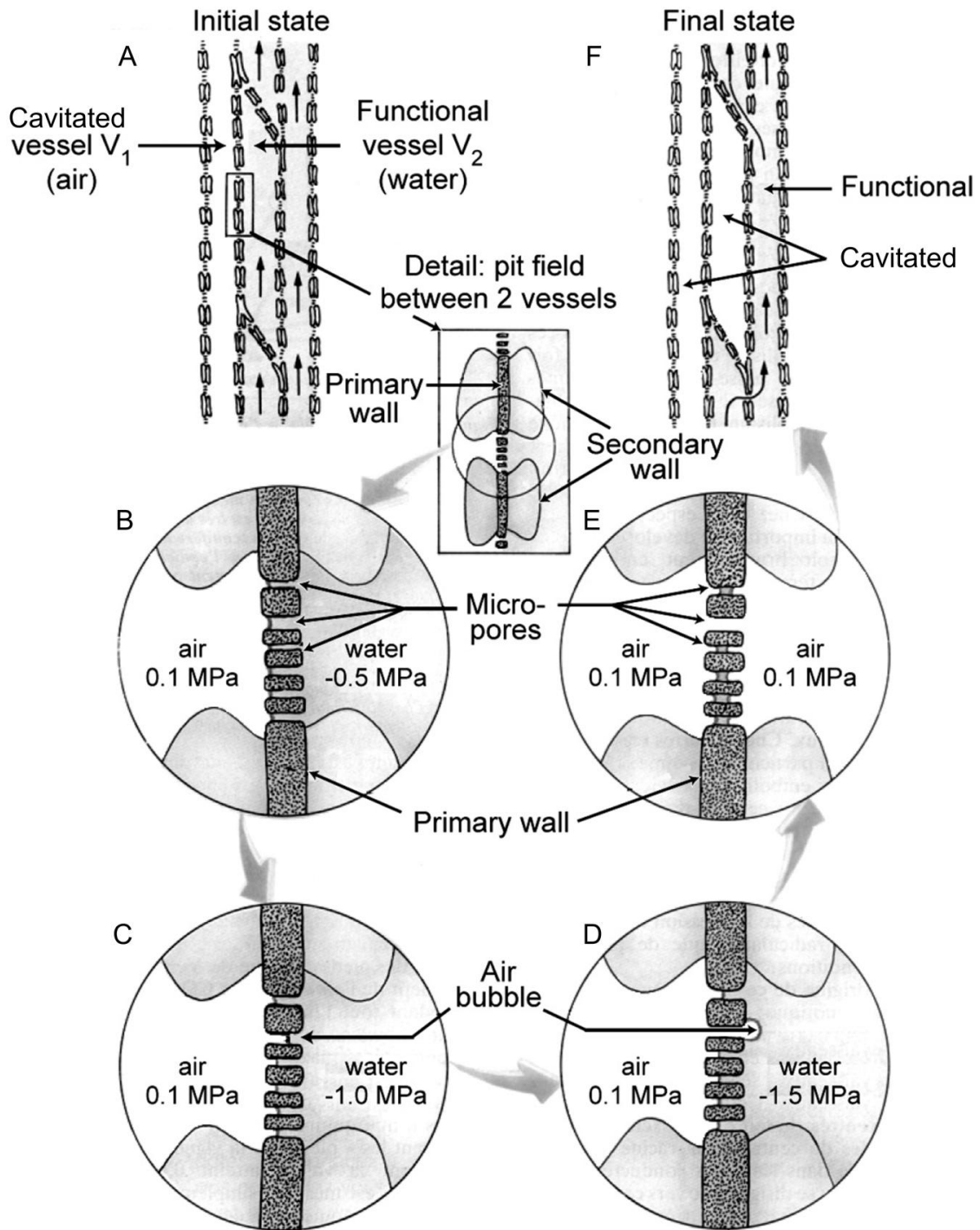


Fig. 2.6 Schematic overview of drought-induced cavitation according to the air-seeding hypothesis. Initially, vessel V_1 is cavitated (filled with air) while the adjacent vessel V_2 is still functional (filled with water) (A). Air-water menisci are created at the pit membrane pores and can stand medium tensions (B). Due to transpiration or dehydration, the pressure difference between V_1 and V_2 builds up and gradually pulls an air bubble through the largest pore, as large pores are most sensitive to high tensions (C). When the critical threshold for the pressure difference is surpassed, the air bubble is pulled into vessel V_2 (D). The gas bubble expands and fills V_2 entirely (E), resulting in a cavitated vessel that is no longer functional (F) (adapted from Cruziat and Tyree (1990)).

2.2 Influence of plant water status on grapevine development and productivity

Growth, development and productivity of grapevines are highly influenced by soil water availability. Excessive water may lead to excessive vegetative and/or reproductive growth (Fig. 2.7), which are both undesired for several reasons. Excessive reproductive growth or yield indicates an imbalance between fruit development and vegetative growth. If grapevines invest too much energy in fruit development, it may be detrimental for their ripening, the shoot and leaves growth, as well as for the fruit development of the next season. Indeed, an imbalance leads to inappropriate partitioning of assimilates between canopy and fruit production. Furthermore, the rate of fruit maturation is influenced by crop level: larger crops require more time to ripen their grapes compared to smaller crops. Finally, a high yield delays the ripening of branches and shoots and delays sugar accumulation, thus depleting the reserves for the consecutive winter (Smart et al., 1990; Dokoozlian, 2000; Creasy and Creasy, 2009; Keller, 2010a; b).

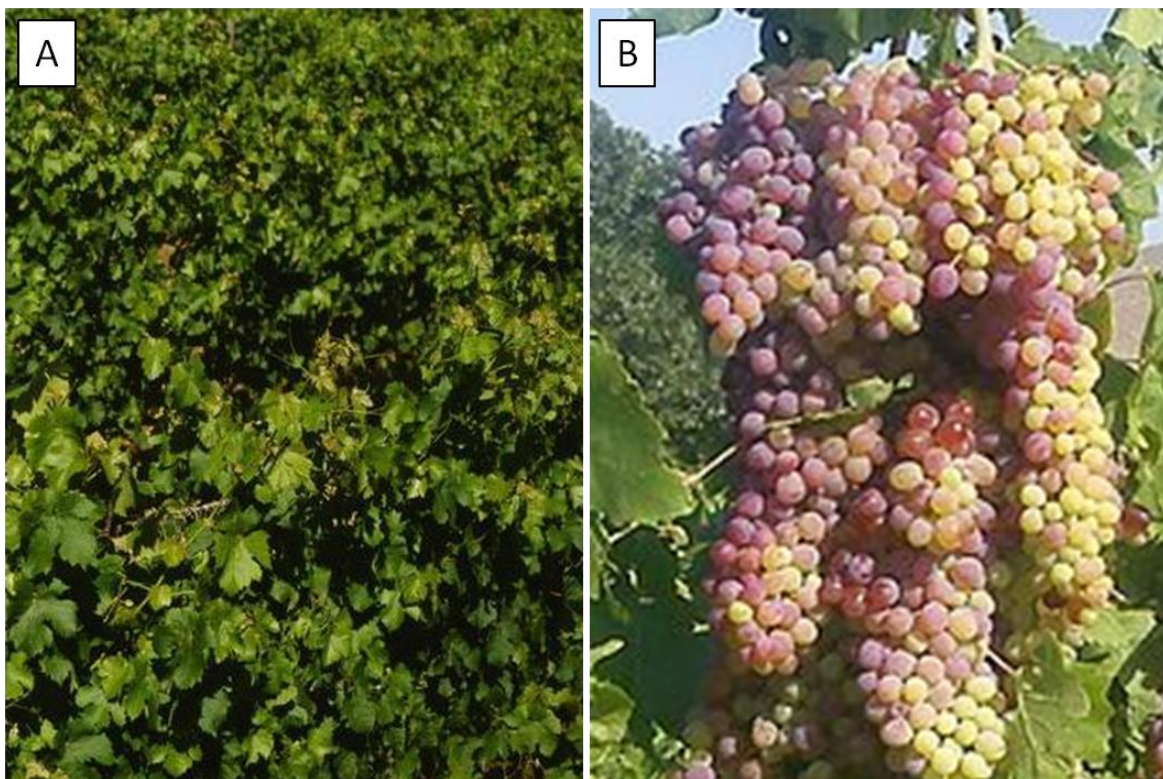


Fig. 2.7 Example of excessive vegetative (A) and reproductive (B) growth in grapevines (adapted from <http://en.wikipedia.org/wiki/Grape>; <http://homeguides.sfgate.com/prune-grape-vine-buds-50029.html>).

Excessive vegetative growth, on the other hand, may compete with flower formation for sugars, nutrients and water. In a later stage, it competes with the grapes and may jeopardise fruit quality (Smart et al., 1990; Creasy and Creasy, 2009; Keller, 2010a; b). A large plant growth alters the microclimate and increases the indirect light within the canopy. Indirect light has a different light quality and quantity as direct sun light, resulting in a significant physiological effect on leaves as well as grapes. Grape temperature is close to ambient air temperature in shaded berries, while up to 13°C (or even 17°C) elevated temperature has been observed in sun exposed grapes, e.g. in semi-arid climates (Smart and Sinclair, 1976; Spayd et al., 2002; Tarara et al., 2008; Keller, 2010a). Shading can lead to diminished fruit set, yield, berry size, delayed ripening and decreased and heterogeneous grape quality (Smart et al., 1990; Dokoozlian, 2000; Creasy and Creasy, 2009). Note that also excessive crop load, thus the grapes itself, can cause shadow within the canopy. An altered microclimate (not only light conditions and temperature but also humidity and wind speed) may change grape composition and may enhance the risk for diseases (Smart et al., 1990), although it is often unclear whether the adverse effects of inadequate sun exposure arise from a decrease in light or temperature (Keller, 2010a). Finally, a larger canopy complicates the maintenance and management of the vineyard and makes it more labour-intensive. Larger canopies increase time-consuming practices such as pruning, spraying, leaf-removal in the fruit zone and shoot thinning (Smart et al., 1990; Creasy and Creasy, 2009).

Severe water deficiency, called drought stress, is not desired as well, as it may limit important plant processes such as growth and photosynthesis. The plant water status determines the turgor pressure in the plant cells, which is the driving force for cell (and plant) growth (Lockhart, 1965; Jones, 1992; Williams, 2000). One of the first visible signs of drought stress is a diminished shoot growth. Under moderate stress the shoot length, rate of elongation, leaf size, total leaf area, trunk biomass and diameter are decreased. Under severe or very rapid onset of drought stress, the shoot tip may even die (Williams, 2000). Plant water status influences opening and closing of the stomata through which water escapes while CO₂ gas is taken up during photosynthesis. This process synthesises sugars and is of utmost importance for maintenance, growth, grapevine and fruit development (Jones,

1992; Dokoozlian, 2000; Williams, 2000; Chaves et al., 2010). During the growing season, sugars are mainly transported to non-photosynthetic organs such as the roots and stem. After veraison (colouring and ripening of the grapes), the grapes become the main sink (Dokoozlian, 2000). Even fruit set of the next year can be hindered by a reduced photosynthetic capacity (Creasy and Creasy, 2009), as the reproductive development of grapevines is expanded over two years: shoots formed out of buds in the first growing season carry fruit in the following growing season (Keller, 2010a).

Level and timing of drought stress during the growing season is crucial. Sufficient soil water availability at the start of the growing season is needed to develop a large enough canopy for capturing sufficient sun light (Smart et al., 1990; Acevedo-Opazo et al., 2010). Especially near flowering, grapevines are very sensitive to water deficit. Mild drought stress may promote inflorescence initiation (flower cluster), but more severe drought stress reduces the number of inflorescences (Keller, 2010a) and strongly reduces fruit set (Hardie and Considine, 1976; Creasy and Creasy, 2009).

Recent vineyard practices try to find a good balance between vegetative and reproductive growth by limiting excessive crop or canopy growth. A grapevine should obtain a sufficient canopy to maintain photosynthesis and ripen its fruits without resulting in vigorous vines that require intensive management. Currently, one of the major objectives is to produce uniformly ripe grapes (homogeneous ripeness) with great flavour and aroma, as it is difficult to determine the optimal and most practical harvest time when berry maturity shows large variation (Kennedy, 2002; Creasy and Creasy, 2009; Stafne and Martinson, 2012). Most growers strive to minimise not only spatial, but also annual variation in grape yield and quality (Keller, 2010a; b). The optimal balance is case-specific: it depends on the year, climate, cultivar, type of wine, management and location (Creasy and Creasy, 2009).

2.3 Influence of plant water status on grape and wine composition

2.3.1 What defines grape and wine quality?

Quality is not easy to define or quantify and strongly depends on the intended end-use (table or wine grapes, type of wine). Grapes or wines are considered of high quality when visual, taste and aroma characters are considered above average. Quality depends on the perception of pleasant and attractive flavours and aromas. Components interactively contributing to the grape and wine impression are their size and shape (for table grapes), pH, sugars, acids, tannins, colour and other phenolic and volatile chemicals (Jackson and Lombard, 1993; Creasy and Creasy, 2009; Keller, 2010b).

2.3.2 Growth phases of the grape

To understand the effect of water status on grape quality, it is important to obtain insight into berry growth and development and to know when different components accumulate in the grapes. Grape and wine quality can be modified by regulating berry size, since this alters the contribution of three main constituents of a berry, i.e. skin, seeds and flesh. These tissues show very different compositions and thus attribute in a diverse manner to the final quality. Wines produced from smaller berries, for instance, will generally have a higher share of components derived from the skin and the seeds (Kennedy, 2002; Stafne and Martinson, 2012). The development of berry weight, size and diameter is characterised by two successive sigmoid growth phases (phase I and III), separated by a lag phase of slow or no growth (phase II) (Fig. 2.8: overview of the berry development and typical changes in berry diameter) (Dokoozlian, 2000; Kennedy, 2002; Keller, 2010a; Stafne and Martinson, 2012). The three typical berry growth phases will be discussed in the following paragraphs.

Phase I

The first rapid growth phase starts at bloom and lasts a few weeks (up to 60 days) (Dokoozlian, 2000; Kennedy, 2002). The seed embryos and berry are constituted during phase I, but the berry remains firm and green due to the presence of chlorophyll (Kennedy, 2002; Stafne and Martinson, 2012). In the beginning, mainly

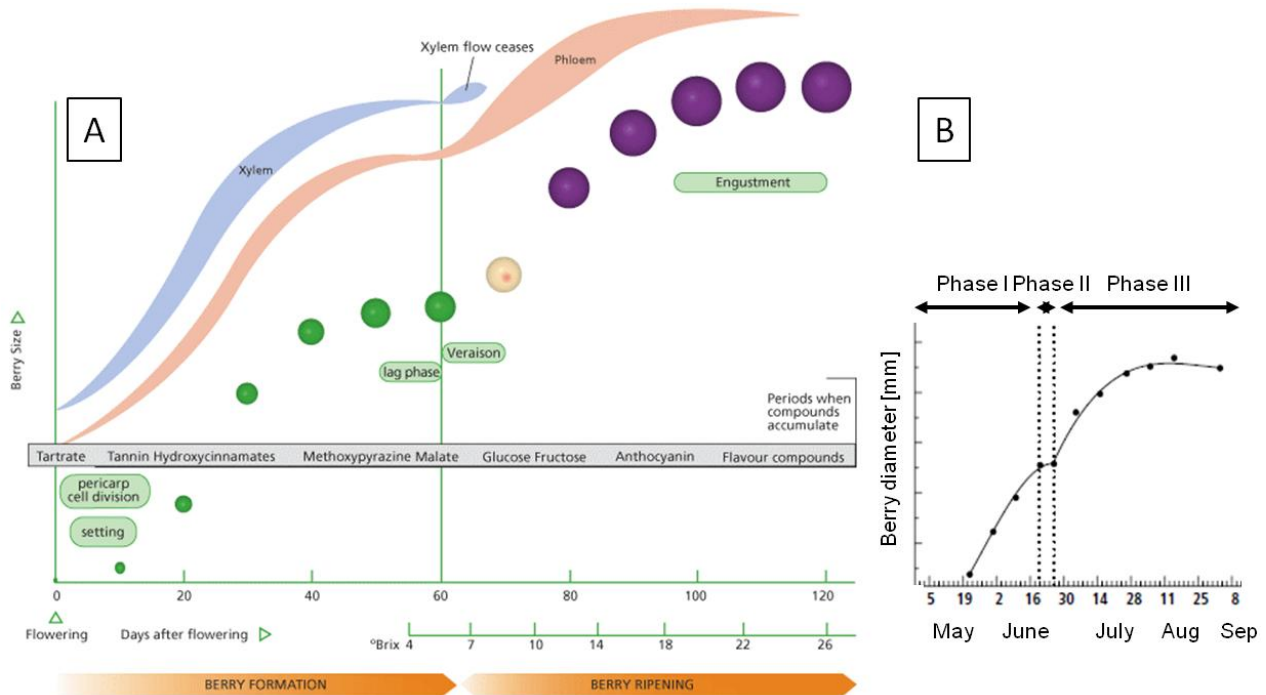


Fig. 2.8 (A) Development of berry size and colour from flowering until harvest. Major events and main components that accumulate during a certain period are indicated in the green and grey boxes, respectively (after Kennedy (2002)). (B) Typical changes in berry diameter during the growing season. Three typical growth phases can be distinguished: two successive sigmoid phases with fast growth (phase I and III) separated by a period of no growth (phase II) (after Dokoozlian (2000)).

fast cell divisions are responsible for the increasing volume and berry diameter (Fig. 2.8B). Near the end of phase I, the number of cells stabilises and new cells are no longer formed. Besides cell volume and organic solute content (sugars), final berry size at harvest is a function of the number of cell divisions during this phase (Dokoozlian, 2000; Kennedy, 2002; Keller, 2010a).

Water import into the berry can occur via both xylem and phloem, but their relative contribution is dependent on the berry growth phase. During phase I and II, water import mainly occurs via the xylem vessels (Fig. 2.8A) (Choat et al., 2009; Dai et al., 2010).

Sugar content remains low (around 2% of berry fresh weight), but soluble solids such as tartaric, malic and hydroxycinnamic acids and tannins accumulate in the berry (Fig. 2.8, 2.9) (Dokoozlian, 2000). Tartaric and malic acids (the main organic acids in grapes) reach their maximum concentration around veraison and contribute to the acidity of the wine. Malic acids mainly occur in the flesh, while the

highest accumulation of tartaric acids is found in the skin (Stafne and Martinson, 2012). Their concentration is crucial for wine balance, stability and aging potential (Dai et al., 2010). Hydroxycinnamic acids, present in the skin and the flesh, act as precursor for volatile phenols (Kennedy, 2002; Stafne and Martinson, 2012). These phenols, such as tannins, anthocyanins and flavones, play a key role for the determination of grape colour, aromas and astringency (Dokoozlian, 2000; Creasy and Creasy, 2009). Tannins are present in seeds and skins and are not only responsible for the specific bitter and astringent taste of red wines, but have a putative role for the mouthfeel, aging potential and stability of the red colour (Dokoozlian, 2000; Stafne and Martinson, 2012). Red pigments in grapes are fragile and their stability depends on the tannins that bind on them. Furthermore, phenols are assumed to play an important role within the context of nutritive value and health benefits, as they can act as antioxidants (Dokoozlian, 2000; Creasy and Creasy, 2009). Finally, also aroma components, amino acids, micro nutrients, vitamins and minerals (mainly potassium, calcium, sodium, phosphor and chloride ions) accumulate during phase I (Dokoozlian, 2000; Kennedy, 2002).

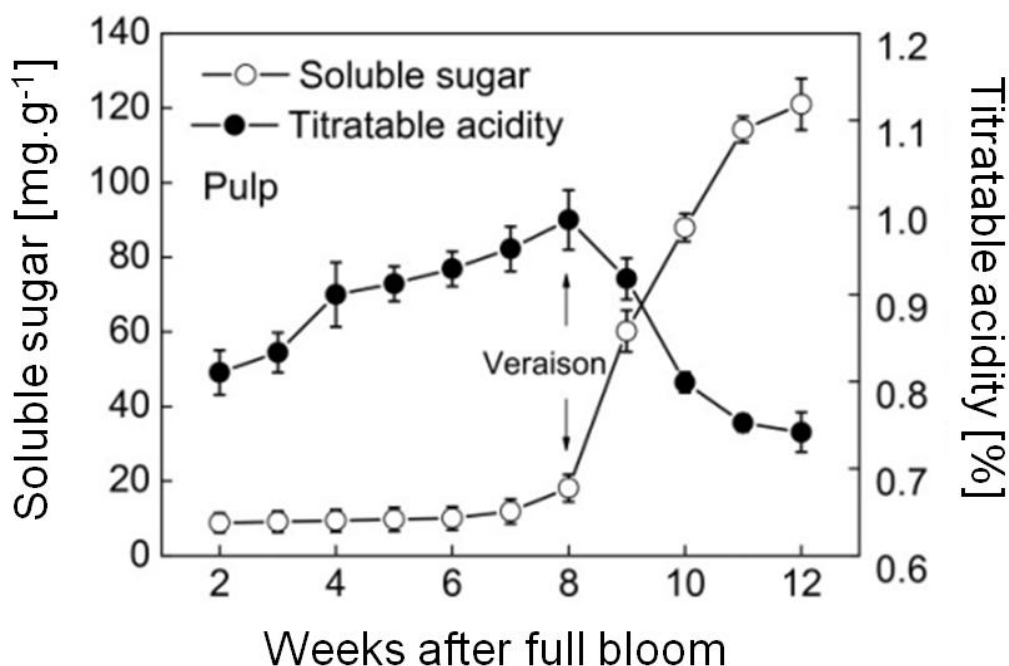


Fig. 2.9 Typical changes in sugar and acid levels during grape berry development. Acids are accumulated during growth phase I, while sugar concentration remains low. After veraison, sugars accumulate in the berry and the acid concentration diminishes (after Sun et al. (2010)).

Phase II

The lag phase lasts approximately two or three weeks (Dokoozlian, 2000) but varies considerably dependent on cultivar (Creasy and Creasy, 2009). Grape berry growth stagnates temporarily and cell division stops. Further increase in volume is solely attributed to cell elongations. During phase II, the seeds in the berry start to grow rapidly and reach their final size before veraison. The berries itself remain hard but start to lose chlorophyll. The organic acids reach their maximum concentration (Dokoozlian, 2000; Stafne and Martinson, 2012).

Phase III

Grape ripening and resumption of rapid berry growth starts with veraison. In this period, the berries soften and change colour (Fig. 2.8A). Their size approximately doubles through cell expansion (Fig. 2.8B), mainly because of sugar and water accumulation. Sugars accumulate up to 25% or more of berry fresh weight at harvest, juice pH rises gradually and the phenol and acid concentration decreases (Fig. 2.9). pH determines the ionic forms of some molecules, possibly affecting the colour of anthocyanins, and is crucial for grape juice and wine biological stability (increased risk for spoilage and wine oxidation occurs when pH > 3.6) (Creasy and Creasy, 2009; Keller, 2010b).

The amount of most components that were accumulated during phase I remain constant, although, their concentration drops remarkably due to volume increase (dilution effect) (Dokoozlian, 2000; Kennedy, 2002; Dai et al., 2010; Stafne and Martinson, 2012). Nevertheless, the absolute amount of malic acids and tannins is diminished by respiration and enzyme degradation (Dokoozlian, 2000; Stafne and Martinson, 2012). Also some important aromatic components decline on a per-berry basis during the ripening process, e.g. methoxypyrazine compounds (related to vegetal characteristics of wines) (Kennedy, 2002).

The most prominent transformation during phase III is the ripening of the grapes and the related strong increase in certain components, in particular sugars (Fig. 2.8, 2.9) and secondary metabolites (i.e. organic compounds which are not core to normal growth, development and survival of the plant). Both sugars and secondary metabolites are of utmost importance for the quality. The latter include anthocyanins (red varieties), certain aroma and volatile flavour compounds, and

their precursors, e.g. terpenoids (white varieties) (Dokoozlian, 2000; Kennedy, 2002; Stafne and Martinson, 2012). Sugars are required for fruit growth, ripening and as constituents for other components such as organic and amino acids (Dokoozlian, 2000). They contribute to wine taste, mouthfeel, body and balance. Importantly, sugars determine the percentage of alcohol in wines as they are converted into alcohol during fermentation (Williams, 2000; Keller, 2010b).

During phase III, xylem constitutes no longer the preferential pathway for water import into the berry, as import mainly occurs via phloem after veraison (Fig. 2.8) (Greenspan et al., 1994; Choat et al., 2009; Dai et al., 2010). This shift in water supply has been assigned to disruption of xylem vessels as a result of berry growth, but recent studies demonstrate that xylem remains functional and that the berries and the grapevine remain hydraulically connected (Keller et al., 2006; Choat et al., 2009; Tilbrook and Tyerman, 2009). Reduction in water supply via xylem may be attributed to an accumulation of solutes in the berry apoplast and hydraulic buffering by water delivered via the phloem (Keller et al., 2006; Choat et al., 2009). This may even lead to an excess of phloem water supply, and may result in water efflux via xylem (from the berries back to the plant), also called xylem backflow (Tyerman et al., 2004; Keller et al., 2006; Dai et al., 2010). Tyerman et al. (2004) and Tilbrook and Tyerman (2009) suggested that xylem backflow may play a key role in observed berry weight loss of certain varieties during the later stages of ripening (e.g. in *Vitis vinifera* L. cv. Shiraz, but rarely in cv. Chardonnay).

2.3.3 Grape and wine composition

As indicated above, any factor changing the grapevine growth or its physiology, in particular water status, will influence grape berry development and composition, either directly or indirectly. The extent of alteration depends on both the drought level and the prevailing berry growth phase (Fig. 2.8). For instance, excessive water availability leads to reduced sugar, colour and higher acidity, while water deficit can both increase or decrease sugar and acid content, pH and colour, dependent on the timing and level (Keller, 2010b). Besides soil water availability, also other factors that limit photosynthesis (e.g. nutrient deficiency) can affect berry size and ripening (Dokoozlian, 2000), but this study focuses on soil water availability.

Berry size

Although berry size itself is not a crucial feature for quality of wine grapes, it has a major influence on grape and wine composition. Berry size defines the degree of dilution of secondary metabolites present in the berry sap (Dai et al., 2010) and, indirectly, the proportion of skin, seeds and sap (Kennedy, 2002).

Water deficits are known to influence berry size, generally resulting in a decline (Dai et al., 2010). Phase I (onset of flowering until decelerated growth) seems most affected by drought. Grapevines subjected to drought during this phase usually have smaller berries compared to well-watered grapevines (Dokoozlian, 2000; Williams, 2000; van Leeuwen et al., 2009; Chaves et al., 2010; Dai et al., 2010). Supplemental irrigation in later stages cannot compensate for this diminished growth, suggesting a decreased number of cells (cell divisions only occur during phase I) or permanent restriction of cell size or volume (Dokoozlian, 2000; Williams, 2000). Decreased berry size can also result from water deficits during phases II and III, but is then caused by diminished cell volume (not number) and reduction in soluble solids such as sugars (Dokoozlian, 2000). Mild to moderate drought stress seems therefore most beneficial when applied during phase I (van Leeuwen et al., 2009; Keller, 2010b).

Sugars

Water availability affects sugar concentration by an interaction of three processes: sugar import, sugar metabolism and water import (Dai et al., 2010). Higher sugar concentrations have been observed in grapevines subjected to certain levels of drought stress compared to well-watered grapevines (Williams and Matthews, 1990; Williams, 2000; van Leeuwen et al., 2009; Chaves et al., 2010; Keller, 2010b). This can be partly explained by diminished sugar accumulation seen in well-watered grapevines (due to increased shadow within large canopies), while drought-stressed grapevines tend to have a smaller yield and thus less sinks that compete for carbohydrate. Finally, water is lost from grapes subjected to drought, resulting in a smaller berry volume and higher sugar concentration (Williams, 2000; Keller, 2010b). Slight to moderate water deficits increase the sugar concentration, however, sugars imported into the grapes need to be produced during photosynthesis. When grapevines close their stomata under more severe

water deficit and photosynthesis stops, also sugar production and transport to the grapes will eventually cease (Dokoozlian, 2000; Keller, 2010b).

Acids

Acids are as important as sugars for the perception of grapes and wine. They contribute to the sharp and astringent taste and mask the effect of sugars (sweetness) (Keller, 2010b). Low levels result in flat wines, high levels give a tart and sour taste (Dai et al., 2010). Tartaric acid is little affected by water status, but malic acid is (Keller, 2010b). Water deficits have been found to result in a declined acidity at harvest, especially when occurred before veraison (Williams and Matthews, 1990; Keller, 2010b). Other studies, however, did not observe an influence of moderate drought stress on titratable acidity (Matthews et al., 1990; Ginestar et al., 1998; Chaves et al., 2010).

Aroma, taste and colour constituents

Water deficits before or after veraison influence the appearance of wine, its aroma, taste and colour. The latter appears the easiest to identify (Matthews et al., 1990). Both anthocyanins (Ginestar et al., 1998; Roby et al., 2004; Acevedo-Opazo et al., 2010; Chaves et al., 2010; Keller, 2010b) and flavonols (Chaves et al., 2010) were found to be greatly affected, their composition possibly in a greater extent than their concentration (Chaves et al., 2010). Matthews et al. (1990) observed highest concentrations of anthocyanins in wines from grapevines subjected to mild drought stress (shortly) before veraison, suggesting that grape ripening is most sensitive around this period. The authors argue that drought either stimulates the production of anthocyanins (Chaves et al., 2010), responsible for the red colour, or limits their conversion to other, not colour-related components. Others state that an increment of the skin-to-pulp ratio (due to decreased berry size) is to a greater extent responsible for improved colour (Acevedo-Opazo et al., 2010; Keller, 2010b). Severe drought, however, may result in uneven ripening and green or poor-coloured grapes and is thus detrimental for colour (Keller, 2010b). Altered aromas were found more noticeable than tastes, which may indicate that volatile components are more affected by water status than soluble constituents (Matthews et al., 1990). Again, severe stress has been observed to impair the aroma potential. Some authors report no effect on the accumulation of tannins and

flavonols (Keller, 2010b), while others did observe an effect on tannins (Roby et al., 2004; van Leeuwen et al., 2009).

As mentioned in section 2.2, grapevines with a large soil water availability tend to develop large canopies. This impedes light interception and is detrimental for grape quality, because such grapevines have been shown to produce grapes with higher pH and malic acids, while sugars, tartaric acids, phenols (aromas) and anthocyanins were diminished (Smart et al., 1990; Creasy and Creasy, 2009). For instance, the amount of methoxypyrazines and monoterpenes (aroma compounds) seems to depend on the light-exposure of the berries. Methoxypyrazines are important and highly concentrated components in unripe grapes. They contribute to vegetal (herbaceous) characteristics found in some wines (e.g. *Vitis vinifera* L. cv. Cabernet Sauvignon and Cabernet Blanc), but the prevailing opinion regards them as undesirable. As their degradation is influenced by light, these flavours can be mitigated by restricting the water availability (which limits canopy growth and shadow) (Smart et al., 1990; Kennedy, 2002; Creasy and Creasy, 2009). The opposite goes for monoterpenes: they are considered favourable and their accumulation is stimulated by light-exposure of the berry. They are associated with tropical, fruity flavours and often dominate and define the typicality of cultivars such as Muscat and Riesling (Creasy and Creasy, 2009). Also Chapman et al. (2005) observed lower astringency, more fruity and less vegetal aromas in wines from drought-stressed Cabernet Sauvignons.

2.4 Using plant measurements as indicators for plant water status

The water status has a great influence on the appearance of the grapevine, its dimension and health and, which is crucial to grape- and wine growers, is decisive for the composition and quality of the grapes. By fine-tuning the appropriate timing and level of water deficits, optimal fruit and wine quality can be achieved. Obtaining this crucial balance seems however difficult, if not impossible, without an accurate monitoring of the plant water status (Naor, 2006). It is internationally recognised that such a monitoring system should rely on plant measurements rather than on soil or climatic measurements, since many plant physiological

processes respond directly to changes in water status of plant tissues (Jones, 2004; Steppe et al., 2008). Therefore, information on the actual water status and the health of the plant is gained by measuring on the plant itself, also called the speaking plant concept (Udink ten Cate et al., 1978). Although various plant variables are applied for this purpose (e.g. review by Jones (2004)), only the three plant variables most crucial for this study will be described in the following paragraphs.

2.4.1 Stem diameter variations

A promising indicator for plant water status is the variation in stem diameter. Stem diameter variations result from both actual stem growth and daily fluctuations of the living tissues due to radial water transport (Génard et al., 2001; Daudet et al., 2005; Steppe et al., 2006). The latter is driven by imbalances between root water uptake and leaf transpiration and occurs between xylem and surrounding, more elastic living tissues that serve as a storage pool for water. In the morning, when transpiration is started but water uptake is lagging behind, water is withdrawn from the internal water storage pool, which causes the stem diameter to decrease. The opposite phenomenon is seen in the evening when elastic storage tissues are replenished, resulting in an expansion of the stem diameter (Tyree and Zimmermann, 2002; Steppe and Lemeur, 2004).

Stem diameter variations can be measured continuously and automatically (Fig. 2.10) and are strongly influenced by drought stress (Vermeulen et al., 2008). They have been applied for automatic monitoring of the plant's physiological condition and water status, including grapevines (Cifre et al., 2005; Kopyt and Ton, 2005; Steppe et al., 2006; De Swaef et al., 2009; Fernández and Cuevas, 2010; Ortuño et al., 2010). Noteworthy is that besides drought stress, also phenological stage and crop load may have an influence on the stem diameter variations (Intrigliolo and Castel, 2006; 2007a; b).

2.4.2 Sap flow rate

Another indicator used worldwide for plant water status is sap flow rate (Fig. 2.11), which additionally provides information on the exact amount of water the plant consumes (Ginestar et al., 1998; Cifre et al., 2005; Patakas et al., 2005; Fernández et al., 2008; Green, 2008). Besides soil water availability, also

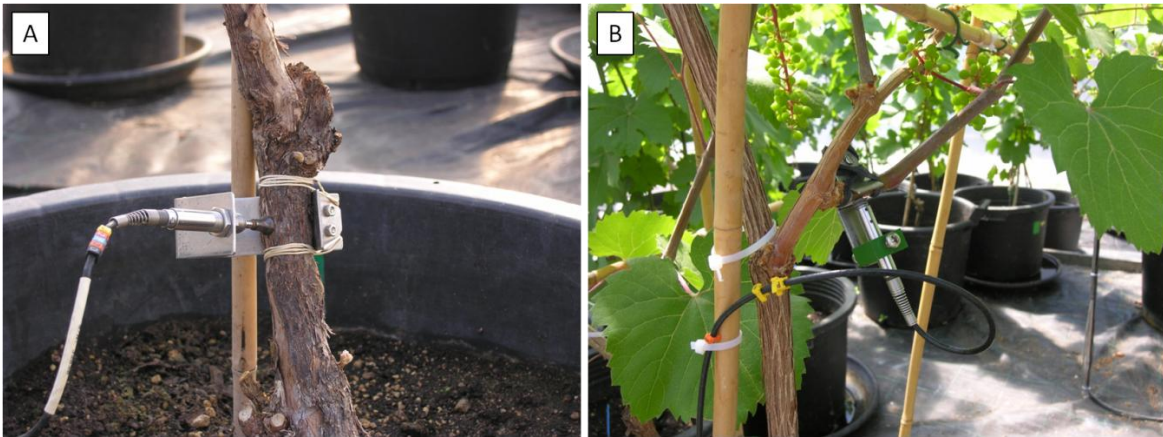


Fig. 2.10 Linear Variable Displacement Transducer (LVDT, accuracy $\pm 1 \mu\text{m}$) installed on a (A) stem and (B) shoot of a grapevine to measure stem diameter variations. A LVDT transforms mechanic movement, due to expansion or shrinkage of the stem, into an electrical, detectable signal that can be registered automatically.



Fig. 2.11 Installation of Dynagage sensors (accuracy $\pm 10\%$) (van Bavel and van Bavel, 1990) to measure sap flow rate in grapevines. These heat balance sensors calculate sap flow rate based on thermodynamics. A controlled, continuous amount of heat is applied to the exterior of the stem. The amount of heat that dissipates in radial and axial direction (by conduction) is measured. The remaining heat transported with the ascending sap (by convection) is calculated to deduce sap flow rate. The higher the convection, the higher the sap flow rate in the plant.

atmospheric water demand affects sap flow rate (De Swaef et al., 2009). Low sap flow rates can therefore result from low soil water availability, but may also be the consequence of a cloudy day.

2.4.3 Stem water potential

Various researchers have proposed stem water potential as one of the most suitable indicators for plant water status (McCutchan and Shackel, 1992; Shackel et al., 1997; Choné et al., 2001; Williams and Araujo, 2002; Patakas et al., 2005; Acevedo-Opazo et al., 2010). Stem water potential is generally measured with a pressure chamber (Scholander et al., 1965), also a well-established method by grape- and wine growers (Williams and Araujo, 2002; Creasy and Creasy, 2009). In this method, leaves are enclosed in two-layered bags, plastic on the inside and aluminium foil on the outside, at least 1 hour prior to the measurements. When equilibrium between the leaf water potential of enclosed leaves and stem xylem water is reached, these leaves are cut off and inserted into the pressure chamber (Fig. 2.12) (McCutchan and Shackel, 1992). It is a destructive, discontinuous and labour-intensive method, which makes it impractical for automatic and continuous purposes. Attempts have been made to measure stem water potential automatically, such as the use of *in situ* stem psychrometers (Dixon and Tyree, 1984; Vogt and Losch, 1999; Vogt, 2001). Although this sophisticated sensor requires a high level of technical skill and appears rather difficult to install and apply for long-standing applications (Jones, 2004; Nizinski et al., 2013), the stem psychrometer seems a promising technique for the future.

2.4.4 Combination of plant measurements

The above outlined physiological indicators for plant water status show both advantages as well as shortcomings. The influence of other factors such as microclimatic conditions, crop load and phenological stage may hamper the use of stem diameter variations and sap flow rate measurements as unambiguous indicators of plant water status when used without additional information. Stem water potential, on the other hand, is until now difficult to measure automatically. Good knowledge of underlying plant mechanisms seems of great importance. Mechanistic models are promising tools for this purpose as they can serve as a soft sensor: by compiling various plant variables, information can be linked and interpreted simultaneously. This enables unravelling plant mechanisms and contributes to our understanding of plant functioning. Such mechanistic models could also be used for automatic water status monitoring and irrigation scheduling.

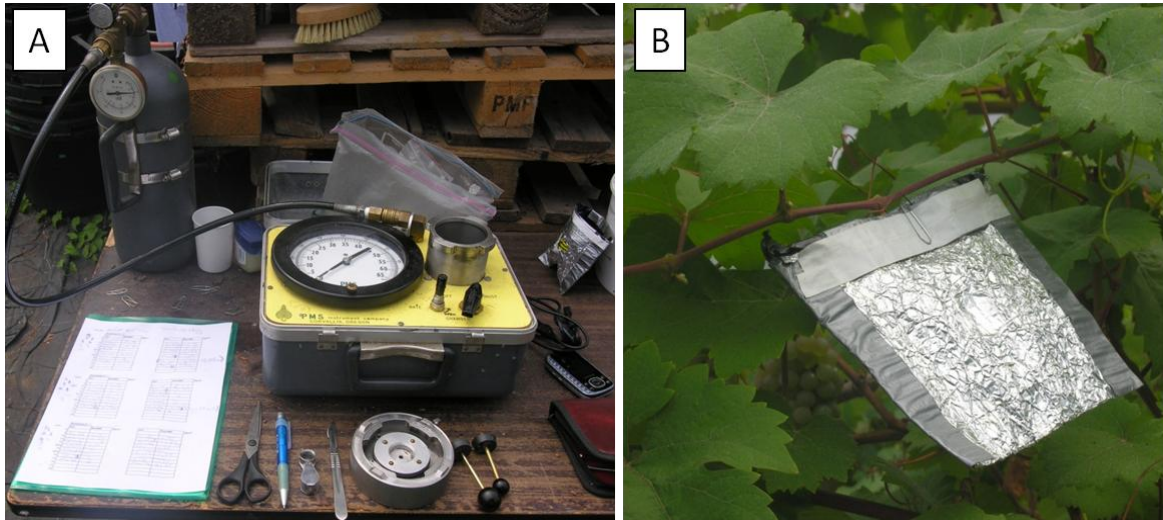


Fig. 2.12 (A) Set-up of the pressure chamber method (accuracy ± 0.05 MPa) (Scholander et al., 1965). When a leaf is cut off, xylem sap drops back below the cut surface due to prevailing xylem tension (i.e. water potential). The pressure in the pressure chamber (where the cut leaf is placed) is gradually raised until sap exudates at the cut end. At that moment, leaf water potential matches applied external pressure and can be read out. (B) When leaves are bagged for at least 1 h prior the measurements, leaf water potential comes into equilibrium with stem xylem water potential.

Steppe et al. (2006; 2008) developed such a mechanistic model for irrigation scheduling of trees. Their water transport and storage model uses measurements of sap flow rate and stem diameter variations as input to describe both the dynamics in stem diameter and axial and radial water transport in a tree. The term storage refers to the fact that the model also considers daily fluctuation and water storage in the stem (as explained in section 2.4.1). The model enables accurate simulations of stem water potential under well-watered conditions, among other plant variables. By combining the information on stem water potential, stem diameter variations and sap flow rate, the water transport and storage model gives a detailed description of the water status and physiological condition of the plant.

2.4.5 Vulnerability curve

The plant's sensitivity to drought is generally described by a vulnerability curve (Fig. 2.13) (Choat et al., 2010; Cochard et al., 2010; Sperry et al., 2012). Such a curve is a graphical representation of the plant's percentage loss of hydraulic conductance (PLC [%]) in the xylem as a function of declining xylem water potential (Ψ [MPa]) (Tyree and Zimmermann, 2002). Alternatively, if the length of the segment is known, PLC is calculated based on hydraulic conductivity

(normalised to the length). In the stem xylem, this loss is mainly the consequence of cavitation (Sperry et al., 2012). For each Ψ value (e.g. Ψ ranging from 0 to -5 MPa), a corresponding PLC value can be calculated as such:

$$PLC = 100 * \left(1 - \frac{K}{K_{max}}\right) \quad (2.3)$$

with K actual hydraulic conductance [$\text{g.MPa}^{-1}.\text{h}^{-1}$] or conductivity [$\text{g.m.MPa}^{-1}.\text{h}^{-1}$] and K_{max} the hydraulic conductance or conductivity when none of the xylem vessels is cavitared. The more sensitive a plant is to cavitation, the more it is prone to cavitation under less negative stem water potentials and thus the more its hydraulic functioning is hindered.

Each species (e.g. Tyree and Sperry, 1989; Tyree and Zimmermann, 2002) or even cultivar (e.g. Alsina et al., 2007) has a characteristic vulnerability curve. A vulnerability curve typically has a sigmoid shape (so-called “s” shape, Fig. 2.13) because not all vessels cavitate under the same stem water potentials. Indeed, the vessels have different dimensions (Cai and Tyree, 2010; Christman et al., 2012) and perhaps more importantly, a different total area of pit membranes (i.e. interconnection between separate vessels) (Wheeler et al., 2005), pit membrane structure and distribution of pores (Sperry and Tyree, 1988; Tyree and Zimmermann, 2002; Choat et al., 2008; Lens et al., 2013). All these important features define a vessel’s resistance against cavitation. Recently, also “r” shaped vulnerability curves have been observed (e.g. blue vulnerability curve in Fig. 2.13), which show a rapid rise in PLC at the beginning of the vulnerability curve (Ψ close to zero) before levelling off in a long tail (Cochard et al., 2010; Christman et al., 2012; Sperry et al., 2012). Especially for species with long vessels, “r” shaped vulnerability curves have been observed with centrifuge and short segment techniques. These curves are considered anomalous and lead to a strong overestimation of plant vulnerability, probably arising from the presence of vessels which were cut open during sampling (called open-vessel artefact) (Choat et al., 2010; Cochard et al., 2010; McElrone et al., 2012; Cochard et al., 2013).

The stem water potential at which 50% of the hydraulic conductance is lost (Ψ_{50} or P_{50}) is often applied as an index to classify the vulnerability of different species or cultivars to cavitation, e.g. as a screening trait for breeding programs (Tyree and

Zimmermann, 2002; Alsina et al., 2007; Choat et al., 2008). Ψ_{50} is therefore an important feature of a vulnerability curve. Values ranging from -0.7 to -11 MPa were found among 60 species from many different climates and growth forms (Tyree et al., 1994).

Construction of the vulnerability curve

Several standard procedures for constructing a vulnerability curve exist. K is calculated by the ratio of mass flow rate of the measurement solution through the segment (F [$\text{g}\cdot\text{h}^{-1}$]) and pressure gradient along its length (ΔP [MPa]), either induced gravimetrically by a hydraulic pressure head (Sperry et al., 1988; 2012; Alsina et al., 2007) or by a XYL'em apparatus (Cochard et al., 2000; Espino and Schenk, 2011):

$$K = \frac{F}{\Delta P} \quad (2.4)$$

Note the similarity with Eq. 2.2. The main difference of how a vulnerability curve is generated lies in the methodology to obtain the (successive) desired negative xylem pressures. These pressures are for instance obtained by bench drying or air dehydration (considered the gold standard) (Sperry and Tyree, 1988; Tyree and Zimmermann, 2002; Cochard et al., 2010; Christman et al., 2012; Urli et al., 2013), dehydration in a pressure chamber, also called air injection (Cochard et al., 1992; Sperry et al., 1998; 2012), or by using centrifugal forces (Alder et al., 1997; Sperry et al., 1998; 2012; Cochard, 2002; Urli et al., 2013). The standard procedures for constructing a vulnerability curve require destructive sampling and most are labour-intensive and time-consuming (Choat et al., 2010). Moreover, results may deviate dependent on the applied method (Choat et al., 2010; Cochard et al., 2010; Jacobsen and Pratt, 2012; Cochard et al., 2013; Wheeler et al., 2013), sample length and/or dimension (Kikuta et al., 2003; Choat et al., 2010; Cochard et al., 2010) and method specifications such as xylem tensions during sample excision (Wheeler et al., 2013), degree of flushing and filtering, chemical composition and level of degassing of the aqueous measurement solution (Canny et al., 2007; Espino and Schenk, 2011; van Doorn et al., 2011; Jacobsen and Pratt, 2012; Sperry et al., 2012).

The use of vulnerability curves seems not so straightforward as first assumed. Besides the difficulties related to constructing and comparing vulnerability curves, other limitations arise. Hydraulic functioning or limitations for a species do not only depend on the plant hydraulic properties, but also on those of the soil. Alternative methods for describing vulnerability based on *in situ* plant (and soil) measurements may be a complementary method to investigate plant vulnerability. As such, hydraulic functioning can be observed under natural conditions and for an extended time period, while conventional vulnerability curves are constructed in a laboratory and at a certain moment in time. Also Hölttä et al. (2005) opted for an alternative vulnerability curve: they used measurements of ultrasonic acoustic emissions and stem diameter variations for studying cavitation dynamics in Scots pine (*Pinus sylvestris* L.) trees under field conditions.

Vulnerability curve of grapevine

The observation that vulnerability curves can vary greatly dependent on the applied procedure or method specifications, and its major implication for the often used benchmark criterion Ψ_{50} is illustrated for grapevine in Fig. 2.13 and Table 2.1, respectively.

2.5 Conclusions

Water transport in grapevines occurs in xylem vessels and is described by the cohesion-tension theory. Since water is under tension, which is a metastable condition, the presence of air bubbles may lead to breakage of the water column. This process is called cavitation and results, in turn, in loss of hydraulic conductance. The loss of conductance as a function of increasing tensions is often depicted in a vulnerability curve, which is a benchmark method for comparing vulnerability of species. Grapevine development, quality of grapes and character of wine are strongly influenced by grapevine water status, and may benefit from some level of drought during certain periods of the growing season. Plant measurements such as sap flow rate, stem diameter variations and stem water potential are considered as good indirect or direct indicators for water status. They are therefore promising for obtaining this crucial balance, especially when their information is combined.

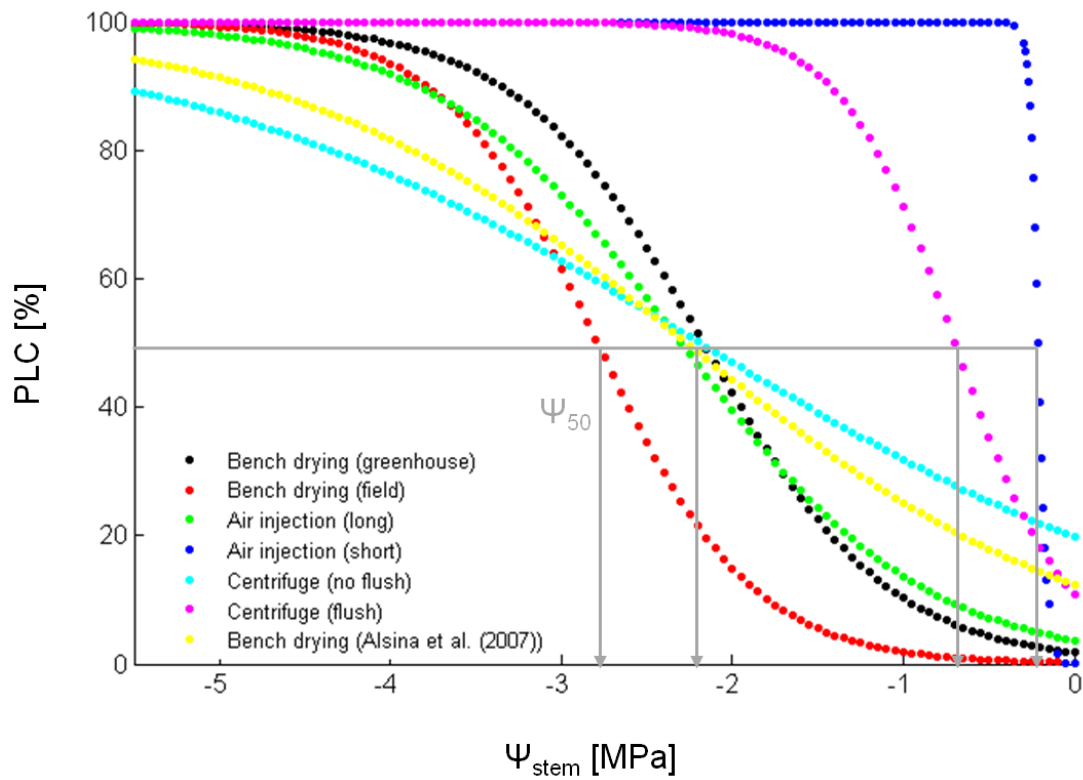


Fig. 2.13 Comparison of vulnerability curves for *Vitis vinifera* L. cv. Chardonnay obtained by different procedures and method specifications. A vulnerability curve depicts the percentage loss of hydraulic conductance (PLC) as a function of declining stem water potential (Ψ_{stem}). An important feature in vulnerability curves is Ψ_{stem} corresponding with 50% PLC (Ψ_{50}). All experiments were performed by Choat et al. (2010), unless stated otherwise.

Table 2.1 Overview of the implications for calculated Ψ_{50} , i.e. stem water potential at which 50% of the hydraulic conductivity is lost, when comparing vulnerability curves obtained with different procedures and method specifications. All experiments were conducted on *Vitis vinifera* L.

Cultivar	Method	Specifications	Ψ_{50} [MPa]	Reference
Chardonnay	Centrifuge	Non-flushed short segments (0.145 m)	-2.19	Choat et al. (2010)
Chardonnay	Centrifuge	Flushed short segments (0.145 m)	-0.70	Choat et al. (2010)
Chardonnay	Bench drying	Field-grown	-2.97	Choat et al. (2010)
Chardonnay	Bench drying	Long segments (0.5 - 0.9 m)	-2.17	Choat et al. (2010)
		Greenhouse-grown		
Chardonnay	Air injection	Long segments (0.9 m)	-2.30	Choat et al. (2010)
Chardonnay	Air injection	Short segments (0.145 m)	-0.21	Choat et al. (2010)
Chardonnay	Bench drying	-	-2.27	Alsina et al. (2007)
Tempranillo	Bench drying	-	-1.17	Alsina et al. (2007)
-	Centrifuge	Short segments (0.142 m)	-0.76	Wheeler et al. (2005)
Glenora	Centrifuge	Short segments (0.14 m)	-0.16	Jacobsen and Pratt (2012)
Glenora	Centrifuge	Short segments (0.27 m)	-0.31	Jacobsen and Pratt (2012)
Glenora	Centrifuge	Short segments (0.14 m)	-0.34	Jacobsen and Pratt (2012)
Glenora	Centrifuge	Short segments (0.27 m)	-0.55	Jacobsen and Pratt (2012)
Glenora	Bench drying	Short segments (0.14 m)	-1.58	Jacobsen and Pratt (2012)
Grenache	Dehydration	Long segments (0.4 m)	-0.91	Lovisol et al. (2008)*
		Pooled data		
Grenache	Air injection	Estimated based on leaf-specific hydraulic conductance	-0.32	Schultz (2003)*
Syrah	Air injection	Estimated based on leaf-specific hydraulic conductance	-0.51	Schultz (2003)*
Chasselas	Bench drying	Estimated based on a vulnerability curve of leaf petioles	-0.41	Zufferey et al. (2011)*

*Studies that reported hydraulic conductance, hydraulic conductivity or percentage loss of hydraulic conductivity data in combination with water potentials, but did not plot the data as a conventional vulnerability curve. Data were therefore extracted and converted to a vulnerability curve to estimate Ψ_{50} for comparison (after Jacobsen and Pratt (2012)).

Chapter 3

Introduction of two statistical techniques for automatic stress detection based on stem diameter variations

After: Baert A, Villez K and Steppe K. 2012. Functional Unfold Principal Component Analysis for automatic plant-based stress detection in grapevine. Functional Plant Biology. 39(6), 516-530.

Abstract

Detection of drought stress is of great importance in grapevines because the plant's water status strongly affects the quality of the grapes and, hence, resulting wine. Measurements of stem diameter variations are very promising for detecting drought stress, but they strongly depend on microclimatic changes. Tools for advanced data analysis might be helpful to distinguish drought from microclimatic effects. To this end, the possibilities of two data mining techniques were explored: Unfold Principal Component Analysis (UPCA), an already established tool in several biotechnological domains, and Functional Unfold Principal Component Analysis (FUPCA), a newer technique combining functional data analysis with UPCA. With FUPCA, the original, multivariate time series of variables are first approximated by fitting the least-squares optimal linear combination of

orthonormal basis functions. The resulting coefficients of these linear combinations are then subjected to UPCA. Both techniques were used to detect when measured stem diameter variations in grapevine deviated from their normal conditions due to drought stress. Stress was detected with both UPCA and FUPCA days before visible symptoms appeared. However, FUPCA is less complex in the statistical sense and more robust compared to original UPCA modelling. Moreover, FUPCA can handle days with missing data, which is not possible with UPCA.

3.1 Introduction

As mentioned in **Chapter 1**, grapevines (*Vitis vinifera* L.) are often subjected to drought stress and this may become more common due to global climate change and increasing scarcity of water (Schultz, 2000; Schultz and Stoll, 2010). Soil water availability has a great influence on both the quality and the quantity of grapevines (**Chapter 2**; Smart et al., 1990; Williams and Matthews, 1990; Creasy and Creasy, 2009). Differences in plant water status thus result in wine with different appearance, aroma, flavour and colour (Smart and Robinson, 1991; Williams, 2000).

It is known that the timing of occurrence of water deficit throughout the growing season is of great importance (Matthews et al., 1990; Keller, 2010a). Well-defined periods with a slight to moderate level of water deficit are therefore needed to improve the quality of grapes, and thus wine, without compromising production (Gaudillère et al., 2002; Möller et al., 2007; Creasy and Creasy, 2009). However, it is difficult to achieve this balance and it requires accurate monitoring of the plant's water status. Early detection of drought stress makes it possible to avoid or at least limit decline in fruit quality (Bacci et al., 1998; Jones, 2004). As discussed in **Chapter 2**, it is generally recognised that the new and innovative strategies meant for this purpose should be plant-based, because plant physiological processes indeed respond directly to changes in the plant water status (e.g. Jones, 1990; 2004; Steppe et al., 2008). Possible indicators are stem or leaf water potential (Jones, 1990). While the latter is strongly influenced by changing microclimatic conditions and therefore less suitable (Jones, 1990; Choné et al., 2001), stem water potential has already been successfully applied for drought stress detection

in grapevines (Choné et al., 2001; Intrigliolo and Castel, 2007b; Möller et al., 2007). Water potential is generally measured with a pressure chamber, a destructive, discontinuous and labour-intensive method, and therefore impractical for continuous monitoring (Jones, 2004; Steppe et al., 2008). A more promising indicator is continuous measurement of variations in stem diameter (Goldhamer and Fereres, 2001; Steppe et al., 2006; Intrigliolo and Castel, 2007b; De Swaef et al., 2009; Fernández and Cuevas, 2010; Ortuño et al., 2010). Stem diameter variations result from both actual radial stem growth and daily fluctuations related to changes in water content in the elastic living tissues that serve as a storage pool for water (Génard et al., 2001; Daudet et al., 2005; Steppe et al., 2006). Changes in water content result from withdrawal (day) or replenishment (night) of internal water storage due to imbalances between root water uptake and leaf transpiration (Tyree and Zimmermann, 2002; Intrigliolo and Castel, 2007b; Steppe et al., 2012). Since stem diameter variations are affected by drought stress (Steppe et al., 2006; De Swaef et al., 2009) and can be measured continuously and automatically using Linear Variable Displacement Transducers (LVDT), they are very applicable for automatic on-line monitoring of the plant's physiological condition.

Before stem diameter variations, and plant-based indicators in general, can be used for stress detection, reference or threshold values are needed. However, an unambiguous method for determination of such values is currently not available (Jones, 2004; Steppe et al., 2008; De Swaef et al., 2009). Another difficulty is the highly dynamic nature of the plant's water status (Goldhamer and Fereres, 2001) and the observation that stem diameter variations are not only affected by drought stress, but also depend on microclimatic conditions (Steppe et al., 2006; De Swaef and Steppe, 2010). Indeed, photosynthetic active radiation and vapour pressure deficit are key driving variables for transpiration and thus have an effect on the daily shrinkage and swelling of the diameter. Consequently, microclimatic measurements should be taken into account to distinguish automatically between changes in stem diameter variations due to daily variations (no detection desired) and changes due to the plant's response to drought stress (detection desired as soon as possible). However, the resulting data set will likely be hard to interpret without additional tools for data analysis.

Specific data mining techniques, such as Principal Component Analysis (PCA), have been developed to facilitate monitoring and diagnosing of such multivariate data sets (Jackson, 1991) (More information on PCA for process monitoring can be found in Box 3.1). PCA is an efficient and powerful method that is commonly applied for statistical process control of processes where accurate mechanistic knowledge is lacking or difficult to achieve (MacGregor and Kourti, 1995; Venkatasubramanian et al., 2003). For instance, examples are found for wastewater treatment (Rosen and Lennox, 2001; Lennox and Rosen, 2002; Lee and Vanrolleghem, 2003; Villez et al., 2008) and fermentation processes (Lennox et al., 2001; Bicciato et al., 2002). Only one application of PCA for stress detection in plant science has been published so far (Villez et al., 2009). These authors used Unfold Principal Component Analysis (UPCA), an extension of PCA (Wold et al., 1987; Nomikos and MacGregor, 1994), for successful drought stress detection in truss tomato (*Solanum lycopersicum* L.) and apple tree (*Malus domestica* Borkh). Another, newer technique called Functional Unfold Principal Component Analysis (FUPCA) combines functional data analysis with UPCA (Chen and Liu, 2001). With FUPCA, each daily time series of the original variables is first approximated by a function. As a result, the data are represented by a smaller number of new values which are further analysed by UPCA (Chen and Liu, 2001).

The aim of the present chapter was to evaluate and compare the performance of both UPCA and FUPCA for automatic, fast and accurate on-line detection of drought stress in grapevine.

Box 3.1 Principal Component Analysis applied for process monitoring

Over a wide range of applications, there is a growing interest for automatic and online data acquisition of industrial processes. Automatic data collection appears very useful, timesaving and convenient, however, once the data are collected, it may be difficult to analyse and interpret the compiled dataset. In many datasets, complex interactions exist between the measured variables. The contribution of a

particular variable to the process performance, which is hoped to be optimised by monitoring the process, may be unclear. The interactions between the measured variables are not always (fully) understood and often knowledge of underlying mechanisms driving the process is lacking. For the controller/supervisor it may be difficult to define the most crucial variables to observe, unravel, extract correlations between the measured variables and assess whether the process behaves as expected or whether action is needed.

Therefore, tools have been developed to support the handling and analysing of large and complex datasets in order to improve process performance and product quality (Kourti, 2002). An often applied, and in some fields already well-established, technique for monitoring a process is Principal Component Analysis (PCA), which has many variants (Venkatasubramanian et al., 2003). PCA is a data mining technique, generally applied to reduce the dimensionality, and therefore surveyability, of a large dataset. By use of PCA, information contained in a great number of measured variables is extracted and subsequently expressed by a smaller number of new variables, called principal components (PCs). Contrary to the original variables, these PCs are uncorrelated. They are ordered as such that most of the variation present in the original variables is captured by only the first PCs. PCA as such considerably reduces the dataset's dimension with only a minimal loss of variation inherent in the data (Jolliffe, 2002). It is assumed that the largest part of the variation that is captured by the PCA model is representative for the amount of retained information underlying the measured variables (Villez, 2007) and that the constructed PCA model properly describes the major trends observed in the data (Venkatasubramanian et al., 2003).

Besides dimension reduction, PCA can be applied to monitor a process, i.e. identify periods of unusual behaviour or indicate when an abnormal event occurs (Aguado et al., 2007). To this end, reference data (so-called historical data) are required to define normal (routine) behaviour for the corresponding process. Data describing the desirable performance forms as such the so-called in-control model. New data are subsequently checked against this in-control model (Chen and Liu, 2001; Kourti, 2002). In some cases, PCA is further employed to diagnose the possible cause of detected abnormal process behaviour (MacGregor and Jaeckle, 1994; Kourti, 2002; Qin, 2003). Although not every problem or cause may be

unambiguously pointed out by PCA, the method generally allows to reveal which group of measured variables contributed most to the deviation from the in-control model, suggesting their responsibility for the abnormal behaviour (MacGregor and Jaeckle, 1994; Kourti, 2002). This considerably narrows down the amount of data the controller/supervisor has to focus on.

PCA has applications in agriculture, biology, chemistry, climatology, demography, ecology, genetics, economics, geology, quality control and so on (Jolliffe, 2002). For a monitoring purpose, the technique has been tested both offline and online (in real-time) for a various range of processes, such as fermentation (Lennox et al., 2001; Monroy et al., 2012) and polymerisation batches (MacGregor and Kourti, 1995), wastewater treatment processes to ensure that effluent quality targets are obtained (Aguado et al., 2007; Villez et al., 2008), steel- (Miletic et al., 2008), polyethylene- (MacGregor and Jaeckle, 1994) and food- (Gurden et al., 2001) manufacturing batches, among others. It has begun to find wide acceptance in industry as well, where it increased safety and returns (Kourti, 2002). As discussed in **Chapters 3** and **4**, a living grapevine can also be considered as an ongoing process with abnormal behaviour occurring during drought stress.

3.2 Material and methods

3.2.1 Plant material and experimental set-up

An experiment was conducted on potted grapevines (*Vitis vinifera* L. cv. Leon Millot) in the greenhouse facilities of the Faculty of Bioscience Engineering of Ghent University, Belgium, during the growing season of 2011. The grapevines were approximately four years old and grown in 50 L containers (0.4 m diameter, 0.4 m height) filled with DCM Mediterra compost and fertilized in summer with DCM organic fertilizer for grapes (magnesium NPK 7-4-7 + 2 MgO). The grapevines were approximately 1.5 m high and had stem diameters of about 16 to 21 mm. They were trained and pruned according to the single Guyot system. One grapevine was chosen for this study and monitored continuously. After a long

control period where the plant was kept well-watered, a period of drought was imposed by withholding irrigation. Irrigation for the stressed plant was resumed when clear visible symptoms of drought stress were observed (colouring and wilting of the leaves). The drought period was followed by a recovery period, in which the plant was again well-watered. The experiment ran from 13 May until 26 July (day of the year (DOY) 133 - 207). Drought stress was imposed from 14 until 28 June (DOY 165 - 179), DOY 165 being the last irrigation before the drought period and DOY 179 the day where irrigation was resumed.

3.2.2 Plant and microclimatic measurements

During the experiment, stem diameter variations as well as microclimatic conditions were monitored (Fig. 3.1). Photosynthetic active radiation (PAR) was measured with a quantum sensor (LI-190S, Li-COR, Lincoln, NE, USA), air temperature (T_{air}) with a thermocouple (type T, Omega, Amstelveen, the Netherlands) and relative humidity (RH) with a RH sensor (type Hygroclip, Rotronic, USA) inserted in a radiation shield. The sensors were installed inside the greenhouse near the grapevines, approximately 2 m above ground. Vapour pressure deficit (VPD) was calculated from RH and T_{air} as the difference between the air's potential and actual vapour pressure value.

Stem diameter variations (D) were measured using a LVDT sensor (Linear Variable Displacement Transducer, model DF 5.0, Solartron Metrology, Bognor Regis, UK), attached to the stem with a custom-made stainless steel holder, which does not require a temperature correction (Steppe and Lemeur, 2004). All sensor signals were recorded every 20 s (DAQ 34970A and multiplexer 34901A, Agilent Technologies, Diegem, Belgium). The analysed data of PAR, VPD and D were included as input for UPCA and FUPCA modelling. All data- and modelling analysis were performed in Matlab[®] (The Mathworks Inc., Natick, MA, USA).

3.2.3 Unfold Principal Component Analysis

Principal Component Analysis (PCA) is a well-established technique for monitoring and diagnosing of processes with large, multivariate data sets, consisting of many variables with strong correlations (Box 3.1; Jackson, 1991; Kourti, 2002; Venkatasubramanian et al., 2003). In this study, PAR, VPD and D measurements were organised in a three-dimensional matrix X ($I \times J \times K$), in which I stands for

the day it was taken, J for the time within the day and K for the variable. To deal with three-dimensional data sets, an extension of PCA, Unfold Principal Component Analysis (UPCA), was needed, which was first proposed by Wold et al. (1987). A detailed description of UPCA can be found in Nomikos and MacGregor (1994) and a more extensive explanation on how UPCA can be applied for on-line plant stress detection in Villez et al. (2009).

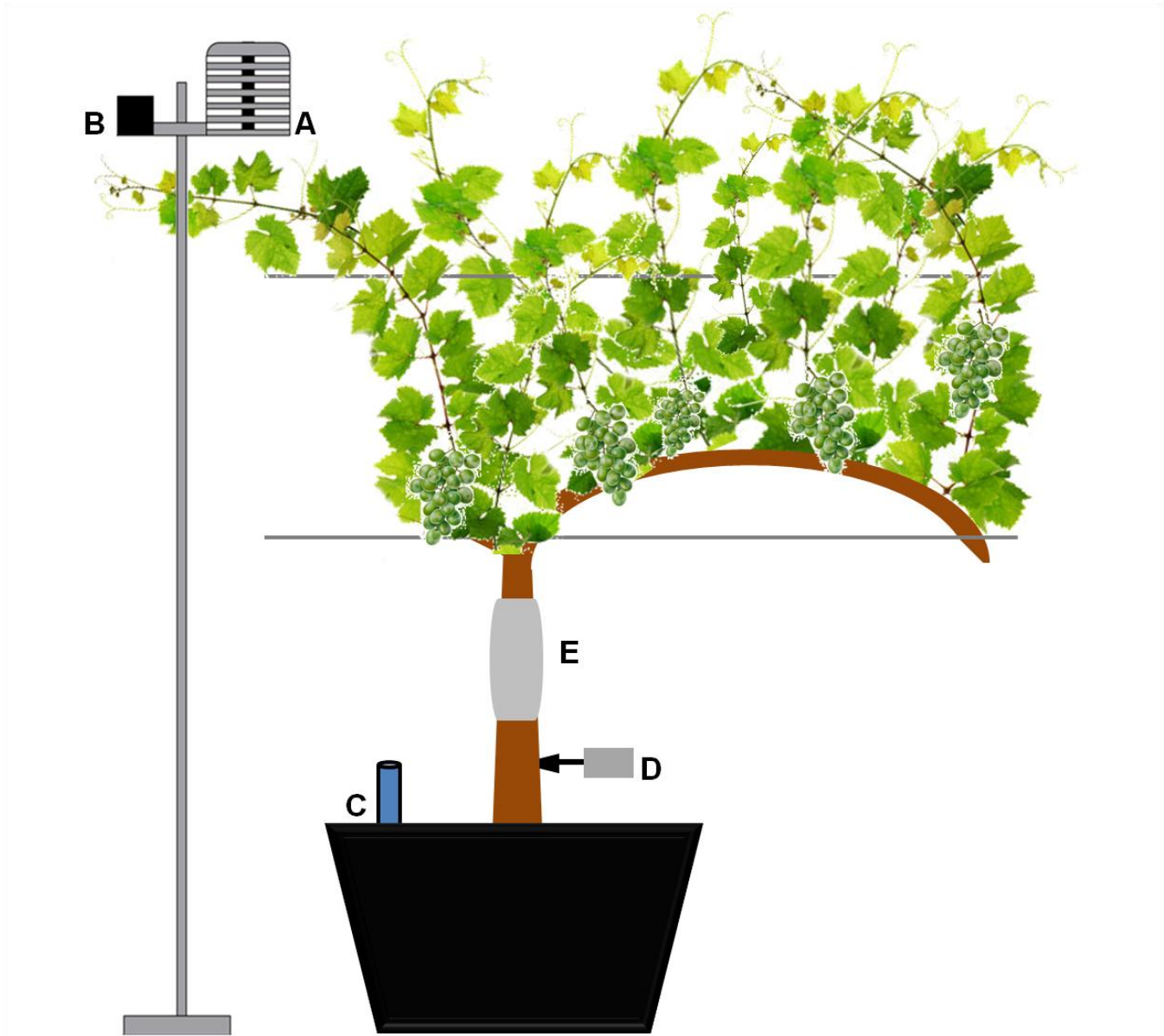


Fig. 3.1 Schematic overview of the sensors installed during a drought stress experiment on grapevine: (A) Relative humidity, air temperature and (B) photosynthetic active radiation were measured above the canopy. Soil water potential was measured with an electronic tensiometer (C), stem diameter variations with a Linear Variable Displacement Transducer (D) and sap flow rate with a heat balance sensor (E).

Days with missing data cannot be considered in classical UPCA, so 18 out of 74 days were omitted from the data set, including four days during the control period (mainly because of electricity failure). The remaining 26 days between DOY 134 and 165 during the well-watered control period were used for calibration (I_{cal}) of the UPCA model, with $I = 56$ days, $J = 4320$ measurements (measurement value every 20 s) and $K = 3$ variables (PAR, VPD and D).

Data pre-processing

Prior to UPCA, the data were pre-processed. First, the daily net growth of the diameter was removed by subtracting the first value of each day from all D measurements of that day. This subtraction was necessary to get an interpretable UPCA model, because each day was considered as a separate and independent cycle for the purpose of PCA modelling (Villez et al., 2009). Next, the data were centred column-wise (Fig. 3.2A) to zero mean by subtracting the mean of all measurements for a specific sensor at a given time during the day from the corresponding measurements. Then, centred data of a specific sensor were divided by the overall standard deviation of the data for that given sensor. This group scaling or single-slab scaling (Fig. 3.2B) balanced the variation in the sensor's measurements without disturbing the data's covariance structure (Gurden et al., 2001). Finally, the data were unfolded batch-wise (Fig. 3.2C) to transform the three-way data set ($I \times J \times K$) into a two-way matrix ($I \times J \cdot K$). A single row now represented all and exclusively data of one single day (0-24 h). After pre-

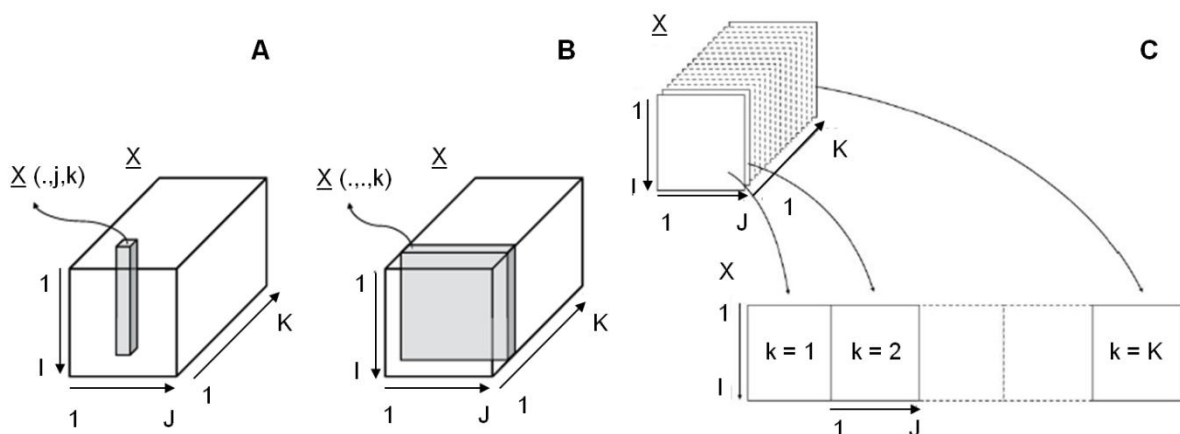


Fig. 3.2 Column-wise centring (A), group scaling or single-slab scaling (B) (after Gurden et al. (2001)) and batch-wise unfolding (C) as part of the pre-processing of data for Unfold Principal Component Analysis. X represents a three-dimensional data matrix in which I stands for the day, J for the time within the day and K for the variable.

processing, the data were suitable for PCA modelling, henceforth referred to as UPCA modelling.

The UPCA model

Since correlation exists in the data, a majority of the data's variation can be captured well by a smaller set of new variables, called principal components (PCs). Those new variables were constructed based on the calibration data and were uncorrelated and orthogonal linear combinations of the original variables. The larger the number of retained PCs (# PCs or c), the larger the proportion of variance of the original data that is captured by the model (Johnson and Wichern, 2002). The proportion of total variance captured by a single PC is referred to as relative variance (RV), while the relative cumulative variance (RCV) is the proportion of variance captured by the first c PCs. As a result, identification of the UPCA model boils down to determining the number c . This is typically done in a subjective manner while attempting to trade off between dimension reduction (c) and captured variance (RCV). Visualisation and analysis by means of the PCs may be easier than working with the complete dataset. To transform the original variables into PCs, the data matrix ($X_{I \times J.K}$) is decomposed into a new score matrix ($T_{I \times c}$) with I observations and c principal components, and a loading matrix P (dimensions $J.K \times c$). This can be written as follows: $X = T.P' + E$, with E the residuals. The c column vectors of P (thus one for each PC) are the c eigenvectors of the calibration data covariance matrix and are also called loading vectors. UPCA modelling can be interpreted as the construction of a relationship between the new variables to obtain a profile of expected, normal conditions.

Stress detection with UPCA

Two conventional statistics were used for statistical stress monitoring: the Q statistic and the Hotelling's T^2 statistic (Hotelling, 1947; Johnson and Wichern, 2002). Calibration data were used to determine the upper control limit of those two statistics (Fig. 3.3). The Q statistic or sum of squared residuals measures the goodness of the model fit:

$$Q(i) = \sum_{n=1}^N M_R(i,n)^2 \quad (3.1)$$

with M_R the matrix of residuals, N the lateral dimension of the two-dimensional data matrix ($N = J \times K$), n the corresponding coordinate inside this matrix and i the coordinate representing the day. Practically, the Q statistic determines the difference between the original and reconstructed data and accounts for the expected variance of the residuals. If the upper control limit of this statistic is violated, residuals are believed not to result from random effects only. The second statistic, Hotelling's T^2 , is defined as the weighted sum of squared scores and is a measure for the distance between the reconstructed data and the origin:

$$T^2(i) = \sum_{c=1}^C \frac{T(i,c)^2}{\lambda_c} \quad (3.2)$$

with T the score matrix, C the number of retained PCs, c the PC index and λ_c the c^{th} largest eigenvalue. Since the use of the Hotelling's T^2 assumes otherwise normal data, accounting for variation within the modelled space (linear subspace spanned by the c selected eigenvectors), this statistic is typically useful to detect extreme events which do not violate the correlation structure as identified via the

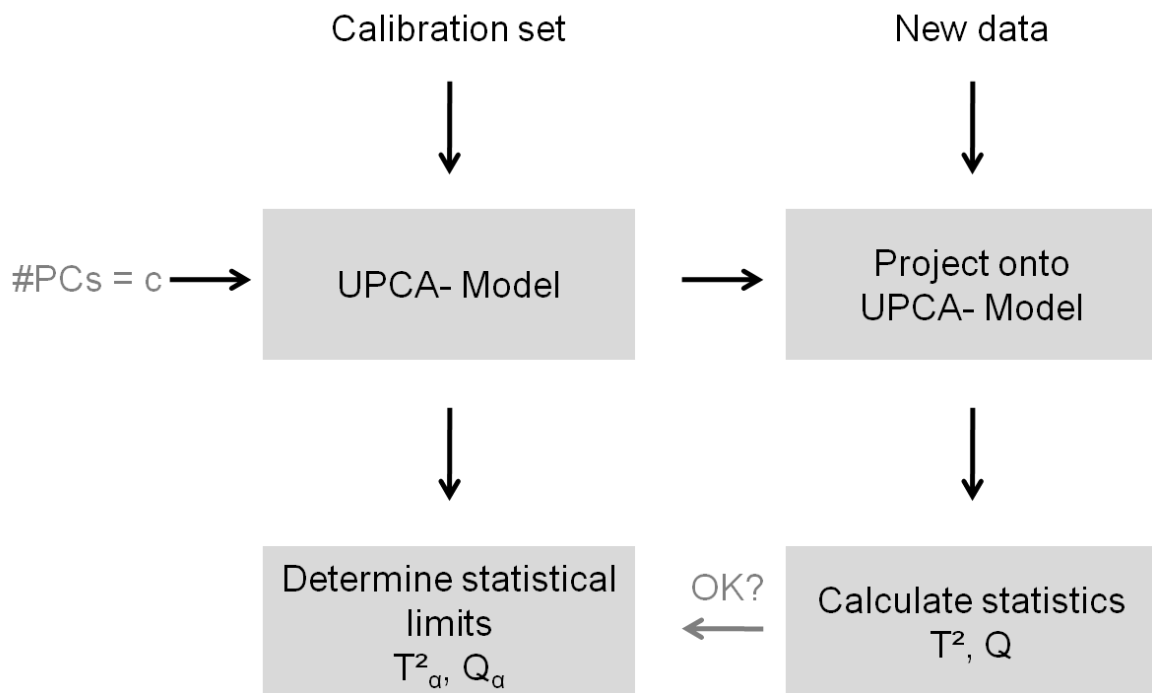


Fig. 3.3 Schematic overview of Unfold Principal Component Analysis (UPCA) for plant stress detection. The UPCA model is constructed by means of a calibration set and statistical limits (T^2_α , Q_α) are determined. Subsequently, new data are projected onto this UPCA model and corresponding statistics (T^2 , Q) are calculated. They are finally compared with the previously determined statistical limits to determine if plant stress occurs.

first c eigenvectors of the covariance matrix. To this end, one first evaluates whether the Q statistic remains under its set limit. Only if this is true, the Hotelling's T^2 is checked against its proper limit, even though it can always be computed. Determining whether drought is detected in new data is done by pre-processing these data in the same manner (removal of D net growth, centring, scaling and unfolding) and projecting them onto the UPCA model. Corresponding statistics (Q , T^2) are then compared with the previously determined statistical limits (Q_α , T^2_α) (Fig. 3.3). If one of the limits is exceeded, it indicates abnormality (drought stress) for the corresponding day.

3.2.4 Functional Unfold Principal Component Analysis

Functional Unfold Principal Component Analysis (FUPCA) was first introduced by Chen and Liu (2001). The method applies functional data analysis prior to UPCA modelling and therefore reduces the set of original variables into a set of new coefficients (via functional data analysis), while preserving the ability to easily monitor a process and detect abnormalities (via UPCA). FUPCA is therefore a promising technique for stress detection in plants.

Functional data analysis

Functional data analysis is a method to represent the data in such a way that it facilitates further analysis (Ramsay and Silverman, 2005). With this analysis, each single daily time series of the original variables (PAR, VPD and D) is approximated by linear combinations of a set of known basis functions (defined below). These basis functions are orthonormal and have been proven to allow arbitrarily good function approximations by linear combination of a sufficiently large number of such basis functions. As a result, the majority of the information contained in the PAR, VPD and D measurements is stored by functional data analysis in a condensed form, since the coefficients of the linear combination are of a lesser number than the original measurements.

In this study, the B-spline basis was chosen. This basis consists of several spline functions, called B-splines, and often needs only a small number of them to approximate the data. B-splines can be computed fast and exhibit great flexibility (Ramsay and Silverman, 2005). The use of B-splines as a basis results in a piece-wise polynomial function.

Two choices have to be made for defining a B-spline. First, the order (n) of the B-splines has to be fixed, which is one more than its degree ($n-1$). For instance, a third order B-spline is from the second degree or piecewise quadratic. Note that the derivatives of the function up to derivative $n-2$ are continuous over the whole argument range of the fitted function. In Fig. 3.4A, B, C, an example of respectively a second, third and fourth order B-spline is shown for the approximation of a sine function. Second, one needs to determine the locations of the so called knots which define the location and width of each of the B-splines, as well as the intervals over which the fitted function is continuous. In this study, a complete day covered in the data set (0-24 h) was divided into equal-length intervals by placing knots uniformly over the argument range. The same

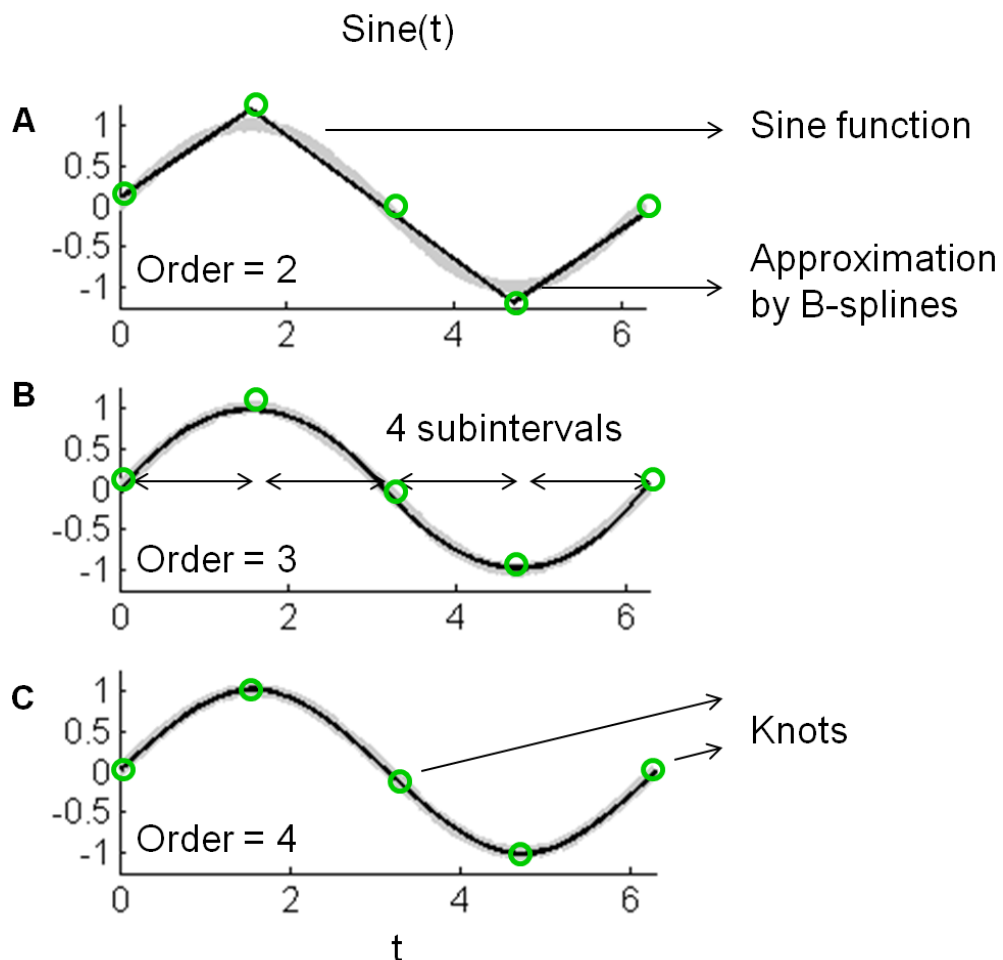


Fig. 3.4 Example of second (A), third (B) and fourth (C) order B-splines (black lines) to approximate a sine function (grey lines). The interval across which the function is to be approximated is divided into subintervals by knots (green circles) (adapted from Ramsay and Silverman (2005)).

placement was used for all days and all variables. Knots were positioned every i^{th} hour of a day [0: i: 24 h]. Different options for i were tested. For instance, a knot could be placed every 6 h or every 6 min. The number of coefficients to define a B-spline is determined by the number of knots and the order (i.e. the interior knots plus the order). The approximation and flexibility of a B-spline can be improved by increasing the order and the number of knots, respectively. Determining the knots and order is therefore a balance between a better approximation (fit) and smoothness (simplicity).

By the opportunity to add constraints to a function, functional data analysis permits incorporation of additional information based on prior knowledge, such as being positive, monotone, convex or concave (Ramsay and Silverman, 2005; Turlach, 2005). In this study, the PAR variable is known only to take non-negative values ($\text{PAR} \geq 0$). For this reason, a positivity constraint was added to ensure that the fitted functions are non-negative over the whole argument range. This was implemented through the shape constrained spline fitting method of Turlach (2005).

More extensive information on functional data analysis and B-splines can be found in Ramsay and Silverman (2005) or Ramsay et al. (2009).

Combination of functional data analysis and UPCA: the FUPCA model

Functional data analysis was in this study applied to generate a smaller set of spline coefficients (originating from the B-splines), which capture the majority of the relevant information. These new coefficients, instead of the original data, were then used for identifying the UPCA model (Chen and Liu, 2001) (Fig. 3.5), henceforth referred to as FUPCA model. This reduced the number of free parameters to be estimated as part of the PCA modelling step. Moreover, functional data analysis can handle missing data, provided that the number of missing data points is not too large. More specifically, a unique set of coefficients can be identified if at least one data point is present in each knot interval and if the total number of data points is equal or larger than the number of estimated coefficients. Therefore, days with empty subintervals were removed from the data set.

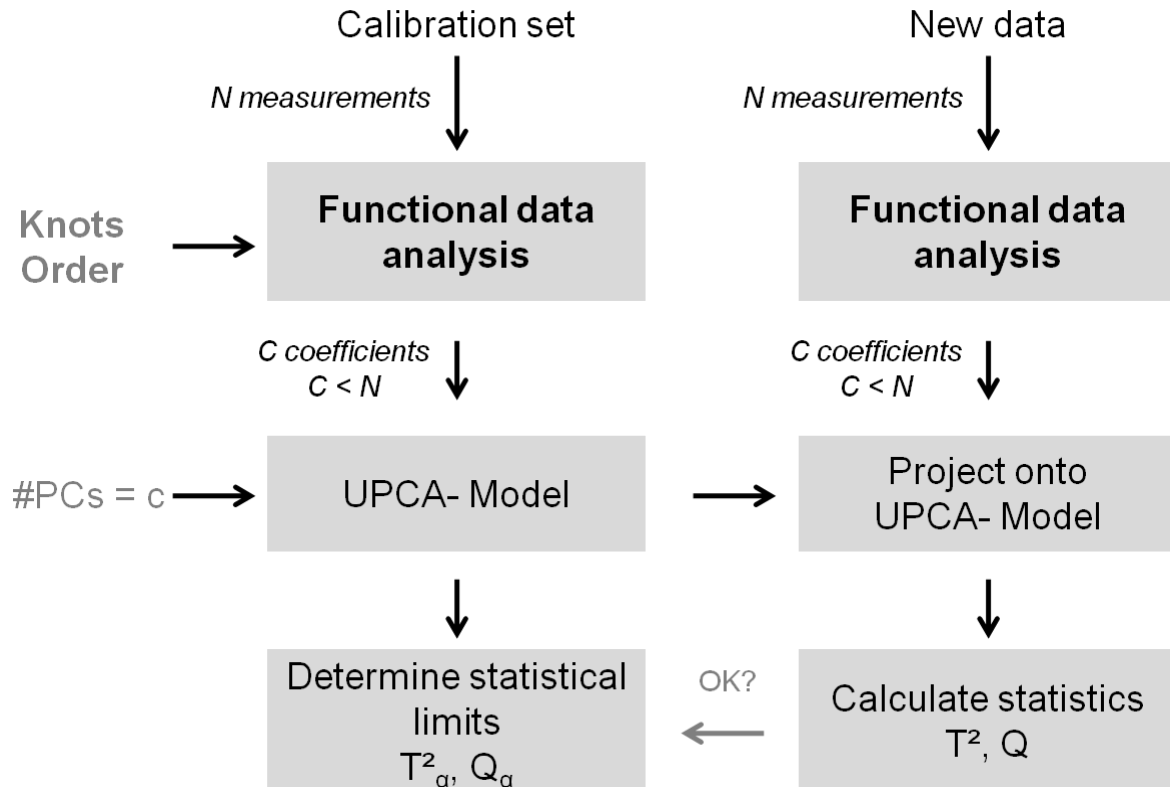


Fig. 3.5 Schematic overview of Functional Principal Component Analysis (FUPCA) for plant stress detection. A calibration set (with N measurements) is first subjected to functional data analysis. Resulting C coefficients are then used to construct a UPCA model with c principal components (PCs) and to determine statistical limits (T^2_α, Q_α). Subsequently, new data are projected onto this UPCA model after the same functional data analysis and corresponding statistics (T^2, Q) are calculated. They are finally compared with the previously determined statistical limits to determine if plant stress occurs.

It is typically assumed in PCA-based applications that the data as analysed contain only independent and identically distributed (IID) noise. Moreover, PCA models are least-squares optimal which means that the resulting model is maximum likelihood optimal only if the measurement errors are assumed to be normal (i.e. Gaussian). Unfortunately, spline function fitting is a (linear) transformation and thus results in a non-identical distribution of the errors in the spline coefficients if the original measurement errors were IID distributed. Spline fitting does preserve normality, however, since it entails a linear transformation only. To counter the effects of spline fitting on the error distribution, a whitening procedure was executed to decorrelate the errors in the spline coefficients due to measurement error in the original data. To this end, the expected correlation matrix for these errors was computed, assuming normal and IID distribution of the measurement errors in the original data. This expected correlation matrix was then

used to apply maximum likelihood scaling to the spline coefficients (Wentzell and Lohnes, 1999) prior to UPCA analysis (Hoefsloot et al., 2006).

Subsequently, to define the FUPCA model, a similar procedure as for classical UPCA modelling (Fig. 3.3) was applied. The difference is that the calibration set was first subjected to functional data analysis. Then, the resulting (smaller) set of coefficients were pre-processed by rotation, centring, scaling and unfolding and used to construct the FUPCA model. New data were projected onto this FUPCA model after the same functional data analysis and pre-processing. Corresponding statistics (Q , T^2) were calculated and finally compared with the previously determined statistical limits (with the calibration set) to determine if plant stress occurred (Fig. 3.5).

3.3 Results

3.3.1 The UPCA model

Microclimatic conditions (PAR and VPD) (Fig. 3.6A) and D (Fig. 3.6B) were monitored. The grapevine showed a net daily growth for D during the control period (DOY 133 - 165). A few days after water was withheld (DOY 165), a clear deviation in the course of D was observed. Irrigation was resumed on DOY 179 because clear visible symptoms of drought stress were detected. Although the grapevine was again well-watered during the recovery period, D showed little or no growth (Fig. 3.6B).

Calibration data (from the control period) were used to identify the UPCA model. The RV and corresponding RCV for the first 12 PCs are plotted in Fig. 3.7A and B, respectively. 60% of the total variance of the dataset was captured by the first PC. The following PCs only captured 10% or less. Since adding an extra PC would only add a small amount of explained variability, while increasing the complexity of the UPCA model, the model with one PC was selected. For all variables, large variability in the loadings of this first PC (Fig. 3.7C) was seen during the day, while the temporal variations were smaller in night time conditions (morning and evening hours, i.e. first and last data points of each variable). Indeed, Fig. 3.6 shows that most variability in PAR, VPD and D between days is found during the daytime. For instance, both sunny and cloudy days were observed, having a very different PAR

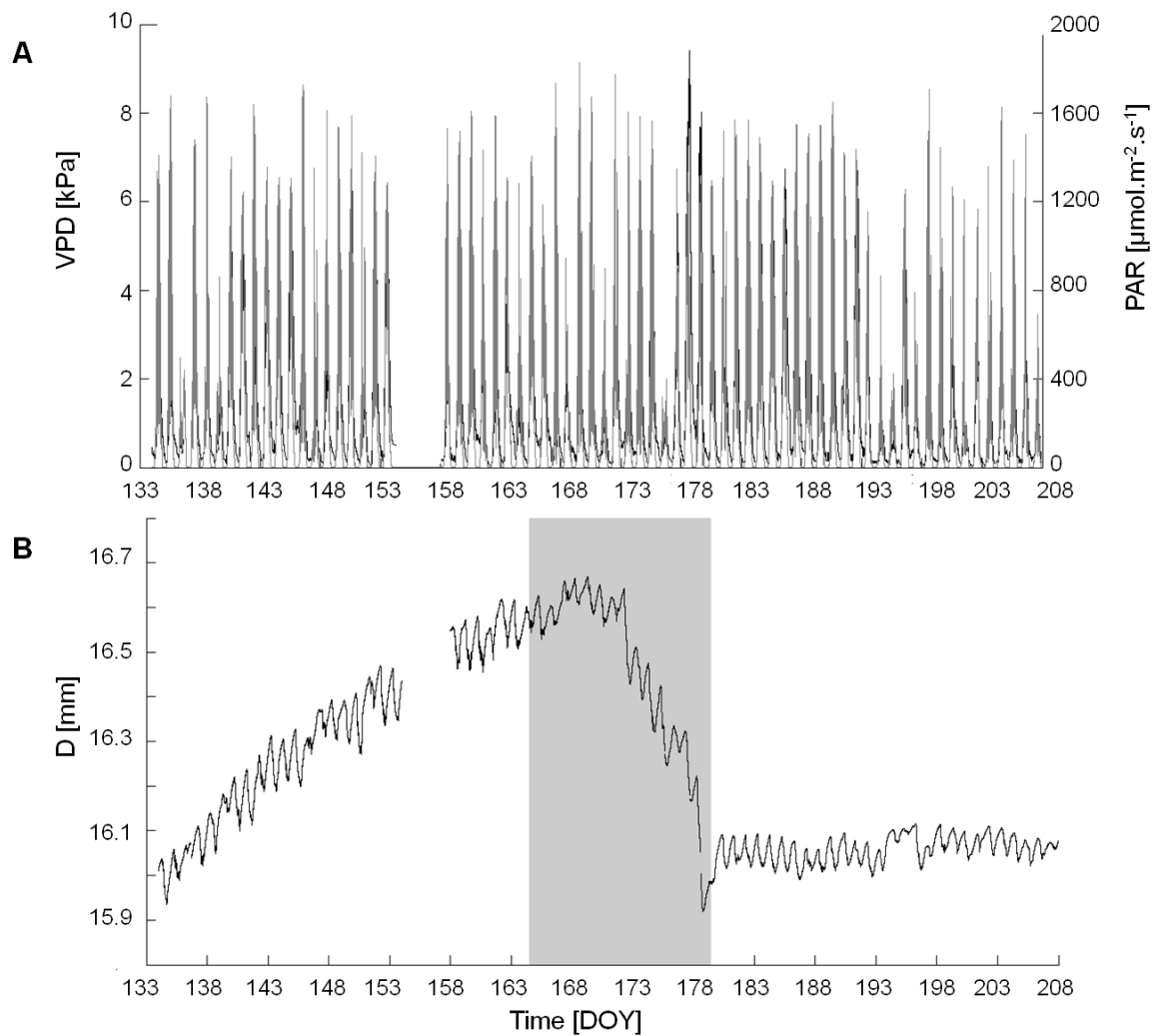


Fig. 3.6 (A) Microclimatic conditions: photosynthetic active radiation (PAR, grey line) and vapour pressure deficit (VPD, black line). (B) Stem diameter variations (D) of a drought-stressed grapevine. The grey area marks the period of drought for the stressed grapevine (DOY 165 - 179).

and VPD pattern. Since PAR and VPD are the key driving variables for transpiration, they also have an effect on the daily shrinkage and swelling of the diameter (Steppe et al., 2006). Moreover, Fig. 3.7C shows that PAR and VPD are positively correlated, while D shows a negative correlation. This negative correlation can be explained as follows: higher PAR and VPD result in higher transpiration and lower water potentials in the plant (Cruziat and Tyree, 1990; De Swaef and Steppe, 2010). If transpiration exceeds water uptake from the soil, the internal water storage is depleted and D shrinks (Tyree and Zimmermann, 2002; Steppe et al., 2006; 2012; Intrigliolo and Castel, 2007b).

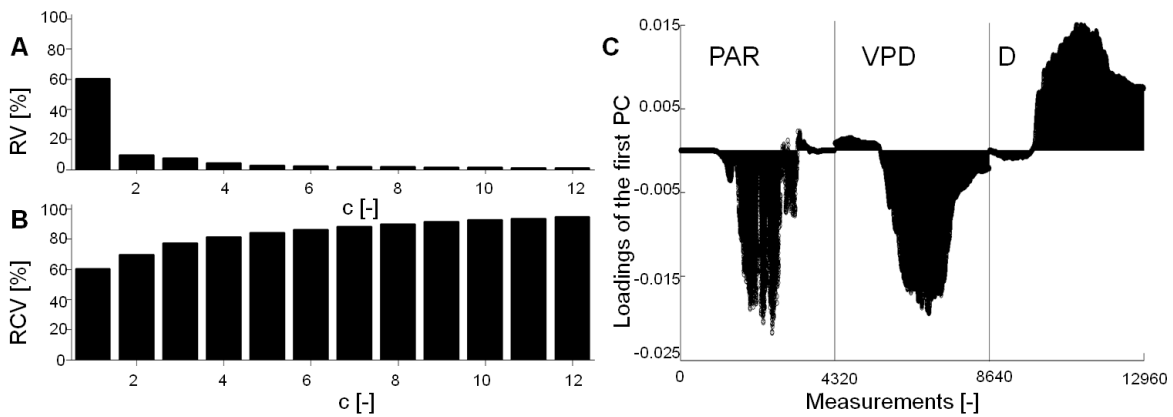


Fig. 3.7 (A) Relative variance (RV) and (B) relative cumulative variance (RCV) as a function of the number of PCs, c . (C) Loadings for all variables, i.e. photosynthetic active radiation (PAR), vapour pressure deficit (VPD) and stem diameter variations (D), of the first principal component of the UPCA model for grapevine.

3.3.2 Stress detection with UPCA

The calibration data were used to determine the statistical limit for the Q statistic and Hotelling's T^2 statistic (Q_α , T^2_α). Subsequently, statistical values for the entire grapevine dataset were calculated using the UPCA model and compared with these limits (Fig. 3.3). Both the Q statistic (Fig. 3.8A) and the Hotelling's T^2 statistic (Fig. 3.8B) stayed within their limit during the control period. The latter needs to be checked only if the Q statistic remains under its set limit, as it is designed to detect extreme events that do not violate the correlation structure. Since the Hotelling's T^2 statistic stayed within its limit, no such events were detected. The Q statistic started violating the 99% limit (Q_α) from DOY 172 until the end of the stress period, except for DOY 173 and 176, where Q did not exceed the limit, and DOY 178, which could not be monitored due to a lack of D data (Fig. 3.6B). The low Q statistics on DOY 173 and 176 can be explained by the low PAR and VPD values of those days, resulting in only a small or even negligible shrinkage of D (Fig. 3.6). On DOY 179, water supply was resumed and the Q statistic remained again below its limit from DOY 180 onward, suggesting recovery of the grapevine. UPCA could hence detect drought stress seven days before visible symptoms appeared.

3.3.3 Functional data analysis

In FUPCA (Fig. 3.5), all data were first transformed by means of B-spline basis functions. The same functional data analysis (same order and distribution of knots)

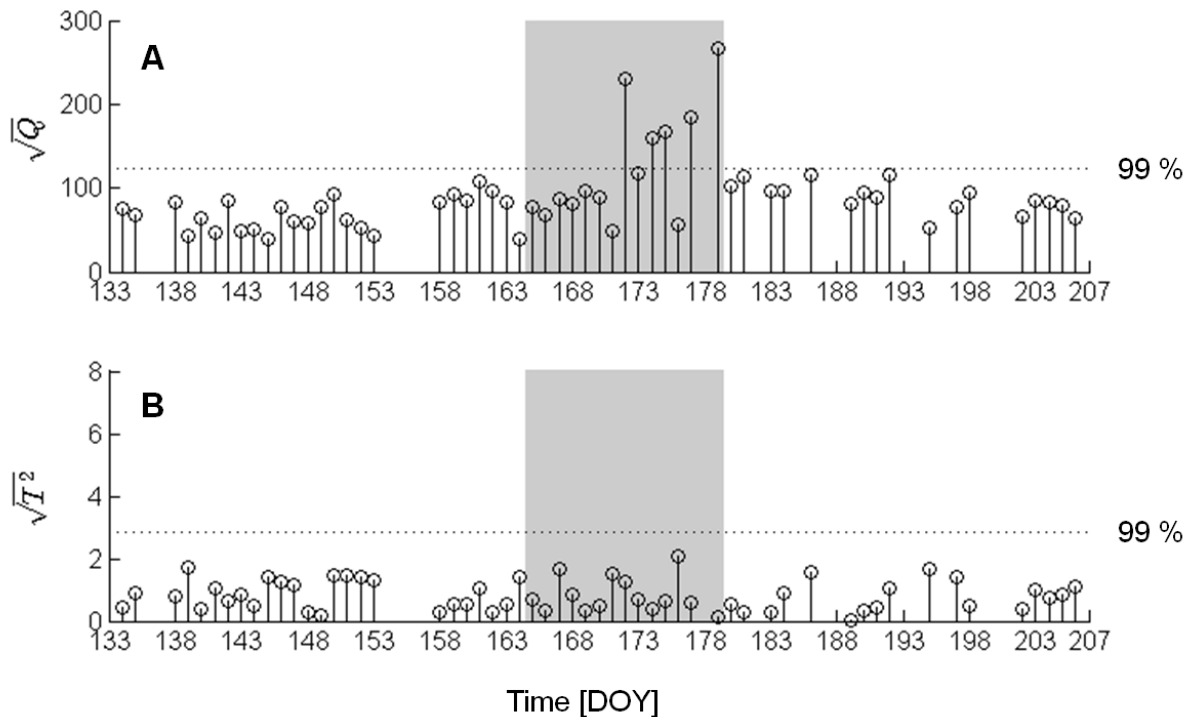


Fig. 3.8 Unfold Principle Component Analysis (UPCA) for grapevine: (A) square root of Q statistic and (B) square root of Hotelling's T^2 statistic as a function of time. The grey area marks the period of drought for the stressed plant (DOY 165 - 179), the dotted lines indicate the statistical 99% limits Q_α and T^2_α .

was performed on each variable. Different numbers of uniformly spaced knots were tested by increasing the length of the subintervals. For instance, in Fig. 3.9, third order B-splines with knots every 6 h (Fig. 3.9A) and every 6 min (Fig. 3.9B) were used to approximate one day of D. To decrease the complexity of the FUPCA model, the longest subinterval that resulted in a satisfying detection was chosen. For a subinterval of 1.5 hours, an early detection with only two false detections (i.e. detection of drought stress during a well-watered period, see below) was obtained. Also for smaller subintervals, one or two false detections were observed. When a greater subinterval was selected, four false detections or more were obtained. Therefore, a knot distribution every 1.5 h was chosen. Also different orders of the B-splines were tested. Third order B-splines were chosen because they resulted in a good data fit, while a greater order, thus also a more complex function, did not significantly improve this. Therefore, all variables were transformed with third order B-splines, knots placed every 1.5 h. This resulted in 18 coefficients per variable as input for the FUPCA model (Fig. 3.10C, discussed below).

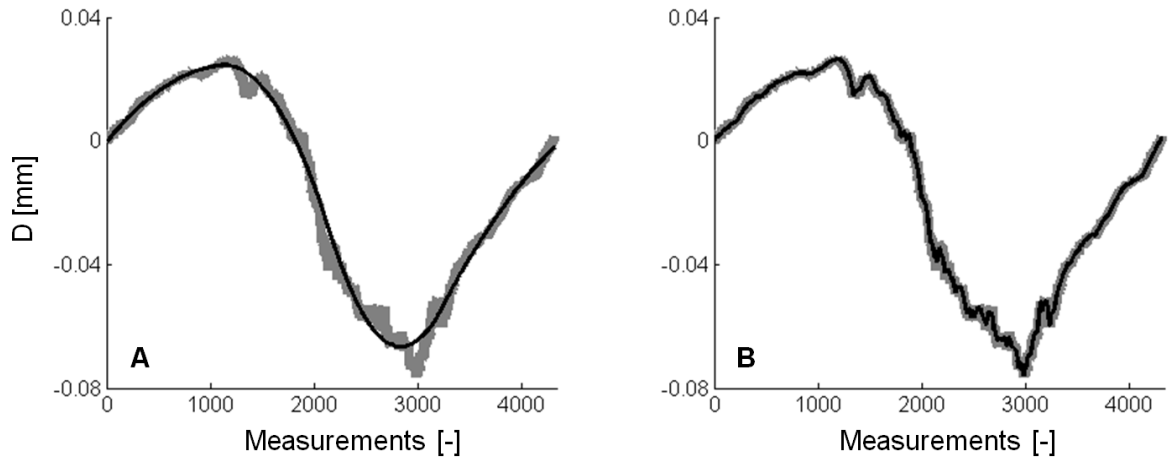


Fig. 3.9 Approximation by functional data analysis (black lines) for one day of diameter variation measurements (D , grey lines) with third order B-splines and subintervals of (A) 6 h or (B) 6 min.

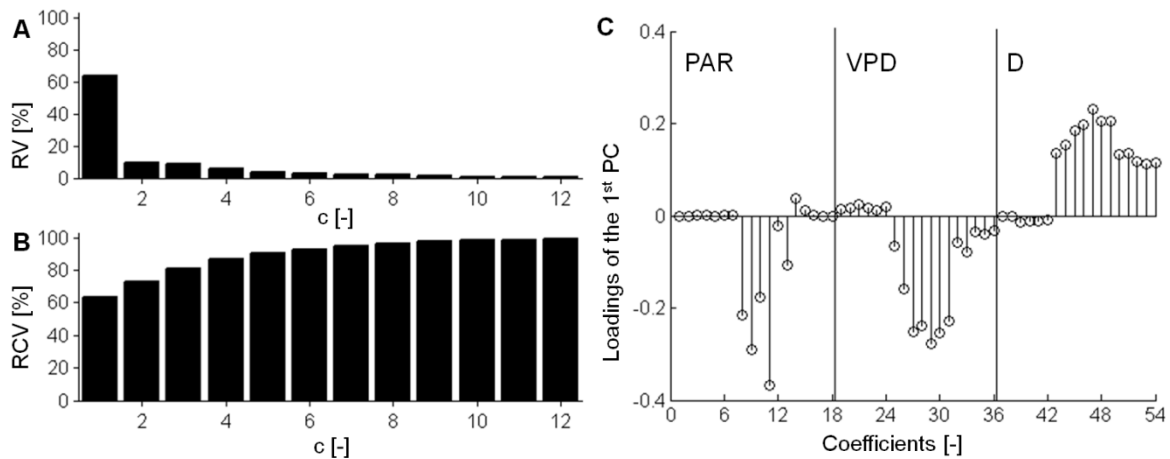


Fig. 3.10 (A) Relative variance (RV) and (B) relative cumulative variance (RCV) as a function of the number of PCs, c . (C) Loadings for all variables, i.e. photosynthetic active radiation (PAR), vapour pressure deficit (VPD) and stem diameter variations (D), of the first principal component of the FUPCA model for grapevine.

3.3.4 Stress detection with FUPCA

In Fig. 3.10A and B, RV and RCV for the first 12 PCs of the FUPCA model, based on the calibration data, are shown respectively. As in classical UPCA, the model with one PC was selected since more than 60% of the total variance of the dataset was captured with the first PC, while the following PCs captured 10% or less. For the FUPCA model, a similar loading pattern of the first PC (Fig. 3.10C) was found as for classical UPCA (Fig. 3.7C), but now with less data points per variable. This

demonstrates that a major part of the information was kept after transformation by functional data analysis, while the complexity greatly reduced.

In order to retain independent and identically distributed noise after functional data analysis, the coefficients were rotated prior to centring and scaling. Therefore, a rotation matrix was constructed, containing the variance of the variables: $246 \mu\text{mol}\cdot\text{m}^{-2}\cdot\text{s}^{-1}$ for PAR, $1.1 \cdot 10^{-4}$ kPa for VPD and $2.5 \cdot 10^{-7}$ m for D.

Next, statistical values for the complete dataset were determined and compared with the statistical limits. Fig. 3.11 shows that the Q statistic and Hotelling's T^2 statistic did not rise above their statistical limit for the entire control period. As in classical UPCA modelling, the Q statistic of the FUPCA model indicated abnormality on DOY 172. Drought stress was therefore detected by FUPCA with the same speed as with classical UPCA.

Only two false detections were found: the Q statistic was violated on DOY 181 and 193, even though those days belong to the recovery period. DOY 193 could not be monitored with classical UPCA (Fig. 3.8) because that day contained missing data.

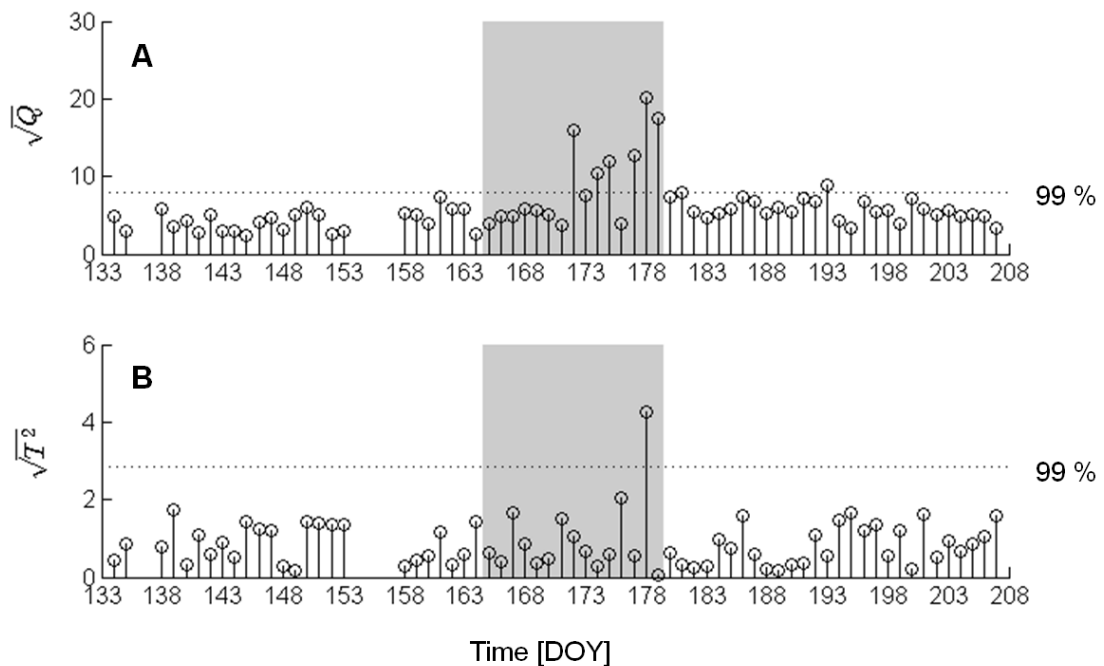


Fig. 3.11 Functional Unfold Principle Component Analysis (FUPCA) for grapevine: (A) square root of Q statistic and (B) square root of Hotelling's T^2 statistic as a function of time. The grey area marks the period of drought for the stressed plant (DOY 165 - 179), the dotted lines indicate the statistical 99% limits Q_α and T^2_α .

Moreover, the false detection on DOY 193 can be explained by the sudden increase in D (Fig. 3.6B). Because neither VPD nor PAR showed notable differences with other days, the sudden increase is caused by an irrigation event, suggesting that the grapevine might have experienced unsatisfying water availability the preceding days.

3.4 Discussion

3.4.1 UPCA and FUPCA to automatically detect plant stress

The proposed UPCA and FUPCA techniques were proven successful for early drought stress detection in grapevine because they could detect drought stress days before visible symptoms appeared (colouring and wilting of the leaves, observed on the day of resumed irrigation). Also Villez et al. (2009) successfully applied UCPA for automatic stress detection in apple tree and truss tomato. The proposed FUPCA technique of this study was tested on those datasets as well, and obtained the same results as with classical UCPA modelling (Baert et al., 2011). This suggests that both techniques will be applicable for other species as well, as long as there is a clear relationship between stem diameter variations and plant water status. The model should then be calibrated using the microclimate and stem diameter variations data of the species of interest during a well-watered period.

Detection in UPCA and FUPCA is based on statistically determining whether new data behave normally, i.e. within the limits defined by a so-called in-control model. This in-control model is abstracted from the calibration data, which are assumed to represent correlations and behaviour belonging to normal conditions (well-watered) (Venkatasubramanian et al., 2003). In fact, one can say that the FUPCA or UPCA model represents the expected pattern under normal conditions. Both techniques therefore circumvent the need of determining a reference or threshold value, which is a difficulty in other methods for automatic stress detection (Fereres and Goldhamer, 2003; Jones, 2004; Steppe et al., 2008; De Swaef et al., 2009). Such thresholds are typically set as boundary lines on monitored plant-based measurements. However, a reference measurement of the plant water status is not only influenced by soil water status, but also by microclimatic conditions

(Ortuño et al., 2010). The threshold is therefore usually based on measurements under well-watered conditions (Fereres and Goldhamer, 2003; Patakas et al., 2005) or relationships between plant responses and the water status (De Swaef et al., 2009). There is however currently not an established method to make this possible. UPCA and FUPCA represent promising alternatives (further discussed in **Chapter 4**).

The UPCA and FUPCA techniques developed in this study detect drought stress based on variations in stem diameter. It is indeed a sensitive parameter in grapevine to monitor the water status (Intrigliolo and Castel, 2007b; Ortuño et al., 2010). After veraison, however, Intrigliolo and Castel (2007b) found that there was no longer a relationship between stem diameter variations and plant water status in grapevine. The time veraison is achieved, stem growth starts to decrease independently from water status, probably because the fruits become a more important sink, and eventually stem growth ceases. Most likely, UPCA and FUPCA would detect an abnormality in that specific period, although the shrinkage in stem diameter is then not caused by drought stress, but by the characteristic behaviour of grapevine after veraison.

The lack of stem diameter growth during the recovery period (Fig. 3.6B) may be explained by the timing during the growing season, as stem diameter growth in grapevines has been observed to cease near the end of the growing season (Ton and Kopyt, 2004; Kopyt and Ton, 2005; Intrigliolo and Castel, 2007b). Hence, UPCA and FUPCA performances will be tested using data from different drought-experiments (timing during the growing season) and different seasons in **Chapter 4**.

Currently, the proposed methods are able to detect abnormality or not, but they do not yet distinguish among different levels of drought stress. This is not necessary for full irrigation management, where drought stress is systematically avoided. In deficit irrigation scheduling, however, a specific level of drought stress is often desired and intended to be maintained over a certain period of time. This might be difficult with the developed models in this study. In future research, it would be interesting to investigate whether the UPCA and FUPCA techniques can be made useful to detect different levels of drought stress in plants (discussed in **Chapter 8**).

3.4.2 Comparison of UPCA and FUPCA

For grapevine, as well as apple tree and truss tomato (Baert et al., 2011), UPCA and FUPCA techniques achieved drought stress detection with the same speed. However, if the dataset contains days with partly missing data, FUPCA modelling is able to monitor more days compared to UPCA modelling. In this study, only 6 days out of 74 needed to be removed in the FUPCA analysis (Fig. 3.11), because on these particular days the gaps of missing data were too large (mainly due to electricity failure). In UPCA, however, 18 days needed to be removed from the same data set (Fig. 3.8). Obviously, the ability of FUPCA modelling to estimate small gaps with missing data is a great advantage for fast stress detection, since more days can be monitored.

Moreover, in FUPCA, all variables were first transformed with functional data analysis to reduce the FUPCA model input. This resulted in 18 coefficients per variable (Fig. 3.10C), while the original variables consisted of 4320 data points each (Fig. 3.7C) as input for the classical UPCA model. Consequently, the FUPCA model is less complex in a statistical sense compared to the original UPCA model. As a result, FUPCA does not capture the short-term (minutes) variations in D caused by fluctuations in the microclimatic conditions (e.g. Fig. 3.9A). Despite this information loss, UPCA and FUPCA performed similarly in this study. This suggests that the information important for the effect of drought is not a matter of minutes, but spread throughout the day, which is captured well by the functional data analysis. More experiments will be performed in **Chapter 4** to confirm this hypothesis.

3.5 Conclusions

Even in temperate climates, grapevines often experience some level of drought stress during the growing season. The water status of grapevines is however of great importance for both fruit quantity and quality. To ensure an appropriate plant water status, an automatic, fast and reliable method for drought stress detection is hence needed. To this end, UPCA and FUPCA were tested and enabled successful stress detection days before visible symptoms appeared. Both methods, after calibration, can be implemented for other species as well, as was

proven for apple tree and truss tomato. It can therefore be concluded that these techniques are very promising for early plant stress detection, although further research is needed to apply UPCA and FUPCA for deficit irrigation scheduling. In grapevine, UPCA and FUPCA might detect an abnormality after veraison independently of the water status, but caused by the characteristic decreasing stem growth during that period. Although the techniques were proven successful for stress detection before veraison, additional research is needed to test the performance of both techniques across the entire growing season of grapevine. Compared to UPCA, FUPCA exhibits a lesser parametric complexity and can handle days with missing data straightforwardly.

Chapter 4

Automatic drought stress detection in grapevines without using conventional threshold values

After: Baert A, Villez K and Steppe K. 2013. Automatic drought stress detection in grapevines without using conventional threshold values. Plant and Soil. 369(1), 439-452.

Abstract

Because the water status of grapevines strongly affects the quality of the grapes and resulting wine, automated and early drought stress detection is important. Plant measurements are very promising for detecting drought stress, but strongly depend on microclimatic changes. Therefore, conventional stress detection methods require threshold values which define when plants start sensing drought stress. There is however no unique method to define these values. In this study, two techniques that overcome this limitation were proposed: Unfold Principal Component Analysis (UPCA) and Functional Unfold Principal Component Analysis (FUPCA). These two statistical methods automatically distinguish between drought and microclimatic effects, based on a short preceding full-irrigated period to extract plant behaviour under normal conditions. Both techniques aimed at detecting when measured sap flow rate or stem diameter variations in grapevine deviated from their normal behaviour due to drought stress. The models based on sap flow

rate had some difficulties to detect stress on days with low atmospheric demands, while those based on stem diameter variations did not show this limitation, but ceased detecting stress when the stem diameter levelled off after a period of severe shrinkage. Nevertheless, stress was successfully detected with both approaches several days before visible symptoms appeared. UPCA and FUPCA based on plant indicators are therefore very promising for early stress detection.

4.1 Introduction

Automated and early detection of plant drought stress is of great importance, because the plant water status greatly influences both the fruit quality and the quantity, as has been shown for tomato (De Swaef and Steppe, 2010), grapevine (Smart et al., 1990; Williams, 2000; Keller, 2010a) and fruit trees (Naor, 2006). Drought stress detection is also a key factor in accurate irrigation scheduling tools (Jones, 2007; Steppe et al., 2008).

Two plant variables used worldwide as plant water status indicator are sap flow rate (Ginestar et al., 1998; Cifre et al., 2005; Fernández et al., 2008) and stem diameter variations (Goldhamer and Fereres, 2001; Steppe et al., 2006; Intrigliolo and Castel, 2007b). Irrespective of the chosen plant-based indicator, threshold or reference values beyond which plants start sensing stress need to be defined (Fereres and Goldhamer, 2003; Jones, 2004). The difficulty with this approach is however that these threshold values are dynamic. Indeed, they are not only influenced by soil water availability, but also by microclimatic conditions (Steppe et al., 2008; De Swaef et al., 2009; De Swaef and Steppe, 2010; Ortuño et al., 2010). Therefore, it is not recommended to use one single, absolute value of any plant-based measurement as a threshold. In addition, the chosen indicator always has to be considered relative to a reference (Fereres and Goldhamer, 2003; Intrigliolo and Castel, 2006).

Two different approaches are conventionally applied for determining such a reference. In a first approach, a simultaneous reference group of plants under non-limiting water conditions is required. Stress is detected when the ratio between the chosen plant variable of the actual (stressed) plants and that of the reference (full-irrigated) plants exceeds a critical value. For instance, Patakas et al. (2005) and

Fernández et al. (2008) used a ratio based on sap flow rate measurements (SF_i/SF_{ref} , with SF_i = actual sap flow rate and SF_{ref} = sap flow rate of a reference (full-irrigated) group of plants), while Ortuño et al. (2009) and Conejero et al. (2011) based their irrigation scheduling on a ratio of maximum daily shrinkage (MDS) extracted from stem diameter variations (MDS_i/MDS_{ref} , with MDS_i = actual MDS and MDS_{ref} = MDS of a reference (full-irrigated) group of plants).

In a second approach, reference equations (baseline relationships) are defined under non-limiting soil conditions or taken from the literature. Such an equation is typically a regression between the plant variable of interest and a meteorological variable closely related to drought stress (Fernández and Cuevas, 2010). For example, Intrigliolo and Castel (2006) determined regression equations between MDS and vapour pressure deficit (VPD), air temperature or evapotranspiration as a reference for irrigation scheduling in plum trees. Similar baselines were defined for citrus (Velez et al., 2007), olive (Moreno et al., 2006) and almond trees (Ferreeres and Goldhamer, 2003), among other species.

Clearly, an unambiguous method for determination of threshold values is not yet available (Jones, 2004; Steppe et al., 2008; De Swaef et al., 2009). Moreover, both described approaches have some disadvantages. Reference equations obtained under certain conditions might not be applicable in other conditions, such as different microclimate, crop load and species size (Velez et al., 2007). The environmental variable most suitable to relate the plant variable to may change with species or cultural conditions (Velez et al., 2007). On the other hand, a full-irrigated reference group of plants is needed in the first approach, which should be often inspected to ensure that they show similar growth and appearance as the treatment plants (Goldhamer and Fereres, 2001; Fernández et al., 2008). In addition, a critical value of the SF_i/SF_{ref} or MDS_i/MDS_{ref} ratio has to be defined. This critical value may be estimated based on the observed relationship between the ratio and stem water potential or photosynthesis (Patakas et al., 2005), but is more often arbitrarily chosen based on experience (Ortuño et al., 2009; Conejero et al., 2011).

A promising alternative to overcome the difficulties of determining conventional threshold values is Unfold Principal Component Analysis (UPCA). This method is an extension of Principal Component Analysis (Wold et al., 1987; Nomikos and

MacGregor, 1994), a data mining technique developed to facilitate monitoring and diagnosing of complex, multivariate data sets (Box 3.1; Jackson, 1991). It is an efficient and commonly used method for process control (MacGregor and Kourti, 1995; Venkatasubramanian et al., 2003), but has only a few applications in plant science so far (Villez et al., 2009; **Chapter 3**). Both studies used UPCA based on stem diameter variations, photosynthetic active radiation (PAR) and VPD measurements for early drought stress detection in truss tomato, apple tree or grapevine. In **Chapter 3**, next to classic UPCA, Functional Unfold Principal Component Analysis (FUPCA) was also successfully applied for drought stress detection, i.e. UPCA in combination with functional data analysis (Chen and Liu, 2001). In both methods, an in-control model is abstracted from calibration data, i.e. data belonging to normal (full-irrigated) conditions, which represents the expected pattern and behaviour under normal conditions. Subsequently, stress detection is based on determining whether new stem diameter variations data, in combination with corresponding VPD and PAR data, behaves below the statistical limits defined by this in-control model. The UPCA and FUPCA techniques therefore circumvent the need of defining conventional threshold values, in contrast to the existing methods. Moreover, UPCA and FUPCA are techniques with simple visual readouts, which makes results easy to interpret. This is of great importance for the applicability of an automatic stress detection system (Fernández and Cuevas, 2010).

Although UPCA and FUPCA successfully detected drought stress in grapevine based on stem diameter variations, as shown in **Chapter 3**, both techniques may always detect an abnormality after veraison, irrespective of the water status. In that specific period, a characteristic shrinkage of the stem diameter can be observed in grapevines, not caused by drought, but by the fruits that are becoming a more important sink (Intrigliolo and Castel, 2007b; Ortuño et al., 2010). A possible solution may be to use another plant indicator, like sap flow rate, which remains related to the plant water status after veraison.

The aim of this chapter was therefore to investigate the performance of UPCA and FUPCA with different stress indicators during drought stress experiments on grapevine. Sap flow rate and stem diameter variations in combination with microclimatic measurements as model input were compared and evaluated. Stress

detection was investigated during two different seasons, different timing during the season and on grapevines of two different ages.

4.2 Materials and methods

4.2.1 Plant material and experimental set-up

Seven experiments (two control and five drought stress experiments) were conducted on potted grapevines (*Vitis vinifera* L.) in the greenhouse facilities of the Faculty of Bioscience Engineering of Ghent University, Belgium, during the growing season of 2010 and 2012. Henceforth, the experiment of 2010 will be referred to as repetition 1, R1, while the experiments of 2012 will be referred to as controls 1 and 2, C1 and C2, and repetitions 2 to 5, R2 to R5. All grapevines were grown in 50 L containers (0.4 m diameter, 0.4 m height) filled with DCM Mediterra compost, fertilised in summer with DCM organic fertiliser for grapes and trained according to the single Guyot system. The plants were two (C1, C2, R2 to R5) and seven (R1) years old, approximately 1.5 m high, and had stem diameters of approximately 9 to 17 mm at the beginning of the experiment. One grapevine (R1) was selected and continuously monitored during an experiment that ran from 1 July until 12 August 2010 (day of the year (DOY) 182 - 224), while six other grapevines (C1, C2 and R2 to R5) were monitored from 25 April until 14 July 2012 (DOY 116 - 196). After a control period in which the plants were at least irrigated every two to three days, irrigation was withheld for R1 to R5 to impose a period of drought stress. When clear visible symptoms of drought stress were observed (colouring and wilting of the leaves), irrigation was resumed for the stressed plants and a recovery period followed. The period of drought stress for R1 lasted from 18 until 29 July (DOY 199 - 210), DOY 199 being the last irrigation event and DOY 210 the day were irrigation was resumed. The period of drought stress for R2, R4 and R5 lasted from 11 until 28 June (DOY 163 - 180), while the period of drought stress for R3 lasted from 21 May until 4 June (DOY 142 - 156). C1 and C2 were control treatments in which the plants were continuously kept fully irrigated. An overview of the experiments can be found in Table 4.1.

Table 4.1 Overview of the Unfold Principal Component Analysis (UPCA) models based on sap flow rate (SF) or stem diameter variations (D) for the control (C1 and C2) and imposed drought stress experiments (R1 to R5) on grapevine. Time is given in day of the year (DOY).

Control or repetition	Experimental period [DOY]	Drought period [DOY]	Based on SF measurements		Based on D measurements		Day of clear visible detection [#]
			Calibration period	Day of detection [#]	Calibration period	Day of detection [#]	
2010							
R1	182 - 224	199 - 210	182 - 196 (not 192 - 194)	3	182 - 196 (not 192 - 194)	2	12
2012							
C1	116 - 196	-	116 - 162	-	116 - 162	-	-
C2	116 - 196	-	116 - 162	-	116 - 162	-	-
R2	116 - 196	163 - 180	142 - 162	10	142 - 162	10	15*
R3	116 - 196	142 - 156			116 - 141	6	15
R4	116 - 196	163 - 180	142 - 162	10	142 - 162	10	18
R5	116 - 196	163 - 180	116 - 162	16	116 - 162	18	18

*In R2, clear visible symptoms of drought stress appeared on DOY 177, while stress was imposed until DOY 180

4.2.2 Microclimatic and plant physiological measurements

The set-up for plant and microclimatic measurements is similar to the experiment explained in **Chapter 3**. Photosynthetic active radiation (PAR) was measured with a quantum sensor (LI-190S, Li-COR, Lincoln, NE, USA), air temperature (T_{air}) with a thermocouple (type T, Omega, Amstelveen, the Netherlands) and relative humidity (RH) with a RH sensor (type Hygroclip, Rotronic, Hauppauge, NY, USA) inserted in a radiation shield. Vapour pressure deficit (VPD) was calculated from RH and T_{air} as the difference between the air's potential and actual vapour pressure value. All sensors were installed inside the greenhouse near the grapevines, approximately 2 m above ground level. With exception of R3, the soil water potential (Ψ_{soil}) was measured in each container with electronic tensiometers (type SWT4R, Delta-T Devices Ltd, Cambridge, UK for R1 and type TensioTrans model 1000 C, Tensio-Technik, Geisenheim, Germany for C1, C2, R2, R4 and R5) (see experimental set-up in Fig. 3.1 and 4.1).

Sap flow rate (SF) was measured at the base of the stem of each grapevine (except for R3) with heat balance sap flow sensors (models SGA10-ws, SGEX-13 or SGB16-ws, Dynamax Inc., Houston, TX, USA). Stem diameter variations (D)

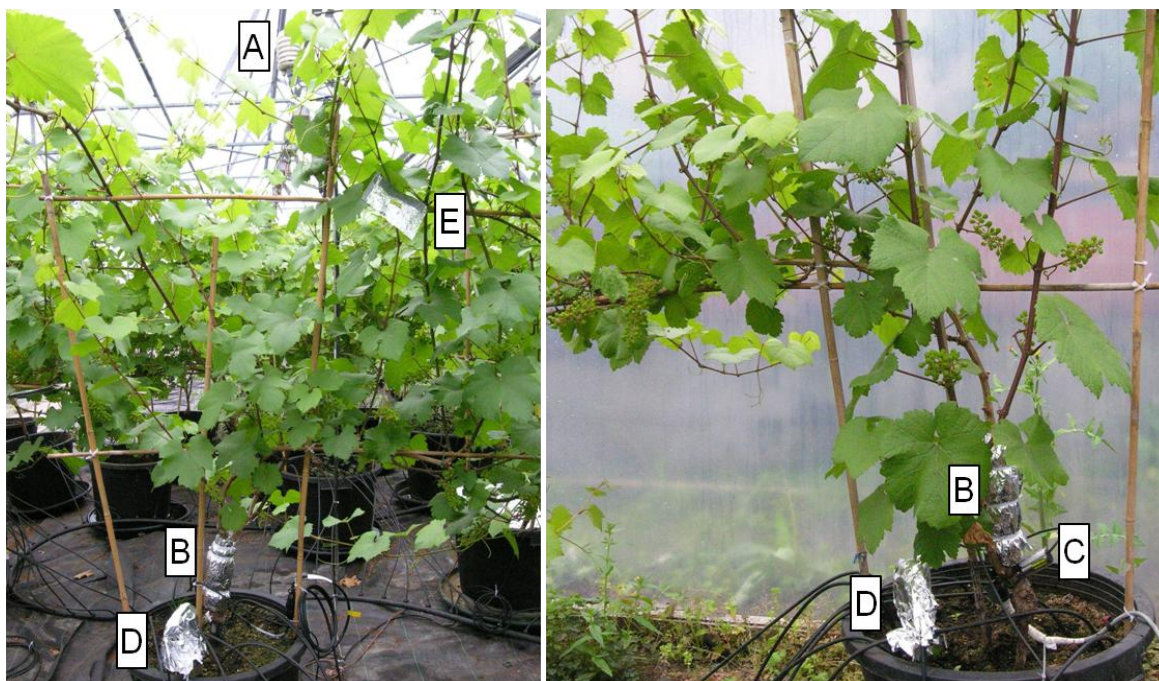


Fig. 4.1 Overview of the measurements performed during a drought experiment on grapevine: (A) microclimatic measurements (relative humidity, air temperature and photosynthetic active radiation), (B) sap flow rate, (C) stem diameter variations, (D) soil water potential and (E) stem water potential.

were measured on all monitored grapevines using Linear Variable Displacement Transducer (LVDT) sensors (model LBB 375-PA-100 and transducer bridge 8C-35, Schaevitz, Hampton, VA, USA or model DF5.0, Solartron Metrology, Bognor Regis, UK), attached to the stem just below the sap flow sensor with a custom-made stainless steel holder, for which no temperature correction is required (Steppe and Lemeur, 2004). All sensor signals were scanned every 20 s and recorded every 5 min (DAQ 34970A and multiplexer 34901A, Agilent Technologies, Diegem, Belgium). Finally, midday stem water potentials (Ψ_{stem}) were measured using a pressure chamber (PMS Instrument Company, Albany, OR, USA) at least twice a week. Occasionally, Ψ_{stem} were measured at several times during the day to examine its daily profile. Therefore, one to three mature, healthy leaves per grapevine per measurement were covered in plastic bags coated with aluminium foil for at least 2 h prior to the measurements and only detached from the plant just before the measurement (Fig. 4.1).

4.2.3 Unfold Principal Component Analysis

Principal Component Analysis (PCA) is a well-established technique for monitoring and diagnosing of processes with large, multivariate data sets, consisting of many variables with strong correlations (**Chapter 3**; Jackson, 1991; Kourti, 2002; Venkatasubramanian et al., 2003). In this chapter, two different sets of analysed data of microclimatic and plant physiological measurements were included as input for PCA modelling. In a first approach, PAR, T_{air} and VPD were combined with SF measurements as input, while in a second approach the same microclimatic measurements were combined with D measurements. Thus, two PCA models were constructed for each experiment. In both approaches, measurements were organised in a three-dimensional matrix X ($I \times J \times K$), in which I stands for the day it was taken, J for the time within the day and K for the variable. Since PCA is not able to handle such three-dimensional data sets, it is necessary to use an extension of PCA, Unfold Principal Component Analysis (UPCA). A detailed description of UPCA, which was first proposed by Wold et al. (1987), can be found in Nomikos and MacGregor (1994). Specific details of PCA-based methods implemented for on-line stress detection in plants are given in **Chapter 3** and Villez et al. (2009).

For R1, the data collected in the period from DOY 182 until 196 (irrigated control period) were used for calibration (I_{cal}) of the UPCA models. As UPCA cannot deal with missing data by default, one day (DOY 194) was omitted from the data set. The missing data was the result of an electricity failure. In addition, DOY 192 and 193 were not included in I_{cal} due to a too negative Ψ_{soil} (discussed below). As a result, the calibration data set included 12 days ($I_{cal} = 12$). Furthermore, $I = 42$ days, $J = 288$ measurements (measurement value every 5 min) and $K = 4$ variables (SF or D, PAR, T_{air} and VPD) in both UPCA approaches. Data from DOY 116 until 162 were used as calibration period for C1, C2 and R5, while data from DOY 142 until 162 were used to calibrate the models of R2 and R4 (Table 4.1).

Data pre-processing

Prior to UPCA, the data were pre-processed in a similar manner as explained in detail in **Chapter 3**. All data were centred column-wise (Fig. 3.2A) to zero mean and divided by the overall standard deviation of the data for that given sensor. This group scaling or single-slab scaling (Fig. 3.2B) (Gurden et al., 2001) was followed by batch-wise unfolding (Fig. 3.2C) to transform the three-way data set ($I \times J \times K$) into a two-way matrix ($I \times J \cdot K$). A single row now represented all and exclusively data of one single day (0-24 h). After pre-processing, the data were suitable for PCA modelling, henceforth referred to as UPCA modelling.

Stress detection with the UPCA model

As explained in **Chapter 3**, a majority of the existing variation in the microclimatic and plant physiological data can be captured well by a smaller set of new variables. Those new variables, called principal components (PCs), are constructed based on the calibration data and are uncorrelated and orthogonal linear combinations of the original variables. A larger proportion of variance of the original data is captured by the model if a larger number of PCs (# PCs or c) is retained (Johnson and Wichern, 2002). This proportion of total variance captured by a single PC is referred to as relative variance (RV), while the relative cumulative variance (RCV) is the proportion of variance captured by the first c PCs. As a result, identification of the UPCA model boils down to the assessment of the number c . The in-control UCPA model, which is abstracted from calibration

data, can be interpreted as the construction of a relationship between the new variables to obtain a profile of expected, normal conditions.

Two conventional statistics are applied for statistical stress monitoring: the Q (sum of squared residuals, Eq. 3.1) statistic, which measures the goodness of the model fit, and the Hotelling's T^2 statistic (weighted sum of squared scores, Eq. 3.2), which is a measure for the distance between the reconstructed data and the origin (Hotelling, 1947; Johnson and Wichern, 2002). The upper control limit of both statistics is determined based on the calibration data. If the upper control limit of the Q statistic is violated, residuals are believed not to result from random effects only and thus indicate abnormality. The Hotelling's T^2 statistic, however, assumes the use of otherwise normal data, accounting for variation within the modelled space (linear subspace defined by the c selected eigenvectors), and is therefore typically useful to detect extreme events which do not violate the correlation structure as identified via the first c eigenvectors of the covariance matrix. To this end, the Q statistic is first evaluated, and only when this statistic remains below its set limit, the Hotelling's T^2 is checked against its proper limit. Nevertheless, the Hotelling's T^2 statistic can always be computed. Determining whether drought is detected in new data is done by pre-processing these data in the same manner and projecting them onto the UPCA model. Corresponding statistics (Q, T^2) are then compared with the previously determined statistical limits (Q_α , T^2_α) (Fig. 3.3). If one of the limits is exceeded, it indicates abnormality (drought stress) for the corresponding day.

4.2.4 Functional Unfold Principal Component Analysis

In FUPCA (first introduced by Chen and Liu (2001)), data are transformed by functional data analysis prior to UPCA modelling. With functional data analysis, the single daily time series of the original variables (SF or D, PAR, T_{air} and VPD) are approximated by linear combinations of a set of known basis functions. Consequently, the data are now represented by a smaller number of parameters than the amount of original data points. The UPCA model is identified using the fitted coefficients instead of the original data, with the same procedure as for classic UPCA modelling (removal of D net growth if applicable, centring, scaling and unfolding). The dimensionality of the input data for the UPCA model is thus strongly reduced. The resulting FUPCA model is, hence, less complex in a

statistical sense compared to the classic UPCA model, while preserving the ability to easily monitor a process and detect abnormalities. Moreover, functional data analysis has the advantage that gaps with missing data can be approximated if not too large, i.e. each knot interval should have at least one data point.

As in **Chapter 3**, the B-spline basis was chosen to construct a family of spline functions. Each available function consists of a linear combination of several splines, in this case B-splines. B-splines can be computed fast, exhibit great flexibility, and data can often be approximated by using only a small number of them (Ramsay and Silverman, 2005). The order (n) of the B-splines defines its degree ($n-1$). A complete day (0-24 h) is divided into equal-length intervals by placing knots uniformly over the argument range (e.g. every i^{th} hour of a day). The locations of these knots determines the location and width of the B-splines, and the successive intervals over which the function is to be fitted to the original data. The number of coefficients to define a B-spline depends on the number of knots (k) and the order ($\# \text{ coefficients} = n + k - 2$) (Ramsay and Silverman, 2005).

Third order B-splines were chosen with a knot distribution every 1.6 h, which resulted in 17 coefficients per variable as input for the FUPCA models. Gaps with missing data could be approximated using this functional data analysis, therefore no days needed to be excluded from the data set of R1, while only one day (DOY 158) needed to be removed from the other data sets (C1, C2, R2 to R5). For calibration of the FUPCA models, the same days as for UPCA were used. For instance, $I = 43$ days, $I_{\text{cal}} = 12$ days, $J = 17$ data points (instead of 288 measurements) and $K = 4$ variables in both FUPCA approaches for R1.

A detailed description of functional data analysis and B-splines can be found in Ramsay and Silverman (2005) or Ramsay et al. (2009). More information on the application of FUPCA for stress detection in plants is given in **Chapter 3**.

4.3 Results

4.3.1 UPCA and FUPCA for drought stress detection

Microclimatic and plant physiological measurements

PAR, T_{air} and VPD during the drought stress experiment in 2010 (R1) are shown as an example in Fig. 4.2, the conditions during the other experiments were similar (Appendix Fig. S1). During the control period of R1 (DOY 182 - 199), the grapevine showed high SF and a daily net growth for D (Fig. 4.3A, B), except for DOY 192, 193 and 199. This is in agreement with the low Ψ_{soil} on those days (Fig. 4.3C). A few days after the last irrigation event (DOY 199), a clear deviation in both SF and D was observed. Midday stem water potentials (Ψ_{stem} , Fig. 4.3C) of -1.5 to -1.7 MPa were measured by the end of the stress period. From DOY 203 onward, the Ψ_{soil} sensor failed due to dehydration of the soil exceeding values of -0.08 MPa, which is beyond the sensor detection limit. Irrigation was resumed on DOY 210 as clear visible symptoms of drought stress were observed. In the following recovery period, SF and D recovered and midday Ψ_{stem} returned to -0.4 MPa on DOY 211. For C1, C2 and R2 up to R5, the grapevines were monitored earlier in the season (DOY 116 - 197). Therefore, low SF and zero or low daily net growth of D occurred at the beginning of the experiments, increasing thereafter along with canopy development (Fig. S2, S4, S6, S9, S11 and S13). When irrigation was withheld in R2 to R4, similar effects as in R1 were observed, i.e. ceased daily net growth of D, followed by shrinkage, and decreased SF and Ψ_{stem} as a result of decreasing Ψ_{soil} . In R5, however, the effects on SF, D and Ψ_{stem} were rather weak (Fig. S13). In the control treatments, daily net growth of D and high SF were maintained during the entire experimental period and Ψ_{stem} did not exceed -0.58 and -0.68 MPa in C1 and C2, respectively, because Ψ_{soil} was kept above -0.01 MPa (Fig. S2, S4).

Determination of the UPCA and FUPCA models

The RV and corresponding RCV for the first eight PCs of the UPCA model based on SF for R1 are shown in Fig. 4.4A and B, respectively. 49% of the total variance of the dataset was captured by the first PC, while the second PC captured 22%. The following PCs only captured 8% or less. In FUPCA based on SF of R1, the

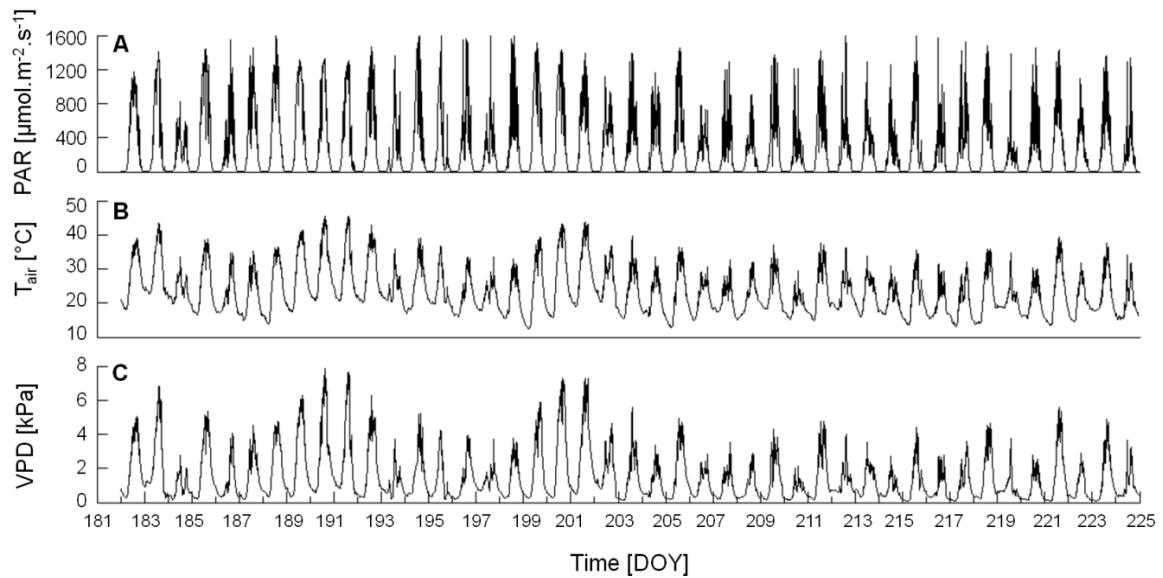


Fig. 4.2 Microclimatic conditions: (A) photosynthetic active radiation (PAR), (B) air temperature (T_{air}) and (C) vapour pressure deficit (VPD) during the experiment in 2010 as an example (R1). Time is given in day of year (DOY).

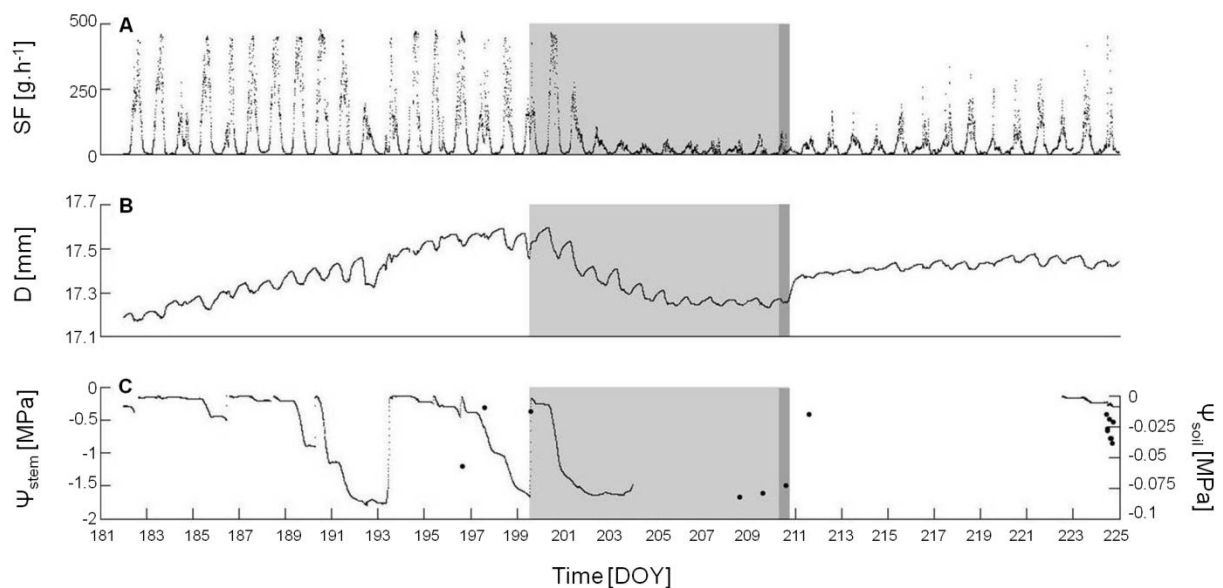


Fig. 4.3 (A) Sap flow rate, SF, (B) stem diameter variations, D, (C) stem water potential, Ψ_{stem} and soil water potential, Ψ_{soil} of the drought-stressed grapevine in R1 as an example. Time is given in day of the year (DOY). The grey area marks the period of drought stress for the plant (DOY 199 - 210), the dark grey area the day of resumed irrigation, until the irrigation event.

first and second PC captured 48% and 26%, respectively. Therefore, both models with two PCs were selected since they captured 71% and 74% of the variance, while adding extra PCs would only add little to the explained variability and would increase the complexity of the models.

The loadings (coefficients) of this first PC of UPCA (Fig. 4.4C) and FUPCA showed a predominantly negative value for all four variables. This indicates that a positive effect on PAR, T_{air} and VPD also has a positive effect on SF. The loadings also indicate a large variability during the day, while the variability is smaller during night. This is in accordance with the high variability found in microclimatic conditions and SF (Fig. 4.2, 4.3A). Indeed, both sunny and cloudy days prevailed during the measurement campaign, with distinct PAR, T_{air} and VPD patterns and

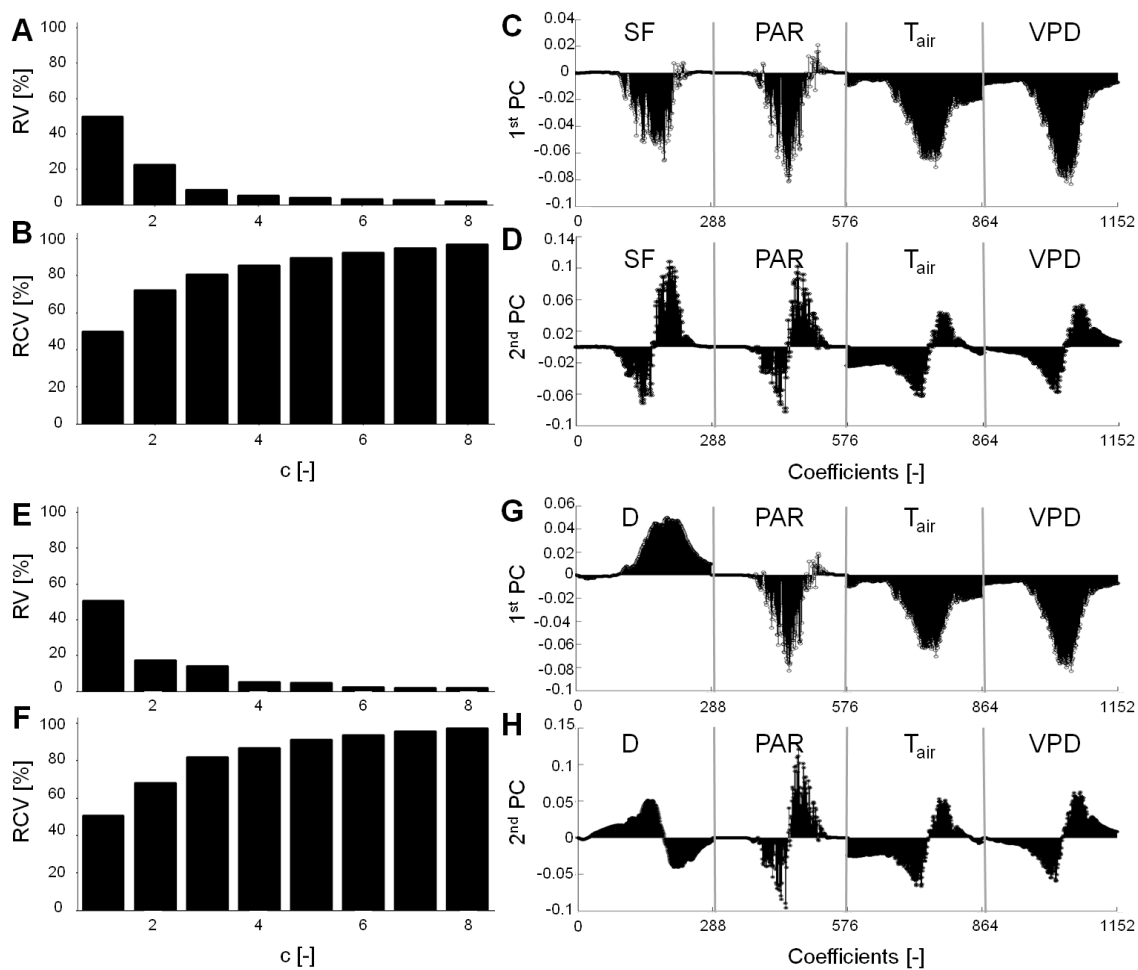


Fig. 4.4 Typical (A) relative variance (RV) and (B) relative cumulative variance (RCV) as a function of the number of principal components, c , of an Unfold Principal Component Analysis (UPCA) model based on sap flow rate (SF) measurements (R1). Loadings for all variables, i.e. SF, photosynthetic active radiation (PAR), air temperature (T_{air}) and vapour pressure deficit (VPD) are shown for the (C) first and (D) second principal component of this UPCA model based on SF. Typical (E) RV and (F) RCV of an UPCA model based on stem diameter variations (D) measurements (R1). Loadings for all variables, i.e. D, PAR, T_{air} and VPD are shown for the (G) first and (H) second principal component of this UPCA model based on D.

thus distinct SF patterns. In Fig. 4.4D, the loadings of the second PC of the UPCA model showed a wavelike pattern for all variables.

Similar results were found for the identification of the UPCA and FUPCA models based on D for R1. RV (Fig. 4.4E) and corresponding RCV (Fig. 4.4F) of the UPCA model showed that the first and second PC captured 50% and 17% of the total variance of the dataset, respectively, while the following PCs captured 13% or less. For FUPCA 48% and 20%, respectively, were captured by the first and second PC (data not shown). Therefore, both models with two PCs were selected, capturing, respectively, 67% and 68% of the variance, exhibiting sufficient explained variability and maintaining an acceptable complexity. In contrast to SF, a positive change in PAR, T_{air} and VPD resulted in a negative change in D (Fig. 4.4G, loadings of the first PC for the UPCA model). Similar to the loadings of the second PC for the SF models, the loadings of the second PC for the D models (Fig. 4.4H, loadings for the UPCA model) showed a wavelike pattern.

Finally, UPCA and FUPCA models based on SF and D, each in combination with PAR, T_{air} and VPD, were constructed for the remaining experiments: C1, C2 and R2 to R5. Data of the specific experiments were used for calibration of the models (Table 4.1). Similar to R1, two PCs were selected for all the models, capturing 56% to 75% of the variance existing in the data.

Stress detection with UPCA and FUPCA based on SF

The Q and Hotelling's T^2 statistical values (Q , T^2) of the UPCA and FUPCA models based on SF were calculated each day and compared with their corresponding statistical limits (Q_{α} , T^2_{α}) determined by the corresponding calibration data.

While the T^2 statistics were never violated in R1 (and therefore not shown), the Q statistic of UPCA (Fig. 4.5A) and FUPCA (Fig. 4.5B) remained below their limits during the control period, except on DOY 192 and 193. On DOY 192 and at the start of DOY 193, very low Ψ_{soil} and SF (Fig. 4.3) occurred, resulting in an abnormality detection by both models. This indicates that an irrigation event every two or three days was insufficient in that period. During the stress period (DOY 199 - 210), the Q statistics of both UPCA and FUPCA exceeded their 99% limit on DOY 201, 203, 205, 209 (plus DOY 208 for FUCPA), indicating abnormality (drought stress) while no visible symptoms of stress could yet be detected. On the

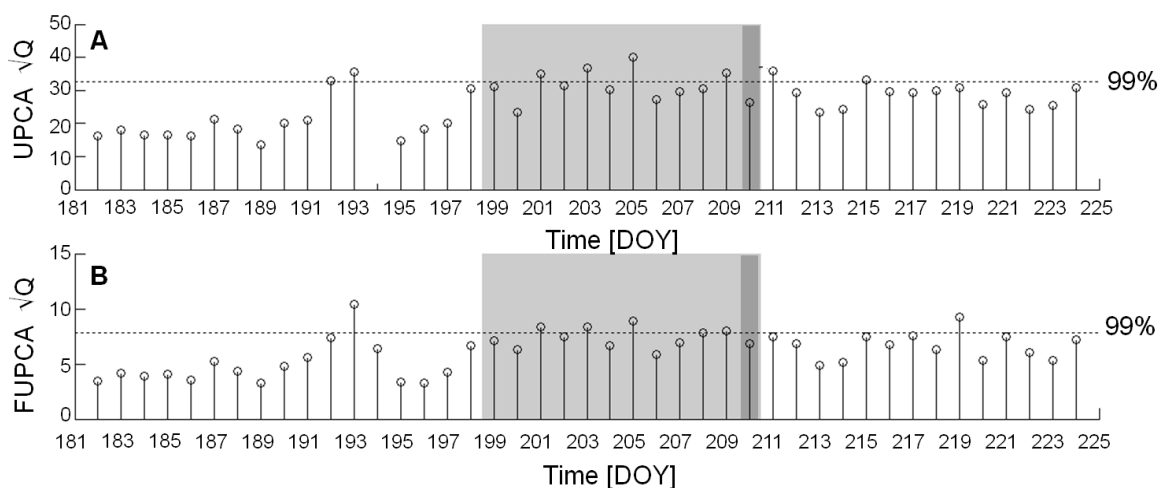


Fig. 4.5 Square root of Q statistic as a function of time (in day of year, DOY) of (A) Unfold Principal Component Analysis (UPCA) and (B) Functional Unfold Principal Component Analysis (FUPCA) based on sap flow rate (SF) for R1 as an example. In both cases, the square root of the statistic is given, enabling a better distinction between values close to the statistical 99% limits Q_{α} (dotted lines). The grey area marks the period of drought stress for the plant (DOY 199 - 210), the dark grey area the day of resumed irrigation.

remaining days, where low SF occurred simultaneously with lower PAR and VPD (Fig. 4.2), the Q statistics did not exceed their limit for both UPCA and FUPCA. When water supply was resumed, the Q statistics remained below their limit (except for one or two days), suggesting recovery of the grapevine.

Other drought stress experiments, i.e. R2 and R4 (Fig. S6-S7, S11-S12), supported the above mentioned results: the Q statistics of the UPCA models exceeded the 99% limit ten days after the last irrigation event. Clear visible stress symptoms were only detected five to eight days later (Table 4.2). Detection failed in both experiments on DOY 173 and DOY 176, when lower SF was observed in combination with lower PAR and VPD, as was also seen in R1. No UPCA model based on SF could be constructed for R3 since SF was not measured. For R5, UPCA only detected abnormality on DOY 178 and 180 (Table 4.2), since SF only showed a small decrease toward the end of the stress period (DOY 163 - 180). Also the absence of shrinkage in D and the fact that Ψ_{stem} never decreased below -0.7 MPa, suggested that this grapevine may not have been greatly influenced by the imposed stress, despite the prevailing low Ψ_{soil} down to -0.08 MPa.

With FUPCA, similar results as with UPCA were found for R4 and R5: abnormality was detected one day earlier using FUPCA in R4, while the FUPCA model of R5 only detected an abnormality on DOY 180. In R2, UPCA scored however better

than FUPCA, since the latter detected abnormality on the same day but failed to detect abnormality on DOY 174, 175 and 177 (Table 4.2).

During the control treatment C1, the Q statistical 99% limit was not exceeded, except for three false detections with UPCA and two ones with FUPCA, while the statistical 99% limit of C2 was never violated with both models. This resulted from the normal SF, D, Ψ_{soil} and Ψ_{stem} behaviour that was observed for C1 and C2 (Fig. S2 to S5).

Stress detection with UPCA and FUPCA based on D

The Q statistical values of the UPCA and FUPCA model based on D of R1 as an example are shown in Fig. 4.6A and B, respectively. The Hotelling's T^2 statistics were never violated and therefore not shown. The Q statistics remained below their limit during the control period, except on DOY 192, 193 and 198. This again can be explained by the low Ψ_{soil} causing a more pronounced shrinkage in D (Fig. 4.3B, C). This confirmed the detection by both models based on SF. During the stress period of R1, the Q statistics of UPCA and FUPCA based on D started violating Q_{α} from DOY 200 until 204. Toward the end of the stress period, the Q values no longer exceeded their 99% limit (except on DOY 210 for FUPCA) although drought stress was still ongoing. D was characterised by a pronounced overall decrease at the beginning of the drought stress period, but this levelled off after a couple of days, explaining the behaviour of the models. On DOY 210, water supply was resumed and the Q statistics remained below their limit afterward, suggesting a recovery, which is in agreement with the increase in D.

In drought stress experiments R2, R3 and R4, the Q statistics of the UPCA models started to exceed the 99% limit six to ten days after the last irrigation event (Table 4.2, Fig. S8, S10, S12). Again, when D levelled off after a couple of days, Q values did no longer exceed their limit, in spite of the continued drought stress. The Q values generally exceeded their limit on the last day of the stress period, i.e. on the transition day with resumed irrigation in the late afternoon, since this had a pronounced effect on D. This was correctly detected by most models as an abnormality. In R5, this was however the only detection (Table 4.2, Fig. S14).

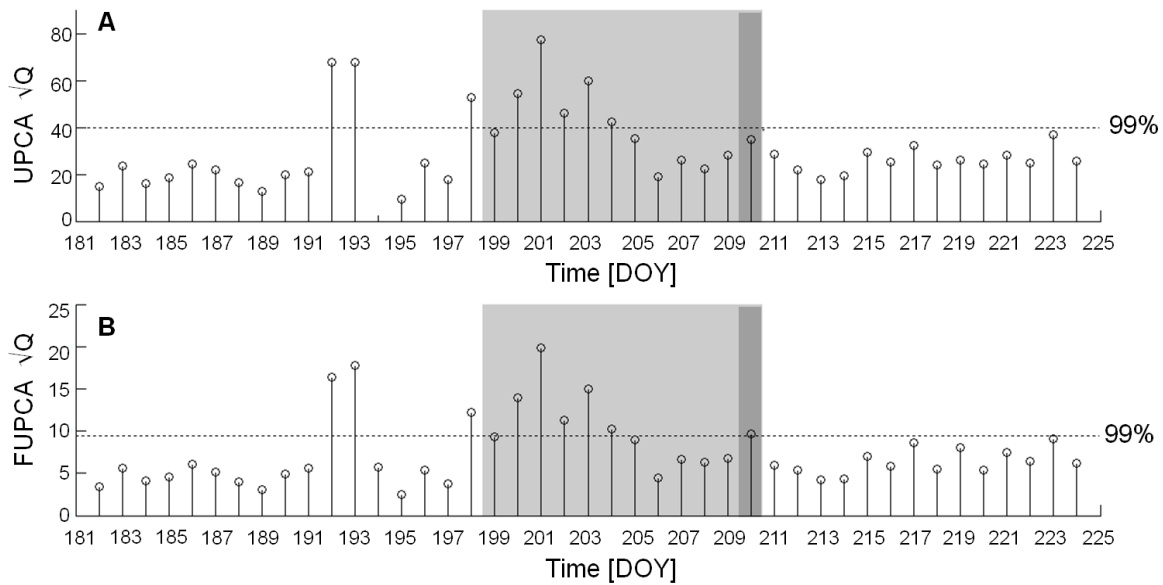


Fig. 4.6 Square root of Q statistic as a function of time (in day of year, DOY) of (A) Unfold Principal Component Analysis (UPCA) and (B) Functional Unfold Principal Component Analysis (FUPCA) based on stem diameter variations (D) for R1 as an example. In both cases, the square root of the statistic is given, enabling a better distinction between values close to the statistical 99% limits Q_{α} (dotted lines). The grey area marks the period of drought stress for the plant (DOY 199 - 210), the dark grey area the day of resumed irrigation.

The results with FUPCA for R2 to R5 were quite similar to the results obtained with UPCA, except for R3 (Table 4.2). In R3, the FUPCA model detected abnormality from DOY 147 to 151, DOY 149 not included, while UPCA detected drought continuously from DOY 147 to 153.

The Q and T^2 statistics of the UPCA and FUPCA models based on D of C1 and C2 were never violated, which is in agreement with a successful control treatment (Fig. S3, S5).

4.3.2 Selection of the calibration period

Another, shorter calibration period was selected in R2 and R4 (Table 4.1). This new calibration period started at DOY 142, when flowering began and leaf canopy was fully developed. Higher SF and more pronounced growth characterised this period (Fig. S6, S11). This particularly resulted in a better detection using SF, and a slight improvement when using D (Fig. S7 and S8, respectively).

4.4 Discussion

4.4.1 Loadings of the principal components

The loadings of the first PCs showed that a positive effect on PAR, T_{air} and VPD had a similar effect on SF, while the contrary was observed for D (Fig. 4.4C and G, respectively). Since PAR and VPD are the key driving variables for transpiration (Jones, 1992; De Swaef et al., 2009), higher PAR and VPD result in higher SF. On the other hand, higher transpiration also results in lower water potentials in the plant (Cruziat and Tyree, 1990; De Swaef and Steppe, 2010). Subsequently, if transpiration exceeds root water uptake, the internal water storage pool is depleted, which results in a shrinkage of D (Steppe et al., 2006; Intrigliolo and Castel, 2007b; Steppe et al., 2012).

A more complex pattern for all variables was observed for the second PCs (Fig. 4.4D, H). Villez et al. (2009) found a similar wavelike pattern for the second PC in their UPCA models for apple tree and truss tomato. Multiplying the main trajectory of the second PC with an arbitrary chosen positive multiple resulted in a forward shift in time of the peaks in PAR and VPD measurements compared to the mean trajectories, as well as a drop in D measurements. A negative multiple resulted in a backward shift of the trajectories (e.g. Fig. 7 in Villez et al. (2009)). Therefore, the authors suggested a temporal variability in the daily cycles captured by the second PC. Also in other cyclic processes, such as weather station data or gait cycles of children, behaviour of the second PC was attributed to a time shift or temporal effect (Ramsay and Silverman, 2005).

4.4.2 UPCA and FUPCA for drought stress detection

UPCA and FUPCA based on SF detected the first symptoms of drought stress five to nine days before any visible signs were noticed, but some difficulties arose with distinguishing low soil water availability from low atmospheric water demand on cloudy days. Indeed, low SF may result from low soil water availability, but also from a low water demand by the atmosphere (low PAR and VPD). For instance, Fig. 4.3A shows that also on fully irrigated days, lower PAR and VPD (Fig. 4.2) resulted in lower SF. Since this dependency was included in the calibration of the models, they did not detect any abnormality when low SF occurred in combination with lower atmospheric demand.

Table 4.2 Overview of the difference in drought stress detection between Unfold Principal Component Analysis (UPCA) and Functional Unfold Principal Component Analysis (FUPCA) based on measurements of sap flow rate (SF) or stem diameter variations (D) for the control (C1 and C2) and imposed drought stress experiments (R1 to R5) on grapevine. Time is given in day of the year (DOY), underlined values highlight differences between UPCA and FUPCA.

Control or repetition	Drought period [DOY]	Detected days based on SF measurements		Detected days based on D measurements	
		UPCA	FUPCA	UPCA	FUPCA
2010					
R1	199 - 210	201, 203, 205, 209	201, 203, 205, <u>208</u> , 209	200 - 204	200 - 204, <u>210</u>
2012					
C1	-	-	-	-	-
C2	-	-	-	-	-
R2	163 - 180	172, 174, 175, 177, 178 - 180	172, 178 - 180	172, <u>174</u> , 175, 177, 180	172, 175, 177, 180
R3	142 - 156			147, 148, <u>149</u> , 150, 151, 152, 153	147, 148, 150, 151
R4	163 - 180	172, <u>174</u> , 175, 177 - 180	<u>171</u> , 172, 175, 177 - 180	172, <u>174</u> , 175, 177, 180	172, 175, 177, 180
R5	163 - 180	<u>178</u> , 180	180	180	-

Models based on D performed much better in these situations, but stopped detecting stress as soon as the measured stem diameter levelled off several days after initiation of severe drought stress, as was clearly observed in R1 (Fig. 4.3B, 4.6) and in a lesser extent in R2, R3 and R4 (Fig. S6 to S12). Water storage pools were largely emptied by then and could no longer be recharged during the night, causing a less pronounced stem shrinkage and swelling pattern compared to the start of the drought stress (Fernández and Cuevas, 2010). This caused the models to indicate that plant behaviour returned to normal. Also in past studies, it has been observed that maximum daily shrinkage of measured stem diameter decreased, and even became smaller than those of the control when the drought cycle was applied long enough (Klepper et al., 1973; De Swaef et al., 2009; Ortuño et al., 2010). The purpose of the proposed techniques was however to detect drought stress at an early stage, in the context of an early-warning system, which was achieved five to seven days before the diameter started to level off and five to ten days before visual drought stress symptoms appeared. In addition, the ability to warn for deviating D behaviour due to insufficient irrigation (e.g. warnings during the control period of R1) was demonstrated. Above remarks indicate that a certain level of experience is in any case preferable to make a good evaluation of the model output. The end-user must have the capability to assess the model performance and reliability. The end-user should be able to link the results to microclimatic conditions or past events and evaluate whether plant recovery is the plausible cause if the model output returns to normal conditions.

Only in R5, the models were not able to detect drought stress (Fig. S13, S14). Examination of the plant-physiological data of R5 suggests that this particular grapevine was not greatly affected by drought, even though irrigation was withheld for 18 days. Indeed, D barely shrank, SF only slightly diminished and Ψ_{stem} never decreased below -0.7 MPa, a value close to -0.63 MPa measured during the control period (Fig. S13). Also visibly, the grapevine appeared to be healthy, since only two leaves were coloured by the end of the drought period. The behaviour of this grapevine was hence in great contrast with the other grapevines. The unexpected response of R5 illustrates the possible existence of plant-to-plant variability in response to drought stress, already mentioned by others for various species, including grapevines (Naor, 2006; Velez et al., 2007; Fernández and

Cuevas, 2010; Montoro et al., 2012). It is therefore recommended to always monitor a representative plant when automatic drought stress detection is applied for a whole group of plants. This number not only depends on the plant-to-plant variability, but also on the root-zone and vineyard-wide spatial variability (Naor, 2006). Naor (2006) and Fernández et al. (2008) suggested that recent developments such as remote sensing may help to identify representative plants and may reduce the required number of monitored individuals. Remote thermal imagery, for instance, is a technique that measures canopy temperature. Canopy temperature depends on changes in stomatal closure and leaf transpiration and is therefore recognised as a measure for plant stress (Maes and Steppe, 2012). The technique has been explored for screening canopy temperature variability over large areas, as well as for detecting biotic and abiotic stresses (Jones, 2007; Jones et al., 2009; Alchanatis et al., 2010; Maes and Steppe, 2012).

UPCA and FUPCA can be implemented for other plant species as well, considering a proper calibration, as was already demonstrated for apple tree and truss tomato (Villez et al., 2009; **Chapter 3**). In this study, SF and D were chosen as plant water status indicator because of their easy continuous monitoring and worldwide appreciation, both for research and field applications (e.g. Cifre et al., 2005).

The preference for UPCA or FUPCA, as well as the choice for which plant variable to use as stress indicator, will depend on the application and availability, price and quality of the sensors. FUPCA requires an extra processing step (functional data analysis), but can monitor days with gaps of missing data. In case the risk for those gaps is high (e.g. caused by sensor, data acquisition or electricity failure), FUPCA will be the technique of choice, otherwise UPCA might suffice. In some cases (R3 and the SF approach in R2), UPCA resulted in a better or longer drought stress detection, although slightly better outcomes of FUPCA were observed in others cases (Table 4.2). Although FUPCA was able to detect drought stress in an early stage, its performance may be improved by adapting the knot distribution for the functional data analysis, dependent on the case study.

4.4.3 Selection of the calibration period

Both UPCA and FUPCA were successfully applied in this study to detect abnormalities in plant behaviour and drought stress without the need to define conventional threshold values for SF or D. Instead, both techniques require a calibration data set, which can be a preceding control period in which the plant is fully irrigated. The length of this control period depends on the prevailing microclimatic variability, because the model eventually needs to abstract normal plant behaviour. Days with both low and high atmospheric demand were included in the calibration data set of this study, because the aim was to distinguish between microclimatic driven changes in plant behaviour and changes caused by drought stress.

Also the phenological stage may influence the selection of the calibration period. When the calibration period contains too many days with zero or low daily net growth of D and low SF, typical for the beginning of the growing season, the models did not detect drought stress as abnormal, since they were taught to recognise these low values as expected. By selecting a proper, representative calibration period, defined for instance by a fully developed canopy, the models successfully detected drought stress.

As the introduced methods still need a fully irrigated control period for calibration purposes, they may seem in essence not different from any other conventional method. The proposed approach, however, only needs a limited control period, while conventional methods need a continuous monitoring of the control group and this group has the risk to lose its property as being representative (Goldhamer and Fereres, 2001; Fernández et al., 2008). In addition, the critical threshold to be exceeded in order to warn for drought stress is determined in a statistical way in this study, while it is mostly chosen rather arbitrarily in conventional methods (e.g. Conejero et al., 2011). On the other hand, the latter permits to easily impose different degrees of drought stress, what might be desirable to improve fruit quality (Möller et al., 2007; Creasy and Creasy, 2009). This may also be possible with UPCA and FUPCA, but requires further investigation (discussed in **Chapter 8**).

4.5 Conclusions

An automatic and reliable method for fast drought stress detection in grapevine is recommended to ensure an appropriate plant water status, since it influences both fruit quantity and quality. Current stress detection methods need the determination of threshold values beyond which the plant starts sensing drought stress. Determination of these values is however difficult due to their dynamic nature. Unfold Principal Component Analysis (UPCA) and Functional Unfold Principal Component Analysis (FUPCA) can circumvent this difficulty. The techniques are able to automatically abstract the plant's behaviour in normal conditions, which pattern is used to compare the new data with, and are able to define the detection limit in a statistical way. Two UPCA and FUPCA models were proposed here: one based on sap flow rates and another based on stem diameter variations. All models enabled successful stress detection days before visible symptoms appeared irrespective of plant age, timing or season. It can be concluded that UPCA and FUPCA based on plant indicators are very promising for early stress detection. Nevertheless, care should be taken when selecting a few representative plants for automatic stress detection of a whole group.

Chapter 5

Development of a mechanistic water transport and storage model for grapevine

After: Baert A, De Schepper V and Steppe K. Variable hydraulic resistances and their impact on plant drought response modelling. Plant, Cell and Environment. (Submitted)

Abstract

Plant drought responses are still not fully understood. Improved knowledge on drought responses is, however, crucial to better predict the impact of expected drought on individual plant and ecosystem functioning. Mechanistic plant models in combination with plant measurements are promising for obtaining information on the whole-plant water status. This unique combination can greatly assist us in better understanding the effect of limiting soil water availability and drought stress associated with climate change. While existing water transport models are reliable under sufficient soil water availability, they generally fail under dry conditions as not all appropriate mechanisms seem yet implemented. The aim of this chapter was therefore to identify mechanisms underlying plant drought responses, and to investigate the behaviour of hydraulic resistances encountered in the soil and xylem for grapevine. The model-based study demonstrated that a variable hydraulic soil-to-stem resistance is necessary to describe plant drought responses. In addition, the implementation of a variable soil-to-stem hydraulic resistance in an existing water transport and storage model enabled the generation of an *in situ*

soil-to-stem vulnerability curve which might be a valuable alternative to the conventional curves. Furthermore, a daily recalibration of the adapted model revealed a drought-induced increase in the radial hydraulic resistance between xylem vessels and elastic living tissues. The ability to obtain accurate information on plant hydraulic resistances and to simulate plant drought responses can foster important discussions regarding the functioning of plants and ecosystems during climate change induced droughts.

5.1 Introduction

Increasing drought-induced hydraulic plant and tree failure has been observed worldwide, leading to forest decline and mortality (Martínez-Vilalta et al., 2002; Allen et al., 2010; Choat et al., 2012). Examining plant water status and its underlying mechanisms will contribute to our understanding of plant and tree functioning and their vulnerability to drought, which is crucial if we aspire to predict the impact of climate change, as more extreme drought events are expected to occur (Schultz and Stoll, 2010; Choat et al., 2012). Therefore, accurate information on the encountered hydraulic resistances in the soil to plant continuum is desired as this highly influences the plant water status.

A first challenge is to understand the mechanisms determining plant hydraulic resistance. This resistance, or its reciprocal conductance, might be altered on a short-scale by a changed expression or activation of plasma membrane aquaporins (water channel proteins). The role of these aquaporins is mainly demonstrated in roots, leaves and fruits (Cochard et al., 2007; Choat et al., 2009; Lovisolo et al., 2010), and just recently in branches (Steppe et al., 2012). In addition, diurnal changes in xylem resistance have been observed (Tsuda and Tyree, 2000), possibly as a result of light-mediated changes in potassium concentration in the xylem sap (Sellin et al., 2010). Furthermore, cavitation increases the xylem resistance. During cavitation the xylem vessel loses its hydraulic function as water vapour replaces the xylem sap under tension (Sperry and Tyree, 1988; Cruiziat and Tyree, 1990; Lovisolo et al., 2010). Cavitation and refilling of cavitated xylem vessels occur on a daily basis, however, the cavitation events are enhanced by drought conditions (Brodersen et al., 2010; Zufferey et al.,

2011; Meinzer et al., 2013; Schenk et al., 2013). Consequently, the hydraulic resistance in the xylem depends on the balance between vessel cavitation and vessel refilling which varies during the day (Meinzer et al., 2013). Vulnerability curves are commonly used to quantify cavitation by describing the relationship between declining stem water potential (Ψ_{stem}) and increasing resistance. The latter is depicted as percentage loss of hydraulic conductivity (PLC).

A second challenge is to comprehend the hydraulic behaviour of the soil and its interaction with plant roots (Green et al., 2006; Damour et al., 2010). Soil water flow resistances increase with drying soil (Gardner, 1960; Tuzet et al., 2003; Zweifel et al., 2007). Soil texture is identified as the major factor determining the steepness of the water potential gradient between roots (Ψ_{root}) and the soil rhizosphere (Ψ_{soil}) (Sperry et al., 1998), but root water uptake might substantially enlarge this gradient (Gardner, 1960; Tuzet et al., 2003; Zweifel et al., 2007).

Mechanistic modelling in combination with plant measurements is often applied to obtain deeper insight in the mechanisms underlying observed plant responses (Perämäki et al., 2001; Steppe et al., 2008; Diaz-Espejo et al., 2012), and is therefore considered as a promising tool for comprehending plant responses to drought. However, the application of models during drought conditions is complex and not straightforward (Martínez-Vilalta et al., 2002; Tuzet et al., 2003; Zweifel et al., 2007; Steppe et al., 2008; Damour et al., 2010; Egea et al., 2011; Diaz-Espejo et al., 2012; Zhou et al., 2013). Therefore, an urge for improved models with better mechanistic descriptions exists. For example, the dynamic water transport and storage model of Steppe et al. (2006), which enables amongst other variables simulation of Ψ_{stem} , one of the best plant water status indicators (Choné et al., 2001; Fereres and Goldhamer, 2003; Acevedo-Opazo et al., 2010), performs well under well-watered conditions (Steppe et al., 2006; 2008) and mild drought stress (De Pauw et al., 2008a), but fails under severe drought conditions. Modelling plant water transport during severe drought stress can enhance our understanding of important plant processes occurring during these conditions.

The objectives of this chapter were to (1) reveal the behaviour of hydraulic resistances encountered from soil to stem, in particular when exposed to drought conditions, and (2) seek if these new insights can be exerted to better describe drought responses. To address this, introducing a variable hydraulic resistance in

an existing water transport and storage model (Steppe et al., 2006; 2008) was investigated as a means to improving predictions of plant responses to drought. The model performance of the adapted model was verified for grapevine (*Vitis vinifera* L.). The applied mechanistic model is considered as generic, therefore, its contribution to a better understanding of plant drought responses was assessed and its importance in predicting plant functioning during drought was highlighted.

5.2 Materials and methods

5.2.1 Experimental set-up

Experiments were conducted on four two-year-old grapevines (*Vitis vinifera* L. cv. Chardonnay) (repetitions R1 to R4). The grapevines were planted in 50 L containers (0.4 m diameter, 0.4 m height), filled with DCM Mediterra compost and fertilised in summer with DCM organic fertiliser for grapes. They were pruned and trained according to the single Guyot system and grown in the greenhouse facilities of the Faculty of Bioscience Engineering at Ghent University, Belgium. At the beginning of the growing season, the grapevines were about 1.5 m high and had stem diameters ranging from 9 to 17 mm at the stem base. The greenhouse facility allowed a strict control of the soil water availability of the grapevines, while the microclimate varied freely dependent on the prevailing conditions. Irrigation was stopped after a control period in which the plants were irrigated at least twice a week to ensure adequate water availability. Drought was imposed from 11 until 28 June 2012 (day of the year (DOY) 163 - 180) for R1, R2 and R4, whereas drought lasted from 21 May until 7 June 2012 (DOY 142 - 159) for R3. Flowering occurred around DOY 142.

5.2.2 Microclimatic and soil measurements

Photosynthetic active radiation (PAR), air temperature (T_{air}) and relative humidity (RH) were measured approximately 2 m above ground level with a quantum sensor (LI-190S, Li-COR, Lincoln, NE, USA), thermocouple (type T, Omega, Amstelveen, the Netherlands) and RH sensor (type Hygroclip, Rotronic, Hauppauge, NY, USA) which was inserted in a radiation shield. An electronic tensiometer (type TensioTrans model 1000 C, Tensio-Technik, Geisenheim, Germany) was inserted in each container to measure soil water potential (Ψ_{soil}).

5.2.3 Plant physiological measurements

Stem diameter variations (D) were measured with Linear Variable Displacement Transducers (LVDT, model DF5.0, Solartron Metrology, Bognor Regis, UK or model LBB 375-PA-100 and transducer bridge 8C-35, Schaevitz, Hampton, VA, USA) attached to the stem base with custom-made stainless steel holders, which do not require temperature correction (Steppe and Lemeur, 2004). Sap flow rate (SF) was measured above each LVDT with heat balance sap flow sensors (SGEX-13 or SGA10-ws, Dynamax Inc., Houston, TX, USA). A data logger (DAQ 34970A and multiplexer 34901A, Agilent Technologies, Diegem, Belgium) scanned all sensor signals every 20 s.

Stem water potential (Ψ_{stem}) was measured using a pressure chamber (PMS Instrument Company, Albany, OR, USA). Mature, healthy leaves were covered in plastic bags coated with aluminium foil for at least 2 h prior to the measurements to ensure hydraulic equilibration with stem xylem water (McCutchan and Shackel, 1992). Midday Ψ_{stem} was measured at least twice a week. Occasionally, Ψ_{stem} was measured at several times during the day to examine its daily dynamics. One to three leaves were chosen per record. Simultaneous measurements of Ψ_{stem} and Ψ_{soil} were used to calculate the integrated hydraulic resistance of the soil-to-stem segment (R^X [MPa.h.g⁻¹]) according to Ohm's law using the water potential difference [MPa] and prevailing sap flow rate (SF [g.h⁻¹]) in the soil-to-stem segment (cf. Tsuda and Tyree, 2000; Sellin et al., 2010):

$$R^X = \frac{\Psi_{\text{soil}} - \Psi_{\text{stem}}}{\text{SF}} \quad (5.1)$$

5.2.4 Model description

An existing water transport and storage model (Steppe et al., 2006; 2008), which describes water transport dynamics in a single plant, was adapted in this study. Model structure and equations are shown in Fig. 5.1. The basic principles from the original model of Steppe et al. (2006; 2008) were conserved. When transpiration starts in the morning, Ψ_{stem} decreases. The developed water potential difference between stem and soil induced water uptake from the soil. Since living tissues and xylem are hydraulically connected, stored water in the living tissues can contribute to the transpiration stream (Génard et al., 2001; Steppe et al., 2006; 2012) causing

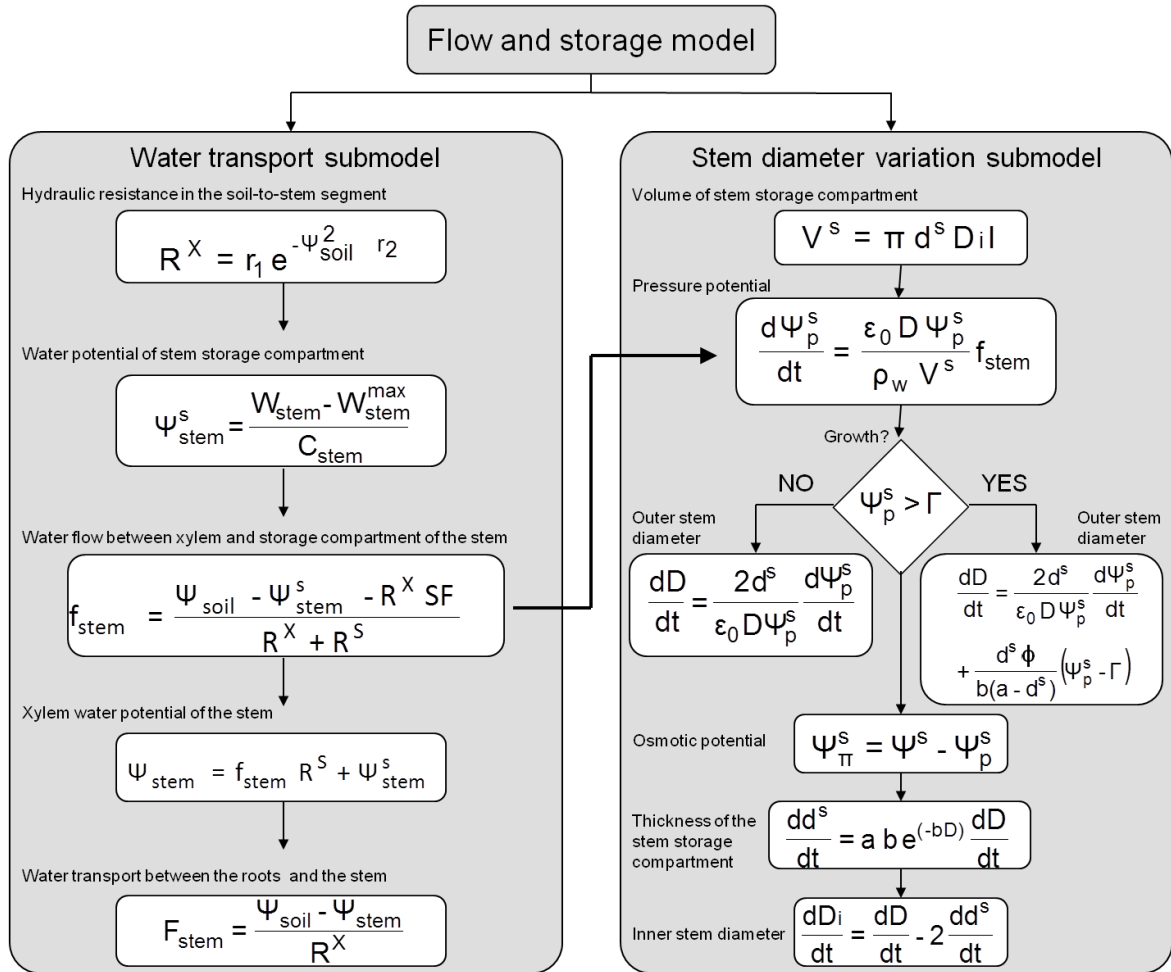


Fig. 5.1 Schematic overview of the model equations. The model consists of two submodels: a water transport submodel (left panel) for describing the dynamics of plant sap flow and storage, linked to a stem diameter variations submodel (right panel) that describes stem diameter changes and growth. Following parameters and variables are used in the model: F_{stem} , water flow between the roots and the stem; Ψ_{soil} , soil water potential; Ψ_{stem} , stem water potential; R^X , integrated hydraulic resistance in the soil-to-stem segment; f_{stem} , water flow between xylem and storage compartment; R^S , radial hydraulic resistance between the xylem and elastic storage tissues; Ψ_{stem}^s , water potential of storage compartment; SF, sap flow rate; W_{stem} , water content of the storage compartment; $W_{\text{stem}}^{\text{max}}$, maximum W_{stem} ; C_{stem} , capacitance of the water storage tissues in the stem compartment; r_1 , r_2 , parameters for calculation of R^X ; V^s , volume of the storage compartment; D_i , inner stem diameter; d^s , thickness of the storage compartment; l , length of the stem segment; D , outer diameter of the stem segment; Ψ_p^s , turgor pressure potential of the storage compartment; ϵ_0 , proportionality constant; ρ_w , density of water; Γ , threshold at which cell wall-yielding occurs; ϕ , cell wall extensibility; a , b , allometric parameters; Ψ_{π}^s , osmotic potential of the storage compartment.

the stem diameter to shrink. The model has two input variables (measurements of SF and Ψ_{soil}) and consists of two submodels. The first submodel describes the dynamic axial and radial water transport within the rigid xylem and between the

xylem and the living tissues. The second submodel simulates the dynamics in D , resulting from both irreversible growth (Lockhart, 1965) and reversible daily shrinkage and swelling of living tissues (Génard et al., 2001; Steppe et al., 2006). When the turgor pressure (Ψ_p^s) exceeds a critical wall-yielding threshold (Γ), the living cells grow irreversibly. Ψ_p^s depends on the radial water flow between the xylem and the living tissues, which is derived from the water transport submodel and, hence, represents the link between both submodels. A more detailed description can be found in Steppe et al. (2006; 2008).

The existing model uses a constant parameter value for the hydraulic resistance in the xylem (Steppe et al., 2006; 2008; Baert and Steppe, 2013). To obtain better drought response simulations, the constant xylem resistance was replaced by a variable hydraulic resistance which is related to Ψ_{soil} [MPa] and accounts for changes in overall hydraulic resistance experienced during upward water transport in the entire soil-to-stem segment (R^X [MPa.h.g⁻¹]):

$$R^X = r_1 e^{-\Psi_{\text{soil}}^2 r_2} \quad (5.2)$$

with r_1 [MPa.h.g⁻¹] and r_2 [MPa⁻²] parameters dependent on plant and soil characteristics. It should be noted that the adapted model integrates the resistances of the soil, the roots and the stem in one variable R^X that changes in function of Ψ_{soil} .

Model calibration, simulation and identifiability analysis

Model implementation, simulation, calibration and identifiability analysis were conducted using the plant modelling software PhytoSim (Phyto-IT BVBA, Mariakerke, Belgium). Model simulation was performed with a fourth-order Runge-Kutta numerical integrator with variable step size (integrator settings: accuracy = $1 \cdot 10^{-6}$ and maximum step size = 0.1 s). Model calibration was based on the simplex method (Nelder and Mead, 1965) and minimised the weighted sum of squared errors for the variables D and Ψ_{stem} . Measurements of SF and Ψ_{soil} were used as model inputs and measurements of D and Ψ_{stem} for model calibration.

Two types of identifiability analysis exist: structural (theoretical) or practical identifiability. Structural identifiability can be performed prior to data collection and without prior knowledge on the parameter values. This analysis deals with the

question whether it is theoretically possible to find unique values for the model parameters given the model structure and available measurements (De Pauw et al., 2008a). In this study, however, a practical identifiability analysis was performed. A practical identifiability determines whether model parameters can be accurately estimated using the amount and quality of the available data. A model parameter is then defined to be identifiable if it has sufficient influence on the model output (i.e. high sensitivity) and is at the same time is not correlated with other model parameters (i.e. no linear dependencies with other model parameters) (De Pauw et al., 2008a; Steppe et al., 2008). To compare the original and adapted model, calibration parameters were selected based on such practical identifiability analysis (De Pauw et al., 2008a) including available measurements of D and Ψ_{stem} . The selected calibration parameters of the original model were the capacitance of the water storage tissues in the stem compartment (C_{stem}), the cell wall extensibility (ϕ), the radial hydraulic resistance between the xylem and the storage compartment (R^S) and the hydraulic xylem resistance (R^X). For the adapted model, five identifiable calibration parameters were selected based on a second practical identifiability analysis (De Pauw et al., 2008a), as parameter R^X was replaced by Eq. 5.2: C_{stem} , ϕ , R^S , r_1 and r_2 . The remaining non-calibrated model parameters were assigned a fixed value based on the literature or direct measurements (Table 5.1). A set of ten consecutive days during the most severe drying soil conditions was used for calibrating and comparing the original and adapted model. The calibrated models were compared using the objective model selection criteria sum of squared errors (SSE) and final prediction error (FPE) (e.g. Dochain and Vanrolleghem, 2001; Steppe et al., 2006):

$$\text{FPE} = \frac{\text{SSE}}{N} + \frac{2p \text{SSE}}{N(N-p)} \quad (5.3)$$

with N the number of data points and p the number of estimated parameters. The FPE evaluates both the model fit (first term) and the number of parameters (second term, penalises too complex models). The smaller the criteria, the better the model.

Additional model calibrations were performed for each grapevine. The five identifiable parameters of the adapted model were recalibrated daily based on a five-day moving window to investigate their variability in response to soil drying.

This analysis resulted in calibrated parameter values for each day of the complete drought period.

5.3 Results

5.3.1 R^X exponentially increases with decreasing Ψ_{soil}

A clear relationship was observed between measured Ψ_{soil} [MPa] and R^X calculated according to Eq. 5.1 [MPa.h.g⁻¹] (Fig. 5.2). This observed relationship could be described by Eq. 5.2 and justified its implementation in the adapted water transport and storage model.

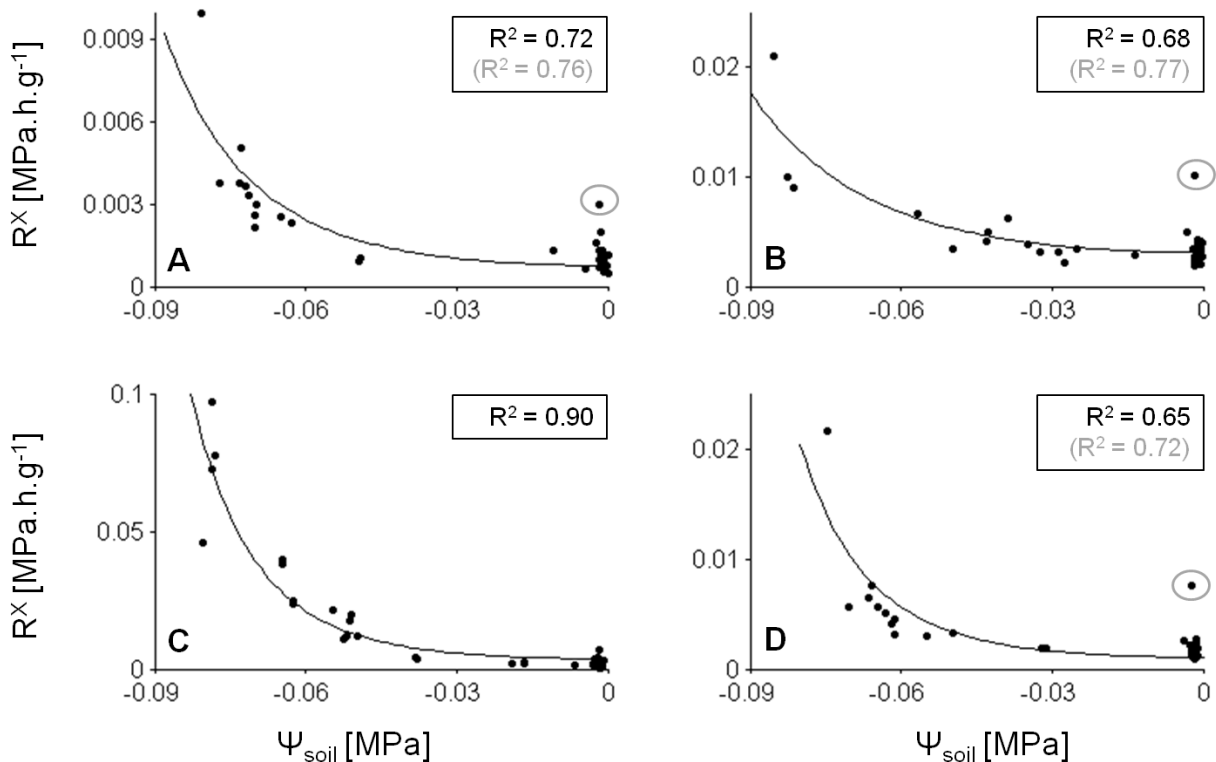


Fig. 5.2 Integrated hydraulic resistance in the soil-to-stem segment (R^X) as a function of soil water potential (Ψ_{soil}) shows a clear trend for all four grapevines R1 to R4 (A-D). The equation $R^X = r_1 e^{-\Psi_{\text{soil}}^2} r_2$ (solid lines), with r_1 , r_2 proportionality parameters, was fitted to the measurements. The coefficient of determination (R^2) ranged between 0.65 and 0.90, and improved to the range of 0.72 and 0.90 when one outlier (on a very cloudy day) was removed (indicated with grey circles).

Table 5.1 Definition, values (range over grapevines R1 to R4), unit and reference of the model parameters used in the water transport and storage model with variable soil-to-stem hydraulic resistance.

Parameter	Definition	Value	Unit	Reference
Obtained during calibration				
C_{stem}	Capacitance of the water storage tissues in the stem compartment	2.48 - 9	g.MPa^{-1}	-
ϕ	Cell wall extensibility	0.0003 - 0.0043	$\text{MPa}^{-1}.\text{h}^{-1}$	-
R^S	Radial hydraulic resistance between the xylem and the elastic living tissues	0.86 - 1.78	MPa.h.g^{-1}	-
r_1	Proportionality parameter for calculation of the integrated soil-to-stem hydraulic resistance	0.0002 - 0.0035	MPa.h.g^{-1}	-
r_2	Proportionality parameter for calculation of the integrated soil-to-stem hydraulic resistance	180 - 502	MPa^{-2}	-
Obtained from measurements or the literature				
l	Length of the stem segment	1	m	Measured
a	Allometric parameter	0.002968	m	Génard et al. (2001)
b	Allometric parameter	32	m^{-1}	Génard et al. (2001)
Γ	Critical threshold value which must be exceeded to produce stem growth	0.9	MPa	Génard et al. (2001)
ε_0	Proportionality constant for calculation of the bulk elastic modulus	1100	m^{-1}	Steppe et al. (2006)

5.3.2 Drought stress simulated with constant or variable R^X

Measured SF (Fig. 5.3A, Appendix Fig. S15A, D, G) and daily net growth of D (Fig. 5.3B, S15B, E, H) decreased in all grapevines (R1 to R4) with declining soil water availability (Fig. 5.3C, S15C, F, I), although this was less pronounced in R2. A similar trend was observed in measurements of Ψ_{stem} (Fig. 5.3C, S15C, F, I).

For all grapevines, except for R2, the adapted model (variable R^X , Eq. 5.2) showed a distinct enhancement in simulating the decreasing trend in D and Ψ_{stem} observed in drought-stressed grapevine compared to the original model that failed in describing the plant drought responses (Fig. 5.3, S15). These findings are also

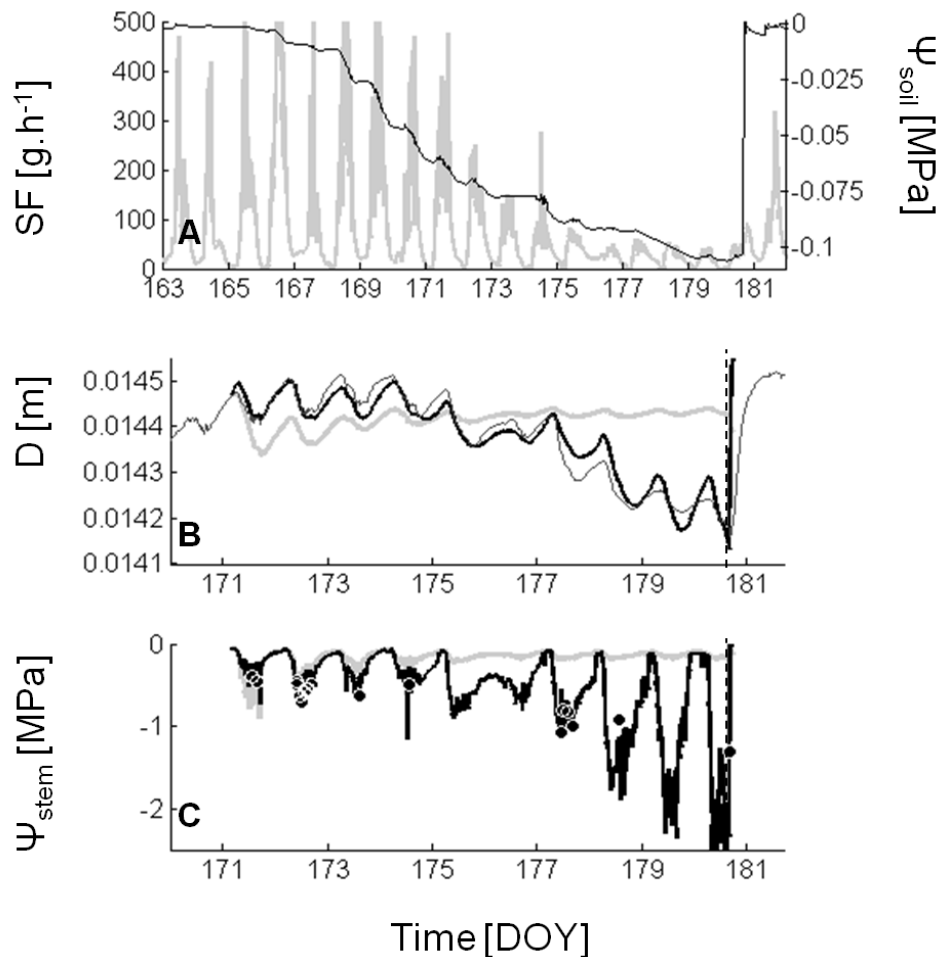


Fig. 5.3 Model inputs and simulations of a typical grapevine. The used model inputs were (A) sap flow rate (SF, grey lines) and soil water potential (Ψ_{soil} , black lines); (B) Comparison between measurements of stem diameter variations (D, thin grey line) with model outputs of the original (constant hydraulic resistance in the xylem, thick grey lines) and adapted (integrated variable hydraulic resistance in the soil-to-stem segment, black lines) model; (C) Comparison between measurements (black dots) of stem water potential (Ψ_{stem}) with model outputs of the original (thick grey lines) and adapted (black lines) model.

reflected in both SSE and FPE values with higher values for the original model (Table 5.2). Table 5.1 gives an overview of range within which optimised parameter values occurred in the adapted model for R1 to R4.

5.3.3 Vulnerability curve

When drought stress progressed, the hydraulic functioning gradually declined as indicated by the declining modelled soil-to-stem hydraulic conductance ($K^X = 1/R^X$) (Fig. 5.4). The curve in Fig. 5.4, which depicts modelled K^X as a function of modelled midday Ψ_{stem} , strongly resembles the commonly applied vulnerability curve. Similar to such vulnerability curves, which describe the relationship between Ψ_{stem} and loss of hydraulic conductivity in the plant (PLC [%]) (e.g. Choat et al., 2010; Cochard et al., 2010), $\Psi_{\text{stem},50}$ and $\Psi_{\text{stem},90}$ were determined as modelled stem water potential corresponding with 50% and 90% loss of hydraulic soil-to-stem conductance. $\Psi_{\text{stem},50}$ and $\Psi_{\text{stem},90}$ were -0.4 ± 0.1 MPa and -0.8 ± 0.1 MPa, respectively. When Ψ_{stem} dropped below $\Psi_{\text{stem},90}$ no full recovery of the stem diameter took place during the night, which resulted in a continuous decrease of the stem diameter (Fig. 5.3, S15).

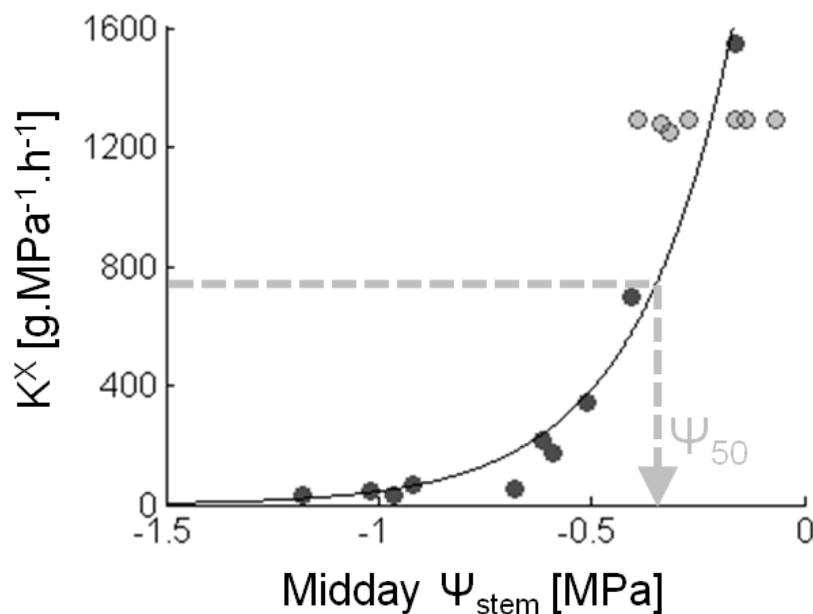


Fig. 5.4 A modelled vulnerability curve representing modelled soil-to-stem hydraulic conductance (K^X) as a function of modelled midday stem water potential (Ψ_{stem}) for a grapevine during soil drying. Ψ_{50} represents Ψ_{stem} at which 50% of the initial (not stressed) soil-to-stem hydraulic conductance is lost. The light grey values were averaged to obtain an appropriate fit.

Table 5.2 Sum of squared errors (SSE) and final prediction error (FPE) for simulations of stem diameter variations (D) or stem water potential (Ψ_{stem}). Simulations with a constant (original model) or variable (adapted model) hydraulic resistance in the soil-to-stem segment (R^X) are compared for grapevine R1 to R4.

n°	SSE for D [mm ²]		SSE for Ψ_{stem} [MPa ²]	
	Constant R^X	Variable R^X	Constant R^X	Variable R^X
R1	$3.6 \cdot 10^{-5}$	$1.8 \cdot 10^{-6}$	3.4	0.5
R2	$1.8 \cdot 10^{-6}$	$1.6 \cdot 10^{-6}$	0.5	0.2
R3	$2.1 \cdot 10^{-5}$	$1.2 \cdot 10^{-5}$	6.4	1.5
R4	$2.6 \cdot 10^{-5}$	$4.4 \cdot 10^{-6}$	2.5	0.2

n°	FPE for D [mm ²]		FPE for Ψ_{stem} [MPa ²]	
	Constant R^X	Variable R^X	Constant R^X	Variable R^X
R1	$1.3 \cdot 10^{-8}$	$6.6 \cdot 10^{-10}$	0.30	0.06
R2	$6.1 \cdot 10^{-10}$	$5.4 \cdot 10^{-10}$	0.06	0.03
R3	$7.1 \cdot 10^{-9}$	$4.1 \cdot 10^{-9}$	0.76	0.17
R4	$9.2 \cdot 10^{-9}$	$1.6 \cdot 10^{-9}$	0.28	0.02

5.3.4 Dynamics in the hydraulic resistances R^X and R^S during soil drying

R^X showed a diurnal pattern under adequate water availability: maximum values prevailed during the night, while the lowest values were observed in the afternoon (Fig. 5.5A). These daily dynamics continued under drying soil (Fig. 5.5B) but a pronounced net increase in R^X was superimposed on these daily fluctuations.

The values for radial hydraulic resistance between the xylem and the elastic living tissues (R^S [MPa.h.g⁻¹]), recalibrated daily based on a moving window, were exponentially related to Ψ_{soil} [MPa] for all grapevines, with the exception of R2 (Fig. 5.6). In analogy with R^X (Fig. 5.2, Eq. 5.2), the following equation fitted well through the measurements:

$$R^S = s_1 e^{-\Psi_{\text{soil}}} s_2 \quad (5.4)$$

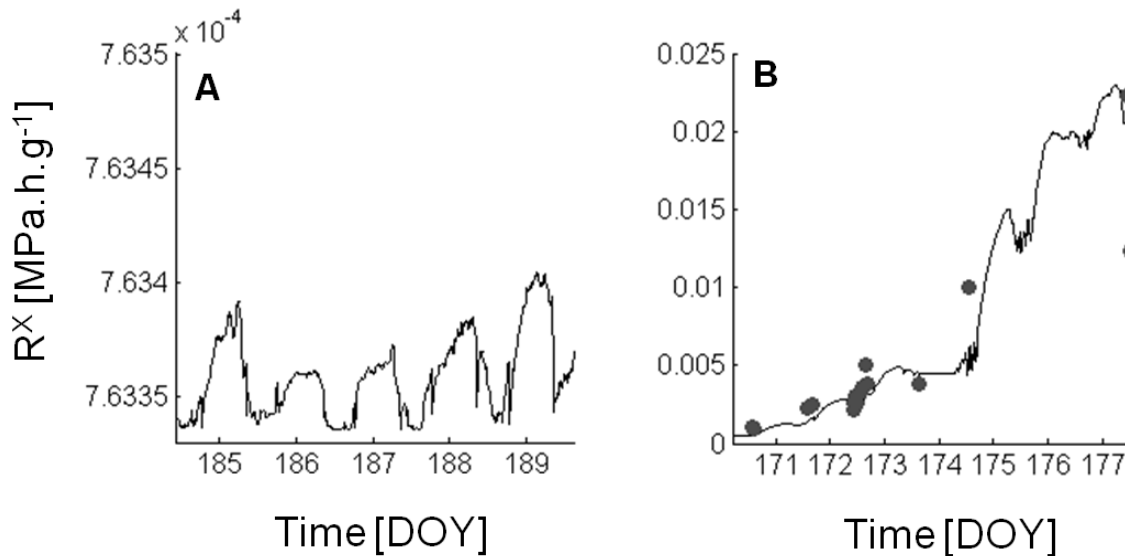


Fig. 5.5 The simulated soil-to-stem hydraulic resistance (R^x) shows (A) daily dynamics in wet conditions and (B) drought-induced dynamics in stressed conditions. If measurements were available, R^x (grey dots) calculated according to Eq. 5.1 is also shown. Time is given in day of the year (DOY).

with s_1 [MPa.h.g⁻¹] and s_2 [MPa⁻¹] proportionality parameters dependent on plant and soil characteristics. No similar trends were found in the model parameters C_{stem} , ϕ , r_1 or r_2 .

5.4 Discussion

5.4.1 Plant drought response modelling requires variable hydraulic resistances

Accurate modelling and understanding plant responses to water deficit remains a challenging objective despite the increasing awareness of its necessity in many fields (Tuzet et al., 2003; Damour et al., 2010; Egea et al., 2011; Diaz-Espejo et al., 2012). This study demonstrates that the commonly accepted use of a constant hydraulic plant resistance as imbedded in water transport and storage models (e.g. Steppe et al., 2006; 2008; Zweifel et al., 2007; De Schepper and Steppe, 2010; De Swaef and Steppe, 2010), fails to describe plant responses under severe drought conditions (Fig. 5.3, Appendix Fig. S15). To assess the impact of future droughts on crops and forests, a variable hydraulic resistance in soil and plants (Fig. 5.2) should be considered.

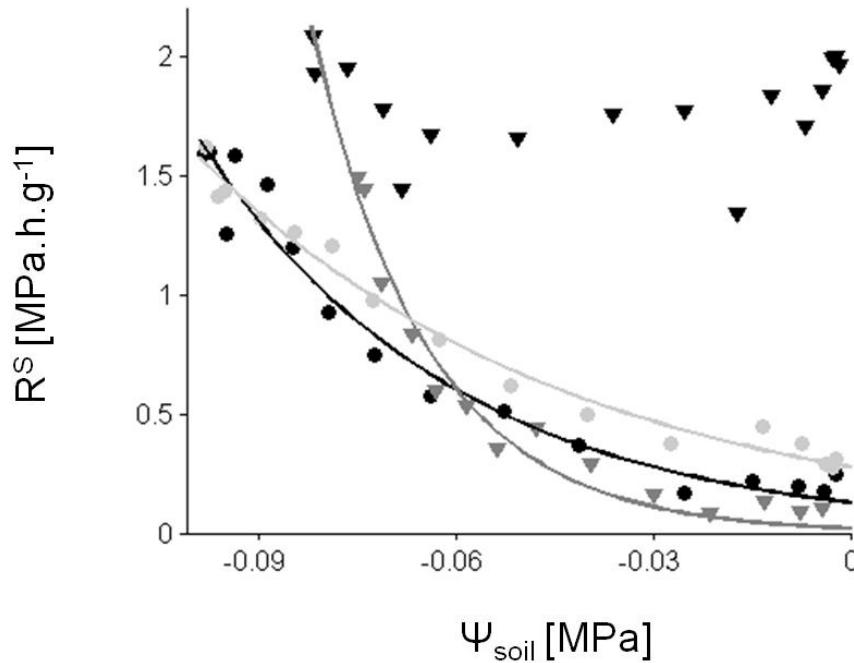


Fig. 5.6 Increase in radial hydraulic resistance between xylem and elastic storage tissues (R^S) with decreasing soil water potential (Ψ_{soil}) for grapevines R1 (black circles), R3 (grey triangles) and R4 (grey circles), but not for R2 (black triangles).

The equation $R^S = s_1 e^{-\Psi_{\text{soil}} s_2}$ (solid lines), with s_1 , s_2 both proportionality parameters, was fitted to the measurements. Coefficients of determination (R^2) were 0.95 (R1), 0.93 (R3) and 0.97 (R4).

5.4.2 Advantage of an integrated soil-to-stem hydraulic resistance

In the literature, soil and plant hydraulic resistances are often separately studied. A first group of researchers relates the plant hydraulic resistances in roots, stems and leaves to declining water potentials (Lovisolo and Schubert, 1998; Sperry et al., 1998; Lovisolo et al., 2010; Johnson et al., 2012). A second group deals with soil water availability under drying soil conditions, because the water potential near the roots strongly differs from the soil water potential measured at a certain distance (Gardner, 1960; Tuzet et al., 2003; Green et al., 2006; Zweifel et al., 2007). An integrated soil-plant approach seems promising as the physical properties of water flow in soil and xylem are similar (Sperry et al., 2002) and their resistances are extremely difficult to separate since the soil resistance depends on micro-gradients around the root zone (Tuzet et al., 2003). Therefore, the improved model of this study (Fig. 5.1) incorporated a variable integrated hydraulic resistance R^X that captures the entire upward water flow pathway from soil to stem

(Eq. 5.2, Fig. 5.2). Also Diaz-Espejo et al. (2012) used an integrated resistance and implemented a constant parameter for the soil-to-leaf hydraulic resistance in their stomatal conductance model based on Buckley et al. (2003). They observed a fourfold increase in this resistance when olive trees were exposed to a drying soil (determined by fitting the model for four days during a regulated deficit irrigation treatment). The approach of one variable hydraulic resistance integrating both soil and plant aspects avoids the implementation of multiple hydraulic resistances, often entailing uncertain model parameters which might be difficult to estimate.

5.4.3 Modelled soil-stem integrated vulnerability curve

The modelled relationship between soil-to-stem conductance and stem water potential (Fig. 5.4) integrates the information which was previously obtained from separate soil desorption and plant vulnerability curves (e.g. Gardner, 1960; Choat et al., 2010; Cochard et al., 2010). This integrated model approach might have several advantages compared to experimental approaches. For instance, a soil desorption curve has to be defined for each soil type, because of strong dependence on soil properties. Hence, a general description of a soil desorption curve requires a complex set of equations (e.g. Gardner, 1960; Tuzet et al., 2003). In addition, as demonstrated in **Chapter 2**, various and strongly diverging plant vulnerability curves can be found in the literature dependent on sample length and/or dimension (Kikuta et al., 2003; Choat et al., 2010; Cochard et al., 2010), on the applied method (Choat et al., 2010; Cochard et al., 2010; Jacobsen and Pratt, 2012; Cochard et al., 2013) and on the method specifications such as the degree of flushing and filtering, chemical composition and degassing level of the measurement solution (Canny et al., 2007; Espino and Schenk, 2011; van Doorn et al., 2011; Jacobsen and Pratt, 2012; Sperry et al., 2012). Furthermore, conventional plant vulnerability curves require destructive sampling and investigate each plant organ separately (e.g. stem, branches, twigs and leaves). Unless one aims at distinguishing vulnerability of specific organs, it seems difficult to represent whole-plant hydraulic functioning by the hydraulic properties of the individual plant organs. Therefore, the use of conventional vulnerability curves to estimate the whole-plant *in situ* hydraulic functioning seems not straightforward. Alternative methods such as the proposed model approach (Fig. 5.4, 5.5), based

on automatic *in situ* plant and soil measurements, can be a valuable alternative for studying plant survival and vulnerability to drought. The model approach allows studying hydraulic functioning under natural conditions for an extended time period, whereas conventional vulnerability curves are constructed in a laboratory and at a certain moment in time. Hölttä et al. (2005) also developed an alternative vulnerability curve by using *in situ* measurements of ultrasonic acoustic emissions and stem diameter variations to study cavitation dynamics in Scots pine trees under field conditions.

Reported values of $\Psi_{\text{stem},50}$ in the literature are -0.70 MPa to -2.97 MPa for *Vitis vinifera* L. cv. Chardonnay (Wheeler et al., 2005; Alsina et al., 2007; Choat et al., 2010). These values are notably lower than the ones determined from this modelling approach (-0.4 ± 0.1 MPa). However, this difference can be attributed to the fact that reported vulnerability curves only examine the hydraulic conductance of the stem xylem, whereas this model approach integrates the hydraulic conductance in soil, roots and stem. $\Psi_{\text{stem},90}$ of the modelled vulnerability curve corresponded with a severe loss of conductance which apparently inhibited refilling of the elastic water storage tissues during the night and resulted in a continuous decrease of the stem diameter.

5.4.4 Dynamics in axial and radial hydraulic resistances

In addition to the drought-induced change of soil-to-stem hydraulic resistance, R^x showed a diurnal pattern, in which lowest hydraulic resistance occurred in the afternoon and highest hydraulic resistance during the night (Fig. 5.5A). In this study, the diurnal pattern is driven by dynamics in soil water potential as a result of daily watering during the control periods (Eq. 5.2). Tsuda and Tyree (2000) also observed such a diurnal behaviour, in which the lowest hydraulic resistance of each day corresponded with the highest daily transpiration rate occurring in the afternoon, but the observed fast changes in plant hydraulic resistance were related to changing temperature and transpiration. Other studies noticed significant lower leaf (e.g. Cochard et al., 2007; Sellin et al., 2011; Guyot et al., 2012) and stem (Sellin et al., 2010; 2011) hydraulic resistances with increased light irradiance and linked these rapid changes to regulation of aquaporins (Cochard et al., 2007; Sellin et al., 2011; Guyot et al., 2012) or potassium concentration (Sellin et al., 2010). The results from this study suggest that dynamics in soil water potential

might have an influence on plant hydraulic resistance, therefore, timing of water gift should be considered when examining dynamics in plant hydraulic resistances. In addition, a drought induced increase in radial hydraulic resistance between xylem and living tissues (R^S) was observed (Fig. 5.6). This is in agreement with the recent study of Steppe et al. (2012) who elucidated the role of aquaporins in regulating the radial hydraulic resistance in response to drought. This general trend was, however, not observed for grapevine R2 (Fig. 5.6), probably because this plant had a higher drought resistance visible from the smaller decline in SF, D and Ψ_{stem} (Fig. S15). Noteworthy is that also data-driven models UPCA and FUPCA from **Chapter 4** did not detect drought stress for this particular grapevine (i.e. grapevine R5 in **Chapter 4**, Fig. S13, S14). As such, the obtained model results suggest to replace the generally applied constant parameter R^S (Génard et al., 2001; Steppe et al., 2006; De Schepper et al., 2010; De Swaef and Steppe, 2010; De Schepper et al., 2011) with a variable R^S . However, the model performance of the adapted water transport and storage model with a variable R^S did not considerably improve model simulations (data not shown). Nevertheless, an enhanced performance of a model with a variable R^S might be expected for other species, e.g. fruit trees. In contrast to grapevine (Choat et al., 2010; Jacobsen and Pratt, 2012), fruit trees have a strong drought induced decrease in Ψ_{stem} (Shackel et al., 1997; Ortuño et al., 2006; Doltra et al., 2007; Fernández et al., 2011b) which might be reflected in a higher variability of both R^X and R^S and thus a potential model improvement.

5.5 Conclusions

Model implementation of a variable integrated hydraulic resistance for upward water transport improved our understanding of drought stress responses in grapevine (Fig. 5.3, Appendix Fig. S15). Considering a variable hydraulic resistance under drought conditions seems therefore worthwhile to pursue when aspiring accurate drought response modelling in crops and trees. This is not only important for species that benefit from some level of drought for their fruit production and quality (Naor, 2006; Acevedo-Opazo et al., 2010), such as grapevines, but is currently equally important for non-commercial plants, even

ecosystems, that need to survive in regions where droughts associated with climate change are predicted to increase in duration and severity (Allen et al., 2010). Recent findings reveal that drought plays a crucial role in observed forest decline and mortality, caused by so-called hydraulic failure (Martínez-Vilalta et al., 2002; Allen et al., 2010; Choat et al., 2012). Many species function very close to their hydraulic safety margins against harmful levels of drought stress, irrespective of the type of environment they live in (Martínez-Vilalta et al., 2002; Meinzer et al., 2009; Choat et al., 2012). Assessing the impact of future climate change on plants and ecosystems will strongly depend on our mechanistic understanding and ability to model and predict plant responses to drought, an aim to which this chapter contributes.

Chapter 6

Real-time water status monitoring

After: Baert A and Steppe K. Real-time water status monitoring in grapevines using a water transport and storage model. Journal of Agricultural Science. (Submitted)

Abstract

Increasing water shortage and costs make efficient irrigation scheduling inevitable in many viticultural areas, even where it was unnecessary so far, and introduce an increasing need for monitoring of the whole-plant water status. Since specific water deficits play a key role in the production of high quality grapes and wines, reliable monitoring is crucial, in particular under dry conditions. In this chapter, five potted grapevines (*Vitis vinifera* L. cv. Chardonnay), of which three were subjected to a drought treatment before veraison, were continuously monitored during the growing season of 2012. A mechanistic water transport and storage model enabled accurate real-time simulation of stem water potential (Ψ_{stem}) under slight to severe drought stress (soil water potential (Ψ_{soil}) down to -0.09 MPa). Furthermore, the model created added value by supplying information on other relevant plant variables like rapid turgor changes in the elastic storage tissues of the grapevine or changes in both axial and radial hydraulic resistances, and by providing crucial knowledge on the mechanisms underlying plant functioning during drought stress. Finally, the modelling approach enabled generation of soil-to-stem segment vulnerability curves by integrating the hydraulic conductance in

soil and plant. From these curves, Ψ_{stem} at which 50% and 90% loss of conductance in the soil-to-stem segment occurred could be deduced, resulting in a $\Psi_{\text{stem},50}$ of -0.65 ± 0.02 MPa and a $\Psi_{\text{stem},90}$ of -1.07 ± 0.11 MPa for Chardonnay grapevines. Since the model uses only automatic measurements (sap flow rate, stem diameter variations and Ψ_{soil}) as input, it lends to automation and is therefore considered promising for future applications regarding real-time water status monitoring and efficient irrigation scheduling to improve grape quality.

6.1 Introduction

As explained in **Chapter 1**, water shortage is an increasing problem in the world, including viticultural areas (Williams and Matthews, 1990; Schultz, 2000; Hannah et al., 2013a). In central Europe, for instance, a reduction in soil moisture, more extreme temperatures and a higher frequency of summer dry periods are expected to occur (Schultz, 2000). Significant temperature rises have been observed in many regions over the last decades, leading to a growing interest in irrigation scheduling in areas that were completely rain-fed until now (Schultz and Stoll, 2010; Hannah et al., 2013a). Considering that irrigation accounts for approximately 70% of the total water use worldwide (Schultz and Stoll, 2010) and that competition for water and involved costs is increasing, efficient irrigation strategies become a necessity. Such irrigation strategies should minimise water consumption while still providing the adequate amount of water to the grapevines (*Vitis vinifera* L.). Importantly, mild drought stress at the right time enhances grape composition and plays a crucial role in the production of quality wines (**Chapter 2**; Möller et al., 2007; van Leeuwen et al., 2009), resulting in different aromas, flavours and colours (Matthews et al., 1990; Keller, 2010a). On the other hand, both excessive and no drought stress negatively affect the grape's and wine's potential (van Leeuwen et al., 2009). Efficient irrigation is thus not exclusively a story of fulfilling water demand, but rather of defining the optimum level and timing and keeping a tight control of the plant water status.

Accurate irrigation scheduling can therefore benefit from automatic water status monitoring, as this can provide crucial information on the whole-plant water balance. It is internationally acknowledged that such monitoring should rely on

plant measurements (e.g. Jones, 2004; Steppe et al., 2008), of which stem water potential (Ψ_{stem}) is still acknowledged as one of the best indicators (Choné et al., 2001; Intrigliolo and Castel, 2004; Möller et al., 2007; Acevedo-Opazo et al., 2010). Although Ψ_{stem} can be measured with the pressure chamber (Scholander et al., 1965), or with *in situ* stem psychrometers (Jones, 2004; Nizinski et al., 2013), the unique combination of mechanistic modelling with plant measurements offers an interesting alternative with great potential for monitoring whole-plant water status. Indeed, the pressure chamber is a destructive, discontinuous and labour intensive technique and therefore impractical for automatic water status monitoring (Jones, 2004; Intrigliolo and Castel, 2006), while the stem psychrometer is a sophisticated automated sensor, but quite difficult to install and use for long-standing applications (Jones, 2004; Nizinski et al., 2013). While these methods only supply information on Ψ_{stem} , mechanistic plant models can act as soft sensors and also enable simulation of other relevant, but sometimes difficult to measure, plant variables such as axial and radial hydraulic resistances or turgor pressure in the living tissues. As such, mechanistic models provide supplementary information and help in improving our knowledge on plant functioning and their responses to drought by looking at the underlying mechanisms.

Steppe et al. (2006) originally developed a plant model that can be run using easy to measure plant variables. This water transport and storage model mechanistically links sap flow rate (SF), or whole-plant water use, and stem diameter variations (D) and has been used earlier to simulate Ψ_{stem} for irrigation purposes in apple trees (Steppe et al., 2008). For a good model performance under pronounced dry soil conditions, **Chapter 5** introduced new equations dependent on soil water potential to describe (1) the integrated hydraulic resistance encountered by water during its upward transport (R^X , Eq. 5.2) and (2) the radial resistance between xylem and elastic water storage tissues (R^S , Eq. 5.4). Replacing the former constant R^X and R^S by variable ones was necessary to account for increasing water flow resistance of drying soil (Gardner, 1960; Zweifel et al., 2007), cavitating xylem vessels (Sperry et al., 1998; Lovisolo et al., 2010) and the interference of aquaporins (water channel proteins) (Cochard et al., 2007; Lovisolo et al., 2010; Steppe et al., 2012). The improved water transport and storage model proved useful for extending our knowledge on drought responses

(**Chapter 5**; Baert and Steppe, 2013), but has only been tested in an offline set-up and still required manual Ψ_{stem} measurements, which is less desirable in practical applications.

In this chapter, the model's potential for real-time monitoring of different plant variables important for the characterisation of the plant water status (Ψ_{stem} , R^X , R^S and turgor), and for extracting altered plant behaviour due to drought stress was investigated. To this end, grapevines were subjected to both wet and pronounced drought conditions and instantaneous plant behaviour was continuously simulated using the model. Because the choice of the moving window size (Steppe et al., 2008), required for daily model recalibration, has an effect on the responsiveness and stability of the model, three moving window sizes (two, four and six days of past data) were tested. Model simulations of Ψ_{stem} using the defined windows were compared with manual measurements and the associated model performance was evaluated.

6.2 Material and methods

6.2.1 Plant material and set-up

Five two-year-old potted grapevines (*Vitis vinifera* L. cv. Chardonnay) were continuously monitored during the 2012-growing season. The grapevines were grown in 50 L containers (0.4 m diameter and height) filled with DCM mediterranea compost and fertilised in summer with DCM organic fertiliser for grapes. They were grown inside the greenhouse facility of the Faculty of Bioscience Engineering at Ghent University, Belgium, to have control over the soil water availability. The plants were pruned and trained according to the single Guyot system. Data from 21 May (day of flowering) until 8 July 2012 (day of the year, DOY 142 - 190) were selected for this study: three grapevines were subjected to drought stress (repetitions R1 to R3) and two plants served as control (R4 and R5). At the start of the growing season, they had base stem diameters ranging from 9 to 17 mm. The grapevines were irrigated at least twice a week to guarantee adequate water supply, unless subjected to drought stress. The drought period lasted from 11 until 28 June (DOY 163 - 180) for R1 and R3 and from 21 May until 7 June (DOY 142 - 159) for R2. The first day represents the last irrigation event, the last day the day

on which irrigation was resumed. All drought treatments were conducted during the first fast growth phase of grape berry development (section 2.3.2; Dokoozlian, 2000; Keller, 2010a), thus before veraison, which was setting in between the middle and end of July. Noteworthy is that results from a fourth drought-stressed grapevine in 2012 (R5 in **Chapter 4** = R2 in **Chapter 5**) will not be presented in this chapter. Since that particular grapevine showed a higher drought resistance, it acted more like a control treatment and was therefore less interesting for this chapter.

6.2.2 Microclimatic, soil and plant measurements

Photosynthetic active radiation was measured with a quantum sensor (LI-190S, Li-COR, Lincoln, NE, USA), air temperature with a thermocouple (type T, Omega, Amstelveen, the Netherlands) and relative humidity (RH) with a RH sensor (type Hygroclip, Rotronic, Hauppauge, NY, USA) inserted in a radiation shield. All sensors were installed near the grapevines at approximately 2 m above ground level.

Sap flow rate (SF) was monitored with heat balance sap flow sensors (models SGA10-ws or SGEX-13, Dynamax Inc., Houston, TX, USA) and stem diameter variations (D) with Linear Variable Displacement Transducers (LVDT, model LBB 375-PA-100 and transducer bridge 8C-35, Schaevitz, Hampton, VA, USA or model DF5.0, Solartron Metrology, Bognor Regis, UK), attached below the SF sensors with custom-made stainless steel holders, for which no temperature correction was required (Steppe and Lemeur, 2004).

Soil water potential (Ψ_{soil}) in each grapevine container was measured using an electronic tensiometer (type TensioTrans model 1000 C, Tensio-Technik, Geisenheim, Germany). All sensor signals were recorded every 20 s (DAQ 34970A and multiplexer 34901A, Agilent Technologies, Diegem, Belgium).

Stem water potential (Ψ_{stem}) measurements, used for initial model calibration and for verifying the real-time Ψ_{stem} model simulations during the actual application, were taken with a pressure chamber (PMS Instrument Company, Albany, OR, USA) at least twice a week around noon, and occasionally at several times during the day to examine the daily dynamics. One to three mature, healthy leaves per grapevine were chosen per record and covered in plastic bags coated with

aluminium foil for at least 2 h prior to Ψ_{stem} measurements to ensure hydraulic equilibrium with stem xylem water (McCutchan and Shackel, 1992).

6.2.3 Model description

As explained in **Chapter 5**, the basic principles of the applied water transport and storage model originated from the tree water transport and storage model of Steppe et al. (2006; 2008) and were conserved. Model structure and equations are shown in Fig. 6.1. The model describes the water transport in a single plant and is composed of two submodels: a water transport submodel describing the rigid xylem and surrounding living tissues (Fig. 6.1, left panel), and a submodel inferring the dynamics in D (Fig. 6.1, right panel). The latter result from both irreversible growth and reversible daily shrinkage and swelling caused by radial water transport (Génard et al., 2001; Steppe et al., 2006). Cells grow proportionally to the cell wall extensibility (ϕ) when the turgor pressure (Ψ^s_p) surpasses a critical wall-yielding threshold (Γ) (Lockhart, 1965). Ψ_{stem} decreases when plants start to transpire in the morning, developing a water potential gradient between stem and soil. Consequently, water uptake is induced, but also stored water contributes to the transpiration stream, causing the stem to shrink, because water in xylem and living storage tissues is hydraulically connected (Goldstein et al., 1998; Génard et al., 2001; Steppe et al., 2006; 2012).

To improve plant drought response simulations, the former constant hydraulic resistances of the original model were replaced by new equations in **Chapter 5**: the hydraulic resistance encountered during radial water transport (R^S , Eq. 5.4), as well as the integrated hydraulic resistance experienced during upward water transport through the soil-to-stem segment (R^X , Eq. 5.2), became dependent on Ψ_{soil} (Fig. 6.1). More details on the basic principles can be found in Steppe et al. (2006; 2008), and on the variable hydraulic resistances in **Chapter 5** and Baert and Steppe (2013).

6.2.4 Model calibration and simulation

Model development, simulation, calibration and identifiability analysis were conducted with PhytoSim (Phyto-IT BVBA, Mariakerke, Belgium), software developed for plant modelling and simulation. For model simulation, a fourth-order Runge-Kutta numerical integrator with variable step size was used (integrator

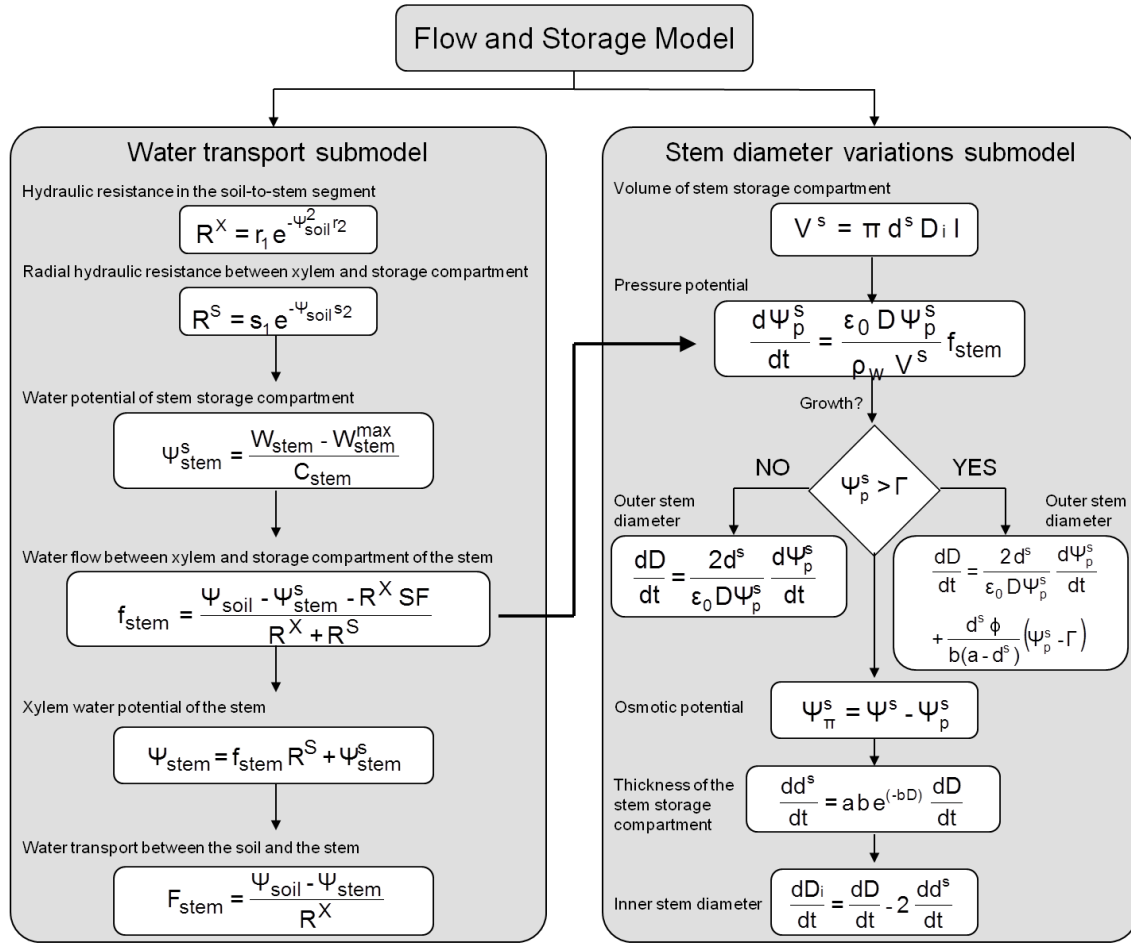


Fig. 6.1 Schematic overview of the model equations. The model consists of two submodels: a water transport submodel (left panel) for describing the dynamics of plant sap flow and storage, linked to a stem diameter variations submodel (right panel) that describes stem diameter changes and growth. Following parameters and variables are used in the model: F_{stem} , water flow between the roots and the stem; ψ_{soil} , soil water potential; ψ_{stem} , stem water potential; R^X , integrated hydraulic resistance in the soil-to-stem segment; f_{stem} , water flow between xylem and storage compartment; R^S , radial hydraulic resistance between the xylem and elastic storage tissues; ψ_{stem}^s , water potential of storage compartment; SF, sap flow rate; W_{stem} , water content of the storage compartment; W_{stem}^{max} , maximum W_{stem} ; C_{stem} , capacitance of the water storage tissues in the stem compartment; s_1 , s_2 , proportionality parameters for calculation of R^S ; r_1 , r_2 , proportionality parameters for calculation of R^X ; V^s , volume of the storage compartment; D_i , inner stem diameter; d^s , thickness of the storage compartment; l , length of the stem segment; D , outer diameter of the stem segment; ψ_p^s , turgor pressure potential of the storage compartment; ϵ_0 , proportionality constant; ρ_w , density of water; Γ , threshold at which cell wall-yielding occurs; ϕ , cell wall extensibility; a , b , allometric parameters; ψ_{π}^s , osmotic potential of the storage compartment.

settings: accuracy = $1 \cdot 10^{-6}$ and maximum step size = 0.1 s). For model calibration, the simplex method, originally developed by Nelder and Mead (1965) and available in PhytoSim, was used to minimise the weighted sum of squared errors between the measured data and the model simulations. Measurements of SF and

Ψ_{soil} were used as model inputs and measurements of D to calibrate the model (Fig. 6.2). While simulation of Ψ_{stem} is the actual target, the model additionally simulates other important features of plant functioning, such as R^X , R^S and turgor.

Model parameters were either fixed beforehand based on the literature or direct measurements, or assigned a value during initial model calibration, or daily recalibration (Table 6.1). Calibration parameters were selected based on two practical identifiability analysis (**Chapter 5**; De Pauw et al., 2008a), which investigated both the sensitivity of the parameters (i.e. sufficient influence on the model output) and their correlation with other model parameters (i.e. no linear dependencies with other model parameters) (De Pauw et al., 2008a; Steppe et al., 2008). The identifiability analysis for initial model calibration, including available measurements of D and Ψ_{stem} , revealed that parameters C_{stem} (stem capacitance), ϕ (cell wall extensibility), r_1 , r_2 (parameters for calculation of R^X) and s_2 (parameter for calculation of R^S) could be assigned unique values to. Since it seems logical to assume that some physiological characteristics of the plant (e.g. r_1 , r_2 , C_{stem}) do not remain constant throughout the growing season (Lechaudel et al., 2007; Steppe et al., 2008), the model was recalibrated daily for the actual application, using solely automatic D measurements. A second identifiability analysis demonstrated that the parameters C_{stem} , ϕ and r_2 were identifiable when only D measurements were used. In practice, unique values were first assigned to r_1 and s_2 using a short, initial measurement campaign with both D and manual Ψ_{stem} measurements. This initial calibration period was set equal to the moving window size (see below), in which several Ψ_{stem} measurements (around noon) at a sunny day were sufficient. Thereafter, the model was recalibrated on a daily basis. Each morning, at 4.00 h, new calibrated values for parameters C_{stem} , ϕ and r_2 were obtained using D measurements of the past two to six days and used for simulating the next day in real-time (Fig. 6.2).

6.2.5 Size of the moving window

The moving window size for model recalibration implies a compromise between (1) responsiveness, as a small moving window reacts rapidly to changing microclimatic and/or physiological conditions, and (2) stability, as a longer moving window is less influenced (or tricked) by the alternation of sunny with cloudy days (Steppe et al., 2008). Three options were tested: a two-, four- and six-day moving

window. Model performances were compared using an objective model selection criterion, called final prediction error (FPE) (e.g. **Chapter 5**; Dochain and Vanrolleghem, 2001; Steppe et al., 2006):

$$\text{FPE} = \frac{\text{SSE}}{N} + \frac{2p\text{SSE}}{(N-p)N} \quad (6.1)$$

with N the number of data points and p the number of estimated parameters (C_{stem} , ϕ and r_2). The lower the FPE, the better the model performance.

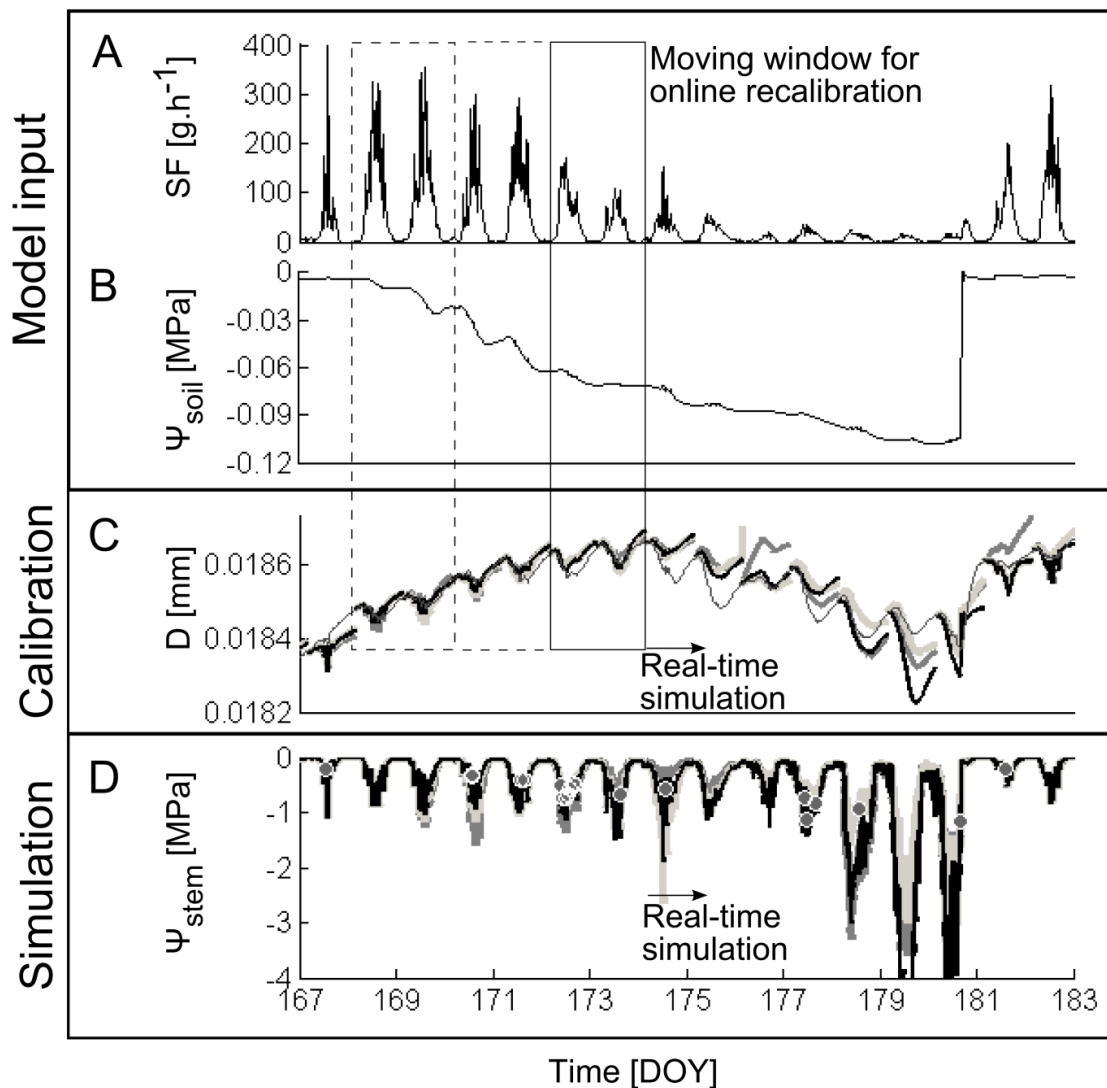


Fig. 6.2 Typical application of the water transport and storage model for real-time simulation of grapevine water status (detail of R1 during drought). (A) Sap flow rate, SF, and (B) soil water potential, Ψ_{soil} , are used as input variables. (C) Stem diameter variations, D, are used for daily model recalibration to simulate (D) stem water potential, Ψ_{stem} . Each morning, the model is recalibrated based on a moving window of past data and used for simulating the next day. Results from the model with a moving window of two (thick dark grey lines), four (thick light grey lines) or six (thick black lines) days are compared with measured D (thin grey line in C) and Ψ_{stem} (grey dots in D). Time is given in day of the year (DOY).

Table 6.1 Definition, value, unit and reference of the parameters used in the mechanistic water transport and storage models of R1 to R4, covering conditions from fully irrigated to severe drought.

Parameter	Definition	Value	Unit	Reference
Obtained from measurements, the literature or estimations				
l	Length of the stem segment	1	m	Measured
a	Allometric parameter	0.002968	m	Génard et al. (2001)
b	Allometric parameter	32	m^{-1}	Génard et al. (2001)
Γ	Critical threshold value for stem growth	0.9	MPa	Génard et al. (2001)
ϵ_0	Proportionality constant for calculation of the bulk elastic modulus	1100	m^{-1}	Steppe et al. (2006)
s_1	Proportionality parameter for calculation of the radial hydraulic resistance between xylem and elastic living tissues	0.02	$MPa \cdot h \cdot g^{-1}$	Estimated (Chapter 5)
Obtained during initial or daily (re)calibration				
C_{stem}	Capacitance of the water storage tissues in the stem compartment	1 - 10	$g \cdot MPa^{-1}$	Daily recalibrated
ϕ	Cell wall extensibility	0.0004 - 0.0063	$MPa^{-1} \cdot h^{-1}$	Daily recalibrated
r_1	Proportionality parameter for calculation of the integrated hydraulic resistance in the soil-to-stem segment	0.0007 - 0.0027	$MPa \cdot h \cdot g^{-1}$	Initially calibrated
r_2	Proportionality parameter for calculation of the integrated hydraulic resistance in the soil-to-stem segment	8 - 998	MPa^{-2}	Daily recalibrated
s_2	Proportionality parameter for calculation of the radial hydraulic resistance between xylem and elastic living tissues	52 - 63	MPa^{-1}	Initially calibrated

6.3 Results and discussion

6.3.1 Daily model recalibration

Measurements of D were used to recalibrate the model by comparing them with model simulations of D (Fig. 6.3A and 6.4A for R1 and R2, respectively; results of R3 to R5 are similar and therefore not shown). Every night, new values were assigned to the parameters C_{stem} , ϕ and r_2 by observing past data. These parameter values, containing plant information of the past days, were then applied for simulating the next day in real-time (24 h). The model thus simulated plant responses on a specific day using information on past plant behaviour. As a consequence, the model accurately simulated D when little differences existed in

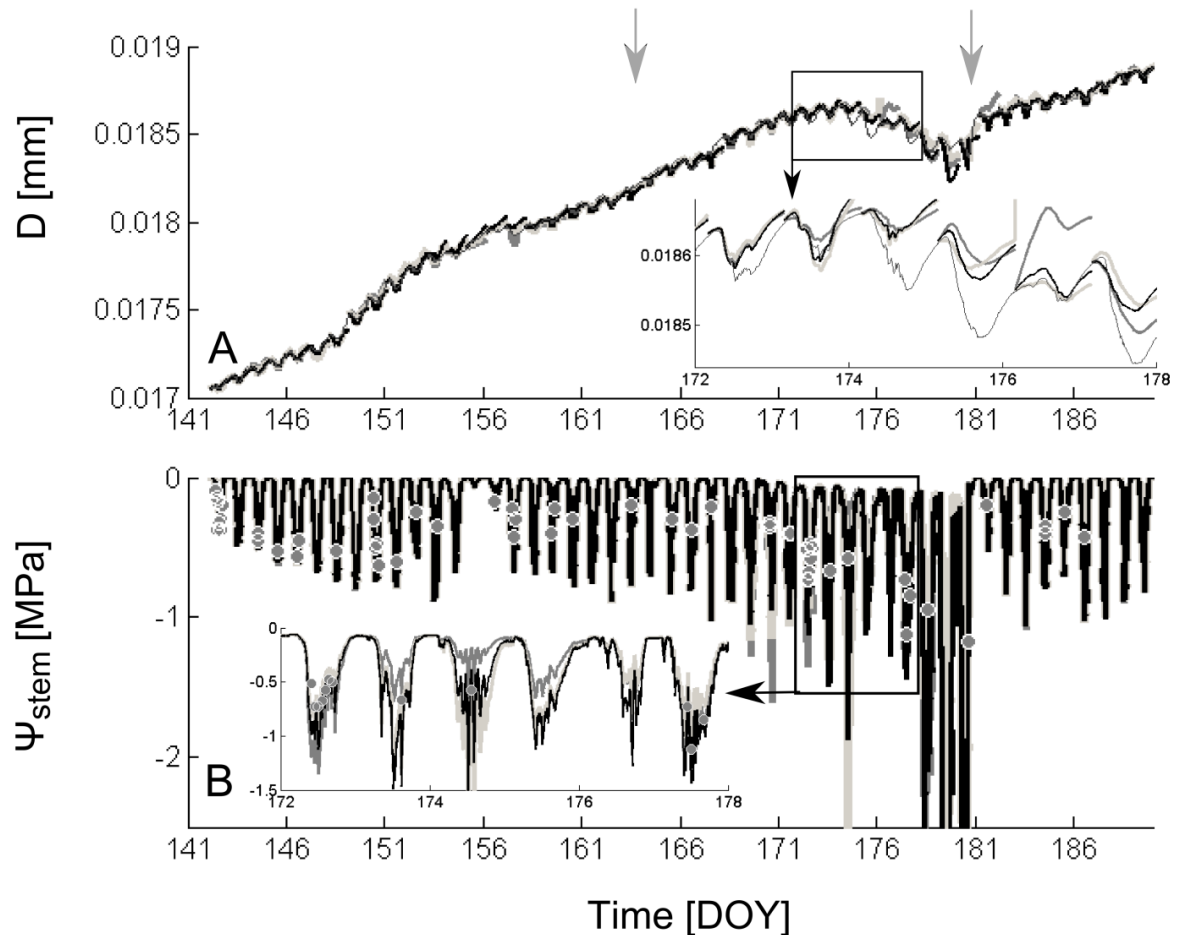


Fig. 6.3 Model simulations of (A) stem diameter variations, D , and (B) stem water potential, Ψ_{stem} , of R1 using a moving window for daily recalibration of two (thick dark grey lines), four (thick light grey lines) or six (thick black lines) days. Measured D (thin grey line in A) and Ψ_{stem} (grey dots in B) are indicated. Time is given in day of the year (DOY). Drought was imposed from DOY 163 - 180, as indicated by the grey arrows.

plant behaviour between consecutive days (Fig. 6.3A and 6.4A, e.g. model simulations before and after the drought period), but D simulations deviated from the measurements when the growth pattern altered between consecutive days. D simulations were then adapted day-by-day when D flattened out (Fig. 6.3A, DOY 152 - 158), or adjusted gradually when strong decreases in D occurred due to drought stress (e.g. detail in Fig. 6.3A). However, in the envisaged application, D measurements and corresponding model simulations mainly serve for daily recalibration. It is noteworthy that changes in D could be captured more accurately when model simulations were performed across the period of model calibration and no real-time simulations of the next day were intended (Fig. 6.5, calibration and simulation over a four-day period). However, in such an approach information on a specific day is not available until the next day, while this study aimed at real-time simulation of grapevine behaviour to enable a continuous, real-time monitoring of the plant water status.

6.3.2 Real-time simulation of the plant behaviour and water status

The water transport and storage model was used for real-time water status monitoring in grapevine, covering conditions from full irrigation to severe drought. The range within which optimised parameter values occurred, covering these various conditions and plants, are shown in Table 6.1. During wet and slight to severe drought conditions (Ψ_{soil} down to -0.09 MPa, e.g. Fig. 6.2B), the model performed well in simulating Ψ_{stem} dynamics (Fig. 6.3B (R1) and 6.4B (R2)), in spite of the adjustments the model already was required to make for capturing the effects on D dynamics under moderate drought conditions (Ψ_{soil} around -0.07 MPa, Fig. 6.2B, C). During the most severe drought conditions (last days of the imposed drought period), the model however tended to underestimate Ψ_{stem} , as it simulated lower values than those observed. In R1, this occurred from DOY 178 - 180 with the two- and six-day moving window (25-90% underestimation), while the model with a four-day moving window still simulated realistic Ψ_{stem} on DOY 178 (Fig. 6.3B). In R2, the model predicted realistic Ψ_{stem} across the entire period with a two-day moving window, except on DOY 151, but underestimated Ψ_{stem} on DOY 152, 154 and 156 with the other two moving windows (50-89%) (Fig. 6.4B). Finally, in R3, Ψ_{stem} was underestimated from DOY 177 onward (20-213%). This suggests that some plant mechanisms involved in grapevine drought responses under the

most extreme conditions are not yet, or not yet properly, included in the model. Note however that such conditions ($\Psi_{\text{soil}} < -0.09$ MPa) are extreme and will not be deliberately imposed in practice since it is known that excessive drought stress negatively affects the quality of grapes and associated wines (van Leeuwen et al., 2009). Model underestimation of Ψ_{stem} was also reflected in the deviation from the 1:1 line under lower Ψ_{soil} and Ψ_{stem} , but model simulations were accurate and realistic under less extreme soil conditions ($\Psi_{\text{soil}} > -0.09$ MPa) (Fig. 6.6).

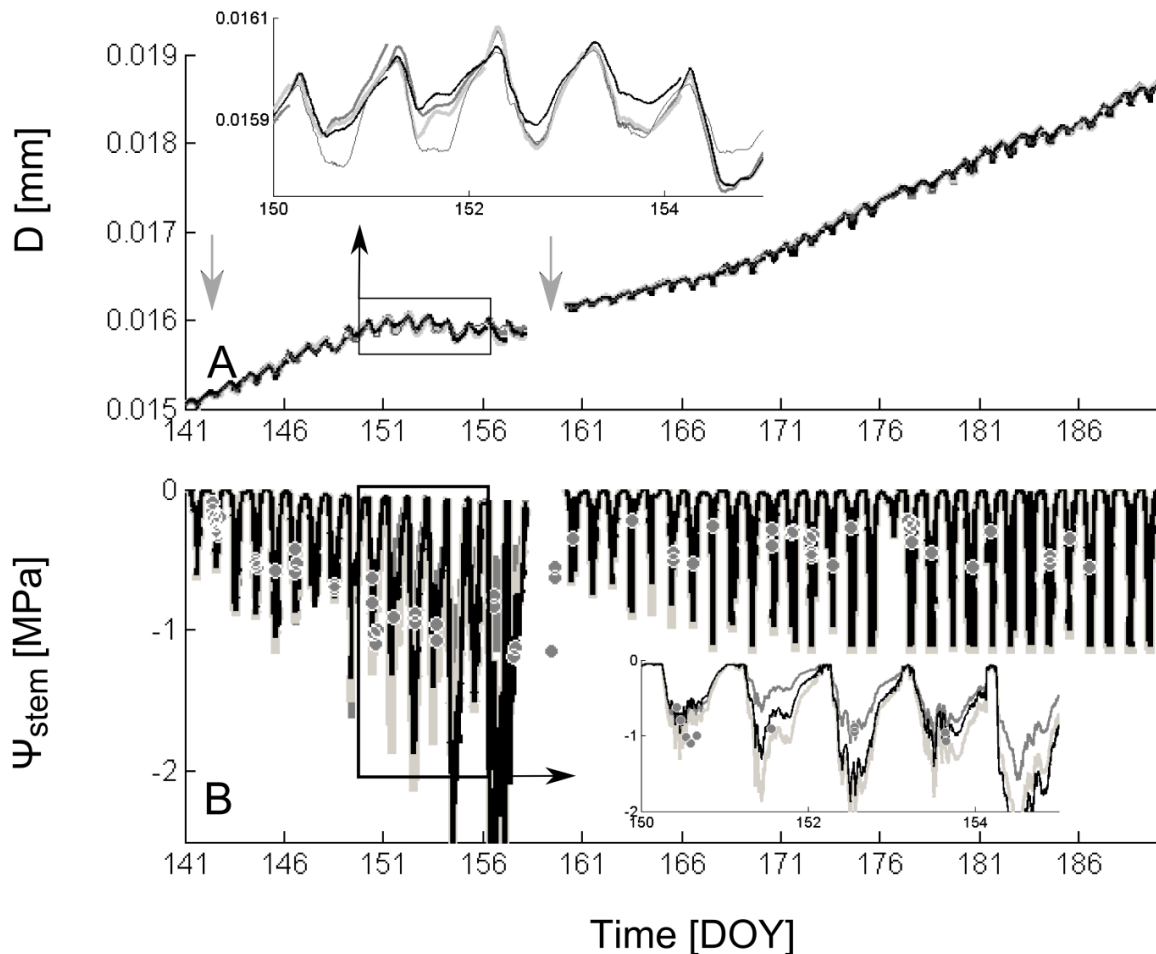


Fig. 6.4 Model simulations of (A) stem diameter variations (D) and (B) stem water potential (Ψ_{stem}) of R2 using a moving window for daily recalibration of two (thick dark grey lines), four (thick light grey lines) or six (thick black lines) days. Measured D (thin grey line in A) and Ψ_{stem} (grey dots in B) are indicated. Time is given in day of the year (DOY). Drought was imposed from DOY 142 - 159, as indicated by the grey arrows.

The model not only grasped the well-known effects of drought on D and Ψ_{stem} , but also revealed other drought responses of grapevine. Both the axial (R^X) and the radial (R^S) hydraulic resistance increased exponentially as water availability decreased and drought intensified (Fig. 6.7A and 6.7B, respectively). The increase

in R^X resulted from the assumed increase in water flow resistance in the soil with drought (Gardner, 1960; Tuzet et al., 2003; Zweifel et al., 2007), as well as the increase in resistance against upward water transport in the plant with decreasing water potential due to cavitated xylem vessels (Sperry et al., 1998; Lovisolo et al., 2010). Recently, a similar trend has also been suggested for R^S (Chapter 5; Steppe et al., 2012; Mencuccini et al., 2013). Both R^X and R^S in existing water transport models are however still assumed constant (e.g. Zweifel et al., 2007; De Pauw et al., 2008a; Steppe et al., 2008; De Schepper et al., 2010; De Swaef and Steppe, 2010; De Schepper et al., 2011), which might explain their limitation in performing well under severe drought conditions.

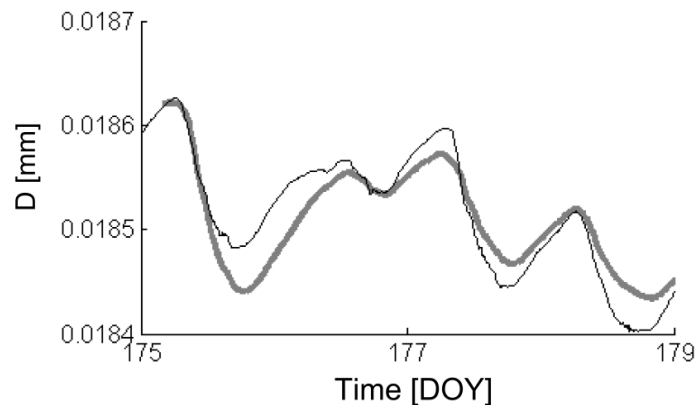


Fig. 6.5 Typical simulation of the stem diameter variations (D , thick grey line), of a grapevine (R1) using the model parameters obtained during model calibration for those days (no real-time simulation is intended). Measured D (black line) is also shown. Time is given in day of the year (DOY).

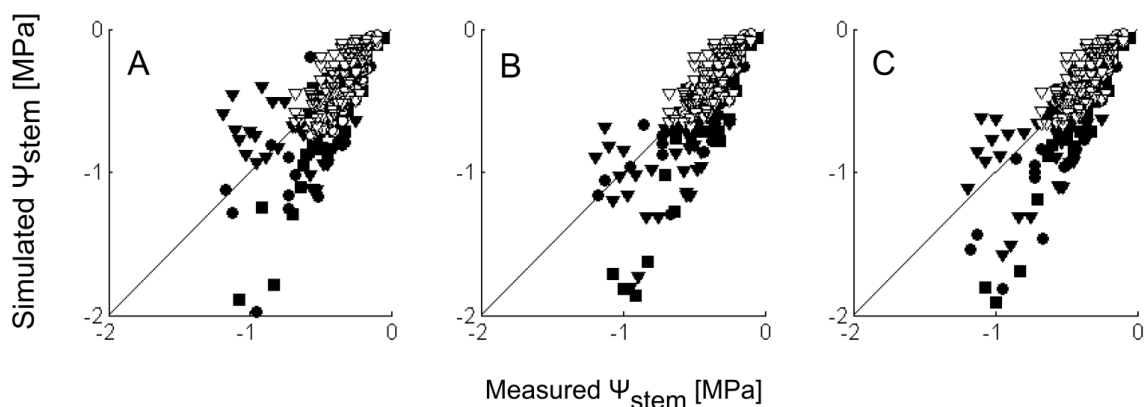


Fig. 6.6 Comparison of stem water potential (Ψ_{stem}) obtained from measurements (x-axis) or through real-time simulation (y-axis) of three drought-stressed (R1 (closed circles), R2 (closed triangles) and R3 (closed squares)) and two control grapevines (R4 (open circles) and R5 (open triangles)) using a moving window for daily recalibration of (A) two, (B) four or (C) six days.

In contrast to the increasing trends in R^X and R^S , mean turgor in the elastic storage tissues rapidly decreased when irrigation was withheld (Fig. 6.7C). This rapid change in bark turgor during drought has also been reported in a previous study on Scots pine trees (Mencuccini et al., 2013). This substantial drop in turgor with progressive drought resulted in a retarded radial stem growth in the

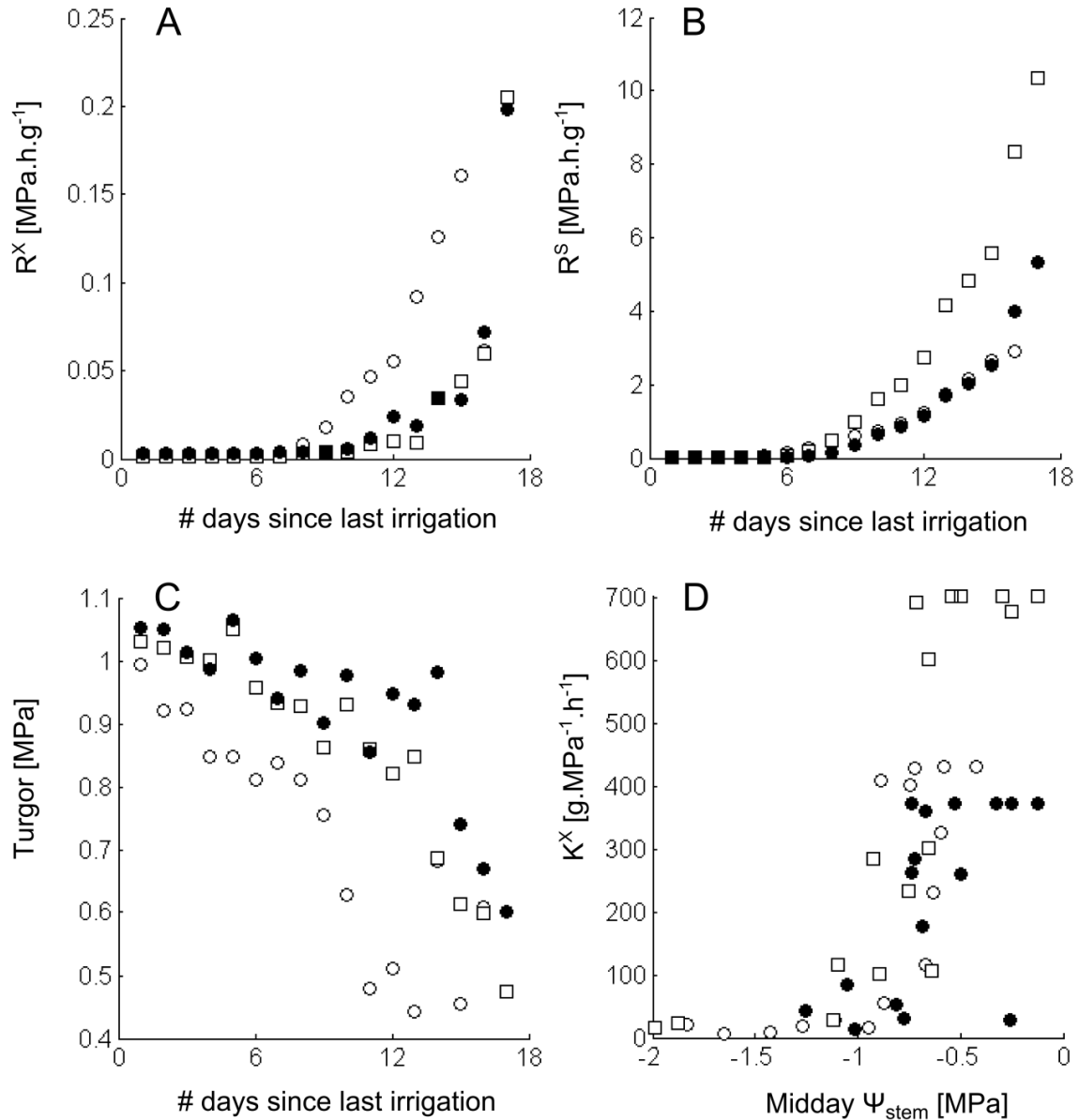


Fig. 6.7 Typical trend in three drought-stressed grapevines ((R1 (closed circles), R2 (open circles) and R3 (open squares)) in: (A) hydraulic resistance in the soil-to-stem segment, R^X , (B) radial hydraulic resistance between xylem and elastic storage tissues, R^S , and (C) turgor of the storage tissues, Ψ_p , as a function of day since the last irrigation event. (D) Hydraulic conductance in the soil-to-stem segment ($K^X = 1/R^X$) as a function of midday stem water potential, Ψ_{stem} (12.00 - 14.00 h). All values are daily means.

grapevines and overall stem shrinkage was observed when the daily mean turgor dropped below 83% of its critical wall-yielding threshold Γ (Fig. 6.3A and 6.4A).

Although all grapevines showed similar trends in simulated R^X , R^S and turgor under the influence of drought (Fig. 6.7A to C), their absolute values differed from grapevine to grapevine. The existence of such a plant-to-plant variability, also observed in other studies on grapevine (e.g. Fernández and Cuevas, 2010; Montoro et al., 2012; Santesteban et al., 2013), indicates the importance of a model calibration (initial as well as daily recalibration) for each grapevine to obtain optimised model parameters for each monitored individual.

The model-analysis showed a gradual decline in hydraulic functioning when drought stress progressed (lower midday Ψ_{stem}). By depicting the integrated soil-to-stem hydraulic conductance ($K^X = 1/R^X$) as a function of midday Ψ_{stem} (Fig. 6.7D), a curve that strongly resembled the often-applied vulnerability curve was generated, which describes the relationship between the percentage loss of hydraulic conductivity and Ψ_{stem} (e.g. Choat et al., 2010; Cochard et al., 2010). Whereas this classical vulnerability curve only examines the hydraulic conductance in the stem xylem, this study includes the hydraulic conductance in soil and roots as well. From these generated curves the $\Psi_{\text{stem},50}$ (-0.65 ± 0.02 MPa) and the $\Psi_{\text{stem},90}$ (-1.07 ± 0.11 MPa) at which 50% and 90% loss of conductance in the soil-to-stem segment occurred was determined. This $\Psi_{\text{stem},50}$ is higher than the in the literature reported -0.70 MPa to -2.97 MPa for Chardonnay (Wheeler et al., 2005; Alsina et al., 2007; Choat et al., 2010), but this discrepancy can be attributed to the fact that reported vulnerability curves only examine the hydraulic conductance in the stem xylem, whereas this model approach integrates the hydraulic conductance in soil and plant. It was found that when Ψ_{stem} fell below the $\Psi_{\text{stem},90}$ threshold, the water transport function was markedly impaired, leading to the overall shrinkage of the stem diameter (Fig. 6.3 and 6.4).

6.3.3 Size of the moving window

The model was tested using three different moving window sizes of past D data for daily model recalibration in order to search for the best model performance. No consistently better performance was observed when using a two-, four- or six-day moving window (Fig. 6.3 and 6.4), with the exception of days with extreme

drought. Also the FPE results (Table 6.2) reflected small differences, and no consistent trend in FPE with moving window size was found. The best option seems therefore to use a medium (i.e. four-day) moving window size for daily model recalibration, as it represents a good compromise between model stability and responsiveness to physiological changes. Also Steppe et al. (2008) obtained successful irrigation scheduling with a four-day moving window in their study on apple trees under sufficient water supply.

Table 6.2 Final prediction error (FPE) for simulations of stem diameter variations (D) and stem water potential (Ψ_{stem}) with the mechanistic water transport and storage model. Simulations obtained with a two-, four- or six-day moving window for daily model recalibration are compared for three drought-stressed (R1, R2, R3) and two control (R4, R5) grapevines. The lower the FPE (underlined values), the better the model.

Moving window for daily recalibration			
Repetition	two days	four days	six days
FPE for D [mm ²]			
R1	0.0011	0.0008	0.0013
R2	0.0011	0.0015	0.0013
R3	0.0018	0.0028	0.0025
R4	0.0006	0.0010	0.0013
R5	0.0004	0.0005	0.0007
FPE for Ψ_{stem} [MPa ²]			
R1	0.10	0.05	0.08
R2	0.08	0.10	0.08
R3	0.19	0.19	0.27
R4	0.02	0.00	0.01
R5	0.02	0.02	0.02

6.3.4 Step toward accurate irrigation scheduling

This small-scale experiment on five potted grapevines illustrates the first successful combination of a mechanistic water transport and storage model with automatic plant measurements for accurate real-time monitoring of Ψ_{stem} under slight to severe drought stress ($\Psi_{\text{soil}} > -0.09$ MPa) (Fig. 6.3B and 6.4B). A remaining challenge is now to define a threshold or reference value beyond which the plant is considered to sense too much stress and beyond which action (irrigation) is needed (Fereres and Goldhamer, 2003; Jones, 2004) to ensure optimal fruit quality and resulting wine. This will be discussed in detail in **Chapter**

7. Such thresholds should be dynamic, since they are not only influenced by soil water availability, but also by microclimatic conditions (**Chapters 3 and 4**; Steppe et al., 2008; De Swaef et al., 2009; Ortuño et al., 2010) and plant phenology. Furthermore, additional large-scale experiments, including field experiments, are required for further testing the applicability of the water transport and storage model for future practical applications and for determining the required number of measured individuals, as plant-to-plant variability has been observed. For field set-ups, also the positioning of one or more Ψ_{soil} sensors should be carefully considered, as a large spatial variability in soil properties and soil water potential may occur (Gardner, 1960; Jones, 2004).

6.4 Conclusions

In this chapter, it was demonstrated that the use of a mechanistic water transport and storage model in combination with plant measurements could be a valuable alternative for real-time monitoring of the plant water status. The model not only accurately simulated Ψ_{stem} , but it also gave new insights into the behaviour of the grapevines during drought stress via simulation of rapid changes in turgor in the elastic tissues, increases in axial and radial hydraulic resistances and via the generation of soil-to-stem segment vulnerability curves.

Chapter 7

Dynamic thresholds for stem water potential

Abstract

The ability to monitor grapevine water status is of utmost importance to achieve better fruit and wine quality. Even though the stem water potential (Ψ_{stem}) is recognised as one of the best indicators for monitoring plant water status, a generic, high time-resolution, dynamic threshold beyond which the plant is sensing stress is still lacking. Two dynamic Ψ_{stem} thresholds were therefore examined for grapevine (*Vitis vinifera* L. cv. Chardonnay): the first threshold uses vapour pressure deficit (VPD), while the second one uses potential evapotranspiration (λE_p), thus combining VPD and solar radiation, both known as key driving variables for transpiration. The proposed method continuously evaluates whether simulations of actual Ψ_{stem} remain within the limits defined by the dynamic Ψ_{stem} threshold. If not, drought stress is detected. Both approaches detected drought stress 7 to 11 days following the last irrigation event, which is several days before visible symptoms appeared. This system hence achieved early warning of a deviating Ψ_{stem} from behaviour under well-watered conditions and allowed a continuous tight supervision of the grapevine water status by comparing actual simulated Ψ_{stem} against its threshold at any moment. Despite these promising results, the attempt of using one generic threshold for all grapevines occasionally resulted in false detection of drought stress under well-watered conditions. Further

research is therefore recommended on the quantification of generic parameters for the thresholds before testing this method in practice.

7.1 Introduction

Plant measurements are frequently used to verify the plant's health and water status. In many applications, irrigation is scheduled using information from plant measurements (Ginestar et al., 1998; Jones, 2004; Fernández and Cuevas, 2010; Fernández et al., 2011a). Since mild drought stress at specific times can have positive effects on fruit quantity, dimension and composition (Naor, 2006; De Swaef and Steppe, 2010), plant-based irrigation scheduling offers the potential to enhance fruit quality. Certain levels of drought stress can be allowed or even imposed, while still maintaining tight supervision over the plant's water potential and physiological condition.

One of the best indicators of plant water status is stem water potential (Ψ_{stem}) (Choné et al., 2001; Möller et al., 2007; Acevedo-Opazo et al., 2010). To apply Ψ_{stem} (or any plant water status indicator) for irrigation scheduling, a threshold or reference value beyond which the plant starts sensing a certain level of drought stress is required (Ferreles and Goldhamer, 2003; Jones, 2004). This threshold cannot be defined as a fixed constant value, but should be dynamic, because both soil water availability and microclimatic conditions determine its magnitude (**Chapter 4**; Steppe et al., 2008; De Swaef et al., 2009; Ortuño et al., 2010). Several approaches have been proposed to determine dynamic thresholds. Measurements of the selected indicator can be compared with the ones obtained from a reference group of plants, which are maintained under sufficient soil water availability during the entire monitoring period (Patakas et al., 2005; Fernández et al., 2008). The difficulties are however to assign a threshold to this ratio and to ensure that the reference group remains representative for the monitored plants (Goldhamer and Fereres, 2001). Alternatively, baselines or reference relationships between the water status indicator and a microclimatic variable, obtained under sufficient water availability, are used (Intrigliolo and Castel, 2006; Ortuño et al., 2006; Velez et al., 2007; Fernández and Cuevas, 2010). The most suitable microclimatic variable to relate the water status indicator to may change with

species, environment and cultural conditions (Velez et al., 2007). To avoid some of these issues, two Principal Component Analysis (PCA) techniques that define statistical limits beyond which drought stress is detected were proposed in **Chapters 3** and **4**. The techniques do not require determination of the conventional threshold values, but use measurements on selected plants during a short preceding control period in which full irrigation is pursued to calibrate the PCA models.

Although some suitable reference equations linking a microclimatic variable to Ψ_{stem} have previously been developed (e.g. for plum in Intrigliolo and Castel (2006) and for lemon trees in Ortuño et al. (2006)), the elaboration of a generic, high time-resolution, dynamic threshold based on microclimatic measurements is scarce and still lacking for grapevines. Also for grapevines it is known that an accurate monitoring of the plant water status and a plant-based decision of the irrigation supply has a great potential to produce high quality grapes and resulting wines (Matthews et al., 1990; van Leeuwen et al., 2009; Acevedo-Opazo et al., 2010; Chaves et al., 2010; Keller, 2010a). The aim of this chapter was therefore to (1) propose two dynamic Ψ_{stem} thresholds for grapevines (*Vitis vinifera* L. cv. Chardonnay) based on microclimatic variables, and (2) investigate and compare their performance for water status monitoring and fast drought stress detection.

7.2 Material and methods

7.2.1 Plant material and experimental set-up

Data from 21 May (day of flowering) until 8 July 2012 (day of the year, DOY 142 - 190) from six potted grapevines (*Vitis vinifera* L. cv. Chardonnay) were used for this study. The grapevines were planted in 2010 in 50 L containers filled with DCM mediterranean compost and fertilised in summer with DCM organic fertiliser for grapes. They were grown in a greenhouse facility of the Faculty of Bioscience Engineering at Ghent University, Belgium. Diameters at stem base ranged from 9 to 17 mm at the beginning of the 2012-growing season. After a control period in which the plants were irrigated at least twice a week to guarantee adequate soil water availability, four grapevines were subjected to a drought treatment by withholding irrigation. The period of drought lasted from 11 until 28 June 2012 (DOY 163 -

180) for repetitions R1 to R3, while irrigation was withheld from a fourth grapevine (R4) between 21 May and 7 June 2012 (DOY 142 - 159). Control grapevines C1 and C2 were irrigated three times a week the entire growing season.

7.2.2 Water status monitoring

Fig. 7.1 summarises the proposed methodology for plant water status monitoring and drought stress detection using dynamic thresholds based on environmental conditions. Each step will be explained in detail in the following paragraphs. Actual Ψ_{stem} is continuously simulated using a water transport and storage model (**Chapters 5 and 6**; Baert and Steppe, 2013), and compared against a dynamic Ψ_{stem} threshold with uncertainty band. Two options to calculate this threshold are compared: either an approach using only vapour pressure deficit (VPD), or a more elaborate approach using potential evapotranspiration (λE_p). When the actual simulated Ψ_{stem} distinctively moved outside the uncertainty band of the Ψ_{stem} threshold, drought stress is detected.

Actual stem water potential

Actual Ψ_{stem} is simulated with a dynamic water transport and storage model (**Chapters 5 and 6**; Baert and Steppe, 2013). The model uses measurements of sap flow rate (SF) and soil water potential (Ψ_{soil}) as input and stem diameter variations (D) for daily model recalibration. The model enables accurate Ψ_{stem} simulations in grapevines under both wet and dry conditions. More details can be found in **Chapters 5 and 6**.

To be able to apply this model, each grapevine was equipped with a heat balance sap flow sensor to measure SF (model SGA10-ws or SGEX-13, Dynamax Inc., Houston, TX, USA) and a Linear Variable Displacement Transducer to measure D (LVDT, model LBB 375-PA-100 and transducer bridge 8C-35, Schaevitz, Hampton, VA, USA or model DF5.0, Solartron Metrology, Bognor Regis, UK). The LVDTs were attached to the base of the stem with custom-made stainless steel holders for which no temperature correction is required (Steppe and Lemeur, 2004). Ψ_{soil} was measured with electronic tensiometers inserted in each container (type TensioTrans model 1000 C, Tensio-Technik, Geisenheim, Germany). All sensor signals were scanned every 20 s and averaged over 5 min (DAQ 34970A and multiplexer 34901A, Agilent Technologies, Diegem, Belgium).

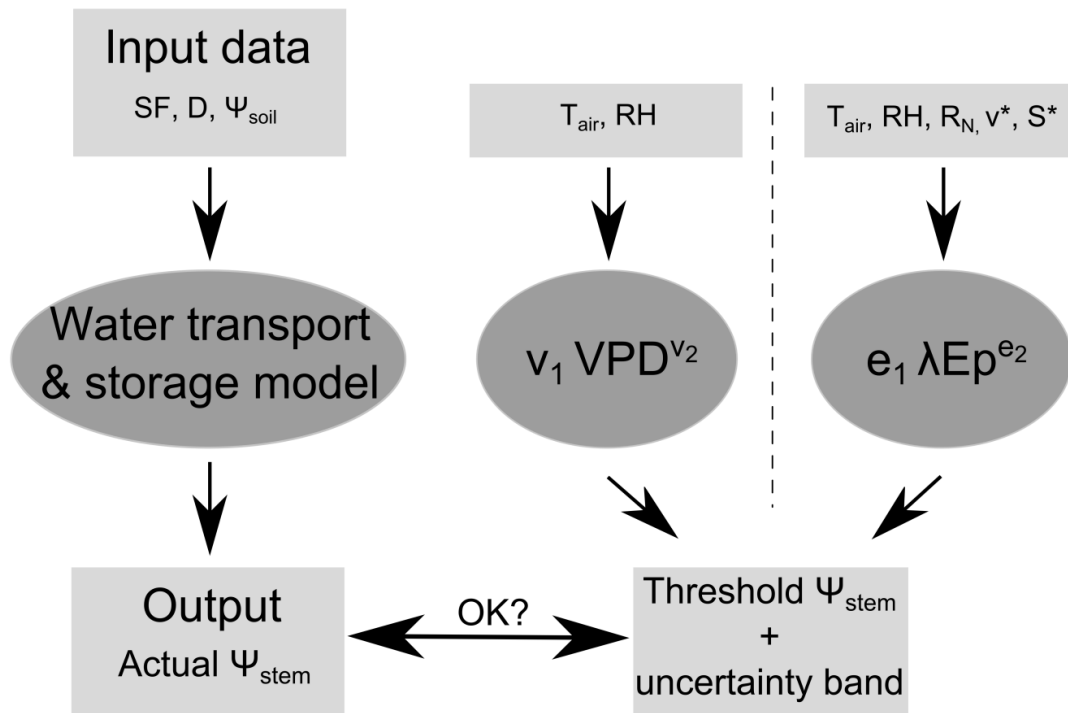


Fig. 7.1 General concept of dynamic thresholds based on environmental conditions to achieve plant-based water status monitoring and fast drought stress detection. Actual stem water potential (Ψ_{stem}) is simulated using a water transport and storage model (**Chapter 6**), in which sap flow rate (SF), stem diameter variations (D) and soil water potential (Ψ_{soil}) are used as input. Subsequently, actual Ψ_{stem} is compared against a Ψ_{stem} threshold (with uncertainty band), which is calculated based on either vapour pressure deficit (VPD) or potential evapotranspiration (λE_p). Both thresholds need air temperature (T_{air}) and relative humidity (RH) measurements as input, while the λE_p -based threshold uses in addition net radiation (R_N), wind speed (v) and soil heat flux (S). *wind speed ($v = 1 \text{ m}\cdot\text{s}^{-1}$) and soil heat flux ($S = 0 \text{ W m}\cdot\text{s}^{-2}$) are assumed constant in this study.

Manual Ψ_{stem} measurements were performed with a pressure chamber (PMS Instrument Company, Albany, OR, USA) and used to verify the actual Ψ_{stem} model simulations. One to three leaves per grapevine were covered in plastic bags coated with aluminium foil for at least 2 h prior to Ψ_{stem} measurements (McCutchan and Shackel, 1992).

Microclimatic variables

Two Ψ_{stem} thresholds are key in this study. A first approach derives the dynamic Ψ_{stem} threshold from VPD, which is calculated from relative humidity (RH) and air temperature (T_{air}) as the difference between the air's potential and actual vapour pressure value. T_{air} was measured with a thermocouple (type T, Omega, Amstelveen, the Netherlands) and RH with a RH sensor (type Hygroclip, Rotronic, Hauppauge, NY, USA) inserted in a radiation shield.

Photosynthetic active radiation (PAR) may have a large influence on plant performance in protected environments such as greenhouse facilities (Vermeulen et al., 2012) and is known to be a key driving variable for plant transpiration besides VPD and soil water availability (Jones, 1992; De Swaef and Steppe, 2010). Therefore, a second dynamic Ψ_{stem} threshold was defined using λE_p to include both VPD and solar radiation. λE_p [$\text{W}\cdot\text{m}^{-2}$] is calculated based on the Penman equation (e.g. Penman, 1948; Allen et al., 1998):

$$\lambda E_p = \frac{s}{s+\gamma}(R_N - S) + \frac{\gamma}{s+\gamma} \frac{\rho_v^0(T_{\text{air}}) - \rho_v(T_{\text{air}})}{r_a / \lambda} \quad (7.1)$$

with s the slope of the curve relating saturation vapour pressure with temperature [$\text{hPa}\cdot\text{C}^{-1}$], γ the psychrometric constant [$\text{hPa}\cdot\text{C}^{-1}$], R_N the net radiation [$\text{W}\cdot\text{m}^{-2}$], S the soil heat flux [$\text{W}\cdot\text{m}^{-2}$], $\rho_v^0(T_{\text{air}})$ and $\rho_v(T_{\text{air}})$ the saturated and actual vapour concentration at air temperature [$\text{g}\cdot\text{m}^{-3}$], respectively, r_a the aerodynamic resistance [$\text{s}\cdot\text{m}^{-1}$] and λ the latent heat of evaporation [$\text{J}\cdot\text{g}^{-1}$]. r_a was calculated based on wind speed (v [$\text{m}\cdot\text{s}^{-1}$]) (Allen et al., 1998), which was assumed low ($v = 1 \text{ m}\cdot\text{s}^{-1}$) since the plants were located in a (ventilated) greenhouse facility (e.g. Jarvis and McNaughton, 1986; Vermeulen et al., 2012). S was assumed negligible because the soil surface in the containers was very small compared to the above leaf area and S is in any case small compared to R_N (Allen et al., 1998). R_N was estimated using PAR measurements, which were conducted with a quantum sensor (LI-190S, Li-COR, Lincoln, NE, USA) installed near the grapevines approximately 2 m above the ground.

Calculation and calibration of dynamic Ψ_{stem} thresholds

Following Liu et al. (2007), Eq. 7.2 was used to calculate a dynamic Ψ_{stem} threshold [MPa] based on VPD [kPa]:

$$\text{Threshold } \Psi_{\text{stem}} = -v_1 \text{ VPD }^{v_2} \quad (7.2)$$

with v_1 and v_2 parameters dependent on microclimatic and plant characteristics. A similar equation was defined for the dynamic Ψ_{stem} threshold [MPa] based on λE_p [$\text{W}\cdot\text{m}^{-2}$]:

$$\text{Threshold } \Psi_{\text{stem}} = -e_1 \lambda E_p^{e_2} \quad (7.3)$$

with e_1 and e_2 parameters dependent on microclimatic and plant characteristics. Calibration of the parameters in Eq. 7.2 and 7.3 was conducted with PhytoSim (Phyto-IT BVBA, Mariakerke, Belgium), a software developed for plant modelling and simulation, by using the simplex search algorithm (Nelder and Mead, 1965) to minimise the weighted sum of squared errors between actual simulated Ψ_{stem} (**Chapter 6**) under well-watered conditions and threshold Ψ_{stem} . All parameters (v_1 , v_2 , e_1 and e_2) were found identifiable (sensitivity and identifiability analysis as explained in De Pauw et al. (2008a)), with v_2 two times more sensitive than v_1 (Eq. 7.2) and e_2 over six times more sensitive than e_1 (Eq. 7.3).

The aim was to develop a generic Ψ_{stem} threshold based on either VPD or λE_p to be used for all plants across the entire monitoring period. To this end, each parameter value, obtained by individual threshold calibration for each well-watered grapevine during the first four days of the experiment (DOY 142 - 146, resulting in a coefficient of determination R^2 ranging from 0.82 to 0.96), was averaged (i.e. grapevines C1, C2 and R1 to R3; R4 was not included as drought was imposed from DOY 142 onward). This four-day calibration period was identical to the initial calibration period of the water transport and storage model used for actual Ψ_{stem} simulation (**Chapter 6**). Resulting mean parameter values constituted the generic Ψ_{stem} thresholds for all grapevines: $v_1 = 0.12 \pm 0.03$, $v_2 = 1.06 \pm 0.12$ for Eq. 7.2 and $e_1 = 1.22 \cdot 10^{-6} \pm 2.47 \cdot 10^{-7}$, $e_2 = 1.75 \pm 0.03$ for Eq. 7.3.

Threshold uncertainty band

Verifying the uncertainty of the dynamic Ψ_{stem} thresholds because of parameter uncertainty is very useful, because the thresholds are intended for prediction of normal Ψ_{stem} behaviour under well-water conditions and, in the future, decision making. A Monte Carlo uncertainty analysis was performed (see procedure in De Pauw et al., 2008b) with PhytoSim (Phyto-IT BVBA, Mariakerke, Belgium). To this end, a normal probability density function was assigned to each parameter (v_1 , v_2 in Eq. 7.2 and e_1 , e_2 in Eq. 7.3) based on the above mentioned parameter values and their respective standard deviation. From these normal distributions associated with the parameters, 1000 samples were generated using Latin hypercube sampling (e.g. Helton and Davis, 2003; De Pauw et al., 2008b). In a next step, the sampled parameter values were propagated through the model to generate the output uncertainty on the Ψ_{stem} thresholds. The upper and lower

limits of the uncertainty band were defined as the 95th and 5th percentile of the resulting output probability distribution constructed from the 1000 different trajectories. This uncertainty band was used to evaluate actual simulated Ψ_{stem} .

7.3 Results and discussion

7.3.1 Calculation of stem water potential thresholds and uncertainty bands

The trajectories of Eq. 7.2 and 7.3 corresponded well with the relationships found between actual simulated Ψ_{stem} and VPD or λE_p during well-watered conditions (Fig. 7.2, data from the well-watered first four days of grapevines C1, C2, R1, R2 R3), and seemed to justify implementation of Eq. 7.2 and 7.3 as dynamic Ψ_{stem} thresholds. The standard deviation on each threshold parameter (v_1 , v_2 in Eq. 7.2 and e_1 , e_2 in Eq. 7.3) resulted in an uncertainty of the thresholds itself, which varied along the day (Fig. 7.2: changes in magnitude of grey bands). The threshold uncertainty was observed to be higher during the day (higher values of VPD or λE_p) compared to nighttime hours, where Ψ_{stem} , VPD and λE_p were close to zero. To account for this variability, an uncertainty analysis (section 7.2.2) was therefore performed, rather than using the parameter values and respective standard deviations directly. In a next step, the thresholds (Eq. 7.2 and 7.3) with corresponding uncertainty bands were used to supervise the plant's water status and detect drought stress.

7.3.2 Dynamic thresholds for water status monitoring

On two typical well-watered sunny (Fig. 7.3A and B) and cloudy (Fig. 7.3C and D) days, actual simulated Ψ_{stem} remained within the uncertainty band of both thresholds, indicating that Ψ_{stem} behaved as predicted for well-watered Chardonnay grapevines under the prevailing microclimatic conditions (VPD or λE_p). The Monte Carlo uncertainty analysis (De Pauw et al., 2008b) translated the observed uncertainty of the respective thresholds (Fig. 7.2) in smaller uncertainty bands at night, when lowest VPD and λE_p occurred, and wider bands in the afternoon when VPD and λE_p were highest (Fig. 7.3). Similarly, lower VPD and λE_p values on cloudy days also resulted in smaller uncertainty bands. On typical drought-stressed days (starting a few days after irrigation was stopped), actual

simulated Ψ_{stem} deviated from its normal behaviour expected under sufficient soil water availability and was observed outside the predicted uncertainty band on the dynamic thresholds (Fig. 7.3E and F, respectively). The more severe the drought stress became and the more it started having a distinct effect on grapevine functioning, the more actual simulated Ψ_{stem} decreased and exceeded the uncertainty bands (e.g. Fig. 7.4A and B for VPD- and λE_p -based threshold, respectively), illustrating that when drought progressed, deviation from predicted normal Ψ_{stem} behaviour intensified.

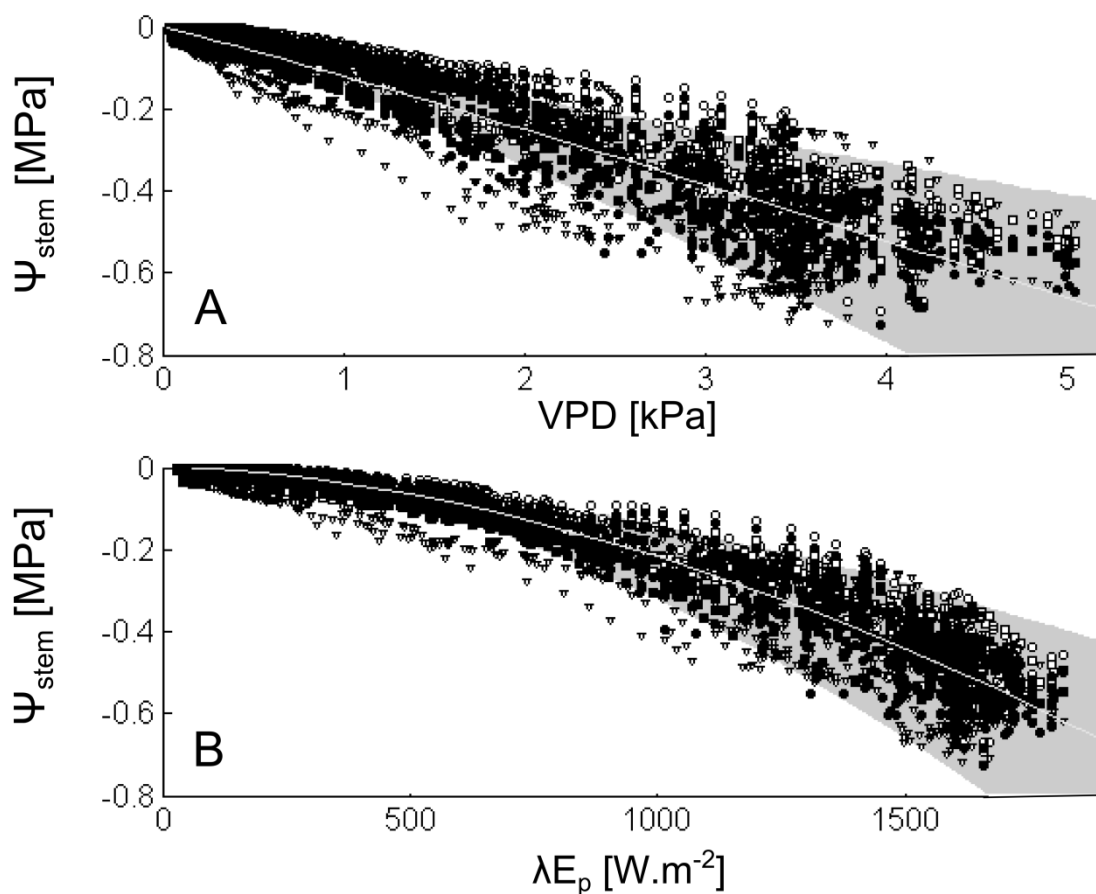


Fig. 7.2 Relationship between actual simulated stem water potential (Ψ_{stem}) and (A) vapour pressure deficit (VPD) or (B) potential evapotranspiration (λE_p) under well-watered conditions. Data from the first four well-watered days of grapevines C1 (open circles), C2 (open triangles), R1 (open squares), R2 (closed circles) and R3 (closed squares), which were used for calibrating a VPD- and λE_p -based dynamic Ψ_{stem} threshold (grey lines), are shown. Standard deviation of the thresholds is also shown (grey bands).

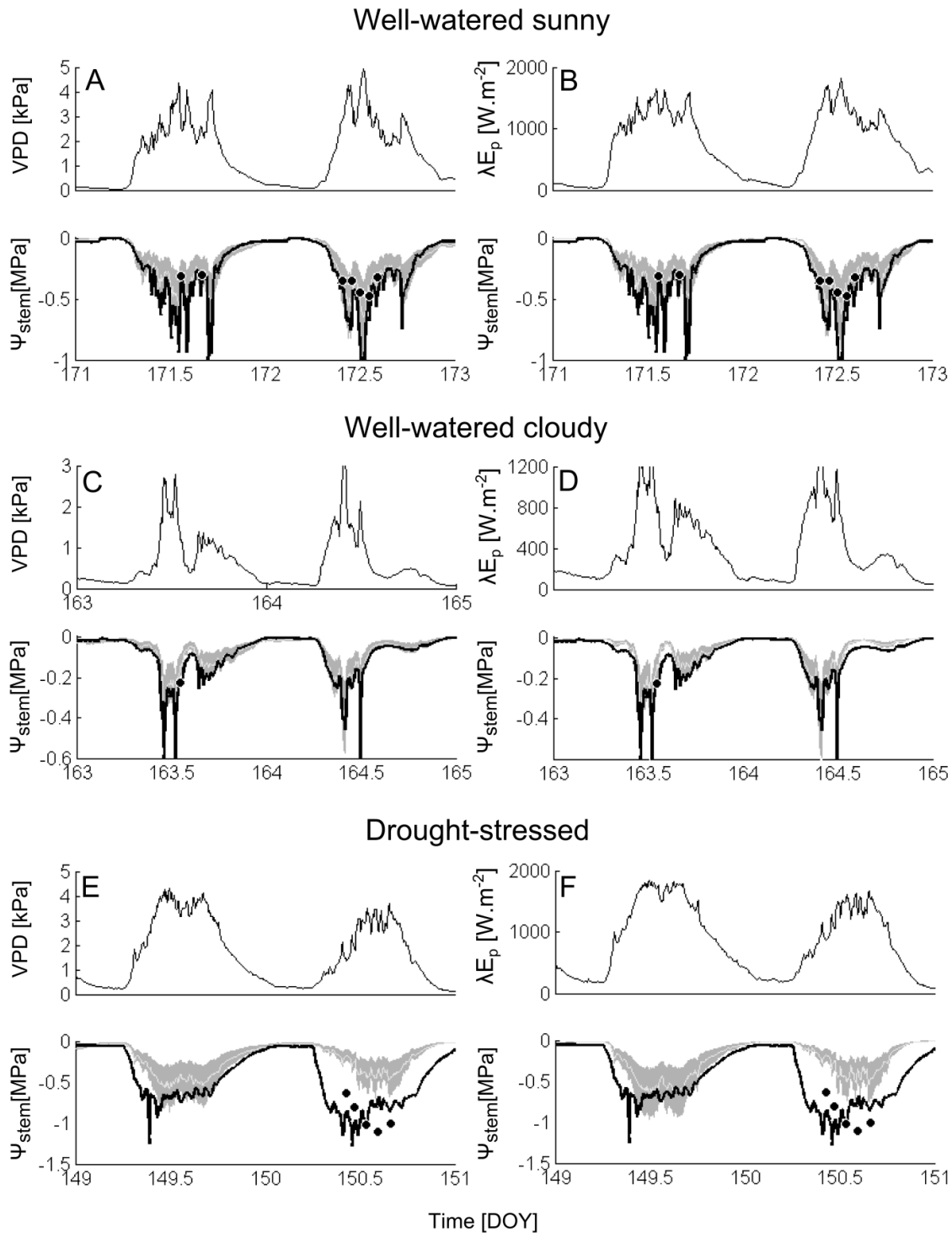


Fig. 7.3 Comparison of two dynamic threshold approaches for water status monitoring and fast drought stress detection. Left: vapour pressure deficit (VPD) and corresponding VPD-based stem water potential (Ψ_{stem}) threshold (white line in grey uncertainty band) for two typical sunny (A) and cloudy (C) well-watered days, and two typical sunny days with drought stress (E). Right: potential evapotranspiration (λE_p) and corresponding λE_p -based Ψ_{stem} threshold (white line in grey uncertainty band) for two typical sunny (B) and cloudy (D) well-watered days, and two typical sunny days with drought stress (F). Actual simulated Ψ_{stem} (black lines) and manual Ψ_{stem} measurements (black dots) are also shown. Time is given in day of the year (DOY).

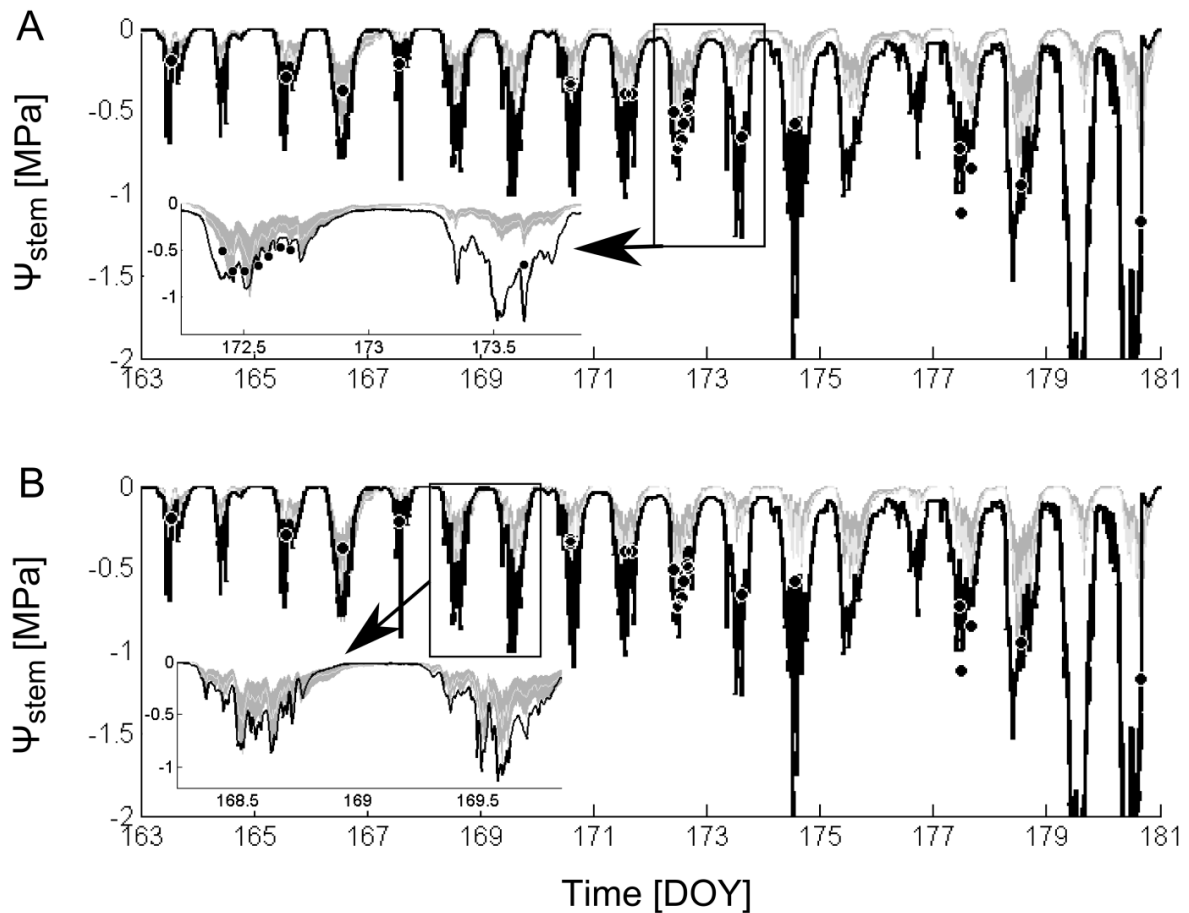


Fig. 7.4 Typical example of actual simulated stem water potential (Ψ_{stem} , black lines) during imposed drought stress (grapevine R3, day of the year (DOY) 163 - 180). Actual simulated Ψ_{stem} is compared against the uncertainty band (grey band) on the dynamic Ψ_{stem} threshold based on (A) vapour pressure deficit (VPD) or (B) potential evapotranspiration (λE_p). Black dots show manual Ψ_{stem} measurements; insets zoom in on two successive days to show that deviation of actual simulated Ψ_{stem} from expected normal behaviour increases when drought progresses.

The dynamic behaviour of the thresholds is important for obtaining reliable plant-based drought detection. Actual Ψ_{stem} values of -0.6 MPa, for instance, would alert the grower for unexpected Ψ_{stem} behaviour on a cloudy day (Fig. 7.3C, D), but not always on a sunny day (Fig. 7.3A, B), because Ψ_{stem} values down to -0.6 MPa and lower are normal under well-watered conditions with high VPD and λE_p . As considered necessary in **Chapter 4** and the literature (Steppe et al., 2008; De Swaef et al., 2009; Ortuño et al., 2010), detection of drought stress with the dynamic system proposed in this study is dependent on both soil water availability (which influences actual Ψ_{stem}) and microclimatic conditions (which influence the magnitude of the threshold bands). Besides dynamic behaviour, the proposed

system also allows a high time-resolution. A tight supervision over the plant water status can be maintained at any moment during the day, as actual simulated Ψ_{stem} can continuously be compared against the expected plant behaviour under well-watered conditions. Furthermore, the magnitude of deviation from the predicted Ψ_{stem} threshold can give information on the level of drought stress. The high time-resolution property of the system entails a huge advantage over several other plant stress indicators such as maximum daily stem shrinkage, daily growth rate (De Swaef et al., 2009; Fernández and Cuevas, 2010; Conejero et al., 2011) and predawn or midday leaf or stem water potential (Williams and Araujo, 2002; Jones, 2004; Acevedo-Opazo et al., 2010), which assess the water status only once a day. Indeed, continuous Ψ_{stem} simulations (and confirmed by manual Ψ_{stem} measurements) revealed that under fluctuating microclimatic conditions, Ψ_{stem} showed strong fluctuations (e.g. fluctuations in Fig. 7.3A and inset in Fig. 7.4A), which may possibly be overlooked when determining the plant water status only at one or a few instants a day.

7.3.3 Performance of generic thresholds for drought stress detection

As intended, actual simulated Ψ_{stem} remained within the expected well-watered behaviour range on the majority of days during well-watered conditions. On some well-watered days, however, actual simulated Ψ_{stem} slightly exceeded the threshold bands (maximum 0.1 MPa). This occurred on only zero to four (out of 49 considered) days in most cases, but up to about ten days for one or both thresholds in C2, R3 and R4, both at the upper (less negative Ψ_{stem} than expected under well-watered conditions) or lower (more negative Ψ_{stem}) limit of the threshold band. The latter may be especially inconvenient when occurring frequently, because it delivers a false positive for a drought stress event to the grower. Multiple reasons may be at the origin of this observed false deviation outside the threshold bands under well-watered conditions. A first explanation lies in the applied Monte Carlo uncertainty analysis (De Pauw et al., 2008b), from which the upper and lower limits of the uncertainty bands were defined as the 95th and 5th percentile. As a result, 5% of well-watered days may be expected outside this range. Although this may partly explain the unexpected deviations from both thresholds, deviations occurred too often in some cases (C2, R4, VPD-based threshold in R3) to be the result of a 5% chance. Therefore, other sources of

uncertainty need to be considered. First, the number of plants under well-watered control conditions ($n = 5$) used for calibrating the parameters (v_1, v_2 in Eq. 7.2 and e_1, e_2 in Eq. 7.3), or the length of the period (four days) may have been too limited to sufficiently account for plant-to-plant or day-to-day variability, respectively. Second, in addition to parameter uncertainty, that arose from plant-to-plant variability and which was accounted for in the Monte Carlo uncertainty analysis, input uncertainty as a result of possible sensor or measurement uncertainty may also play an important role (Vermeulen et al., 2012). Finally, although very convenient for practical applications, optimising Ψ_{stem} threshold parameters (v_1, v_2 in Eq. 7.2 and e_1, e_2 in Eq. 7.3) using a limited calibration period at the start of the measurements and applying these values across the entire growing season, is only justified when parameter variability across the growing season is absent.

Variability in Ψ_{stem} threshold parameters was investigated by recalibrating the parameters across the growing season using well-watered grapevines C1 and C2. To this end, data from 5 May until 24 September 2012 (DOY 126 - 268) were divided in ten-day periods. For each defined ten-day period, v_1, v_2, e_1 and e_2 were assigned optimal values using the calibration module in PhytoSim. Examining changes in optimal parameter values revealed some seasonal influence on the VPD-based threshold (Fig. 7.5A), but a seasonal trend seemed to be absent for the λE_p -based threshold (Fig. 7.5B). Parameter v_1 (VPD-based threshold, Eq. 7.2) in grapevine C2 substantially decreased across the growing season, while parameter v_2 (Eq. 7.2) in grapevine C1 showed the decreasing trend (Fig. 7.5A). In addition, the constant threshold parameters, derived from five plants and considered generic in this study, did not correspond well with the parameter values optimised for one particular plant at all times (Fig. 7.5), as is best illustrated by the deviation of parameter v_1 (of both C1 and C2) from the applied generic threshold parameter value ($v_1 = 0.12 \pm 0.03$). To obtain more realistic threshold parameter values and standard deviations, a larger group of plants might be necessary to use for calibration of the threshold parameters.

7.3.4 Accuracy of automatic water status monitoring

Besides the importance of an appropriate dynamic Ψ_{stem} threshold and associated uncertainty band, the performance and the accuracy of the proposed method is also dependent on the reliability of the actual Ψ_{stem} input. The pressure chamber

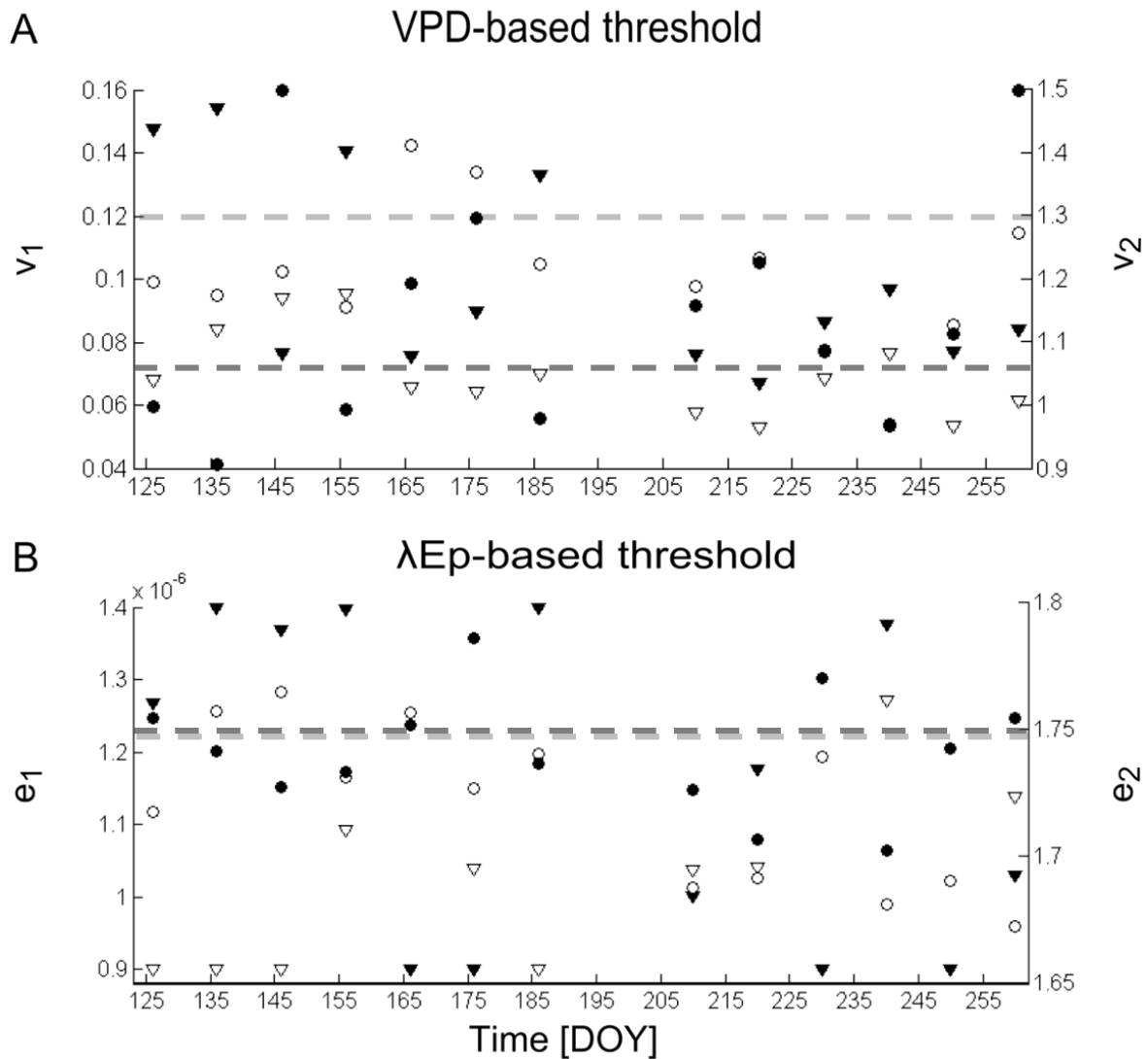


Fig. 7.5 Variability across the growing season (day of the year, DOY) of the dynamic stem water potential (Ψ_{stem}) threshold parameters, using ten-day periods of well-watered grapevines C1 (open symbols) and C2 (closed symbols): parameter (A) v_1 (triangles), v_2 (circles) for the threshold based on vapour pressure deficit (VPD) ($\text{Threshold}\Psi_{\text{stem}} = -v_1 \text{VPD}^{v_2}$) and (B) e_1 (triangles), e_2 (circles) for the threshold based on potential evapotranspiration (λE_p) ($\text{Threshold}\Psi_{\text{stem}} = -e_1 \lambda E_p^{e_2}$). Light grey lines show the applied generic threshold parameter value for v_1 (A) and e_1 (B), dark grey lines the applied value for v_2 (A) and e_2 (B).

(Scholander et al., 1965) is the benchmark method for measuring Ψ_{stem} and is widely used, also for grapevines (e.g. Choné et al., 2001; van Leeuwen et al., 2009; Acevedo-Opazo et al., 2010), but the method is discontinuous, labour intensive, destructive, and cannot be automated (Intrigliolo and Castel, 2006). This

probably explains the lack of dynamic Ψ_{stem} thresholds so far, even though many authors recognise Ψ_{stem} as one of the best indicators for plant water status (McCutchan and Shackel, 1992; Jones, 2004). Attempts have been made to measure Ψ_{stem} automatically with *in situ* stem psychrometers (Dixon and Tyree, 1984; Vogt and Losch, 1999; Vogt, 2001). This sophisticated sensor requires a high level of technical skill and is observed to be difficult to install and apply in the long term (Jones, 2004; Nizinski et al., 2013). The technique may however advance in the future and may become more useful. Such an automatic, reliable sensor for continuous Ψ_{stem} measurements would perfectly complement automatic water status monitoring and drought stress detection in combination with the introduced dynamic Ψ_{stem} thresholds. Alternatively, this study used Ψ_{stem} simulations instead of measurements. These simulations were obtained by using other, automatic plant measurements in combination with a dynamic water transport and storage model (**Chapter 6**), and circumvented as such the difficulty of direct Ψ_{stem} measurements.

7.3.5 Comparison between VPD and λE_p -based thresholds

Overall, the applied thresholds enabled fast detection of drought stress and supervision of its intensity in all grapevines. Drought detection was assumed when actual simulated Ψ_{stem} deviated clearly and consistently from its uncertainty band. The first obvious indication of drought stress with both thresholds was observed on the 8th, 11th and 9th day after irrigation was stopped for R1, R2 and R4, respectively. For R3, drought stress was detected on the 7th and 10th day with the λE_p - and VPD-based threshold, respectively. Interestingly, clear visible symptoms only appeared on the 15th day in R1 and on the 18th day in R3 and R4, but were absent in R2 when irrigation was resumed on day 18. Actual simulated Ψ_{stem} did not exceed the uncertainty bands of the dynamic Ψ_{stem} thresholds in the control treatments (C1 and C2), with the exception of some days (zero to six days, dependent on the threshold and grapevine).

Drought stress was detected rapidly irrespective whether actual simulated Ψ_{stem} was compared against a dynamic threshold calculated using solely VPD, or both VPD and radiation (via the use of λE_p). Despite the similarity in results of both approaches, diverging results may arise in other applications because of a different coupling between the plant canopy and the atmosphere. This coupling

can be expressed by the decoupling coefficient (Ω) and describes the effect of stomatal regulation on transpiration (Jarvis and McNaughton, 1986; Jones, 1992). When the saturation deficit at the leaf surfaces of the canopy is strongly coupled (equal) to that of the surrounding air, the stomata have a tight control over transpiration. In such strongly coupled conditions, Ω is low (close to 0, e.g. conifer needles) and transpiration is mainly driven by VPD. When Ω is high (close to 1, e.g. some broad leaves), the saturation deficit of the air outside the thick boundary layer is completely decoupled from the saturation deficit at the leaf surfaces of the canopy, which reaches a local equilibrium. Because net radiation has a large influence on this local equilibrium, transpiration is no longer controlled by the degree of opening by the stomata, but is mainly driven by net radiation (Jarvis and McNaughton, 1986). In situations where Ω is high and net radiation plays a key role in driving transpiration, more realistic results may be expected with a λE_p -based threshold compared to a threshold based on VPD measurements only. Nevertheless, further investigation is required to verify this hypothesis.

7.4 Conclusions

In this study, proof of principle is given of how dynamic thresholds based on environmental conditions can be used to achieve plant-based (Ψ_{stem} is used as indicator) monitoring of the grapevine water status and fast drought stress detection. Since the proposed methodology can be easily automated, it could be further developed as a practical tool for scheduling irrigation or alerting the grower when irregularities occur and action may be required. Despite promising first results, the protocol for calibrating the generic threshold parameters should be further developed given the observed difficulties (e.g. plant-to-plant variability, seasonal trend and parameter or sensor uncertainty). For practical applications in the future, the performance of the proposed dynamic threshold concept should be carefully investigated under a wide range of environmental conditions (e.g. greenhouse facility versus field experiment) and for the plant species or cultivar of interest, since Ψ_{stem} behaviour under normal conditions (e.g. daily minimum Ψ_{stem}) has been observed to vary dependent on the species or cultivar (e.g. Williams and Araujo, 2002; Chaves et al., 2010).

Chapter 8

General conclusions and future perspectives

If not already a prerequisite now, a great part of the worldwide grapevine cultivation will benefit in the future from efficient and precise irrigation, not only to provide adequate water, but also to improve grape and wine quality. To accomplish precise irrigation scheduling, an accurate monitoring of the plant water status and an early detection of drought stress are crucial. The main objective of this thesis was therefore to develop and evaluate plant-based strategies to fulfil these needs. This final chapter reflects on the most important conclusions of this research and ideas for future research are put forward.

8.1 General conclusions

Two different plant-based strategies for monitoring the grapevine water status were tested. First, water status monitoring and fast drought stress detection were accomplished with a data-driven model approach (**Chapters 3 and 4**). Such an approach does not need a priori information on the underlying plant mechanisms, but the model is constructed using a large amount of historical data. Two different data-driven models were tested and their performances were compared: Unfold Principle Component Analysis (UPCA) and Functional Unfold Principle Component Analysis (FUPCA). In **Chapters 5 to 7**, a mechanistic water transport and storage model was developed and implemented for realising the same aim, but now uses knowledge on underlying mechanisms. Outcomes of both strategies are

summarised in the following paragraphs and their strengths and shortcomings are discussed.

8.1.1 Data-driven modelling

Two expansions of Principal Component Analysis (PCA), a frequently used data-driven technique for monitoring a process in several domains (Box 3.1), were tested for monitoring the grapevine's water status: UPCA and FUPCA (**Chapters 3 and 4**). PCA expresses the information contained in the measured variables, i.e. an indicator of the plant water status such as stem diameter variations (D) (**Chapters 3 and 4**) or sap flow rate (SF) (**Chapter 4**), and measurements of the microclimatic conditions (photosynthetic radiation (PAR), vapour pressure deficit (VPD), air temperature (T_{air})), by a smaller number of new variables. These variables are called principal components (PCs) and describe the major part of the variability (and thus information) in the original data, while the dimensionality of the dataset is greatly reduced. By constructing a relationship between these new PCs, a PCA model extracts the underlying data features and patterns under normal conditions, and as such makes a profile of normal, expected data behaviour (Jolliffe, 2002; Venkatasubramanian et al., 2003; Villez et al., 2009). Monitoring new data implies checking these data against the pattern of normal behaviour, i.e. projecting these data onto the constructed PCA model. Both UPCA and FUPCA enabled a fast detection of drought stress when potted grapevines were subjected to drought, several days (five to ten) before the first clear visible symptoms appeared (colouring and wilting of the leaves).

Difference between UPCA and FUPCA

In this study, UPCA and FUPCA performed quite similar in detecting drought stress at an early stage. UPCA seems the preferred technique in that respect, because unlike FUPCA, UPCA does not require the extra processing step of performing a functional data analysis. However, the functional data analysis in FUPCA involves certain advantages and is worth considering. FUPCA allows estimating gaps of missing data, if not too extensive. This enables water status monitoring of that particular day, which would be impossible with UPCA. Because proper data acquisition was occasionally impeded in this study due to required adjustments of a sensor installation or failure of data logging, electricity or sensors

(**Chapters 3 and 4**), the ability of FUPCA to estimate small gaps of missing data is believed very convenient and increases the usefulness and reliability of the technique. Furthermore, existing knowledge of the data can be incorporated in a functional data analysis (Ramsay and Silverman, 2005), as has been illustrated for the non-negative behaviour of PAR in this study (**Chapter 3**). Due to the considerably reduced amount of input data for the subsequent PCA model, the constructed FUPCA model is less complex compared to the UPCA model.

Unravelling underlying mechanisms

The PCA-based models, in their current use, might seem less suitable for unravelling new insights related to plant water status because underlying processes are not explained. Nevertheless, they can provide valuable supplementary information and could become very powerful when combined with knowledge on plant behaviour or mechanistic models (Kourti, 2002). Note for instance that PCA allows an easy exploration of a (large) dataset to reveal periods of unexpected behaviour and, although not explored in this thesis, can be applied to identify possible causes of unusual behaviour (Kourti, 2002; Box 3.1). Furthermore, the behaviour of the newly constructed variables (PCs) gave insight in the correlations of the original variables (**Chapters 3 and 4**). Indeed, the loadings for all variables (microclimatic measurements plus D or SF) of the first PC indicated that PAR, T_{air} and VPD are positively correlated with SF, which confirms that PAR and VPD are the key driving variables for transpiration and thus SF. On the other hand, they are negatively correlated with D, caused by a more extensive shrinkage of the diameter under higher transpiration (Steppe et al., 2006; Intrigliolo and Castel, 2007b; Steppe et al., 2012). Examination of the second PC revealed other, less obvious mechanisms (e.g. Fig. 4.4D, H). For both SF and D, a wavelike pattern was observed for all variables, which Villez et al. (2009) linked to temporal variability in the daily cycles. Also in other cyclic processes, such as weather station data or gait cycles of children, behaviour of the second PC was attributed to a time shift or temporal effect (Ramsay and Silverman, 2005). The subsequent PCs also account for specific information in the data, although interpretation becomes very difficult. They are not as important as the first and second PC, as they only explain small proportions of the variation in the data.

Monitoring performance depends on the measured plant variable

The performance of the PCA models depends on their input. In **Chapter 4**, the models used either SF as plant indicator, or D. While both performed well, they had different issues to keep in mind. On cloudy days, SF was not able to distinguish between low soil water availability and low atmospheric water demand, since both phenomena result in lower SF values (De Swaef and Steppe, 2010; **Chapter 4**). When D was used as indicator, detection ceased when severe drought initiated. The model then suggested recovery from drought stress, while the plant exhibited more severe drought stress. This observation was caused by a levelling off of the stem diameter because the water storage pools were extensively depleted and could no longer be refilled during the night (e.g. Fig. 4.3B, 4.6). The resulting less pronounced pattern of shrinkage and refilling under severe drought stress compared to the start of the drought stress treatment has been observed in other studies as well (De Swaef et al., 2009; Fernández and Cuevas, 2010; Ortuño et al., 2010). Furthermore, it was hypothesised in **Chapter 3** that the PCA models based on D would fail once veraison of the grapevines is achieved. Grapevines with sufficient soil water availability show a steadily growing diameter before veraison (Fig. 8.1). An impairment of the growth pattern during this period is therefore a clear indication of drought stress. After veraison, however, the stem diameter first shows a characteristic shrinkage irrespective of the water availability and stabilises afterwards (Fig. 8.1) (Ton and Kopyt, 2004; Kopyt and Ton, 2005; Intrigliolo and Castel, 2007b). The colouring and ripening grapes that become a more important sink from veraison onward may be responsible for this phenomenon, as they get priority for receiving photosynthetic assimilates (Dokoozlian, 2000; Intrigliolo and Castel, 2007b). Steered by the shrinking diameter, a PCA model is expected to detect abnormality around the onset of veraison, but is under these circumstances not an explicit sign of drought stress. A promising strategy to overcome the difficulty of changing stem diameter dynamics across the growing season may be to adapt the PCA model to (gradual) changes of the existing relationships between variables, also called adaptive PCA (Li et al., 2000; Lennox and Rosen, 2002; Villez, 2007). An adaptive PCA technique allows updating the PCA model online when new data are available and permits as such that the model follows the evolution/development of the

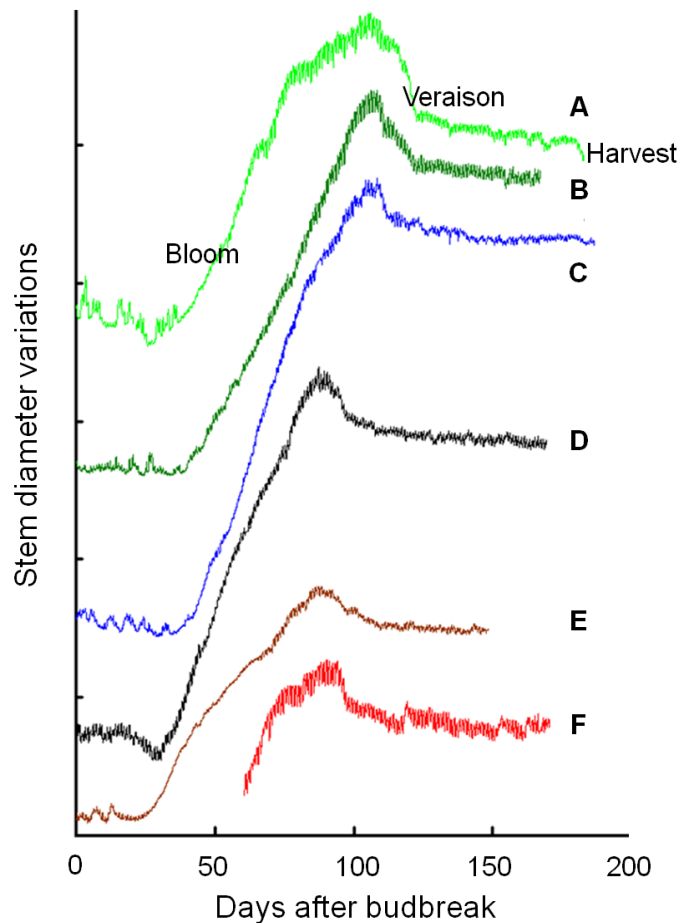


Fig. 8.1 Typical examples of characteristic stem diameter growth curves across the growing season of two table grape cultivars, i.e. (A) Barlinka and (B) Thompson, and four wine grape cultivars, i.e. (C) Cabernet Sauvignon, (D) Merlot, (E) Chardonnay and (F) Shiraz (adapted from Kopyt and Ton (2005)). Typical occurrence of bloom, veraison and harvest are indicated.

grapevine. However, care should be taken that the PCA model does not adapt to abnormal changes in grapevine behaviour (e.g. drought effects), which one wants to detect.

Above remarks on the behaviour of SF and D apply for all techniques that use measurements of SF or D as indicator for plant water status. As mentioned in **Chapter 2**, a better understanding and more thorough and profound knowledge of the plant water status will be obtained when combining several plant measurements. Knowledge of underlying mechanisms and characteristic plant behaviour during specific periods in the growing season proved of utmost importance, even when data-driven models such as UPCA and FUPCA are

applied. Therefore, the use of a mechanistic model that is built from underlying processes seemed a promising alternative.

8.1.2 Mechanistic modelling

A profound understanding of the plant water relations is of utmost importance for a reliable water status monitoring and, in the future, for maintaining the optimal water status level at specific times to optimise fruit quality. In particular, a comprehension of grapevine responses under dry conditions appears crucial, because grapevines are often cultivated under dry conditions and are known to benefit from mild levels of drought stress. Because UPCA and FUPCA were less suited to assist in broadening our knowledge of grapevine physiology, **Chapters 5 to 7** focussed on developing and applying a mechanistic model for describing the water transport and storage in grapevines. A mechanistic model mathematically describes the plant/grapevine by a series of known plant mechanisms and can be considered as a simplified representation of reality. Constructing a mechanistic model allows aligning and integrating several complex plant processes, which each are represented by a mathematical equation (e.g. Fig. 5.1), and interpreting their information simultaneously. As such, the behaviour, the interaction or certain hypotheses of the plant processes and variables can be investigated. Possible outcomes of hypothetical treatments or events can be checked and reasoned out transparently. Mechanistic models can therefore greatly contribute to the understanding of plant functioning and are able to provide explanations on certain observed plant responses.

In **Chapter 5** it was demonstrated that an existing water transport and storage model (Steppe et al., 2006; 2008; De Pauw et al., 2008a), developed for describing water transport and irrigation scheduling in trees, failed when applied for grapevines under dry conditions. Under dry conditions, the original model was not able to correctly simulate D and stem water potential (Ψ_{stem}), which is recognised as one of the best indicators for grapevine water status (Choné et al., 2001; Acevedo-Opazo et al., 2010). The model simulations did not correspond with the actual measurements that indicated a clear decreasing trend in D and Ψ_{stem} when drought intensified (Fig. 5.3, Appendix Fig. S15). As was hypothesised, the generally applied constant parameter for hydraulic resistance in the xylem appeared responsible for this failure. It was proven that the hydraulic

resistance encountered during upward water transport (in the soil-to-stem segment, R^X) cannot be considered constant. R^X showed daily fluctuations, with maximum resistance during the night and minimum resistance during the day (**Chapter 5**), as well as a clear altered trend under the influence of drought (**Chapters 5 and 6**). Daily fluctuations have been observed in other studies as well (Bucci et al., 2003; Lovisolo et al., 2008; Sellin et al., 2010; Zufferey et al., 2011) and assist the plant in enhancing its hydraulic efficiency and water transport capacity while maintaining a moderate water potential drop during the day and avoiding extensive cavitation (Cochard et al., 2007; Nardini et al., 2010; Guyot et al., 2012). Besides this diurnal pattern, R^X was found to increase exponentially due to drought stress (**Chapters 5 and 6**), which can be attributed to the combination of abundant cavitation in the xylem vessels (Sperry and Tyree, 1988; Lovisolo et al., 2010) and increasing water flow resistance in the soil (Gardner, 1960; Tuzet et al., 2003) under dry conditions. Besides the pronounced effect of drought stress on R^X , also the radial hydraulic resistance between xylem and elastic living tissues that serve as a water storage pool (R^S) was proven to be highly influenced by drought stress. The results of this study support the experimental discovery of Steppe et al. (2012) that aquaporins interfere not only in the regulation of upward water transport, but also of radial water transport. Furthermore, in correspondence to other studies (Mencuccini et al., 2013), a marked decline in turgor pressure was observed under drought stress (**Chapter 6**).

Urged by the above new insights, the former constant R^X and R^S of the original water transport and storage model (Steppe et al., 2006; 2008) were replaced by equations (Eq. 5.2 and 5.4) dependent on the soil water potential (Ψ_{soil}) (**Chapter 5**). Once adapted, a good correspondence between measured and simulated data of D , Ψ_{stem} and R^X was obtained. As such, the improved model allowed an accurate description of the grapevine's response under dry conditions and confirmed the reliability of the new mechanisms related to hydraulic resistances implemented in the model. Variable hydraulic resistances are believed necessary for a good description of plant behaviour under dry conditions.

Through the development of an appropriate mechanistic model for describing water transport and storage in grapevines under both wet and dry conditions, **Chapter 5** mainly aimed at broadening the understanding on plant responses.

Once achieved, the improved model was further elaborated and tested to serve as a tool for automatic monitoring of grapevine water status in real-time (**Chapter 6**). To this end, the model was tested for monitoring the plant water status accurately based on automatic measurements alone (SF and Ψ_{soil} as input data and D for daily model recalibration). Particularly under wet and slight to moderate drought conditions, the conditions that predominantly prevail in practice, the model simulations of Ψ_{stem} were accurate. Only under the most severe conditions, the model appeared to underestimate Ψ_{stem} (simulating more negative Ψ_{stem} values than actually measured). This suggests that some plant mechanisms involved in grapevine drought responses under the most extreme conditions are not yet, or not yet properly, included in the model. Note, however, that such severe drought conditions are not favourable for grape and wine quality (**Chapter 2**) and should be avoided in practice.

8.1.3 Model calibration

Prior to the onset of automatic water status monitoring, both the data-driven PCA models and the mechanistic model require calibration, for which historical data from a period where the plant and environmental conditions were optimal are needed. In this thesis, data collected from well-watered plants prior to the actual monitoring period were used for this purpose. A short preceding period is sufficient for the mechanistic model (two to six days, **Chapter 6**), while a longer period (minimum ten days) is preferred for the data-driven models (**Chapters 3 and 4**). In the latter models, as mentioned in section 8.1.1, calibration data are used to construct the PCA model and draw a profile of expected data behaviour and interactions (between meteorological data and D or SF) under well-watered conditions. Furthermore, these data define statistical limits under which new monitored days must stay to be considered as normal. Calibration for the mechanistic model works differently (**Chapters 5 to 7**). Model simulations of D and Ψ_{stem} are aligned with actual D and Ψ_{stem} measurements to find the best model fit. This is achieved by adjusting identifiable model parameters that could not be measured or estimated from the literature. As such, an optimal model parameter set for that particular grapevine is obtained.

The calibration period must be chosen carefully. In both the data-driven or mechanistic approach, the phenological stage must be kept in mind. For the

mechanistic model, data after flowering was used for calibration (e.g. 21 May in 2012, **Chapters 5 to 7**) because the grapevine had developed a full canopy by then. Also for UPCA and FUPCA it is better to avoid an extensive amount of days from the beginning of the growing season, typically showing zero or low daily net growth of D and low SF. It was proven necessary to shorten the calibration period for two out of six grapevines tested in **Chapter 4** to obtain a good stress detection performance. Because the calibration data must teach the PCA models to recognise normal data behaviour expected for the rest of the season, the timing of the calibration period depends on the grapevine (canopy) development, while the length of the calibration period depends on the prevailing microclimatic variability. Since detection of altered plant behaviour on cloudy versus sunny days is not intended, both sunny and cloudy days should be included in the calibration data set. Accidental disturbances during the start-up period, on the contrary, must be excluded from the calibration data set, e.g. unforeseen drought stress or diseases.

8.1.4 Threshold for drought stress detection

Irrespective of the monitoring technique or plant variable that is used as an indicator, threshold or reference values are required to define when plants are considered to experience drought stress (Fereres and Goldhamer, 2003; Jones, 2004). In UPCA and FUPCA (**Chapters 3 and 4**), this threshold is defined by the Q and Hotelling T² statistic (Eq. 3.1 and 3.2, respectively). If one of these limits is exceeded, the model discovers abnormality (e.g. drought stress) on that day. Because UPCA and FUPCA define these thresholds statistically, they seem the more straightforward and objective technique.

Monitoring and evaluating grapevine water status with the mechanistic water transport and storage model, on the other hand, can be made visual and is therefore less abstract. The model provides continuous simulations of Ψ_{stem} (**Chapter 6**). Simultaneously, a dynamic Ψ_{stem} threshold band is constructed. This represents the range within which Ψ_{stem} is expected to fall under well-watered conditions (**Chapter 7**). If Ψ_{stem} starts exceeding this band, the plant experiences more negative Ψ_{stem} than under normal conditions, indicating drought stress for the plant. As outlined in **Chapters 4 and 7**, the dynamic feature of the Ψ_{stem} threshold is of utmost importance, because the plant water status is not only influenced by soil water availability, but also by microclimatic conditions (De Swaef et al., 2009;

Ortuño et al., 2010). Although several approaches have been proposed to determine such dynamic thresholds (e.g. Patakas et al., 2005; Ortuño et al., 2006; Velez et al., 2007), a more practical procedure for determining a generic, high time-resolution dynamic Ψ_{stem} threshold is still lacking, in particular for grapevine. Two different dynamic Ψ_{stem} thresholds were therefore proposed and compared in **Chapter 7**, both based on microclimatic measurements. A first threshold was rather simple as its calculation was based on VPD, the major driving variable for plant transpiration (De Swaef and Steppe, 2010). Besides VPD, also PAR is known as a key driving variable and may greatly affect plant performance in protected environments such as greenhouse facilities (Vermeulen et al., 2012). The second threshold therefore included both VPD and radiation by calculating potential evapotranspiration (λE_p) (Eq. 7.2 and 7.3, respectively).

As with UPCA and FUPCA (**Chapters 3 and 4**), the mechanistic model in combination with either one of the dynamic thresholds allowed a fast detection of drought stress and tight supervision over the plant water status during a drought-exposure experiment on Chardonnay grapevines (**Chapter 7**), as Ψ_{stem} could be continuously compared against expected plant behaviour under well-watered conditions. These first results were very promising, nevertheless, the protocol for calibrating the generic Ψ_{stem} threshold parameters (Eq. 7.2 and 7.3) and defining their uncertainty should be further developed given the observed difficulties with occasional false drought stress detections despite well-watered conditions (as a result of plant-to-plant variability, seasonal trend or parameter and sensor uncertainty) (**Chapter 7**).

8.1.5 Distinguishing between different levels of drought stress

It was pointed out in **Chapter 3** that UPCA and FUPCA are in their current use able to indicate whether data behave normal or abnormal on a certain day, but do not differentiate between gradations in drought stress. This shortcoming does not imply a problem for full irrigation treatments that attempt to avoid any level of drought stress. However, because grape composition benefits from mild levels of drought stress, while it is negatively affected by no or too severe stress (van Leeuwen et al., 2009; Keller, 2010b), a distinction between different levels of drought stress is crucial for grapevines. In future research, it would be interesting to investigate whether the techniques can be adapted for fulfilling this need. One

possibility would be to examine the degree of abnormality once data deviate from normal conditions (indicated by the Q statistic and Hotelling's T^2 statistic). The contribution of each variable to this deviation can be retrieved from the underlying UPCA or FUPCA model (projection model that characterises the relationships under normal conditions). The magnitude of the contribution of the stem diameter variations could indicate how severe the deviation is. MacGregor and Jaeckle (1994) demonstrated this approach for process diagnosis of a polyethylene production reactor. Another option is applied by Dunia and Qin (1998). In their strategy, each abnormality is described by (1) a fixed unit vector, which describes the linear combination of residuals as expected for a particular fault type and (2) a scalar value describing the magnitude of an instance of that fault. Fault diagnosis then boils down to the identification of the scalars for all considered faults. Above strategies seem promising for adapting UPCA and FUPCA. However, it is not recommended to use these techniques in their current set-up when it is targeted to maintain a specific level of drought stress. The mechanistic model lends itself much better for this purpose. More severe drought stress results in a more pronounced decline in D, SF, Ψ_{stem} and turgor, while hydraulic resistances (R^X and R^S) increase considerably, all important plant variables related to the plant water status that can be examined using the water transport and storage model (**Chapters 5 and 6**). As such, information on the stress level of the plant can be extracted from the model outcome.

8.1.6 Data interpretation and practical application

Both the data-driven and mechanistic method consider the collected information simultaneously, which is a great advantage compared to many conventional water status monitoring approaches that do not integrate the data of different sensors/variables. Examining one variable at a time as if it is independent of the other variables, which is seldom the case because their behaviour is probably driven by only one or a few underlying mechanisms, makes their interpretation difficult and defining the underlying cause quite cumbersome.

Instead, via the data-driven models, the information of all measured variables is transformed into a reduced amount of new variables (PCs). The information contained in the several variables is therefore considered simultaneously and is presented in a simpler manner (MacGregor and Jaeckle, 1994; MacGregor and

Kourti, 1995). UPCA and FUPCA also allow a simple and clear graphical representation of the monitoring results (e.g. Fig. 3.8), which are easy to understand and interpret (MacGregor and Jaeckle, 1994; Kourti, 2002). The absence of actual plant processes inherent to data-driven models are a drawback when aiming at testing and interpreting certain specific data/plant behaviour or hypotheses. The fact that a profound a priori understanding is not required, however, is rather an advantage for applying these models in practice because the end-user may lack a profound knowledge or feeling with underlying plant physiological processes. UPCA and FUPCA models can be used for stress detection without seeing or needing the built-in formulas and calculations and for reasoning with incomplete and/or uncertain information. Also the mechanistic water transport and storage model is easy to interpret and recalibrate daily once running, but in contrast to the data-driven models, a broader knowledge and understanding is important for model development and initial model calibration.

A certain level of experience is nevertheless in any case preferable to make a good evaluation of the corresponding model output. Even when either a data-driven or the mechanistic model is started up and is running automatically, the end-user must have the capability to assess the model performance and reliability. The end-user should be able to evaluate whether a drought event is the plausible cause of the detection event or whether there are other possibilities. For instance: Is the vineyard infected by diseases? Does the timing correspond with veraison (Fig. 8.1, **Chapter 3**)? In which stage is the grape development and which level of water availability is optimal for this stage (**Chapter 2**)? Furthermore, a certain feeling is required to make profound decisions on actions to take, if necessary.

It is impossible to equip and monitor all plants in a commercial vineyard with automatic sensors. This limitation is not only applicable for the stress detection techniques proposed in this thesis, but also for other methods based on plant measurements. The required number will depend on the location of the plants and the variability of soil, root-zone and plant (Alchanatis et al., 2010). The existence of plant-to-plant variability has been shown for several species (Naor, 2006; Velez et al., 2007; Fernández and Cuevas, 2010), including grapevines (**Chapters 4, 6 and 7**; Montoro et al., 2012; Santesteban et al., 2013). Recent developments try to provide tools to identify representative plants or troublesome areas (Naor, 2006;

Fernández et al., 2008). Remote thermal imagery is such a technique, used for screening canopy temperature variability over large areas (Fig. 8.2A, B) (Jones, 2007; Jones et al., 2009; Alchanatis et al., 2010; Maes and Steppe, 2012). As such, the required number of measured plants may be reduced and plant selection more underpinned, although more research is still needed on this topic. Canopy temperature depends on changes in stomatal closure and leaf transpiration and is recognised as a measure for plant stress (Maes and Steppe, 2012). Besides scanning for spatial variability, thermal imagery is also explored for detecting biotic and abiotic stress (Fig. 8.2C, D) (Jones, 2004; Chaerle et al., 2007; Grant et al., 2007; Jones et al., 2009; Maes and Steppe, 2012).

8.2 Future research

This thesis focused on developing plant-based strategies for water status monitoring and stress detection in grapevine. Two approaches (data-driven and mechanistic) were elaborated, both achieving a good monitoring of the water status and a fast detection of drought stress during drought experiments on potted grapevines. Although several challenging and crucial steps were taken, some important issues remained unanswered and should be dealt with before these plant-based models can be applied for optimising grape and wine quality in practice. The most prominent ones are discussed below and suggestions for future research are given.

8.2.1 From greenhouse experiments to practice

All experiments described in this thesis were conducted in a greenhouse facility. Such a set-up was most appropriate and convenient for broadening our knowledge on grapevine behaviour, because it allowed having a strict control over the experiments, and in particular, the soil water availability for the grapevines. Indeed, this thesis especially focussed on the effect of drought stress, as it has a crucial influence on grape and wine quality. As such, also developing and testing the data-driven (**Chapters 3 and 4**) and mechanistic (**Chapters 5 to 7**) models occurred under controlled greenhouse conditions. It would be very interesting to conduct additional measurement campaigns under different conditions. First, plant responses and model performances were examined by withholding irrigation from

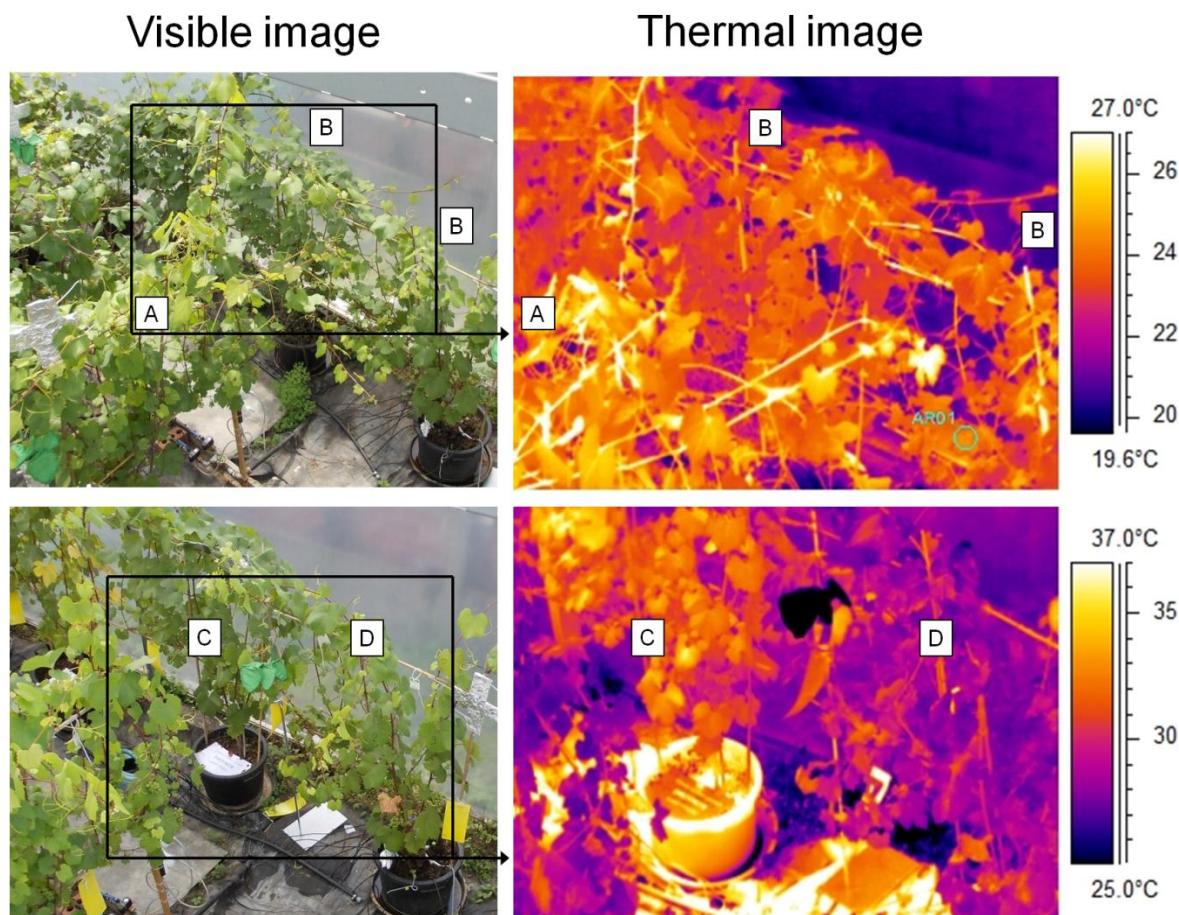


Fig. 8.2 Illustration of using thermal imagery for screening plant-to-plant variability or detecting drought stress by examining differences in canopy temperature. (A, B) Visible and thermal image taken prior to drought stress treatments in 2012. Although grapevine A and grapevines B were all under well-watered conditions, thermal imagery demonstrated plant-to-plant variability due to a difference in canopy temperature (± 26 versus $\pm 24^\circ\text{C}$, respectively). (C, D) Visible and thermal image taken two weeks after irrigation was withheld for grapevine C while D remained irrigated. Based on the considerably higher canopy temperature for grapevine C (± 33 versus $\pm 28^\circ\text{C}$), drought stress for that particular grapevine could be detected.

potted grapevines until visible symptoms appeared. Imposing different levels of stress (e.g. no, mild, slight to moderate and severe drought stress) during different prolonged periods in the growing season (e.g. from flowering until veraison, during ripening or post-harvest) instead of subjecting the grapevines to one relatively short drought shock may provide interesting information on the effect of sustained drought on plant and fruit behaviour. Such drought experiments probably match more tightly to the drought events that grapevine under rain-fed watering or traditional irrigation strategies experience. In addition, imposing different levels of drought stress may reveal different response mechanisms, both on a level of

timing (e.g. when do symptoms and effects on plant functioning appear?) and quantity (e.g. how severe is the effect?). Similar experiments have already been conducted on grapevines, either by varying the levels (Patakas et al., 2005; dos Santos et al., 2007; Acevedo-Opazo et al., 2010; Santesteban et al., 2011) and/or the timing (Hardie and Considine, 1976; Matthews et al., 1990) of water deficits, but these studies rarely consider different plant measurements (such as SF and D) simultaneously or combine them with mechanistic modelling, as has been done in this thesis. Drought exposure experiments were for the first time combined with a data-driven model in this thesis.

Second, besides pot experiments with controlled, prolonged drought levels, field experiments under natural conditions are required for confirming the new findings (e.g. behaviour of dynamic hydraulic plant resistances, **Chapters 5** and **6**) and testing the applicability of the models (**Chapters 6** and **7**) in field conditions.

Finally, now that a more profound understanding of plant responses to drought stress and the underlying mechanisms is attained, the time has come to investigate the influence of drought stress on the fruits. Eventually, optimising the grape and resulting wine quality is the actual target of the grape- and winegrower. Examining the trend in berry size, pH, sugar and acid concentrations across the growing season as a result of different drought stress levels, all important features that contribute to fruit quality (**Chapter 2**), are only a few of the possible measurements to take. The abovementioned variables can be measured directly in the greenhouse or field (e.g. Ginestar et al., 1998; van Leeuwen et al., 2009). More elaborate methods, such as analytical studies in a laboratory or wine sensory tests with trained panellists, can be applied for investigating other fruit and wine quality-related components (aromatic, colour and flavour compounds and impressions) (e.g. Matthews et al., 1990; Roby et al., 2004; Chapman et al., 2005).

8.2.2 Virtual fruit model

As discussed in **Chapter 2**, grape quality is the result of an interaction between many complex biological processes, the fruits and the environment. Among these processes are cell and tissue development, xylem and phloem fluxes, transpiration, photosynthesis and respiration (Génard et al., 2007). The best option for better understanding the effect of the water status on grape quality, and

eventually controlling it, seems to consider the fruit and its development as a system and explicitly investigating the underlying mechanisms. To this end, the major processes and trends related to fruit growth, development and biochemistry should be integrated in a mechanistic model. This enables investigating the combined effect of several interconnected processes on such a complex aspect as fruit quality (Génard et al., 2007; Liu et al., 2007; Dai et al., 2010).

Lescourret and Génard (2005) and Génard et al. (2007) were the first to develop such a virtual fruit model for peach by merging existing submodels for carbon, sugar and water fluxes going in and out of the fruit. Also for other species, research is ongoing for developing virtual fruit models based on biophysical mechanisms, such as tomato (Liu et al., 2007; De Swaef and Steppe, 2011), mango (Lechaudel et al., 2007) and kiwifruit (Cieslak et al., 2011). For grapevine, a few first attempts have been made. Models describing individual aspects related to grape berry development have been introduced, such as the growth model of Dai et al. (2008) (adapted from the peach growth model of Fishman and Génard (1998)) for simulating the response of grape berry growth to environmental conditions and source-to-sink ratio. Other examples are the models of Dreier et al. (2000) and Dai et al. (2009) for describing changes in sugar concentration during ripening. To attain eventually a comprehensive virtual grape model, further research is required, in particular on the integration of knowledge on different processes. Ideas on how to tackle this topic are given in the review of Dai et al. (2010) and potentially valuable frameworks for modelling various processes are extensively discussed.

As explained in **Chapters 3** and **4**, grapevines show a characteristic shrinkage in diameter around the onset of veraison (Fig. 8.1), putatively because the grapes become higher demanding sinks for photosynthetic assimilates. Coupling the mechanistic water transport and storage model (**Chapters 5** to **7**) with a virtual fruit model may enable to comprehend and align the observed behaviour in diameter with the ongoing ripening processes in the grapes. The combination of these models would relate the water relations at the whole-plant level and offer insights into both the plant and fruit development.

Appendix

Supplementary material for Chapter 4

Microclimatic conditions during the experiments in 2012

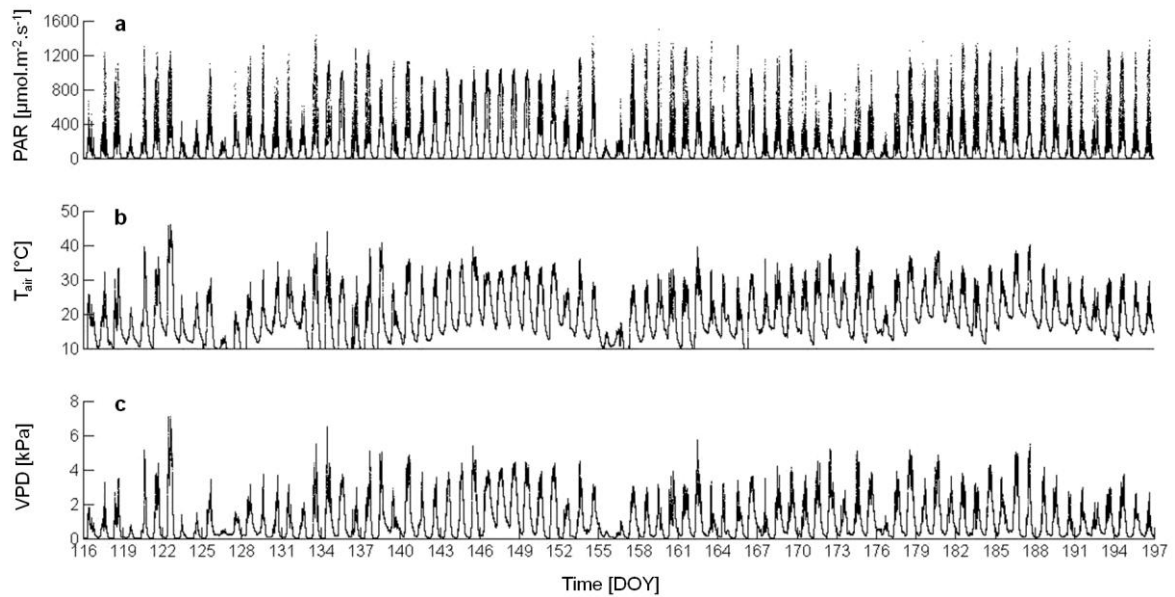


Fig. S1 Microclimatic conditions: (A) photosynthetic active radiation (PAR), (B) air temperature (T_{air}) and (C) vapour pressure deficit (VPD) during the experiments in 2012, i.e. control 1, 2 and repetitions 2 to 5. Time is given in day of the year (DOY).

Analysis of control 1 (2012)

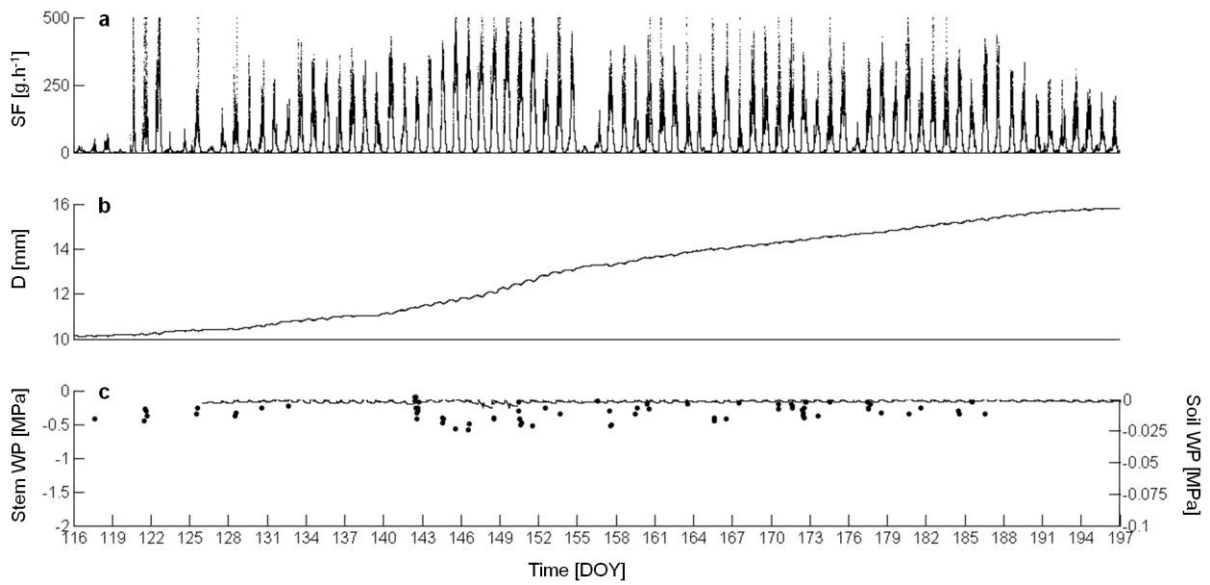


Fig. S2 Control 1: (A) Sap flow rate (SF), (B) stem diameter variations (D) and (C) stem water potential (Ψ_{stem}) and soil water potential (Ψ_{soil}) of a control grapevine. Time is given in day of the year (DOY).

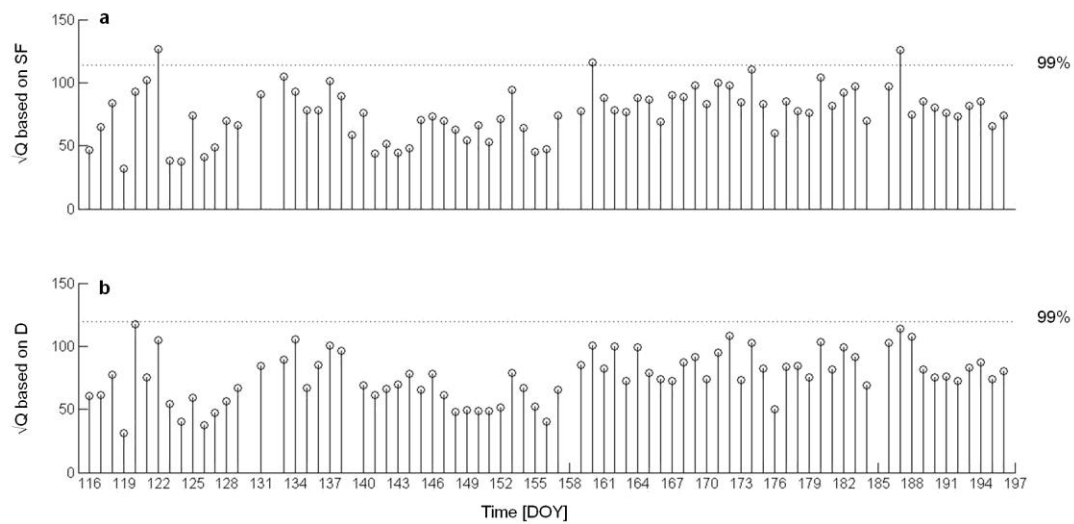


Fig. S3 Control 1: square root of Q statistic as a function of time (in day of the year, DOY) of Unfold Principal Component Analysis (UPCA) based on (A) sap flow rate (SF) and (B) stem diameter variations (D) for a control grapevine. The dotted lines indicate the statistical 99% limits Q_{α} .

Analysis of control 2 (2012)

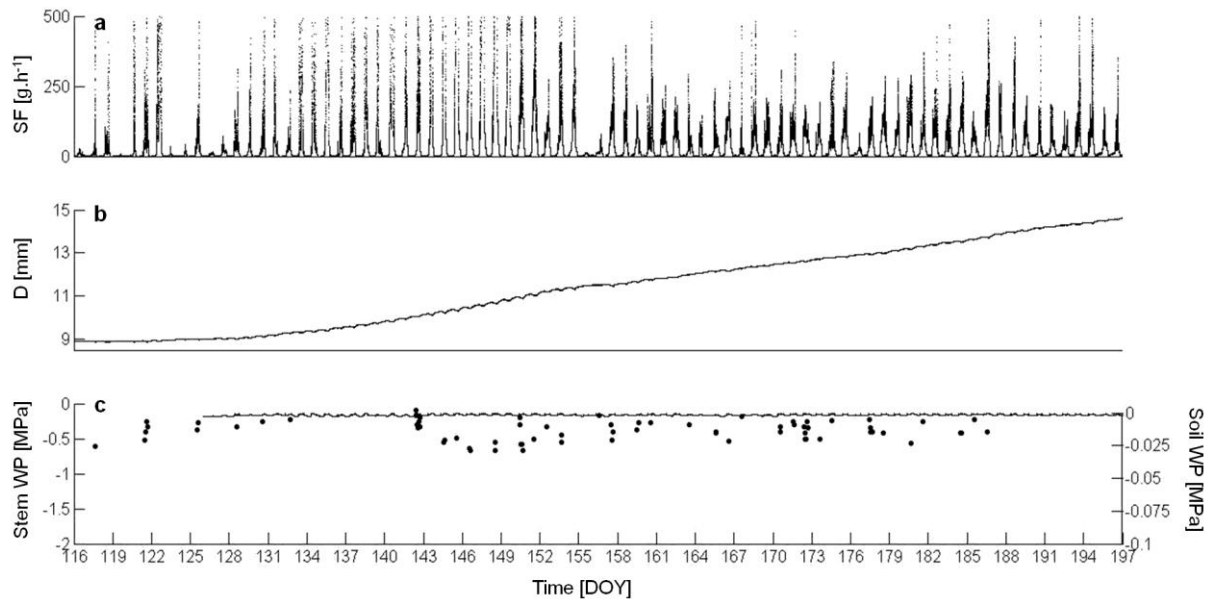


Fig. S4 Control 2: (A) Sap flow rate (SF), (B) stem diameter variations (D) and (C) stem water potential (Ψ_{stem}) and soil water potential (Ψ_{soil}) of a control grapevine. Time is given in day of the year (DOY).

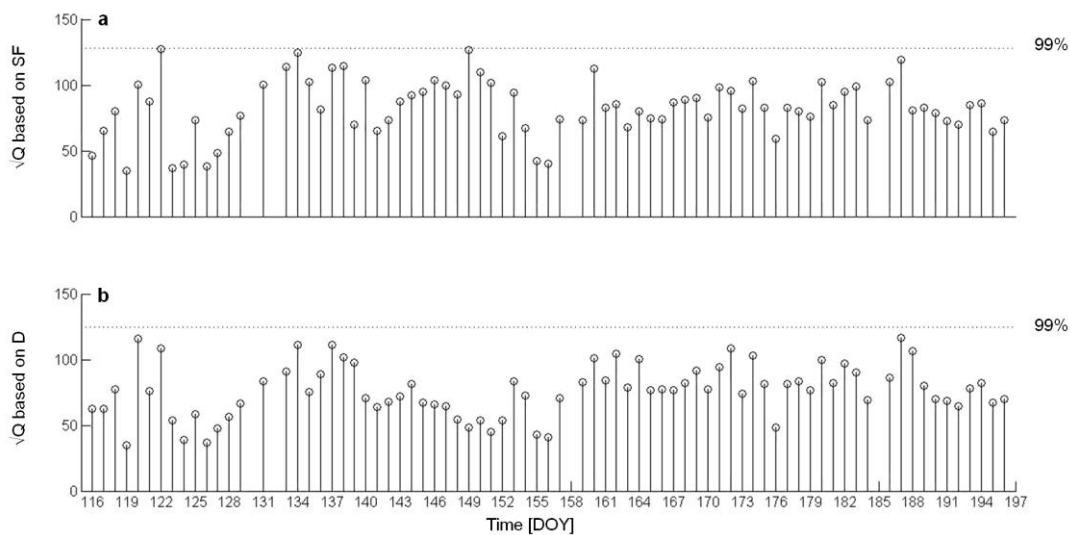


Fig. S5 Control 2: square root of Q statistic as a function of time (in day of the year, DOY) of Unfold Principal Component Analysis (UPCA) based on (A) sap flow rate (SF) and (B) stem diameter variations (D) for a control grapevine. The dotted lines indicate the statistical 99% limits Q_{α} .

Analysis of repetition 2 (2012)

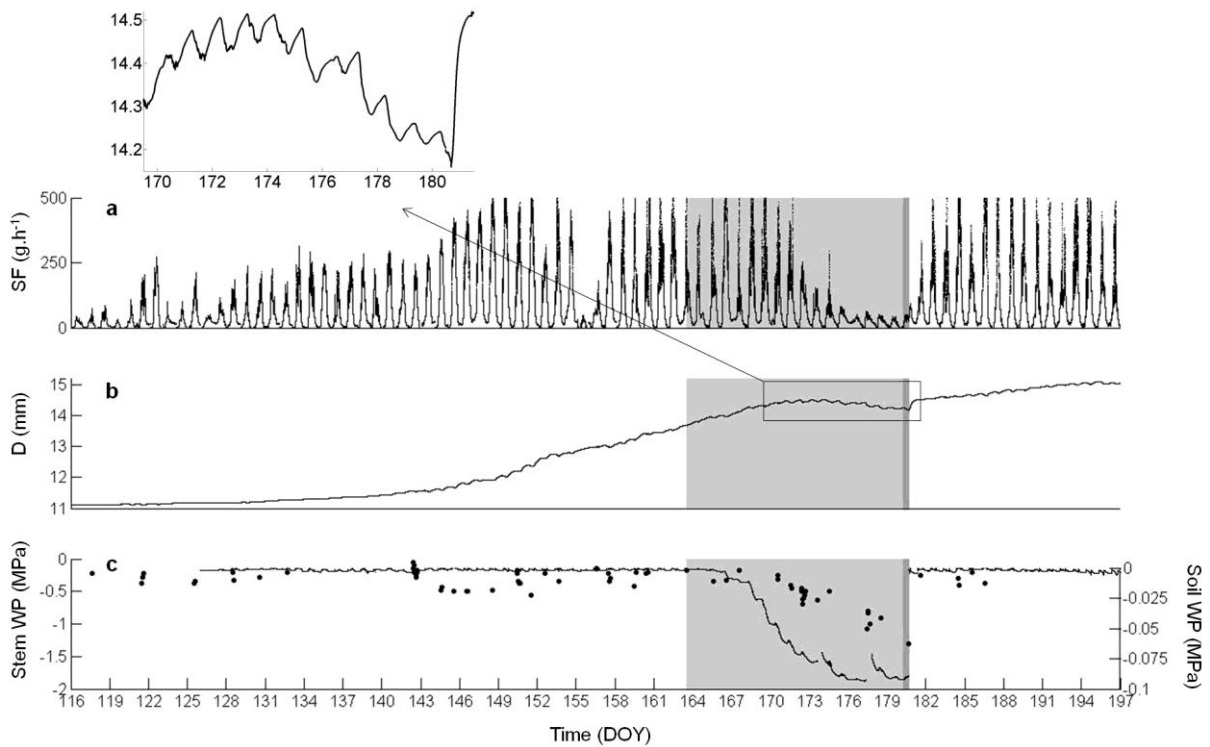


Fig. S6 Repetition 2: (A) Sap flow rate (SF), (B) stem diameter variations (D) and (C) stem water potential (Ψ_{stem}) and soil water potential (Ψ_{soil}) of a drought-stressed grapevine. The grey area marks the period of drought stress for the plant (day of the year (DOY) 163 - 180), the dark grey area the day of resumed irrigation, until the irrigation event

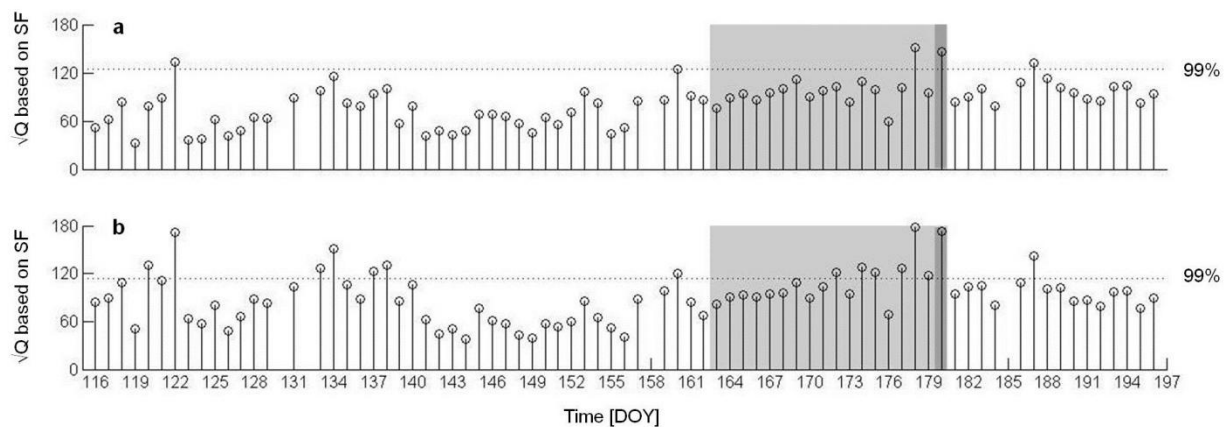


Fig. S7 Influence of a different calibration period for the Unfold Principal Component Analysis (UPCA) model based on sap flow rate, SF, of a drought-stressed grapevine (repetition 2): square root of Q statistic as a function of time for the model calibrated with (A) DOY 116 - 162 or (B) DOY 142 - 162. The dotted lines indicate the statistical 99% limits Q_{α} . The grey area marks the period of drought stress for the plant (DOY 163 - 180), the dark grey area the day of resumed irrigation (until the irrigation event). Clear visible symptoms of drought stress appeared on DOY 177.

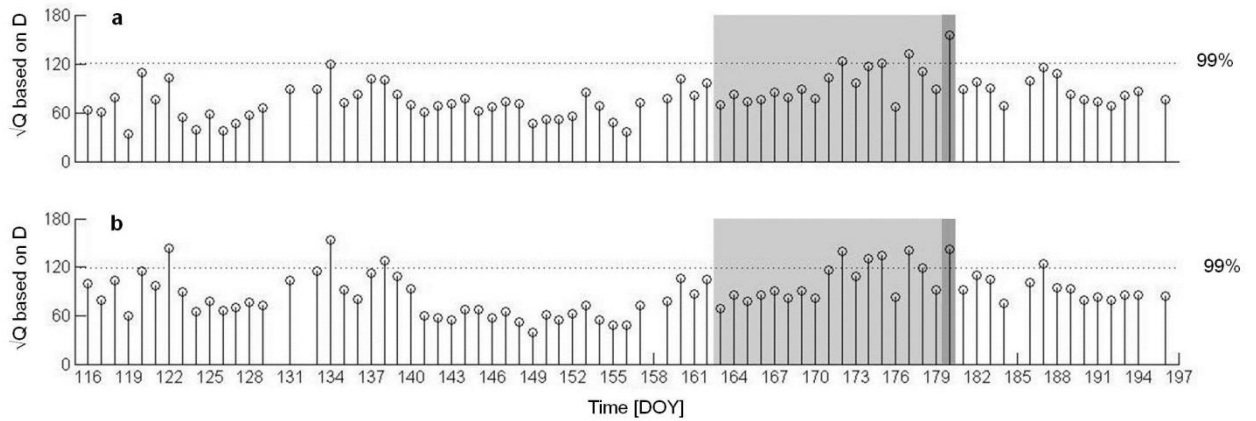


Fig. S8 Influence of a different calibration period for the Unfold Principal Component Analysis (UPCA) model based on stem diameter variations, D , of a drought-stressed grapevine (repetition 2): square root of Q statistic as a function of time for the model calibrated with (A) DOY 116 - 162 or (B) DOY 142 - 162. The dotted lines indicate the statistical 99% limits Q_{α} . The grey area marks the period of drought stress for the plant (DOY 163 - 180), the dark grey area the day of resumed irrigation (until the irrigation event). Clear visible symptoms of drought stress appeared on DOY 177.

Analysis of repetition 3 (2012)

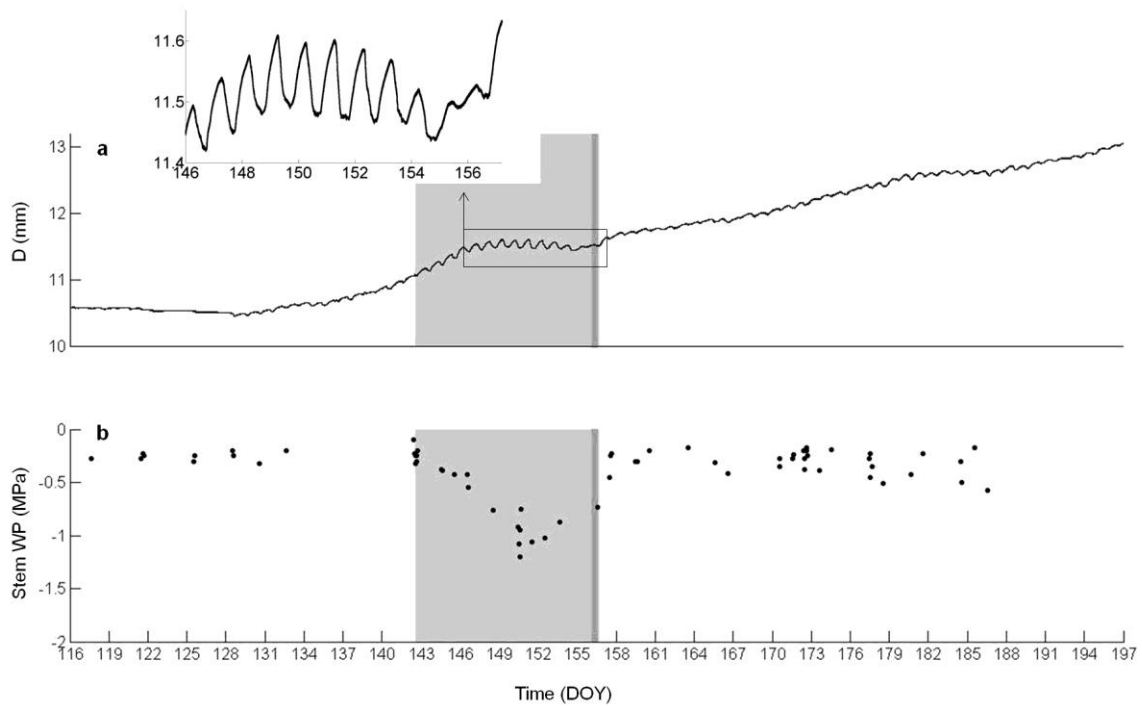


Fig. S9 Repetition 3: (A) stem diameter variations (D) and (B) stem water potential (Ψ_{stem}) of a drought-stressed grapevine. The grey area marks the period of drought stress for the plant (day of the year (DOY) 142 -156), the dark grey area the day of resumed irrigation, until the irrigation event.

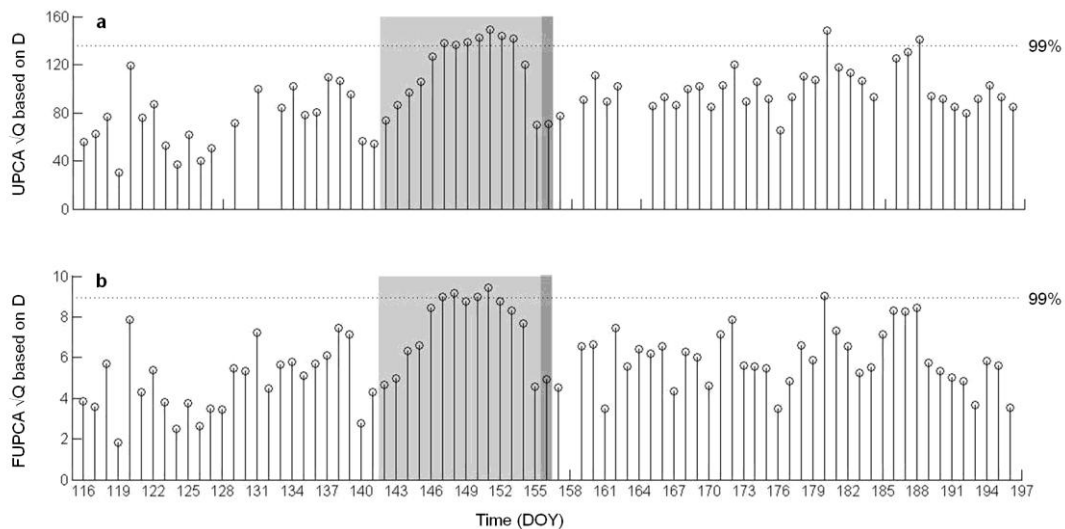


Fig. S10 Repetition 3: square root of Q statistic as a function of time (in day of the year, DOY) of (A) Unfold Principal Component Analysis (UPCA) and (B) Functional Unfold Principal Component Analysis (FUPCA) based on stem diameter variations (D) for a drought-stressed grapevine. The grey area marks the period of drought stress for the plant (DOY 142 - 156), the dark grey area the day of resumed irrigation and the dotted lines indicate the statistical 99% limits Q_{α} .

Analysis of repetition 4 (2012)

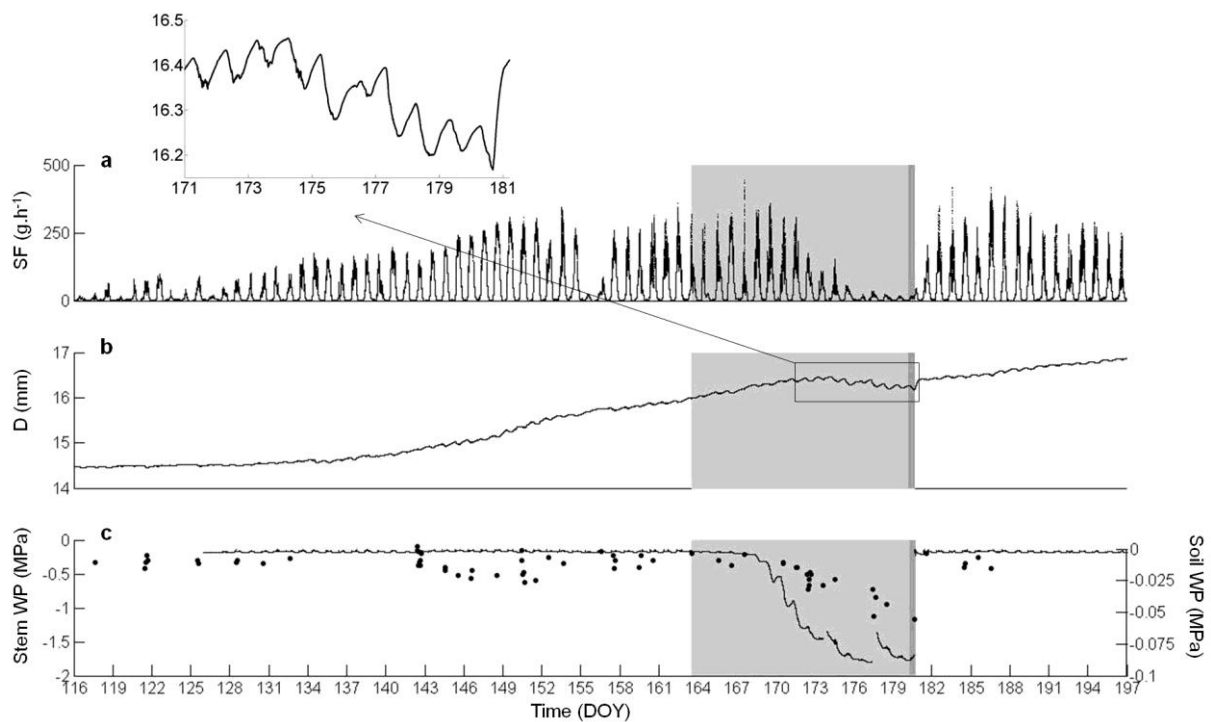


Fig. S11 Repetition 4: (A) Sap flow rate (SF), (B) stem diameter variations (D) and (C) stem water potential (Ψ_{stem}) and soil water potential (Ψ_{soil}) of a drought-stressed grapevine. The grey area marks the period of drought stress for the plant (day of the year (DOY) 163 - 180), the dark grey area the day of resumed irrigation, until the irrigation event.

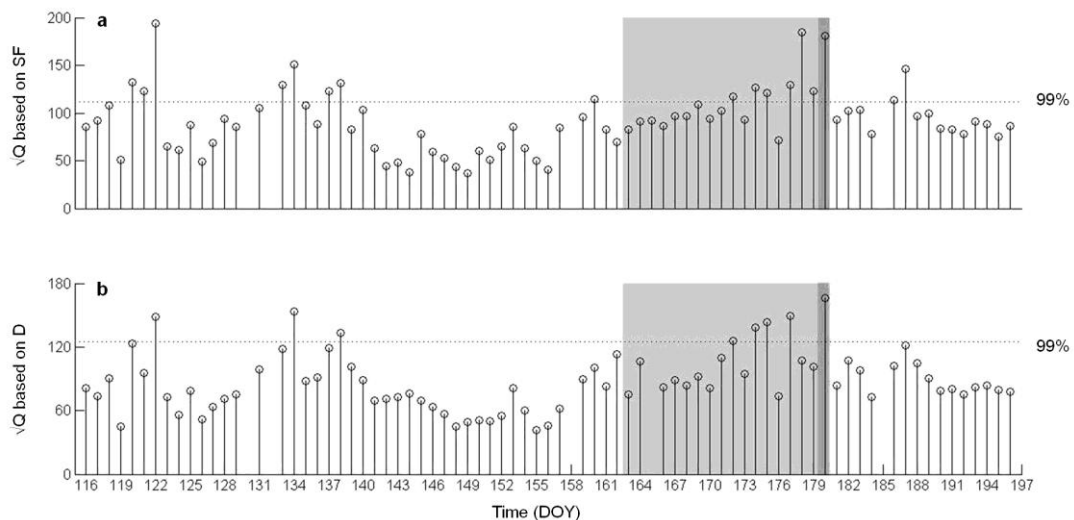


Fig. S12 Repetition 4: square root of Q statistic as a function of time (in day of the year, DOY) of Unfold Principal Component Analysis (UPCA) based on (A) sap flow rate (SF) and (B) stem diameter variations (D) for a drought-stressed grapevine. The grey area marks the period of drought stress for the plant (DOY 163 - 180), the dark grey area the day of resumed irrigation and the dotted lines indicate the statistical 99% limits Q_{α} .

Analysis of repetition 5 (2012)

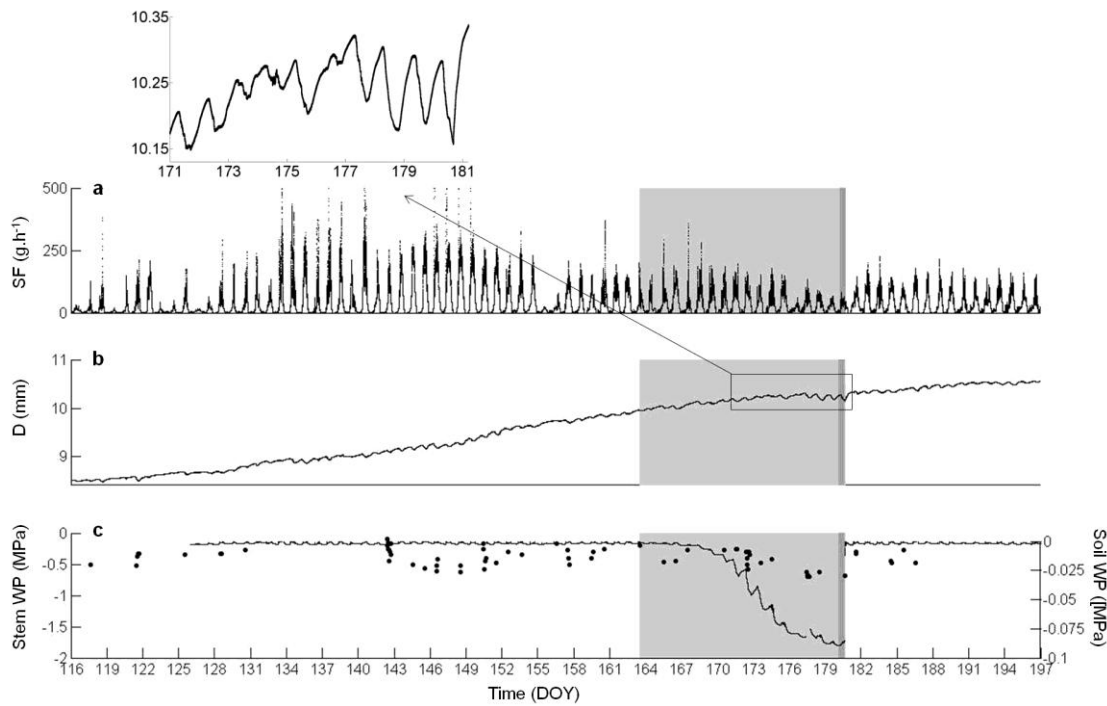


Fig. S13 Repetition 5: (A) Sap flow rate (SF), (B) stem diameter variations (D) and (C) stem water potential (Ψ_{stem}) and soil water potential (Ψ_{soil}) of a drought-stressed grapevine. The grey area marks the period of drought stress for the plant (day of the year (DOY) 163 - 180), the dark grey area the day of resumed irrigation, until the irrigation event.

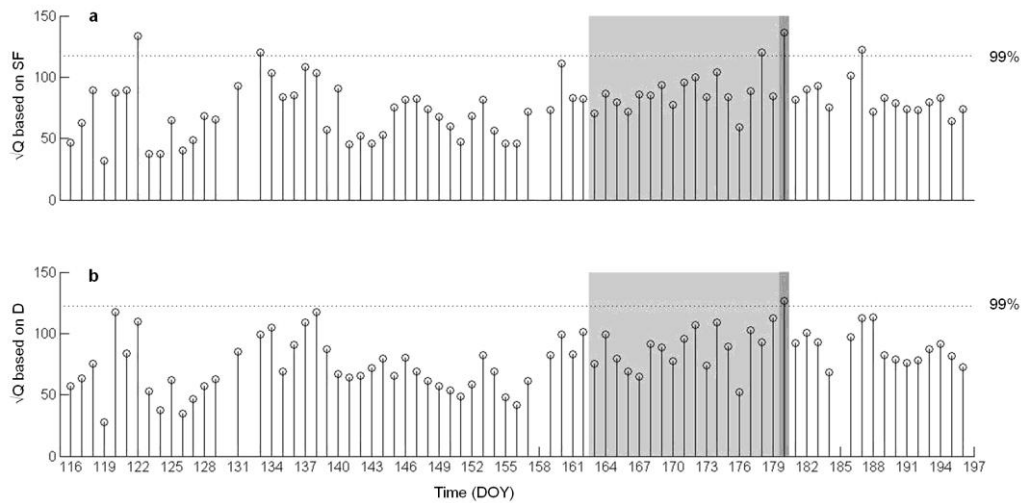


Fig. S14 Repetition 5: square root of Q statistic as a function of time (in day of the year, DOY) of Unfold Principal Component Analysis (UPCA) based on (A) sap flow rate (SF) and (B) stem diameter variations (D) for a drought-stressed grapevine. The grey area marks the period of drought stress for the plant (DOY 163 - 180), the dark grey area the day of resumed irrigation and the dotted lines indicate the statistical 99% limits Q_{α} .

Supplementary material for Chapter 5

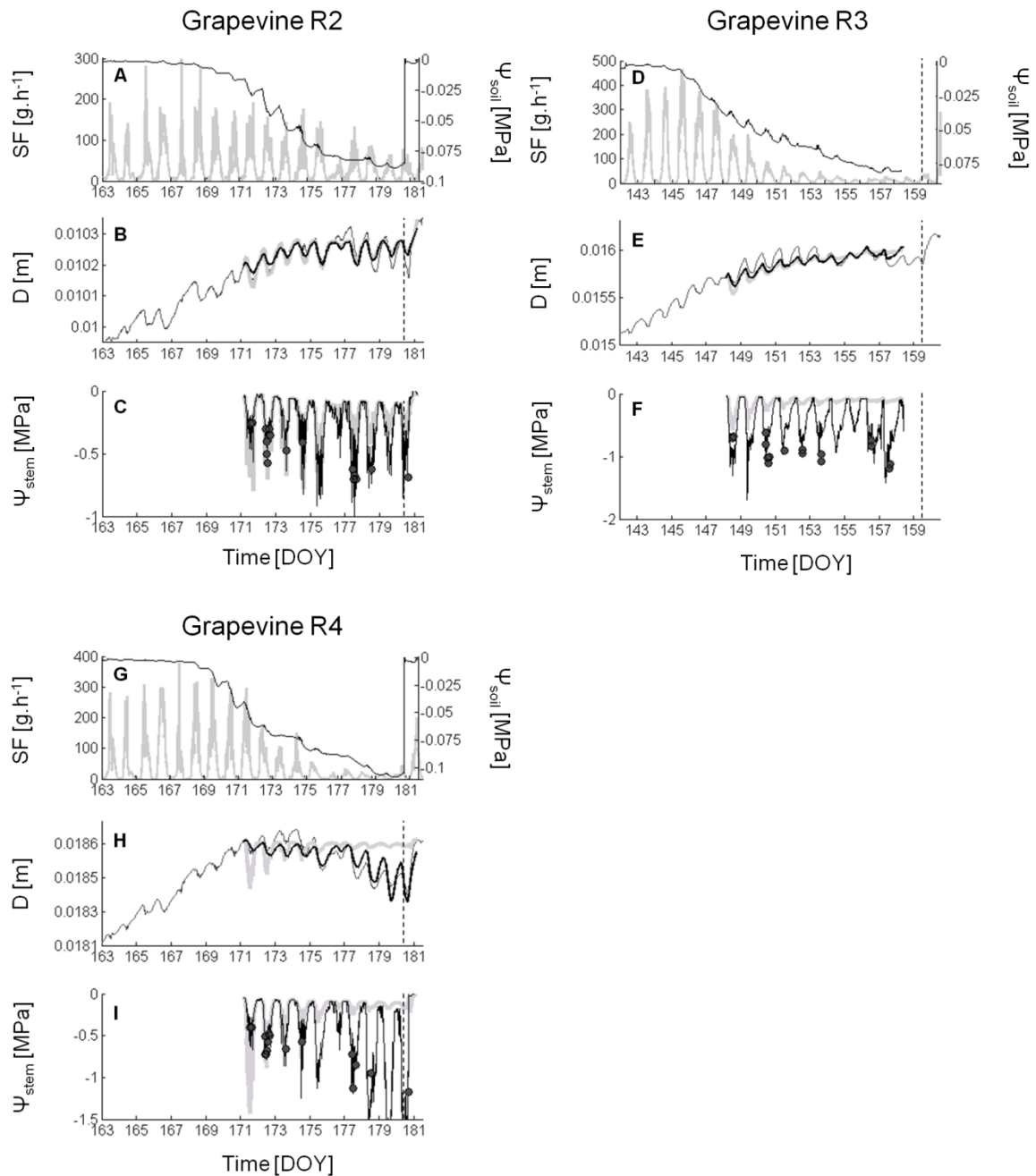


Fig. S15 Model inputs and simulations of grapevine R2 to R4. The used model inputs were (A, D, G) sap flow rate, SF (grey lines), and soil water potential, Ψ_{soil} (black lines); (B, E, H) Comparison between measurements of stem diameter variations, D (thin grey line), with model outputs of the original (constant hydraulic resistance in the xylem, thick grey lines) and adapted (integrated variable hydraulic resistance in the soil-to-stem segment, black lines) model; (C, F, I) Comparison between measurements of stem water potential (Ψ_{stem} , black dots) with model outputs of the original (thick grey lines) and adapted (black lines) model.

References

- Acevedo-Opazo C, Ortega-Farias S and Fuentes S.** 2010. Effects of grapevine (*Vitis vinifera* L.) water status on water consumption, vegetative growth and grape quality: an irrigation scheduling application to achieve regulated deficit irrigation. *Agricultural Water Management*. 97, 956-964.
- Aguado D, Ferrer A, Ferrer J and Seco A.** 2007. Multivariate SPC of a sequencing batch reactor for wastewater treatment. *Chemometrics and Intelligent Laboratory Systems*. 85, 82-93.
- Alchanatis V, Cohen Y, Cohen S, Möller M, Sprinstin M, Meron M, Tsipris J, Saranga Y and Sela E.** 2010. Evaluation of different approaches for estimating and mapping crop water status in cotton with thermal imaging. *Precision Agriculture*. 11, 27-41.
- Alder NN, Pockman WT, Sperry JS and Nuismer S.** 1997. Use of centrifugal force in the study of xylem cavitation. *Journal of Experimental Botany*. 48, 665-674.
- Allen CD, Macalady AK, Chenchouni H, Bachelet D, McDowell N, Vennetier M, Kitzberger T, Rigling A, Breshears DD, Hogg EH, Gonzalez P, Fensham R, Zhang Z, Castro J, Demidova N, Lim J-H, Allard G, Running SW, Semerci A and Cobb N.** 2010. A global overview of drought and heat-induced tree mortality reveals emerging climate change risks for forests. *Forest Ecology and Management*. 259, 660-684.
- Allen RG, Pereira LS, Raes D and Smith M.** 1998. Crop evapotranspiration - Guidelines for computing crop water requirements. Irrigation and drainage paper 56. Rome, IT: FAO.
- Alsina MM, De Herralde F, Aranda X, Savé R and Biel C.** 2007. Water relations and vulnerability to embolism are not related: experiments with eight grapevine cultivars. *Vitis*. 46, 1-6.
- Bacci L, De Vincenzi M, Rapi B, Arca B and Benincasa F.** 1998. Two methods for the analysis of colorimetric components applied to plant stress monitoring. *Computers and Electronics in Agriculture*. 19, 167-186.

- Baert A and Steppe K.** 2013. Putting two water transport models to the test under wet and dry conditions. *Acta Horticulturae*. 991, 359-366.
- Baert A, Villez K and Steppe K.** 2011. Unfold Principal Component Analysis and Functional Unfold Principal Component Analysis for on-line plant stress detection. 9th International Symposium on Modelling in Fruit Research and Orchard Management. Saint-Jean-Sur-Richelieu, Canada. (Under review)
- Bicciato S, Bagnò A, Soldà M, Manfredini R and Di Bello C.** 2002. Fermentation diagnosis by multivariate statistical analysis. *Applied Biochemistry and Biotechnology*. 102-103, 49-62.
- Brodersen CR, McElrone AJ, Choat B, Matthews MA and Shackel KA.** 2010. The dynamics of embolism repair in xylem: in vivo visualizations using high-resolution computed tomography. *Plant Physiology*. 154, 1088-1095.
- Bucci SJ, Scholz FG, Goldstein G, Meinzer FC and Sternberg LDL.** 2003. Dynamic changes in hydraulic conductivity in petioles of two savanna tree species: factors and mechanisms contributing to the refilling of embolized vessels. *Plant, Cell and Environment*. 26, 1633-1645.
- Buckley TN, Mott KA and Farquhar GD.** 2003. A hydromechanical and biochemical model of stomatal conductance. *Plant, Cell and Environment*. 26, 1767-1785.
- Cai J and Tyree MT.** 2010. The impact of vessel size on vulnerability curves: data and models for within-species variability in saplings of aspen, *Populus tremuloides* Michx. *Plant, Cell and Environment*. 33, 1059-1069.
- Campbell NA and Reece JB.** 2008. *Biology*. 8th edn. Amsterdam, NL: Pearson Education.
- Canny MJ, Sparks JP, Huang CX and Roderick ML.** 2007. Air embolisms exsolving in the transpiration water - The effect of constrictions in the xylem pipes. *Functional Plant Biology*. 34, 95-111.
- Chaerle L, Leinonen I, Jones HG and Van der Straeten D.** 2007. Monitoring and screening plant populations with combined thermal and chlorophyll fluorescence imaging. *Journal of Experimental Botany*. 58, 773-784.
- Chapman DM, Roby G, Ebeler SE, Guinard JX and Matthews MA.** 2005. Sensory attributes of Cabernet Sauvignon wines made from vines with different water status. *Australian Journal of Grape and Wine Research*. 11, 339-347.

- Chaves MM, Zarrouk O, Francisco R, Costa JM, Santos T, Regalado AP, Rodrigues ML and Lopes CM.** 2010. Grapevine under deficit irrigation: hints from physiological and molecular data. *Annals of Botany*. 105, 661-676.
- Chen J and Liu J.** 2001. Derivation of function space analysis based PCA control charts for batch process monitoring. *Chemical Engineering Science*. 56, 3289-3304.
- Choat B, Cobb AR and Jansen S.** 2008. Structure and function of bordered pits: new discoveries and impacts on whole-plant hydraulic function. *New Phytologist*. 177, 608-625.
- Choat B, Drayton WM, Brodersen C, Matthews MA, Shackel KA, Wada H and McElrone AJ.** 2010. Measurement of vulnerability to water stress-induced cavitation in grapevine: a comparison of four techniques applied to a long-veined species. *Plant, Cell and Environment*. 33, 1502-1512.
- Choat B, Gambetta GA, Shackel KA and Matthews MA.** 2009. Vascular function in grape berries across development and its relevance to apparent hydraulic isolation. *Plant Physiology*. 151, 1677-1687.
- Choat B, Jansen S, Brodribb TJ, Cochard H, Delzon S, Bhaskar R, Bucci SJ, Feild TS, Gleason SM, Hacke UG, Jacobsen AL, Lens F, Maherali H, Martínez-Vilalta J, Mayr S, Mencuccini M, Mitchell PJ, Nardini A, Pittermann J, Pratt RB, Sperry JS, Westoby M, Wright IJ and Zanne AE.** 2012. Global convergence in the vulnerability of forests to drought. *Nature*. 491, 752-755.
- Choné X, van Leeuwen C, Dubourdieu D and Gaudillère J-P.** 2001. Stem water potential is a sensitive indicator of grapevine water status. *Annals of Botany*. 87, 477-483.
- Christensen JH, Hewitson B, Busuioc A, Chen A, Gao X, Held I, Jones R, Kolli RK, Kwon W-T, Laprise R, Rueda VM, Mearns L, Menéndez CG, Räisänen J, Rinke A, Sarr A and Whetton P.** 2007. Regional climate projections. In: Solomon S, Qin D, Manning M, Chen Z, Marquis M, Averyt KB, Tignor M and Miller HL, Eds. *Climate Change 2007: the physical science basis. Contribution of working group I to the fourth assessment report of the Intergovernmental Panel on Climate Change*. Cambridge, UK: Cambridge University Press.

- Christman MA, Sperry JS and Smith DM.** 2012. Rare pits, large vessels and extreme vulnerability to cavitation in a ring-porous tree species. *New Phytologist*. 193, 713-720.
- Cieslak M, Seleznyova AN and Hanan J.** 2011. A functional-structural kiwifruit vine model integrating architecture, carbon dynamics and effects of the environment. *Annals of Botany*. 107, 747-764.
- Cifre J, Bota J, Escalona JM, Medrano H and Flexas J.** 2005. Physiological tools for irrigation scheduling in grapevine (*Vitis vinifera* L.). An open gate to improve water-use efficiency? *Agriculture Ecosystems & Environment*. 106, 159-170.
- Cochard H.** 2002. A technique for measuring xylem hydraulic conductance under high negative pressures. *Plant, Cell and Environment*. 25, 815-819.
- Cochard H, Badel E, Herbette S, Delzon S, Choat B and Jansen S.** 2013. Methods for measuring plant vulnerability to cavitation: a critical review. *Journal of Experimental Botany*. 64, 4779-4791.
- Cochard H, Bodet C, Ameglio T and Cruiziat P.** 2000. Cryo-scanning electron microscopy observations of vessel content during transpiration in walnut petioles. Facts or artifacts? *Plant Physiology*. 124, 1191-1202.
- Cochard H, Cruiziat P and Tyree MT.** 1992. Use of positive pressures to establish vulnerability curves - Further support for the air-seeding hypothesis and implications for pressure-volume analysis. *Plant Physiology*. 100, 205-209.
- Cochard H, Herbette S, Barigah T, Badel E, Ennajeh M and Vilagrosa A.** 2010. Does sample length influence the shape of xylem embolism vulnerability curves? A test with the Cavitron spinning technique. *Plant, Cell and Environment*. 33, 1543-1552.
- Cochard H, Venisse J-S, Barigah TS, Brunel N, Herbette S, Guilliot A, Tyree MT and Sakr S.** 2007. Putative role of aquaporins in variable hydraulic conductance of leaves in response to light. *Plant Physiology*. 143, 122-133.
- Conejero W, Mellisho CD, Ortuño MF, Moriana A, Moreno F and Torrecillas A.** 2011. Using trunk diameter sensors for regulated deficit irrigation scheduling in early maturing peach trees. *Environmental and Experimental Botany*. 71, 409-415.
- Creasy GL and Creasy LL.** 2009. *Grapes. Crop production science in horticulture* No. 16. Oxfordshire, UK: CABI.

- Cruziat P and Tyree MT.** 1990. La montée de la sève dans les arbres. La recherche. 21, 406-414.
- Dai ZW, Vivin P, Barrieu F, Ollat N and Delrot S.** 2010. Physiological and modelling approaches to understand water and carbon fluxes during grape berry growth and quality development: a review. Australian Journal of Grape and Wine Research. 16, 70-85.
- Dai ZW, Vivin P and Génard M.** 2008. Modelling the effects of leaf-to-fruit ratio on dry and fresh mass accumulation in ripening grape berries. Acta Horticulturae. 803, 283-291.
- Dai ZW, Vivin P, Robert T, Milin S, Li SH and Génard M.** 2009. Model-based analysis of sugar accumulation in response to source-sink ratio and water supply in grape (*Vitis vinifera*) berries. Functional Plant Biology. 36, 527-540.
- Damour G, Simonneau T, Cochard H and Urban L.** 2010. An overview of models of stomatal conductance at the leaf level. Plant, Cell and Environment. 33, 1419-1438.
- Daudet F-A, Améglio T, Cochard H, Archilla O and Lacoite A.** 2005. Experimental analysis of the role of water and carbon in tree stem diameter variations. Journal of Experimental Botany. 56, 135-144.
- De Pauw DJW, Steppe K and De Baets B.** 2008a. Identifiability analysis and improvement of a tree water flow and storage model. Mathematical Biosciences. 211, 314-332.
- De Pauw DJW, Steppe K and De Baets B.** 2008b. Unravelling the output uncertainty of a tree water flow and storage model using several global sensitivity analysis methods. Biosystems Engineering. 101, 87-99.
- De Schepper V and Steppe K.** 2010. Development and verification of a water and sugar transport model using measured stem diameter variations. Journal of Experimental Botany. 61, 2083-2099.
- De Schepper V, Steppe K, Van Labeke M-C and Lemeur R.** 2010. Detailed analysis of double girdling effects on stem diameter variations and sap flow in young oak trees. Environmental and Experimental Botany. 68, 149-156.
- De Schepper V, Vanhaecke L and Steppe K.** 2011. Localized stem chilling alters carbon processes in the adjacent stem and in source leaves. Tree Physiology. 31, 1-10.

- De Swaef T and Steppe K.** 2010. Linking stem diameter variations to sap flow, turgor and water potential in tomato. *Functional Plant Biology*. 37, 429-438.
- De Swaef T and Steppe K.** 2011. Tomato stem and fruit dynamics predicted with a whole-plant water and carbon flow model. *Acta Horticulturae*. 893, 713-719.
- De Swaef T, Steppe K and Lemeur R.** 2009. Determining reference values for stem water potential and maximum daily trunk shrinkage in young apple trees based on plant responses to water deficit. *Agricultural Water Management*. 96, 541-550.
- Diaz-Espejo A, Buckley TN, Sperry JS, Cuevas MV, de Cires A, Elsayed-Farag S, Martin-Palomo MJ, Muriel JL, Perez-Martin A, Rodriguez-Dominguez CM, Rubio-Casal AE, Torres-Ruiz JM and Fernández JE.** 2012. Steps toward an improvement in process-based models of water use by fruit trees: A case study in olive. *Agricultural Water Management*. 114, 37-49.
- Dixon JH and Joly J.** 1895. On the ascent of sap. *Philosophical transactions of the Royal Society of London*. 186, 563-576.
- Dixon MA and Tyree MT.** 1984. A new stem hygrometer, corrected for temperature gradients and calibrated against the pressure bomb. *Plant, Cell and Environment*. 7, 693-697.
- Dochain D and Vanrolleghem PA.** 2001. *Dynamical modelling and estimation in wastewater treatment processes*. London, UK: IWA Publishing.
- Dokoozlian NK.** 2000. Grape berry growth and development. In: Christensen LP, Ed. *Raisin production manual*. Oakland, CA, USA: University of California, Agricultural and Natural Resources No. 3393. 30-37.
- Doltra J, Oncins JA, Bonany J and Cohen M.** 2007. Evaluation of plant-based water status indicators in mature apple trees under field conditions. *Irrigation Science*. 25, 351-359.
- dos Santos TP, Lopes CM, Rodrigues ML, de Souza CR, Ricardo-da-Silva JM, Maroco JP, Pereira JS and Chaves MM.** 2007. Effects of deficit irrigation strategies on cluster microclimate for improving fruit composition of Moscatel field-grown grapevines. *Scientia Horticulturae*. 112, 321-330.
- Dreier LP, Stoll GS and Ruffner HP.** 2000. Berry ripening and evapotranspiration in *Vitis vinifera* L. *American Journal of Enology and Viticulture*. 51, 340-346.
- Dunia R and Qin SJ.** 1998. Subspace approach to multidimensional fault identification and reconstruction. *AIChE Journal*. 44, 1813-1831.

- Egea G, Verhoef A and Vidale PL.** 2011. Towards an improved and more flexible representation of water stress in coupled photosynthesis–stomatal conductance models. *Agricultural and Forest Meteorology*. 151, 1370-1384.
- Espino S and Schenk HJ.** 2011. Mind the bubbles: achieving stable measurements of maximum hydraulic conductivity through woody plant samples. *Journal of Experimental Botany*. 62, 1119-1132.
- Fereres E and Goldhamer DA.** 2003. Suitability of stem diameter variations and water potential as indicators for irrigation scheduling of almond trees. *Journal of Horticultural Science & Biotechnology*. 78, 139-144.
- Fernández JE and Cuevas MV.** 2010. Irrigation scheduling from stem diameter variations: a review. *Agricultural and Forest Meteorology*. 150, 135-151.
- Fernández JE, Green SR, Caspari HW, Diaz-Espejo A and Cuevas MV.** 2008. The use of sap flow measurements for scheduling irrigation in olive, apple and Asian pear trees and in grapevines. *Plant and Soil*. 305, 91-104.
- Fernández JE, Moreno F, Martín-Palomo MJ, Cuevas MV, Torres-Ruiz JM and Moriana A.** 2011a. Combining sap flow and trunk diameter measurements to assess water needs in mature olive orchards. *Environmental and Experimental Botany*. 72, 330-338.
- Fernández JE, Rodriguez-Dominguez CM, Perez-Martin A, Zimmermann U, Rüger S, Martín-Palomo MJ, Torres-Ruiz JM, Cuevas MV, Sann C, Ehrenberger W and Diaz-Espejo A.** 2011b. Online-monitoring of tree water stress in a hedgerow olive orchard using the leaf patch clamp pressure probe. *Agricultural Water Management*. 100, 25-35.
- Fishman S and Génard M.** 1998. A biophysical model of fruit growth: simulation of seasonal and diurnal dynamics of mass. *Plant, Cell and Environment*. 21, 739-752.
- Gardner WR.** 1960. Dynamic aspects of water availability to plants. *Soil Science*. 89, 63-73.
- Gaudillère JP, van Leeuwen C and Ollat N.** 2002. Carbon isotope composition of sugars in grapevine, an integrated indicator of vineyard water status. *Journal of Experimental Botany*. 53, 757-763.
- Génard M, Bertin N, Borel C, Bussières P, Gautier H, Habib R, Lechaudel M, Lecomte A, Lescourret F, Lobit P and Quilot B.** 2007. Towards a virtual fruit

- focusing on quality: modelling features and potential uses. *Journal of Experimental Botany*. 58, 917-928.
- Génard M, Fishman S, Vercambre G, Huguet J-G, Bussi C, Besset J and Habib R.** 2001. A biophysical analysis of stem and root diameter variations in woody plants. *Plant Physiology*. 126, 188-202.
- Ginestar C, Eastham J, Gray S and Iland P.** 1998. Use of sap-flow sensors to schedule vineyard irrigation. II. Effects of post-veraison water deficits on composition of shiraz grapes. *American Journal of Enology and Viticulture*. 49, 421-428.
- Goldhamer D and Fereres E.** 2001. Irrigation scheduling protocols using continuously recorded trunk diameter measurements. *Irrigation Science*. 20, 115-125.
- Goldstein G, Andrade JL, Meinzer FC, Holbrook NM, Cavellier J, Jackson P and Celis A.** 1998. Stem water storage and diurnal patterns of water use in tropical forest canopy trees. *Plant, Cell and Environment*. 21, 397-406.
- Grant OM, Tronina L, Jones HG and Chaves MM.** 2007. Exploring thermal imaging variables for the detection of stress responses in grapevine under different irrigation regimes. *Journal of Experimental Botany*. 58, 815-825.
- Green SR.** 2008. Measurement and modelling the transpiration of fruit trees and grapevines for irrigation scheduling. *Acta Horticulturae*. 792, 321-332.
- Green SR, Kirkham MB and Clothier BE.** 2006. Root uptake and transpiration: from measurements and models to sustainable irrigation. *Agricultural Water Management*. 86, 165-176.
- Greenspan MD, Shackel KA and Matthews MA.** 1994. Developmental changes in the diurnal water budget of the grape berry exposed to water deficits. *Plant, Cell and Environment*. 17, 811-820.
- Gurden SP, Westerhuis JA, Bro R and Smilde AK.** 2001. A comparison of multiway regression and scaling methods. *Chemometrics and Intelligent Laboratory Systems*. 59, 121-136.
- Guyot G, Scoffoni C and Sack L.** 2012. Combined impacts of irradiance and dehydration on leaf hydraulic conductance: insights into vulnerability and stomatal control. *Plant, Cell and Environment*. 35, 857-871.
- Hannah L, Roehrdanz PR, Ikegami M, Shepard AV, Shaw MR, Tabor G, Zhi L, Marquet PA and Hijmans RJ.** 2013a. Climate change, wine, and

- conservation. Proceedings of the National Academy of Sciences of the United States of America. 110, 6907-6912.
- Hannah L, Roehrdanz PR, Ikegami M, Shepard AV, Shaw MR, Tabor G, Zhi L, Marquet PA and Hijmans RJ.** 2013b. Reply to van Leeuwen et al.: Planning for agricultural adaptation to climate change and its consequences for conservation. Proceedings of the National Academy of Sciences of the United States of America. 110, E3053.
- Hardie WJ and Considine JA.** 1976. Response of grapes to water deficit stress in particular stages of development. American Journal of Enology and Viticulture. 27, 55-61.
- Helton JC and Davis FJ.** 2003. Latin hypercube sampling and the propagation of uncertainty in analyses of complex systems. Reliability Engineering & System Safety. 81, 23-69.
- Hoefsloot HCJ, Verouden MPH, Westerhuis JA and Smilde AK.** 2006. Maximum likelihood scaling (MALS). Journal of Chemometrics. 20, 120-127.
- Holbrook MN, Ahrens ET, Burns MJ and Zwieniecki MA.** 2001. In vivo observation of cavitation and embolism repair using magnetic resonance imaging. Plant Physiology. 126, 27-31.
- Hölttä T, Cochard H, Nikinmaa E and Mencuccini M.** 2009. Capacitive effect of cavitation in xylem conduits: results from a dynamic model. Plant, Cell and Environment. 32, 10-21.
- Hölttä T, Vesala T, Nikinmaa E, Perämäki M, Siivola E and Mencuccini M.** 2005. Field measurements of ultrasonic acoustic emissions and stem diameter variations. New insight into the relationship between xylem tensions and embolism. Tree Physiology. 25, 237-243.
- Hotelling H.** 1947. Multivariate quality control illustrated by the testing of sample bombsights. In: Eisenhart O, Ed. Selected techniques of statistical analysis. New York, USA: McGraw-Hill. 113-184.
- Intrigliolo DS and Castel JR.** 2004. Continuous measurement of plant and soil water status for irrigation scheduling in plum. Irrigation Science. 23, 93-102.
- Intrigliolo DS and Castel JR.** 2006. Usefulness of diurnal trunk shrinkage as a water stress indicator in plum trees. Tree Physiology. 26, 303-311.
- Intrigliolo DS and Castel JR.** 2007a. Crop load affects maximum daily trunk shrinkage of plum trees. Tree Physiology. 27, 89-96.

- Intrigliolo DS and Castel JR.** 2007b. Evaluation of grapevine water status from trunk diameter variations. *Irrigation Science*. 26, 49-59.
- IPCC.** 2007. *Climate Change 2007: the physical science basis. Contribution of working group I to the fourth assessment report of the Intergovernmental Panel on Climate Change.* Cambridge, UK: Cambridge University Press.
- IPCC.** 2013. *Climate Change 2013: the physical science basis. Working group I contribution to the fifth assessment report of the Intergovernmental Panel on Climate Change.* (In press).
- Jackson DI and Lombard PB.** 1993. Environmental and management practices affecting grape composition and wine quality - A review. *American Journal of Enology and Viticulture*. 44, 409-430.
- Jackson JE.** 1991. *A user's guide to principal components.* New York, USA: Wiley-Interscience.
- Jacobsen AL and Pratt RB.** 2012. No evidence for an open vessel effect in centrifuge-based vulnerability curves of a long-vesselled liana (*Vitis vinifera*). *New Phytologist*. 194, 982-990.
- Jarvis PG and McNaughton KG.** 1986. Stomatal control of transpiration: scaling up from leaf to region. In: MacFadyen A and Ford ED, Eds. *Advances in ecological research*, vol 15. London, UK: Academic Press, Inc. 1-49.
- Johnson DM, McCulloh KA, Woodruff DR and Meinzer FC.** 2012. Evidence for xylem embolism as a primary factor in dehydration-induced declines in leaf hydraulic conductance. *Plant, Cell and Environment*. 35, 760-769.
- Johnson RA and Wichern DW.** 2002. *Applied multivariate statistical analysis.* 5th edn. New Jersey, USA: Prentice-Hall Inc.
- Jolliffe IT.** 2002. *Principal component analysis.* Springer series in statistics, 2nd edn. New York, USA: Springer.
- Jones GV, White MA, Cooper OR and Storchmann K.** 2005. Climate change and global wine quality. *Climatic Change*. 73, 319-343.
- Jones HG.** 1990. Plant water relations and implications for irrigation scheduling. *Acta Horticulturae*. 278, 67-76.
- Jones HG.** 1992. *Plants and microclimate. A quantitative approach to environmental plant physiology.* 2nd edn. Cambridge, UK: Cambridge University Press.

- Jones HG.** 2004. Irrigation scheduling: advantages and pitfalls of plant-based methods. *Journal of Experimental Botany*. 55, 2427-2436.
- Jones HG.** 2007. Monitoring plant and soil water status: established and novel methods revisited and their relevance to studies of drought tolerance. *Journal of Experimental Botany*. 58, 119-130.
- Jones HG, Serraj R, Loveys BR, Xiong L, Wheaton A and Price AH.** 2009. Thermal infrared imaging of crop canopies for the remote diagnosis and quantification of plant responses to water stress in the field. *Functional Plant Biology*. 36, 978-989.
- Keller M.** 2010a. Managing grapevines to optimise fruit development in a challenging environment: a climate change primer for viticulturists. *Australian Journal of Grape and Wine Research*. 16, 56-69.
- Keller M.** 2010b. *The science of grapevines. Anatomy and physiology*. London, UK: Academic Press.
- Keller M, Smith J and Bondada BR.** 2006. Ripening grape berries remain hydraulically connected to the shoot. *Journal of Experimental Botany*. 57, 2577-2587.
- Kennedy J.** 2002. Understanding grape berry development. *Practical Winery & Vineyard Journal*. July/August. <http://www.practicalwinery.com/julyaugust02/julaug02p14.htm>
- Kikuta SB, Hietz P and Richter H.** 2003. Vulnerability curves from conifer sapwood sections exposed over solutions with known water potentials. *Journal of Experimental Botany*. 54, 2149-2155.
- Klepper B, Taylor HM, Huck MG and Fiscus EL.** 1973. Water relations and growth of cotton in drying soil. *Agronomy Journal*. 65, 307-310.
- Kopyt M and Ton Y.** 2005. Grapevine trunk expansion and microvariations: application for irrigation management. *Australian & New Zealand Grapegrower & Winemaker*. 497, 27-35.
- Kourti T.** 2002. Process analysis and abnormal situation detection: from theory to practice. *IEEE Control Systems Magazine*. 22, 10-25.
- Lechaudel M, Vercambre G, Lescouret F, Normand F and Génard M.** 2007. An analysis of elastic and plastic fruit growth of mango in response to various assimilate supplies. *Tree Physiology*. 27, 219-230.

- Lee DS and Vanrolleghem PA.** 2003. Monitoring of a sequencing batch reactor using adaptive multiblock principal component analysis. *Biotechnology and Bioengineering.* 82, 489-497.
- Lennox B, Montague GA, Hiden HG, Kornfeld G and Goulding PR.** 2001. Process monitoring of an industrial fed-batch fermentation. *Biotechnology and Bioengineering.* 74, 125-135.
- Lennox J and Rosen C.** 2002. Adaptive multiscale principal components analysis for online monitoring of wastewater treatment. *Water Science and Technology.* 45, 227-235.
- Lens F, Tixier A, Cochard H, Sperry JS, Jansen S and Herbette S.** 2013. Embolism resistance as a key mechanism to understand adaptive plant strategies. *Current Opinion in Plant Biology.* 16, 287-292.
- Lescouret F and Génard M.** 2005. A virtual peach fruit model simulating changes in fruit quality during the final stage of fruit growth. *Tree Physiology.* 25, 1303-1315.
- Li WH, Yue HH, Valle-Cervantes S and Qin SJ.** 2000. Recursive PCA for adaptive process monitoring. *Journal of Process Control.* 10, 471-486.
- Liu H-F, Génard M, Guichard S and Bertin N.** 2007. Model-assisted analysis of tomato fruit growth in relation to carbon and water fluxes. *Journal of Experimental Botany.* 58, 3567-3580.
- Lockhart JA.** 1965. An analysis of irreversible plant cell elongation. *Journal of Theoretical Biology.* 8, 264-275.
- Lovisolo C, Perrone I, Carra A, Ferrandino A, Flexas J, Medrano H and Schubert A.** 2010. Drought-induced changes in development and function of grapevine (*Vitis* spp.) organs and in their hydraulic and non-hydraulic interactions at the whole-plant level: a physiological and molecular update. *Functional Plant Biology.* 37, 98-116.
- Lovisolo C, Perrone I, Hartung W and Schubert A.** 2008. An abscisic acid-related reduced transpiration promotes gradual embolism repair when grapevines are rehydrated after drought. *New Phytologist.* 180, 642-651.
- Lovisolo C and Schubert A.** 1998. Effects of water stress on vessel size and xylem hydraulic conductivity in *Vitis vinifera* L. *Journal of Experimental Botany.* 49, 693-700.

- MacGregor JF and Jaeckle C.** 1994. Process monitoring and diagnosis by multiblock PLS methods. *AIChE Journal*. 40, 826-838.
- MacGregor JF and Kourti T.** 1995. Statistical process control of multivariate processes. *Control Engineering Practice*. 3, 403-414.
- Maes WH and Steppe K.** 2012. Estimating evapotranspiration and drought stress with ground-based thermal remote sensing in agriculture: a review. *Journal of Experimental Botany*. 63, 4671-4712.
- Martínez-Vilalta J, Piñol J and Beven K.** 2002. A hydraulic model to predict drought-induced mortality in woody plants: an application to climate change in the Mediterranean. *Ecological Modelling*. 155, 127-147.
- Matthews MA, Ishii R, Anderson MM and O'Mahony M.** 1990. Dependence of wine sensory attributes on vine water status. *Journal of the Science of Food and Agriculture*. 51, 321-335.
- McCully ME.** 1999. Root xylem embolisms and refilling. Relation to water potentials of soil, roots, and leaves, and osmotic potentials of root xylem sap. *Plant Physiology*. 119, 1001-1008.
- McCully ME, Huang CX and Ling LEC.** 1998. Daily embolism and refilling of xylem vessels in the roots of field-grown maize. *New Phytologist*. 138, 327-342.
- McCutchan H and Shackel KA.** 1992. Stem-water potential as a sensitive indicator of water stress in prune trees (*Prunus domestica* L. cv. French). *Journal of the American Society for Horticultural Science*. 117, 607-611.
- McElrone AJ, Brodersen CR, Alsina MM, Drayton WM, Matthews MA, Shackel KA, Wada H, Zufferey V and Choat B.** 2012. Centrifuge technique consistently overestimates vulnerability to water stress-induced cavitation in grapevines as confirmed with high-resolution computed tomography. *New Phytologist*. 196, 661-665.
- Meinzer FC, Clearwater MJ and Goldstein G.** 2001. Water transport in trees: current perspectives, new insights and some controversies. *Environmental and Experimental Botany*. 45, 239-262.
- Meinzer FC, Domec JC, Johnson DM, McCulloh KA and Woodruff DR.** 2013. The dynamic pipeline: homeostatic mechanisms that maintain the integrity of xylem water transport from roots to leaves. *Acta Horticulturae*. 991, 125-131.
- Meinzer FC, Johnson DM, Lachenbruch B, McCulloh KA and Woodruff DR.** 2009. Xylem hydraulic safety margins in woody plants: coordination of stomatal

control of xylem tension with hydraulic capacitance. *Functional Ecology*. 23, 922-930.

Mencuccini M, Hölttä T, Sevanto S and Nikinmaa E. 2013. Concurrent measurements of change in the bark and xylem diameters of trees reveal a phloem-generated turgor signal. *New Phytologist*. 198, 1143-1154.

Miletic I, Boudreau F, Dudzic M, Kotuza G, Ronholm L, Vaculik V and Zhang Y. 2008. Experiences in applying data-driven modelling technology to steelmaking processes. *Canadian Journal of Chemical Engineering*. 86, 937-946.

Möller M, Alchanatis V, Cohen Y, Meron M, Tsipris J, Naor A, Ostrovsky V, Sprintsin M and Cohen S. 2007. Use of thermal and visible imagery for estimating crop water status of irrigated grapevine. *Journal of Experimental Botany*. 58, 827-838.

Monroy I, Villez K, Graells M and Venkatasubramanian V. 2012. Fault diagnosis of a benchmark fermentation process: a comparative study of feature extraction and classification techniques. *Bioprocess and Biosystems Engineering*. 35, 689-704.

Montoro A, Fereres E, Lopez-Urrea R, Manas F and Lopez-Fuster P. 2012. Sensitivity of trunk diameter fluctuations in *Vitis vinifera* L. Tempranillo and Cabernet Sauvignon cultivars. *American Journal of Enology and Viticulture*. 63, 85-93.

Moreno F, Conejero W, Martín-Palomo MJ, Girón IF and Torrecillas A. 2006. Maximum daily trunk shrinkage reference values for irrigation scheduling in olive trees. *Agricultural Water Management*. 84, 290-294.

Naor A. 2006. Irrigation scheduling and evaluation of tree water status in deciduous orchards. In: Janick J, Ed. *Horticultural reviews*, vol 32. New York, USA: Wiley. 111-166.

Nardini A, Grego F, Trifilo P and Salleo S. 2010. Changes of xylem sap ionic content and stem hydraulics in response to irradiance in *Laurus nobilis*. *Tree Physiology*. 30, 628-635.

Nelder JA and Mead R. 1965. A simplex method for function minimization. *The Computer Journal*. 7, 308-313.

- Nizinski JJ, Montoroi J-P, Silvera N and Lointier M.** 2013. Use of the Dixon-Tyree stem hygrometer in a rubber tree plantation. *Agricultural and Forest Meteorology*. 173, 100-106.
- Nomikos P and MacGregor JF.** 1994. Monitoring batch processes using multiway principal component analysis. *AIChE Journal*. 40, 1361-1375.
- Ortuño MF, Conejero W, Moreno F, Moriana A, Intrigliolo DS, Biel C, Mellisho CD, Pérez-Pastor A, Domingo R, Ruiz-Sánchez MC, Casadesus J, Bonany J and Torrecillas A.** 2010. Could trunk diameter sensors be used in woody crops for irrigation scheduling? A review of current knowledge and future perspectives. *Agricultural Water Management*. 97, 1-11.
- Ortuño MF, García-Orellana Y, Conejero W, Pérez-Sarmiento F and Torrecillas A.** 2009. Assessment of maximum daily trunk shrinkage signal intensity threshold values for deficit irrigation in lemon trees. *Agricultural Water Management*. 96, 80-86.
- Ortuño MF, García-Orellana Y, Conejero W, Ruiz-Sánchez MC, Mounzer O, Alarcón JJ and Torrecillas A.** 2006. Relationships between climatic variables and sap flow, stem water potential and maximum daily trunk shrinkage in lemon trees. *Plant and Soil*, 229-242.
- Patakas A, Noitsakis B and Chouzouri A.** 2005. Optimization of irrigation water use in grapevines using the relationship between transpiration and plant water status. *Agriculture Ecosystems & Environment*. 106, 253-259.
- Penman HL.** 1948. Natural evaporation from open water, bare soil and grass. *Proceedings of the Royal Society of London A Mathematical and Physical Sciences*. 193, 120-145.
- Perämäki M, Nikinmaa E, Sevanto S, Ilvesniemi H, Siivola E, Hari P and Vesala T.** 2001. Tree stem diameter variations and transpiration in Scots pine: an analysis using a dynamic sap flow model. *Tree Physiology*. 21, 889-897.
- Qin SJ.** 2003. Statistical process monitoring: basics and beyond. *Journal of Chemometrics*. 17, 480-502.
- Ramsay JO, Hooker G and Graves S.** 2009. *Functional data analysis with R and MATLAB*. New York, USA: Springer.
- Ramsay JO and Silverman BW.** 2005. *Functional data analysis*. 2nd edn. New York, USA: Springer.

- Roby G, Harbertson JF, Adams DA and Matthews MA.** 2004. Berry size and vine water deficits as factors in winegrape composition: anthocyanins and tannins. *Australian Journal of Grape and Wine Research*. 10, 100-107.
- Rosen C and Lennox JA.** 2001. Multivariate and multiscale monitoring of wastewater treatment operation. *Water Research*. 35, 3402-3410.
- Santesteban LG, Guillaume S, Royo JB and Tisseyre B.** 2013. Are precision agriculture tools and methods relevant at the whole-vineyard scale? *Precision Agriculture*. 14, 2-17.
- Santesteban LG, Miranda C and Royo JB.** 2011. Regulated deficit irrigation effects on growth, yield, grape quality and individual anthocyanin composition in *Vitis vinifera* L. cv. 'Tempranillo'. *Agricultural Water Management*. 98, 1171-1179.
- Schenk HJ, Espino S, Mendez AN and McElrone AJ.** 2013. Limitations in the hydraulic pathway: effects of xylem embolism on sap velocity and flow. *Acta Horticulturae*. 991, 323-332.
- Scholander PF, Hammel HT, Bradstreet ED and Hemmingen EA.** 1965. Sap pressure in vascular plants. *Science*. 148, 339-346.
- Schultz HR.** 2000. Climate change and viticulture: a European perspective on climatology, carbon dioxide and UV-B effects. *Australian Journal of Grape and Wine Research*. 6, 2-12.
- Schultz HR.** 2003. Differences in hydraulic architecture account for near-isohydric and anisohydric behaviour of two field-grown *Vitis vinifera* L. cultivars during drought. *Plant, Cell and Environment*. 26, 1393-1405.
- Schultz HR and Stoll M.** 2010. Some critical issues in environmental physiology of grapevines: future challenges and current limitations. *Australian Journal of Grape and Wine Research*. 16, 4-24.
- Sellin A, Öunapuu E and Karusion A.** 2010. Experimental evidence supporting the concept of light-mediated modulation of stem hydraulic conductance. *Tree Physiology*. 30, 1528-1535.
- Sellin A, Sack L, Öunapuu E and Karusion A.** 2011. Impact of light quality on leaf and shoot hydraulic properties: a case study in silver birch (*Betula pendula*). *Plant, Cell and Environment*. 34, 1079-1087.
- Shackel KA, Ahmadi H, Biasi W, Buchner R, Goldhamer D, S. Gurusinghe, Hasey J, Kester D, Krueger B, Lampinen BB, McGourty G, Micke W,**

- Mitcham E, Olsen B, Pelletrau K, Philips H, Ramos D, Scheankl L, Sibbert S, Snyder R, Southwick S, Stevenson M, Thorpe M, Weinbaum S and Yeager J.** 1997. Plant water status as an index of irrigation need in deciduous fruit trees. HortTechnology. 7, 23-29.
- Smart RE, Dick JK, Gravett IM and Fisher BM.** 1990. Canopy management to improve grape yield and wine quality - Principles and practices. South African Journal of Enology and Viticulture. 11, 3-17.
- Smart RE and Robinson M.** 1991. Sunlight into wine. A handbook for winegrape canopy management. Adelaide, AU: Winetitles.
- Smart RE and Sinclair TR.** 1976. Solar heating of grape berries and other spherical fruits. Agricultural Meteorology. 17, 241-259.
- Spayd SE, Tarara JM, Mee DL and Ferguson JC.** 2002. Separation of sunlight and temperature effects on the composition of *Vitis vinifera* cv. Merlot berries. American Journal of Enology and Viticulture. 53, 171-182.
- Sperry JS, Adler FR, Campbell GS and Comstock JP.** 1998. Limitation of plant water use by rhizosphere and xylem conductance: results from a model. Plant, Cell and Environment. 21, 347-359.
- Sperry JS, Christman MA, Torres-Ruiz JM, Taneda H and Smith DD.** 2012. Vulnerability curves by centrifugation: is there an open vessel artefact, and are 'r' shaped curves necessarily invalid? Plant, Cell and Environment. 35, 601-610.
- Sperry JS, Donnelly JR and Tyree MT.** 1988. A method for measuring hydraulic conductivity and embolism in xylem. Plant, Cell and Environment. 11, 35-40.
- Sperry JS, Hacke UG, Oren R and Comstock JP.** 2002. Water deficits and hydraulic limits to leaf water supply. Plant, Cell and Environment. 25, 251-263.
- Sperry JS and Tyree MT.** 1988. Mechanism of water stress-induced xylem embolism. Plant Physiology. 88, 581-587.
- Stafne E and Martinson T.** 2012. Stages of grape berry development. Extension. <http://www.extension.org/pages/31096/stages-of-grape-berry-development>
- Steppe K, Cochard H, Lacoite A and Ameglio T.** 2012. Could rapid diameter changes be facilitated by a variable hydraulic conductance? Plant, Cell and Environment. 35, 150-157.

- Steppe K, De Pauw DJW and Lemeur R.** 2008. A step towards new irrigation scheduling strategies using plant-based measurements and mathematical modelling. *Irrigation Science*. 26, 505-517.
- Steppe K, De Pauw DJW, Lemeur R and Vanrolleghem PA.** 2006. A mathematical model linking tree sap flow dynamics to daily stem diameter fluctuations and radial stem growth. *Tree Physiology*. 26, 257-273.
- Steppe K and Lemeur R.** 2004. An experimental system for analysis of the dynamic sap-flow characteristics in young trees: results of a beech tree. *Functional Plant Biology*. 31, 83-92.
- Sun L, Zhang M, Ren J, Qi J, Zhang G and Leng P.** 2010. Reciprocity between abscisic acid and ethylene at the onset of berry ripening and after harvest. *BMC Plant Biology*. 10, 257.
- Tarara JM, Lee J, Spayd SE and Scagel CF.** 2008. Berry temperature and solar radiation alter acylation, proportion, and concentration of anthocyanin in Merlot grapes. *American Journal of Enology and Viticulture*. 59, 235-247.
- Tilbrook J and Tyerman SD.** 2009. Hydraulic connection of grape berries to the vine: varietal differences in water conductance into and out of berries, and potential for backflow. *Functional Plant Biology*. 36, 541-550.
- Ton Y and Kopyt M.** 2004. Phytomonitoring in realization of irrigation strategies for wine grapes. *Acta Horticulturae*. 652, 167-173.
- Tsuda M and Tyree MT.** 2000. Plant hydraulic conductance measured by the high pressure flow meter in crop plants. *Journal of Experimental Botany*. 51, 823-828.
- Turlach BA.** 2005. Shape constrained smoothing using smoothing splines. *Computational Statistics*. 20, 81-103.
- Tuzet A, Perrier A and Leuning R.** 2003. A coupled model of stomatal conductance, photosynthesis and transpiration. *Plant, Cell and Environment*. 26, 1097-1116.
- Tyerman SD, Tilbrook J, Pardo C, Kotula L, Sullivan W and Steudle E.** 2004. Direct measurement of hydraulic properties in developing berries of *Vitis vinifera* L. cv Shiraz and Chardonnay. *Australian Journal of Grape and Wine Research*. 10, 170-181.
- Tyree MT.** 1988. A dynamic model for water flow in a single tree: evidence that models must account for hydraulic architecture. *Tree Physiology*. 4, 195-217.

- Tyree MT, Davis SD and Cochard H.** 1994. Biophysical perspectives of xylem evolution - Is there a tradeoff of hydraulic efficiency for vulnerability to dysfunction? *International Association of Wood Anatomists Journal*. 15, 335-360.
- Tyree MT and Sperry JS.** 1989. Vulnerability of xylem to cavitation and embolism. *Annual Review of Plant Physiology and Plant Molecular Biology*. 40, 19-38.
- Tyree MT and Zimmermann MH.** 2002. Xylem structure and the ascent of sap. 2nd edn. Berlin, DE: Springer-Verlag.
- Udink ten Cate AJ, Bot GPA and van Dixhoorn JJ.** 1978. Computer control of greenhouse climates. *Acta Horticulturae*. 87, 265-272.
- Urli M, Porte AJ, Cochard H, Guengant Y, Burlett R and Delzon S.** 2013. Xylem embolism threshold for catastrophic hydraulic failure in angiosperm trees. *Tree Physiology*. 33, 672-683.
- van Bavel MG and van Bavel CHM.** 1990. Dynagage installation and operation manual. Houston, TX, USA: Dynamax Inc.
- van den Honert TH.** 1948. Water transport in plants as a catenary process. *Faraday Society Discussions*. 3, 146-153.
- van Doorn WG, Hiemstra T and Fanourakis D.** 2011. Hydrogel regulation of xylem water flow: an alternative hypothesis. *Plant Physiology*. 157, 1642-1649.
- van Leeuwen C, Schultz HR, Garcia de Cortazar-Atauri I, Duchêne E, Ollat N, Pieri P, Bois B, Goutouly J-P, QuénoI H, Touzard J-M, Malheiro AC, Bavaresco L and Delrot S.** 2013. Why climate change will not dramatically decrease viticultural suitability in main wine-producing areas by 2050. *Proceedings of the National Academy of Sciences of the United States of America*. 110, E3051-E3052.
- van Leeuwen C, Tregoat O, Choné X, Bois B, Pernet D and Gaudillère J-P.** 2009. Vine water status is a key factor in grape ripening and vintage quality for red Bordeaux wine. How can it be assessed for vineyard management purposes? *Journal International des Sciences de la Vigne et du Vin*. 43, 121-134.
- Velez JE, Intrigliolo DS and Castel JR.** 2007. Scheduling deficit irrigation of citrus trees with maximum daily trunk shrinkage. *Agricultural Water Management*. 90, 197-204.

- Venkatasubramanian V, Rengaswamy R, Kavuri SN and Yin K.** 2003. A review of process fault detection and diagnosis. Part III: process history based methods. *Computers & Chemical Engineering*. 27, 327-346.
- Vermeulen K, Aerts J-M, Dekock J, Bleyaert P, Berckmans D and Steppe K.** 2012. Automated leaf temperature monitoring of glasshouse tomato plants by using a leaf energy balance model. *Computers and Electronics in Agriculture*. 87, 19-31.
- Vermeulen K, Steppe K, Linh NS, Lemeur R, De Backer L, Bleyaert P, Dekock J, Aerts JM and Berckmans D.** 2008. Simultaneous response of stem diameter, sap flow rate and leaf temperature of tomato plants to drought stress. *Acta Horticulturae*. 801, 1259-1266.
- Villez K.** 2007. Multivariate and qualitative data-analysis for monitoring, diagnosis and control of sequencing batch reactors for wastewater treatment. PhD thesis. Ghent, BE: Ghent University.
- Villez K, Ruiz M, Sin G, Colomer J, Rosén C and Vanrolleghem PA.** 2008. Combining multiway principal component analysis (MPCA) and clustering for efficient data mining of historical data sets of SBR processes. *Water Science and Technology*. 57, 1659-1666.
- Villez K, Steppe K and De Pauw DJW.** 2009. Use of Unfold PCA for on-line plant stress monitoring and sensor failure detection. *Biosystems Engineering*. 103, 23-34.
- Vogt UK.** 2001. Hydraulic vulnerability, vessel refilling, and seasonal courses of stem water potential of *Sorbus aucuparia* L. and *Sambucus nigra* L. *Journal of Experimental Botany*. 52, 1527-1536.
- Vogt UK and Losch R.** 1999. Stem water potential and leaf conductance: a comparison of *sorbus aucuparia* and *Sambucus nigra*. *Physics and Chemistry of the Earth (B)*. 24, 121-123.
- Wentzell PD and Lohnes MT.** 1999. Maximum likelihood principal component analysis with correlated measurement errors: theoretical and practical considerations. *Chemometrics and Intelligent Laboratory Systems*. 45, 65-85.
- Wheeler JA, Huggett BA, Tofte AN, E RF and Holbrook MN.** 2013. Cutting xylem under tension or supersaturated with gas can generate PLC and the appearance of rapid recovery from embolism. *Plant, Cell and Environment*. 36, 1938-1949.

- Wheeler JA, Sperry JS, Hacke UG and Hoang N.** 2005. Inter-vessel pitting and cavitation in woody *Rosaceae* and other vesselled plants: a basis for a safety versus efficiency trade-off in xylem transport. *Plant, Cell and Environment*. 28, 800-812.
- Williams LE.** 2000. Grapevine water relations. In: Christensen LP, Ed. Raisin production manual. Oakland, CA, USA: University of California, Agricultural and Natural Resources Publication No. 3393. 121-126.
- Williams LE and Araujo FJ.** 2002. Correlations among predawn leaf, midday leaf, and midday stem water potential and their correlations with other measures of soil and plant water status in *Vitis vinifera*. *Journal of the American Society for Horticultural Science*. 127, 448-454.
- Williams LE and Matthews MA.** 1990. Grapevines. In: Stewart BA and Nielsen DR, Eds. Irrigation of agricultural crops. Agronomy monograph No. 30. Madison, USA: American Society of Agronomy. 1019-1055.
- Wold S, Geladi P, Esbensen K and Öhman J.** 1987. Multi-way principal components and PLS-analysis. *Journal of Chemometrics*. 1, 47-56.
- Zhou S, Duursma RA, Medlyn BE, Kelly JWG and Prentice IC.** 2013. How should we model plant responses to drought? An analysis of stomatal and non-stomatal responses to water stress. *Agricultural and Forest Meteorology*. 182-183, 204-214.
- Zufferey V, Cochard H, Ameglio T, Spring JL and Viret O.** 2011. Diurnal cycles of embolism formation and repair in petioles of grapevine (*Vitis vinifera* cv. Chasselas). *Journal of Experimental Botany*. 62, 3885-3894.
- Zweifel R, Steppe K and Sterck FJ.** 2007. Stomatal regulation by microclimate and tree water relations: interpreting ecophysiological field data with a hydraulic plant model. *Journal of Experimental Botany*. 58, 2113-2131.

Curriculum vitae

Personal information

Name: Baert Annelies
Date of birth: 23 January 1986
Place of birth: Ghent (Belgium)
Nationality: Belgian
Address: Oogststraat 56, B-9032 Wondelgem
E-mail: Aebaert.Baert@UGent.be

Education

1998 - 2004 Secondary school, Science-Mathematics, Sint-Lievenscollege, Ghent, Belgium

2004 - 2007 Bachelor in Bioscience Engineering (Environmental Technology), Faculty of Bioscience Engineering, Ghent University, Belgium

2007 - 2009 Master in Bioscience Engineering (Environmental Technology), Faculty of Bioscience Engineering, Ghent University, Belgium

Master thesis:

Performed at the Laboratory of Plant Ecology, Department Applied Ecology and Environmental Biology, Faculty of Bioscience Engineering, Ghent University, Belgium

Dutch title: “Stamdiameter, sapstroom en ultrasone akoestische emissies in jonge fruitbomen tijdens extreme droogte”

2010 - 2012 Winegrower-winemaker, entrepreneurial training at Syntra Midden-Vlaanderen

2010 - 2013 Doctoral training programme in Bioscience Engineering,
Faculty of Bioscience Engineering, Ghent University, Belgium

Courses followed in the framework of this programme:

“Ecofysiologie” (2010)

“Meteorology and climatology” (2010)

“Project management” (2010)

“Creative thinking” (2010)

“Advanced academic English: writing skills” (2010)

“Personal effectiveness” (2010)

“Wijnbouwer-wijnmaker: wijnproeven; technologie druiventee”
(2011)

Professional experience

1 Nov - 31 Dec Project from the Special Research Fund (BOF), Department
2009 Veterinary Public Health and Food Safety, Faculty of Veterinary
Medicine, Ghent University, Belgium

Title: “Quantification of phytosterols in grape”

2010 - Present PhD in Applied Biological Sciences, Laboratory of Plant
Ecology, Department Applied Ecology and Environmental
Biology, Faculty of Bioscience Engineering, Ghent University,
Belgium

Title: “Development of a plant-based strategy for water status
monitoring and stress detection in grapevine”

International study experience

30 Jan - 30 Jun Erasmus, Danmarks Tekniske Universitet, Denmark

13 Feb - 20 March Research visit, University of Purdue, Forney Hall of Chemical
2011 Engineering, West Lafayette, Indiana, USA

Grants and prizes

- Dec 2009 Strategic Basic Research from Agency for Innovation by Science and Technology in Flanders (IWT) for the PhD research at Ghent University, Belgium
- Feb 2010 Grant from Scientific Research Committee (CWO) for the research visit at the University of Purdue, Forney Hall of Chemical Engineering, West Lafayette, Indiana, USA
- June 2011 Grant from Scientific Research Committee (CWO) for participation in the conference 9th International Symposium on Modelling in Fruit Research and Orchard Management, Saint-Jean-sur-Richelieu, Québec, Canada
- April 2013 Grant from Research Foundation Flanders (FWO) for participation in the conference 9th International Symposium on Grapevine Physiology and Biotechnology, La Serena, Chile
- Feb 2013 Best Poster Award at the 18th National Symposium on Applied Biological Sciences, Ghent, Belgium, for the poster “Baert A, Villez K and Steppe K. 2013. Unfold Principal Component Analysis for plant-based automatic drought stress detection without using conventional threshold values”

Educational activities

- 2010 - Present Guest lecturer in the course “Plant water relations” and practical guidance during the exercises of the course “Ecophysiology” and “Meteorology”
- 2011 - 2012 Guidance of the Master thesis of Lies Kips: “Ecofysiologisch onderzoek naar het effect van droogtestress op de cavitatie- en hydraulische geleidbaarheidsdynamiek bij druif (*Vitis vinifera* L. cv. Chardonnay)”
- 2013 - 2014 Guidance of the Master thesis of Nina Biesemans, Nele De Lamper and Jonas Goeteyn: “Gecontroleerd waterregime bij druivelaar voor het sturen van wijnkwaliteit”

Scientific publications

International publications with peer review

Baert A, Villez K and Steppe K. 2012. Functional Unfold Principal Component Analysis for automatic plant-based stress detection in grapevine. *Functional Plant Biology*. 39, 519-530.

Baert A, Villez K and Steppe K. 2013. Automatic drought stress detection in grapevines without using conventional threshold values. *Plant and Soil*. 369, 439-452.

Baert A, De Schepper V and Steppe K. Variable hydraulic resistances and their impact on plant drought response modelling. *Plant, Cell and Environment*. (Submitted)

Baert A and Steppe K. 2013. Real-time water status monitoring in grapevines using a water transport and storage model. *Journal of Agricultural Science*. (Submitted)

Baert A and Steppe K. 2013. Dynamic thresholds for stem water potential in grapevines. *Irrigation Science*. (In preparation)

De Swaef T, Mellisho CD, Baert A, De Schepper V, Ortuño MF, Torrecillas A, Conejero W and Steppe K. Model-assisted evaluation of crop load effects on fruit growth and stem diameter in peach. *Annals of Botany*. (Submitted)

International publications without peer review (proceedings)

Baert A, Villez K and Steppe K. 2011. Unfold Principal Component Analysis and Functional Unfold Principal Component Analysis for on-line plant stress detection. *Acta Horticulturae*. (Under review)

Baert A and Steppe K. 2013. Putting two water transport models to the test under wet and dry conditions. *Acta Horticulturae*. 991, 359-366.

Vergeynst LL, Bogaerts J, Baert A, Kips L and Steppe K. 2013. New type of vulnerability curve gives insight in the hydraulic capacitance and conductivity of the xylem. *Acta Horticulturae*. 991, 341-347.

Baert A and Steppe K. 2013. Automatic plant-based water status monitoring in grapevine using an improved water transport and storage model. *Acta Horticulturae*. (Under review)

De Swaef T, Mellisho CD, Baert A, De Schepper V, Conejero W and Steppe K. 2013. Crop load effects on stem diameter variations in peach evaluated with an integrated plant and fruit model. *Proceedings of the 7th International Conference on Functional - Structural Plant Models*, Saariselkä, Finland, 9-14 June 2013. 156-158.

Participation in conferences, symposia and workshops

Baert A and Steppe K. 2010. Influence of drought stress on grapevine. 16th PhD Symposium on Applied Biological Sciences, Ghent, Belgium, 20 December 2010. (poster)

Baert A, Vanhaecke L, Steppe K and De Brabandere H. 2011. Development of a U-HPLC-MS/MS method for the high-throughput quantification of phytosterols in grape. *Mass Spectrometry in Food and Feed*, Merelbeke, Belgium, 9 June 2011. (poster)

Baert A, Villez K and Steppe K. 2011. Unfold Principal Component Analysis and Functional Unfold Principal Component Analysis for on-line plant stress detection. 9th International Symposium on Modelling in Fruit Research and Orchard Management, Saint-Jean-Sur-Richelieu, Canada, 19-23 June 2011. (lecture)

Baert A, Villez K and Steppe K. 2013. Unfold Principal Component Analysis for plant-based automatic drought stress detection without using conventional threshold values. 18th National Symposium on Applied Biological Sciences, Ghent, Belgium, 8 February 2013. (poster)

Baert A and Steppe K. 2013. Automatic plant-based water status monitoring in grapevine. 9th International Symposium on Grapevine Physiology and Biotechnology, La Serena, Chile, 21-26 April 2013. (poster)

Baert A and Steppe K. 2013. Putting two water transport models to the test under wet and dry conditions. 9th International Workshop on Sap Flow, Ghent, Belgium, 4-7 June 2013. (lecture)

Goeteyn J, Van de Wal BAE, Baert A, Biesemans N, De Lamper N and Steppe K. 2013. Quantification of sugars and acids during berry development of grapevines subjected to different levels of drought stress. Trends in Food Analysis VII, Ghent, Belgium, 19 September 2013. (poster)